UNCLASSIFIED

SECURITY CLASSIFICATION OF THIS PAGE

REPORT DOCUMENTATION PAGE

Form Approved OMB No. 0704-0188

1a. REPORT SECURITY CLASSIFICATION: UNCLASSIFIED	1b. RESTRICTIVE MARKINGS
2a. SECURITY CLASSIFICATION AUTHORITY	3. DISTRIBUTION/AVAILABILITY OF REPORT: Approved for public release; distribution unlimited.
2b. DECLASSIFICATION/DOWNGRADING SCHEDULE	
4. PERFORMING ORGANIZATION REPORT NUMBER(S): GIT-85-019	5. MONITORING ORGANIZATION REPORT NUMBER(S): N/A AFOSR-TR- 90-0121
6a. NAME OF PERFORMING ORGANIZATION: Georgia Institute of Technology; 6b. OFFICE SYMBOL (If applicable):	7a. NAME OF MONITORING ORGANIZATION: Air Force Office of Scientific Research (AFOSR) Directorate of Physical & Geophysical Sciences
6c. ADDRESS (City, State, and ZIP Code): School of Physics, Georgia Institute of Technology, Atlanta, Georgia 30332	7b. ADDRESS (City, State, and ZIP Code): AFOSR/NP, Bolling Air Force Base, Bldg. 410, Washington, D. C. 20332-6448
8a. NAME OF FUNDING/SPONSORING ORGANIZATION: AFOSR; 8b. OFFICE SYMBOL (If applicable): NP	9. PROCUREMENT INSTRUMENT IDENTIFICATION NUMBER: AFOSR-84-0233
8c. ADDRESS (City, State, and ZIP Code): Building 410, Bolling AFB, D.C. 20332-6448	10. SOURCE OF FUNDING NUMBERS: PROGRAM ELEMENT NO. 61102F; PROJECT NO. 2301; TASK NO. A4; WORK UNIT ACCESSION NO. N/A

11. TITLE (Include Security Classification)

Termolecular Association of Ions in Gases, Recombination and Electron-Atom Collisions

12. PERSONAL AUTHOR(S)

M. R. Flannery

13a. TYPE OF REPORT	13b. TIME COVERED	14. DATE OF REPORT (Year, Month, Day)	15. PAGE COUNT
Final Report	FROM 7/1/84 TO 7/30/89	9/30/89	171

16. SUPPLEMENTARY NOTATION

17. COSATI CODES			18. SUBJECT TERMS (Continue on reverse if necessary and identify by block number)
FIELD	GROUP	SUB-GROUP	Recombination, Master Equation, Variational Principle, Diffusional Method, Bottleneck Method, Strong-Collision, Coupled Nearest-Neighbor, Radiative, Dissociative
N/A	N/A	N/A	

19. ABSTRACT (Continue on reverse if necessary and identify by block number)

A list of publications of the research performed during the period 7/1/84 - 7/30/89 of the Grant AFOSR - 84-0233 is provided. Theoretical research has been conducted on (a) Termolecular Association and Recombination (b) electron - (excited) atom collisions and on (c) analytical solutions of the Time-Dependent Debye-Smoluchowski equation for transport influenced reactions.Papers on all of the above topics have been written up and published as papers, with reprints sent to AFOSR at various times during the period. The exact Master Equation Method, a Variational Principle discovered during the course of this research, and various approximate treatments are presented is Special Highlights of this research. In addition, the Appendixes include a major review of Recombination Process in General.

20. DISTRIBUTION/AVAILABILITY OF ABSTRACT: ☒ UNCLASSIFIED/UNLIMITED ☐ SAME AS RPT. ☐ DTIC USERS	21. ABSTRACT SECURITY CLASSIFICATION: UNCLASSIFIED
22a. NAME OF RESPONSIBLE INDIVIDUAL: Dr. Ralph E. Kelley	22b. TELEPHONE (Include Area Code): (202) 767-4904; 22c. OFFICE SYMBOL: NP

DD Form 1473, JUN 86 — Previous editions are obsolete. — SECURITY CLASSIFICATION OF THIS PAGE: UNCLASSIFIED

CONTENTS

Abstract

A list of publications of the research performed during the period 7/1/84 - 7/30/89 of the Grant AFOSR-84-0233 is provided. Theoretical research has been conducted on (a) Termolecular Association and Recombination (b) electron-(excited) atom collisions and on (c) analytical solutions of the Time Dependent Debye-Smoluchowski equation for transport influenced reactions. Papers on all of the above topics have been written up and published as papers, with reprints sent to AFOSR at various times during the period. The Exact Master Equation Method, a Variational Principle discovered during the course of this research, and various approximate treatments are presented as Special Highlights of this research. In addition, the Appendices include a major review of Recombination Processes in General.

1. Accomplishments due to AFOSR Support

PRINCIPAL INVESTIGATOR: M. R. Flannery

School of Physics, Georgia Institute of Technology

Grant AFOSR-84-0233, Period 7/1/84 - 7/30/89

Program Element No. 61102F, Project No. 2301, Task No. A4

1.1 Research Objectives

There are two main objectives to this research program:

(1) Basic formulation and development of the theory of termolecular association processes

$$A^+ + B^- + M \rightarrow AB + M \qquad (1)$$

and

$$A^+ + B + M \rightarrow AB^+ + M \qquad (2)$$

(2) Development of scattering theories for the electron-(excited) atom collision process

$$e + A^* \rightarrow e + A^{**} \qquad (3)$$

It is important to conduct an exhaustive theoretical investigation of (1) since not only is (1) of great significance in its own right to many important applications (e.g., exciplex lasers, KrF^*, $XeCl^*$ etc.) but also it represents the simplest three-body chemical reaction. It can therefore be considered as serving as a prototype of three body processes in general.

During this grant period, this objective has been achieved for gases M at low densities. In addition to the Exact Master Equation Treatment of (1), a new Variational Principle has been discovered. This Variational Principle is applicable not only to ion-ion recombination (1) but to three-body processes

in general. It represents the first rigorous Variational Principle in Chemical Physics Collision Processes and is fully documented in §3.2.

Also various simpler but approximate treatments of (1) have been investigated - the Diffusion, Bottleneck, Strong Collision and Coupled Nearest-Neighbor Methods. These are discussed fully in §3.

The second main objective is the development of scattering theories for process (3). Now that some experimental activity is beginning to emerge it is important to develop theories for electron-(excited) atom collisions. This objective has been achieved and progress is detailed in Appendix B.

1.2 Full List of Refereed Publications in Scientific Journals (1984-1989)

1. "Ion-Ion Recombination at High Ion-Density", M. R. Flannery, J. Phys. B: Atom. Molec. Phys. 18, 5 (1985).

2. "Selected Bibliography on Atomic Collisions", M. R. Flannery, E. W. McDaniel and S. T. Manson, Atomic Data and Nuclear Data Tables 33, 1-148 (1985).

3. "The Rate for Transport-Influenced Reactions", M. R. Flannery, J. Phys. B: Atom. Molec. Phys. 18, L747-L749 (1985).

4. "Basic Expression for Termolecular Recombination and Dissociation", M. R. Flannery, J. Phys. B: Atom. Molec. Phys. 18, L839-L844 (1985).

5. "Connection Between Microscopic and Thomson Theories of Recombination", M. R. Flannery, J. Phys. B: Atom. Molec. Phys. 19, L227-L233 (1986).

6. "Orientation and Alignment Parameters for e-He($1\,^1S \rightarrow 3\,^1D$) Collisions", M. R. Flannery and E. J. Mansky, J. Phys. B: Atom. Molec. Phys. 20, L235-L239 (1987).

7. "Macroscopic and Microscopic Perspectives of Termolecular Association of Atomic Reactants in a Gas", M. R. Flannery, in Recent Studies in Atomic and Molecular Processes, ed. A. E. Kingston (Plenum Press, London, 1987), pages 167-191.

8. "Representations of the Transport Equation for Reactive Processes", M. R. Flannery, J. Phys. B: Atom. Molec. Phys. 20, 4929-4938 (1987).

9. "Diffusional Theory of Termolecular Recombination and Association of Atomic Species in A Gas", M. R. Flannery, J. Chem. Phys. 87, 6947-6956 (1987).

10. "Termolecular Recombination at Low Gas Density: Strong-Collision Bottleneck and Exact Treatments", M. R. Flannery and E. J. Mansky, J. Chem. Phys. 88, 4228-4241 (1988).

11. "Variational Principle for Termolecular Recombination in a Gas", M. R. Flannery, J. Chem. Phys. 89, 214-222 (1988).

12. "Termolecular Recombination: Nearest-Neighbor Limit and Uncoupled-Intermediate-Levels Limit", M. R. Flannery and E. J. Mansky, J. Chem. Phys. 89, 4086-4091 (1988).

13. "Analytical and Numerical Solutions of the Time-Dependent Debye-Smoluchowski Equation for Transport-Influenced Reactions", M. R. Flannery and E. J. Mansky, Chem. Phys. 132, 115-136 (1989).

14. "Recombination Processes", M. R. Flannery in Molecular Processes in Space: 'Physics of Atoms and Molecules' Series, edited by T. Watanabe, I. Shimamura, M. Shimizu and Y. Itikawa (Plenum Press, London, 1990).

Six reprints of each of the above publications were submitted to AFOSR as reprint reports with numbers GIT-85-002, 003, 006, 007, 004, 010, 012, 011, 015, 016 017 and 018, respectively.

1.3 Chapters in Books

1. "Macroscopic and Microscopic Perspectives of Termolecular Association of Atomic Reactants in a Gas", in Recent Studies in Atomic and Molecular Processes, ed. A. E. Kingston (Plenum Press, London, 1987) pages 167-191.

2. "Recombination Processes", in Molecular Processes in Space: 'Physics of Atoms and Molecules' Series, edited by T. Watanabe, I. Shimamura, M. Shimizu and Y. Itikawa (Plenum Press, London, 1990).

3. "The Numerical Solution of Partial Differential Equations in Atomic Scattering Theory", by E. J. Mansky in Proceedings of the Summer School of Computational Atomic and Nuclear Physics, edited by C. Bottcher, M. R. Strayer and J. B. McGrory (World Scientific, 1990).

4. "Iterative Solution of Large Linear Systems and Heavy Particle Collisions: Ion-Ion Recombination", by E. J. Mansky in Proceedings of the Summer School of Computational Atomic and Nuclear Physics, edited by C. Bottcher, M. R. Strayer and J. B. McGrory (World Scientific, 1990).

5. "Electron Collision Cross Sections Involving Excited States", by E. J. Mansky, in Proceedings of the NATO-Advanced Study Institute on "Non-Equilibrium Processes in Partially Ionized Gases", edited by M. Capitelli and J. N. Bardsley (Plenum Press, 1990).

Chapter #1 has been published. Six reprints have already been sent to AFOSR under Reprint Report GIT-85-012.

Chapters #2, 3, 4, 5 are in press. Reprints will be sent when available. These chapters are included as Appendices A, B, C and D of this report.

1.4 Annual Reports (7/1/84 - 7/30/88)

Full Annual Reports of the research performed during the previous twelve month period were prepared and submitted to AFOSR. The Performing Organization Report Numbers for the periods 7/1/84-6/30/85; 7/1/85-6/30/86; 7/1/86-6/30/87 and 7/1/87-7/30/88 were GIT-85-001, GIT-85-008, GIT-85-009 and GIT-85-014, respectively.

1.5 Funding History

Project AFOSR-84-0233:

7/1/84 - 6/30/85:	73,403
7/1/85 - 6/30/86:	70,188
7/1/86 - 6/30/87:	86,730
7/1/87 - 7/30/88:	92,845
8/1/88 - 7/30/89:	99,311
TOTAL:	$422,311

1.6 Personnel

1. Professor M. R. Flannery - Principal Investigator
2. Dr. E. J. Mansky - Research Scientist II
3. Mr. M. S. Keehan - Graduate Student
4. Mr. P. Smith - Graduate Student
5. Mr. A. Haffad - Graduate Student
6. Mr. A. Mekki - Graduate Student

2. Invited and Contributed Papers Presented at Professional Scientific Conferences (1984-1988)

1984: The following papers were presented at the 37th Annual Gaseous Electronics Conference, October 9-12, 1984 held at the University of Colorado. Abstracts were published in Bull. Amer. Phys. Soc. (1985) and in Annual Report GIT-85-001.

1. "Association/Dissociation in Dense Gases and Adsorption/Desorption on Surfaces", by M. R. Flannery.
2. "Analytical and Numerical Solutions of the Time Dependent Debye-Smoluchowski Equation", by M. R. Flannery and E. J. Mansky.
3. "Electron-Excited Hydrogen and Helium Collisions", by E. J. Mansky and M. R. Flannery.
4. "Symmetric Charge-Transfer Cross Sections in Rare Gas (Rg^+-Rg) Systems", by E. J. Mansky and M. R. Flannery.

1985: The following paper was presented at the 38th Annual Gaseous Electronics Conference, October 15-18, 1985, held at the Naval Postgraduate School, Monterey, California. The abstract was published in Bull. Amer. Phys. Soc. (1986) and in Annual Report GIT-85-008.

1. "Variational Principle for Association/Dissociation in Dense Gases", by M. R. Flannery, was presented at the 38th Annual Gaseous Electronics Conference, October 15-18, 1985, at the Naval Postgraduate School, Monterey, California.

1986: The following papers were presented at the 39th Annual Gaseous Electronics Conference, October 7-10, 1986, held at University of Wisconsin, Madison, Wisconsin. The abstracts were published in Bull. Amer. Phys. Soc. (1987) and in Annual Report GIT-85-009.

1. "Microscopic Perspective to Termolecular Ion-Molecule Reactions", by M. R. Flannery.
2. "Detailed Investigation of the Thomson Model of Termolecular Recombination", by E. J. Mansky and M. R. Flannery.

An invited lecture entitled:

3. "Termolecular Association in Gases", by M. R. Flannery was presented at a Conference held in Honor of Sir David Bates' 70th Birthday at Queen's University, Belfast, November 17 and 18, 1986.

The lecture was published as a Chapter in the book "Recent Studies in Atomic and Molecular Processes", edited by A. E. Kingston (Plenum Press, New York, 1987).

1987: Invited and Contributed Papers

1. An invited paper entitled "Termolecular Recombination", by M. R. Flannery, was presented at the 40th Annual Gaseous Electronics Conference, Atlanta, held at Georgia Institute of Technology, Georgia, Oct. 13-16, 1987. It is published in Bull. Amer. Phys. Soc. 33, \$2 (1988) p. 122.
2. A contributed paper entitled "Orientation and Alignment Parameters for $e + He(2^{1,3}S) \rightarrow e + He(3^{1,3}P, 3^{1,3}D)$ Collisions", by E. J. Mansky and M. R. Flannery, was presented at the 40th Annual Gaseous Electronics Conference, Atlanta, held at Georgia Institute of Technology, Georgia, Oct. 13-16, 1987. It is published in Bull. Amer. Phys. Soc. 33, \$2 (1988) p. 141.
3. A contributed paper entitled "Termolecular Recombination and Electrical Networks", by M. R. Flannery and E. J. Mansky was presented at the 1988 Spring Meeting of the American Physical Society (APS) in conjunction with the Annual Meeting of the APS Division of Atomic and Molecular and Optical Physics held at Baltimore, Maryland, April 18-21 (1988).

The abstracts were included in the Annual Report GIT-85-014.

1988:

(a) A long paper entitled "Multichannel Eikonal Theory of Electron-(Excited) Atom Collisions", by M. R. Flannery and a contributed paper entitled "Integral and Differential Cross Sections for e-He ($2^{1,3}S$) Collisions", by E. J. Mansky and M. R. Flannery were presented at the 41st Annual Gaseous Electronics Conference held at University of Minnesota, Minneapolis, Minnesota, Oct. 18-21, 1988. The abstracts are published in Bull. Amer. Phys. Soc. 34, #2 (1989) p. 302 and p. 315.

(b) Two contributed papers entitled "The Poincare Sphere for the 2^1P, 3^1P and 3^1D States of Helium", by E. J. Mansky and M. R. Flannery and "Orientation and Alignment Parameters for e-H(1s→3p,3d) Collisions", by E. J. Mansky were presented at the 20th Annual Meeting of the (APS) Division of Atomic, Molecular and Optical Physics held at the University of Windsor, Windsor, Ontario, May 17-19, 1989. The abstracts are published in Bull. Amer. Phys. Soc. 34, #5 (1989) p. 1371 and p. 1407.

(c) An invited paper entitled "Electron Cross Sections Involving Excited States", by E. J. Mansky was presented to the NATO-Advanced Study Institute, "Non-Equilibrium Processes in Partially Ionized Gases" held at Maratea, Italy, June 4-17, 1987. It is published as a Chapter in the Book, listed in §1.2.

(d) Two invited papers entitled "The Numerical Solution of Partial Differential Equations in Atomic Scattering Theory", and "Iterative Solutions in Large Linear Systems and Heavy Particle Collisions", by E. J. Mansky were presented to the Summer School of Computational Atomic and Nuclear Physics held at University of the South, Sewanee, Tennessee, June 16-July 7, 1989. They are published as Chapters in the Book, listed in

§1.3.

(e) A contributed paper entitled "Stokes Parameter Analysis of the 3^1D State of Helium", by E. J. Mansky and M. R. Flannery was delivered to 16th International Conference on the Physics of Electronic and Atomic Collisions held at New York, July 26 - Aug. 1, 1989.

3. Special Highlights

In a series of papers, #9 - #12 of the list in § 1.1, the Termolecular Recombination Process

$$A^+ + B^- + M \rightarrow AB + M \qquad (1)$$

was explored in depth. Exact treatments based on a Master Equation and on a New Variational Principle discovered by M. R. Flannery were developed and applied. Various approximate treatments as (a) The Diffusional Theory (b) Strong Collision and Bottleneck Models and (c) a Coupled Nearest-Neighbor Limit and Uncoupled Intermediate Levels Limits were also provided and compared with experiment. In order to explain the research fully, the resulting publications in J. Chem. Phys. are reproduced in the following Sections 3.1 - 3.4.

In §3.1, the Exact Treatment is discussed together with the Strong Collision and Bottleneck Methods.

In §3.2, the New Variational Principle is developed and applied.

In §3.3, the Diffusional Treatment is presented.

In §3.4, methods of Coupled Nearest-Neighbor and Uncoupled Intermediate Levels are presented and applied.

Since the Termolecular Process (1) is the simplest type of three-body Chemical Process, it is essential to understand it in required depth, not only because of its great significance in general applications but also because it serves as a prototype for three-body reactions. In the following sections, attempt is made to provide an exhaustive understanding.

Also a major review of Recombination Processes in General is included in Appendix A.

3.1 Exact Treatment, Strong Collision and Bottleneck Treatments.

Termolecular recombination at low gas density: Strong collision, bottleneck, and exact treatments

M. R. Flannery and E. J. Mansky
School of Physics, Georgia Institute of Technology, Atlanta, Georgia 30332

(Received 23 November 1987; accepted 24 December 1987)

On introducing the probabilities for association as a function of internal separation R and internal energy E of the associating (A–B) species the strong collision model is thoroughly investigated and compared, as a case study, with the exact treatment of termolcular ion–ion recombination at low gas densities. A bottleneck model is also investigated. Analytical expressions for the one way equilibrium energy-change rates at fixed R are provided in the Appendix.

I. INTRODUCTION

The theory of termolecular ion–ion recombination,

$$A + B + M \underset{k}{\overset{\alpha}{\rightleftarrows}} AB + M \tag{1.1}$$

between positive and negative atomic ions A and B in a low density gas thermal M is now well established.[1–5] The distribution $n_i(E_i,t)$ per unit interval dE_i of recombining pairs AB with internal energy E_i a time t is governed by the collisional input–output Master equation[1–5]:

$$\frac{d}{dt} n_i(E_i,t) = \frac{\partial n_i}{\partial t} - F_i$$

$$= -\int_{-D}^{\infty} [n_i \nu_{if} - n_f \nu_{fi}]\, dE_f$$

$$= -\frac{\partial}{\partial E_i} J_i(E_i,t), \tag{1.2}$$

where ν_{if} is the frequency per unit interval dE_f for $E_i \to E_f$ transitions by collisions between AB and M, where J_i is the upward current in energy space past level E_i and where $-D$ is the energy of the lowest vibrational level of AB relative to the dissociation limit taken as zero energy. For dissociated pairs with $E_i > 0$, F_i is the net flux per unit interval dE_i of (contracting) AB pairs generated with energy E_i at infinite internal separation R. For bound pairs with $E_i < 0$, F_i is zero. The net rate for association is[4]

$$R^A(t) = \int_{-D}^{\infty} P_i^S \left(\frac{dn_i}{dt}\right) dE_i$$

$$= \alpha N_A(t) N_B(t) - k n_s(t), \tag{1.3}$$

where P_i^S is the probability that E_i pairs are collisionally connected to the product channel, i.e., have been stabilized against dissociative collisions with thermal M. The effective two-body rate constant for the association of A and B with (cm^{-3}) concentrations $N_A(t)$ and $N_B(t)$ is α ($cm^3\,s^{-1}$), and k (s^{-1}) is the frequency for dissociation of those tightly bound pairs of concentration $n_s(t)$, which are considered to be fully associated with energies E_i within a block $\mathscr{S}$ of low lying fully stabilized levels in a range $-S > E_i > -D$ within which the stabilization probability P_i^S is calculated to be unity. When the quasi-steady-state (QSS) condition $dn_i/dt = 0$ is satisfied for pairs in a block $\mathscr{B}$ of highly excited levels in the energy range $0 > E > -S$ between the dissociation limit at zero energy and level $-S$ the rate (1.3) reduces to[4]

$$R^A(t) = \int_{-D}^{-S} \left(\frac{dn_i}{dt}\right) dE_i$$

$$= \int_0^{\infty} F_i\, dE_i = -\int_{-E}^{\infty} \left(\frac{dn_i}{dt}\right) dE_i$$

$$= -J(-E,t) \tag{1.4}$$

for a steady-state ($\partial n_i/\partial t = 0$) distribution of pairs in the block $\mathscr{C}$ of fully dissociated states in the energy range $0 < E < \infty$, over which the stabilization probability P_i^S vanishes. The rate (1.3) therefore reduces[4] under QSS to the downward current $-J(-E,t)$ of pairs past energy level $-E$ in bound block $\mathscr{B}$.

At low gas densities the expansion[4]

$$\gamma_i(t) = \frac{n_i(E_i,t)}{\tilde{n}_i(E_i)} = P_i^D(E_i) \left[\frac{N_A(t) N_B(t)}{\tilde{N}_A \tilde{N}_B}\right] + P_i^S(E_i) \left[\frac{n_s(t)}{\tilde{n}_s}\right] \tag{1.5a}$$

$$\equiv P_i^D(E_i)\gamma_c(t) + P_i^S(E_i)\gamma_s(t) \tag{1.5b}$$

permits separation of variables E_i and t in the collisional part of Eq. (1.2). Here γ_i, γ_c, and γ_s are the various time-dependent distributions of states in blocks $\mathscr{B}$, $\mathscr{C}$, and $\mathscr{S}$ normalized to their respective equilibrium values $\tilde{n}_i, \tilde{N}_{A,B}$, and $\tilde{n}_s$. For $\mathscr{B}$ states, P_i^S and $P_i^D = 1 - P_i^S$ are the probabilities that state i is collisionally connected to the sink $\mathscr{S}$ and to the source $\mathscr{C}$. For $\mathscr{C}$ states at low gas densities P_i^D, the collision survival probability is unity when equilibrium conditions in E_i and R can be assumed in the collision part of Eq. (1.2). When Eq. (1.5) is inserted the collisional part of Eq. (1.2), then Eqs. (1.4) and (1.3) yield the expressions[4]

$$\alpha \tilde{N}_A \tilde{N}_B = -j(-E) = k\tilde{n}_s$$

$$= \int_{-E}^{\infty} dE_i \int_{-D}^{-E} (P_f^S - P_i^S) C_{if}\, dE_f \tag{1.6}$$

for the rate coefficients α and k in Eq. (1.1). The collision kernel C_{if} is the collisional rate $\tilde{n}_i \nu_{if}$ ($cm^3\,s^{-1}$) per unit element $dE_i\, dE_f$ for $E_i \to E_f$ transitions and varies linearly with the gas density N. At low N, α is linear in N so that $P_i^{S,D}$ are required only to zero order in N. The net downward time-dependent collisional current across arbitrary level $-E$ in block $\mathscr{B}$ separates as

 0021-9606/88/074228-14$02.10

$$-J(-E,t) = -j(-E)\,[N_A(t)N_{B(t)}/\tilde{N}_A\tilde{N}_B - n_s(t)/\tilde{n}_s] \tag{1.7}$$

which under conditions of full thermodynamic equlibrium tends therefore to zero.

The multicollisional stochastic aspect of the theory becomes apparent by correctly identifying the (time-independent and density-independent) stabilization probability as

$$P_i^S(E_i) = \left[\int_{-D}^{0} (n_i\nu_{if})\,P_f^S\,dE_f\right] \Big/ \left[\int_{-D}^{\infty} n_i\nu_{if}\,dE_f\right] \tag{1.8a}$$

which is the fraction of all collisions which result in association. Equation (1.8a) is consistent with the concept of a Markov element chain, and when rewritten in the form of an integral equation

$$P_i^S \int_{-D}^{\infty} C_{if}\,dE_f = \int_{-D}^{0} C_{if}P_f^S\,dE_f \tag{1.8b}$$

is seen, after substituting Eq. (1.5b) in Eq. (1.2), to be equivalent to the assumption of a quasi-steady-state (QSS) E_i distribution of pairs with energy within the highly excited block $\mathscr{E}$.

The rate (1.6) holds for $E=0$ and $E=S$ to give, respectively,

$$\alpha\tilde{N}_A\tilde{N}_B = -j(0) = \int_0^{\infty} dE_i \int_{-D}^{0} C_{if}P_f^S\,dE_f = k\tilde{n}, \tag{1.9}$$

as the collisional rate from the fully dissociated states i to bound states f which are then collisionally stabilized with probability P_f^S, and

$$\alpha\tilde{N}_A\tilde{N}_B = j(-S) = \int_{-D}^{-S} dE_i \int_{-S}^{\infty} C_{if}P_f^D\,dE_f = k\tilde{n}, \tag{1.10}$$

as the collisional rate from the fully associated states i to levels f which are then collisionally disrupted with probability P_f^D. Note that Eq. (1.9) or Eq. (1.6) is the QSS rate for association of a full equilibrium concentration $\tilde{N}_A\tilde{N}_B$ of dissociated pairs into a perfectly absorbing sink $\mathscr{S}$ maintained at zero population, i.e., $\gamma_c = 1$ and $\gamma_s = 0$ in Eq. (1.5b). Similarly Eq. (1.10) is the QSS rate for dissociation which would result from an equilibrium population $\tilde{n}_s$ of associated $\mathscr{S}$ pairs being dissociated into states $\mathscr{E}$ maintained at zero population, i.e., $\gamma_c = 0$ and $\gamma_s = 1$ in Eq. (1.5b).

In this paper two simplifications to the above exact treatment at low gas densities N are investigated in detail. In the strong collision and bottleneck models, the probabilities P_i^S are preassigned without recourse to Eq. (1.8). The first model assumes that P_i^S for all bound pairs with internal separation R is unity for R within the range $0<R<R_T$, where R_T is some preassigned radius, outside which P_i^S is zero. In this strong collision (or Thomson-style[7]) model, bound pairs with $R<R_T$ are therefore considered to be fully associated and those with $R>R_T$ cannot be stabilized. In the bottleneck model, P_i^S for bound pairs at all accessible R is unity for $E_i<E^*$, and is zero for $E>E^*$ and E^* is a (bound) energy level within $\sim 2kT$ below the dissociation limit and past which the one-way equilibrium rate is a minimum which therefore acts as a bottleneck to the current. The level E^* is, in effect, a transition state. Each model therefore subdivides the two dimensional (R,E) space into regions of some physical signficance. The Thomson model has previously been addressed via a Monte Carlo simulation method[8] and indirectly by an analytical approach[9] based on collisional deactivation of dissociated pairs to levels lower than various bound levels. A more exhaustive and detailed investigation is undertaken here. The bottleneck model has also received some previous consideration.[1,2]

Not only will these models elucidate interesting dynamics underlying the recombination mechanism (1.1) at low gas densities N, but subsequent modification to cover higher gas densities proves quite valuable towards a study (in progress) of the variation of the recombination rate α with gas density N.

II. THEORY

The detailed investigation of the strong-collision model requires the generalization of the Master equation (1.2) to $(\mathbf{R},E)$ space and use of the frequencies $\nu_{if}(R)$ for $E_i \to E_f$ transitions per unit interval $d\,\mathbf{R}\,dE_f$ by collisions between M and the pair AB *at fixed internal separation* R. The appropriate input–output Master equation satisfied by the distribution $n_i(\mathbf{R})$ of (A–B) pairs per unit interval $d\,\mathbf{R}\,dE_i$ has been shown[10] to be the continuity equation

$$\frac{d}{dt}n_i(\mathbf{R},t) = \frac{\partial n_i}{\partial t} + \frac{1}{R^2}\frac{\partial}{\partial R}\left[R^2 j_i^d(R)\right]_{E_i}$$
$$= -\int_{V(R)}^{\infty} \left[n_i(\mathbf{R})\nu_{if}(R) - n_f(\mathbf{R})\nu_{fi}(R)\right]dE_f$$
$$\equiv -\int_{V(R)}^{\infty} S_{if}(R)\,dE_f, \tag{2.1}$$

where $j_i^d(R)$ is the net outward transport current of pairs expanding at R, where S_{if} is the net two level collisional-absorption rate, and where $V(R)$ is the energy of interaction between A and B. Integration of Eq. (2.1) over all accessible R yields the customary Master equation (1.2) for dissociated and bound states.

A. Rates and stabilization probabilities

The steady-state rate (1.4), with the aid of Eq. (2.1), is

$$R^A(t) = -\int_0^{\infty} \lim_{R_T\to\infty}\left[4\pi R_T^2 j_i^d(R_T)\right]dE_i$$
$$= \int_0^{\infty} dE_i \int_0^{\infty} d\,\mathbf{R} \int_{V(R)}^{0} S_{if}(R)\,dE_f \tag{2.2}$$

which either is the net inward flux of dissociated pairs contracting by transport across a sphere of infinite radius R_T or is the net collisional downflow across the dissociation limit at $E_i = 0$.

Now assume (a) that there is a finite radius R_T for which all E_i pairs with $R>R_T$ are in energy equilibrium at each R, i.e.,

$$\frac{n_i(\mathbf{R})}{n(\mathbf{R})} = \frac{\tilde{n}_i(\mathbf{R})}{\tilde{n}(\mathbf{R})}, \quad R>R_T, \tag{2.3a}$$

where

$$n(\mathbf{R}) = \int_{V(R)}^{\infty} n_i(\mathbf{R}) dE \tag{2.3b}$$

is the concentration per unit interval $d\mathbf{R}$ of all pairs with separation R. Thus S_{if} in Eq. (2.2) vanishes for $R>R_T$ to yield

$$R^{A}(t) = \int_0^{\infty} dE_i \int_0^{R_T} d\mathbf{R} \int_{V(R)}^{0} S_{if}(R) dE_f \tag{2.4}$$

which is the steady-state rate of association of dissociated pairs with $R<R_T$.

Association of R_T complex: At low gas densities N, the distribution $n_i(\mathbf{R})$ is independent of N so that the collision term S_{if} remains linear in N. On the right-hand side of Eq. (2.1) $n_i(R)$ is equilibrium with respect to $\mathbf{R}$, so that

$$\frac{n_i(\mathbf{R},E_i)}{n_i(E_i)} = \frac{\tilde{n}_i(\mathbf{R},E_i)}{\tilde{n}_i(E_i)}, \tag{2.5a}$$

where the distribution per unit interval dE_i is

$$n_i(E_i) = \int_0^{R_i} n_i(\mathbf{R}) d\mathbf{R} \tag{2.5b}$$

and R_i is the classical turning point of E_i motion. The separation (1.5) is then valid so that Eq. (2.4) yields

$$\alpha \tilde{N}_A \tilde{N}_B = \int_0^{\infty} dE_i \int_0^{R_T} d\mathbf{R} \int_{V(R)}^{0} C_{if}(R) P_f^S dE_f = k_s \tilde{n}_s \tag{2.6}$$

for the rate of association of dissociated pairs in the complex of radius R_T. The required one-way equilibrium rate

$$C_{if}(R) = \tilde{n}_i(R) v_{if}(R) = C_{fi}(R) \tag{2.7}$$

at each R is related to the R-averaged rate C_{if} previously used[1-3] in Eq. (1.6) by

$$C_{if} = \tilde{n}_i v_{if} = \int_0^{R_{if}} \tilde{n}_i(\mathbf{R}) v_{if}(R) d\mathbf{R} = \int_0^{R_{if}} C_{if}(R) d\mathbf{R}, \tag{2.8}$$

where R_{if} is the lesser of the two outermost turning points R_i and R_f associated with levels E_i and E_f, of which one at least is bound. Detailed expressions for $C_{if}(R)$ are presented in the Appendix.

Strong collision rate: In addition to Eq. (2.3a), assume (b) that all bound states f with $R<R_T$ are fully stabilized, i.e.,

$$P_f^S = 1, \quad R<R_T, \ E_f<0 \tag{2.9}$$

so that the required strong collision rate is

$$\alpha(R_T) \tilde{N}_A \tilde{N}_B = \int_0^{\infty} dE_i \int_0^{R_T} d\mathbf{R} \int_{V(R)}^{0} C_{if}(R) dE_f \tag{2.10}$$

which is the one-way equilibrium rate that dissociated pairs with $R<R_T$ are collisionally deexcited across the dissociation limit. The "complex" assumption (2.3a) is equivalent either to assigning in Eq. (2.2) zero probability $P_f^S = 0$ for $R>R_T$ and $E_f<0$, i.e., to the overall neglect of association or to inclusion in Eq. (2.4) of upward equilibrating transitions past $E_i = 0$ for $R>R_T$. The *strong-collision* assumption (2.9) is equivalent to the neglect in Eq. (2.4) of the rate $\int_V^0 n_f(R) v_{fi}(R) dE_f$ for upward redissociation of pairs with $R<R_T$.

The physical basis to the two assumptions (2.3) and (2.9) can be illustrated by Fig. 1. Bound states at large R arise from highly elliptical Coulomb orbits with low angular momenta where the possible velocity vectors for relative (A–B) motion lie within a narrowly focused region. Upon collision with the gas, the velocity vector is mainly deflected into directions outside this region so that the post-collision velocity vector cannot be consistent with bound states at large R. Collisional dissociation of these highly excited levels at large R is therefore most likely to occur,[8] and stabilization of bound levels f is not viable so that $P_f^S(R>R_T) = 0$ in keeping with assumption (2.3) underlying complex formation for association to proceed.

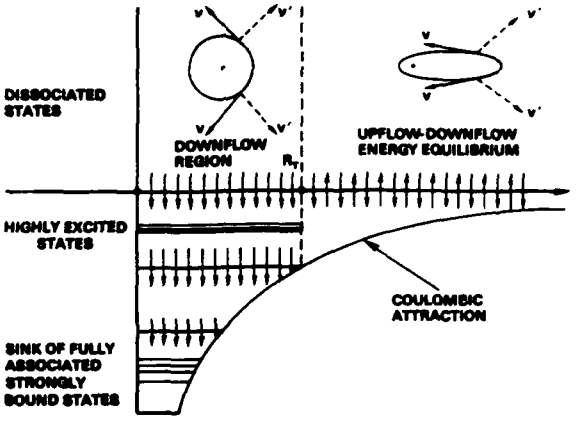

FIG. 1. Schematic basis for strong collisions within an assumed complex of radius R_T. A–B relative motion in circular and highly elliptical (large R) orbits with speeds v and v' before and after ion–neutral collision.

For intermediate R, however, the post-collision velocity can be accomodated by many angular-momentum bound orbits, more final angular momentum levels are accessible at these $R \simeq e^2/2|E_i|$, the radius of the circular orbit, and the number of accessible orbits at a given R increase with increasing binding. Collisional deexcitation of highly excited levels at smaller R therefore tends to occur and pairs with $R<R_T$ in all bound levels can be fully stabilized, in keeping with the strong-collision assumption (2.9).

The averaged kernels (2.8) have been previously derived for symmetrical resonance charge transfer,[1] hard-sphere,[2] and polarization[3] binary collisions between either ion A or B and the gas M. The R-dependent one-way equilibrium kernels $C_{if}(R)$ are not only required for this sudy but also for ongoing investigations of the nonlinear variation of α with gas density N. They are provided in the Appendix as a comprehensive package for present and future use and reference.

The exact low density rate (1.6) and the strong-collision rate (2.10) reduce to a sum[9,11] of rates α_A and α_B, each arising from A–M and B–M binary collisions, respectively, and α_A can be presented[1-3,5,9] as a universal function [cf. Eq. (A55)] of the mass parameter

$$a = \frac{M_B M_g}{M_A (M_A + M_B + M_g)}, \tag{2.11}$$

where M_A, M_B, and M_g are the masses of the reacting atomic ions and gas atoms, respectively.

Calculation of Eq. (1.6), the exact low density rate α_E,

and of the variation of the strong collision rate (2.10) with R_T can now be performed. For the exact rate (1.6), highly accurate converged solutions P_i^S of the integral equation (1.6), discretized as in Ref. 3 into an equivalent set of 100 algebraic equations, have been obtained. Previous results[1-3] were based on 36 coupled equations at most. Convergence of α_E to within 0.5% is found to be much more rapid for intermediate mass parameters a ($\sim 1/3$) than for small and large a which required 100 coupled equations for convergent rates.[5]

In contrast to ion–atom association where the radius R_T may, with some justification, be identified with the location of the centrifugal barrier, no such assignment for ion–ion recombination (without any centrifugal barrier) exists, although Thomson[7] suggested $R_T = 2e^2/3kT$ where the relative kinetic energy ($\frac{1}{2}kT + e^2/R$) is reduced to $\frac{1}{2}kT$ upon collision. Hence bound pairs with $E_f = e^2(1/R_T - 1/R) < 0$ can be formed within $R < R_T$.

The variation with R_T of the ratio $\alpha(R_T)/\alpha_E$ for the recombination of *equal-mass* ions via symmetrical resonance charge-transfer (CX), polarization (POL), and hard-sphere (HS) collisions with an *equal-mass* gas ($a = 1/3$) is displayed in Fig. 2. The ratio is unity for R_T in the range (0.48–0.55) (e^2/kT), in good agreement with Thomson's suggestion. The neglect in Eq. (2.6) of a positive contribution to association from possible collisional stabilization of those bound levels with $R > R_T \approx 0.5$ (e^2/kT) is effectively offset by the neglect in Eq. (2.10) via Eq. (2.9) of a negative contribution arising from redissociation of those bound states with $R < R_T$.

The strong collision model is therefore capable of high accuracy *provided* R_T can be preassigned; realistic assignment to R_T for recombination being only feasible[9] after the exact treatment is performed! The radius R_T, once assigned, may however be adopted in models under development for variation of α with gas density N.

As R_T becomes large the rate (2.10) however tends rapidly to

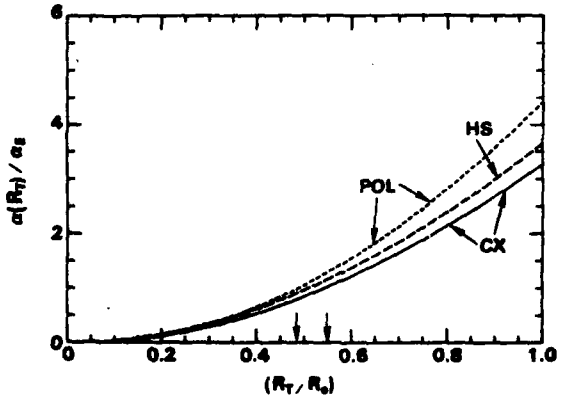

FIG. 2. R_T variation of $\alpha(R_T)$, the strong-collision rate (2.10) normalized to α_E, the exact rate (1.6), for equal-mass components and model ion–neutral interactions (POL: polarization; HS: hard sphere; CX: symmetrical resonance charge transfer). Arrows indicate where $\alpha(R_T) = \alpha_E$ for POL and CX in units of $R = e^2/kT$.

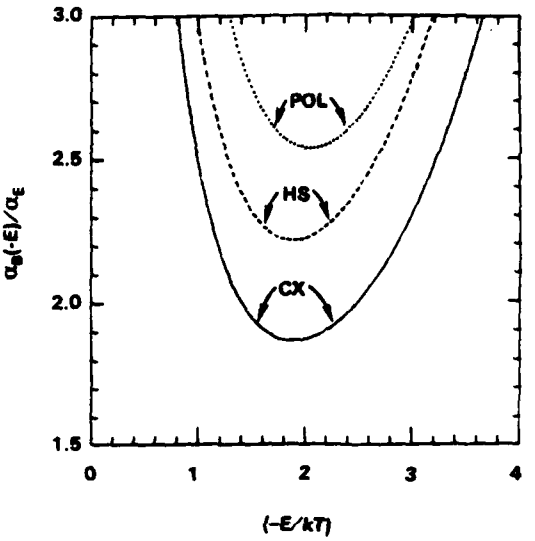

FIG. 3. One-way equilibrium rates $\alpha_{BN}(-E)$, Eq. (2.13), normalized to α_E, the exact rate (1.6), across energy level $-E$ for model ion–neutral interactions POL, HS, and CX.

$$\alpha(R_T \to \infty)\tilde{N}_A\tilde{N}_B = \int_0^\infty dE_i \int_{-D}^{0} C_{if}\, dE_f \qquad (2.12)$$

which is of course infinite owing to the divergence, as $E_i \to 0$, of the equilibrium density $\tilde{n}_i(E_i) \sim |E_i|^{-5/2}\exp(-E_i/kT)$ of Coulomb bound states per unit interval dE_i. As $R_T \to \infty$, the physical basis for adopting the one-way equilibrium rate (2.10) becomes untenable since bound states with large R_T are more readily redissociated (cf. Fig. 1). Upward collisions past the dissociation limit must therefore be included for large R_T. The strong collision assumption is therefore no longer justified for large R_T.

This divergence can be eliminated not only by maintaining R_T finite but also by considering the one-way equilibrium rate

$$\alpha_{BN}(-E)\tilde{N}_A\tilde{N}_B = \int_{-E}^\infty dE_i \int_{-D}^{-E} C_{if}\, dE_f \qquad (2.13)$$

across any bound level $-E$ in block $\mathscr{E}$. Figure 3 illustrates that this rate decreases from the infinite limit (2.12) at $E = 0$ to a pronounced minimum at an energy $E^* = 2kT$ below the dissociation limit. Since Eq. (2.13) is an upper limit to the exact rate by taking $P_i^S(E_i > -E)$ and $P_f^S(E_f < -E)$ within Eq. (1.6) to be zero and unity, respectively, then its minimum value $\alpha_{BN}(-E^*)$ is the least upper limit and is the one-way rate past the effective bottleneck to the curent at $-E^*$ which, in effect, is a transition state. Although this bottleneck model (2.13) is physically different from the previous strong collision model (2.10), it is worth noting that $E^* = 2kT$ corresponds to a turning point R_T of $\frac{1}{2}(e^2/kT)$ for which the strong collision model is effectively exact (cf. Fig. 2). Figure 3 shows that the bottleneck result is however a factor of 1.9–2.5 times larger than the exact rate α_E. In contrast to the strong-collision model (2.10), Eq. (2.13) is always an upper limit since in order to obtain the bottleneck result (2.13) from Eq. (1.6), the ne-

glected terms cannot cancel since they always remain negative. This search for the least upper limit to the one-way equilibrium rate across transition state E^* is identical in principle to the variational phase-space theory of Keck[13] as applied to termolecular ion–ion recombination. The strong collision (Fig. 2) and bottleneck pictures (Fig. 3) have been previously displayed in a recent review[12]; the present CX results in Fig. 2 correct those in Ref. 12.

B. Association probabilities

To obtain these, the low density rate (2.6) for association of dissociated pairs in the R_T complex may also be expressed with the aid of Eq. (2.2) as

$$\alpha(R_T)\tilde{N}_A\tilde{N}_B = \int_0^\infty [4\pi R_T^2 \tilde{j}_i^-(R_T)]P_i^A(R_T)dE_i, \tag{2.14}$$

the net inward transport rate across the R_T sphere where

$$P_i^A(R_T) = [\tilde{n}_i^-(R_T) - n_i^+(R_T)]/\tilde{n}_i^-(R_T) \tag{2.15}$$

now specifies the desired probability that fully dissociated E_i pairs which are originally contracting at R_T will associate within the spherical complex of radius R_T. The distribution of dissociated pairs contracting at R_T is $\tilde{n}_i^-(R_T)$, the equilibrium value characteristic of low gas densities N, and is a nonequilibrium value $n_i^+(R_T)$ for pairs expanding at R_T. The one-way incident current at temperature T and pertinent to low N is the one-way equilibrium current

$$\tilde{j}_i^-(R)dE_i = \tfrac{1}{2}\tilde{n}_i^-(R)v_i(R)dE_i = \tfrac{1}{4}\tilde{n}_i(R)v_i(R)dE_i \tag{2.16}$$

$$= \frac{1}{4}\left(\frac{8kT}{\pi M_{AB}}\right)^{1/2}\tilde{N}_A\tilde{N}_B[1 - V(R)/E_i]$$

$$\times (E_i/kT)\exp(-E_i/kT)d(E_i/kT), \tag{2.17}$$

where M_{AB} is the reduced mass of the pair (A–B) and where $\tilde{n}_i$ is $\tilde{n}_i^+ + \tilde{n}_i^-$. By direct comparison of Eqs. (2.14) and (2.16) the exact association probability of fully dissociated pairs within $R<R_T$ at low gas densities is

$$P_i^{AE}(E_i>0,R_T) = [\pi R_T^2\tilde{n}_i(R_T)v_i(R_T)]^{-1}$$

$$\times \int_0^{R_T} d\mathbf{R}\int_{V(R)}^0 C_{if}(R)P_f^S(R)dE_f \tag{2.18}$$

which increases linearly with gas density N via C_{if}. The stabilization probabilities P_f^S which are solutions of Eq. (1.8) do not vary with N. As $R_T\to\infty$, Eq. (2.18) in Eq. (2.14) yields

$$\alpha_i(E_i>0,R_T) = \pi R_T^2\tilde{n}_i(R_T)v_i(R_T)P_i^{AE}(E_i>0,R_T), \tag{2.19}$$

the rate per unit interval dE_i for association of dissociated E_i pairs with $R<R_T$. As $R_T\to\infty$, Eq. (2.19) saturates to the exact partial rate.

The association rate per unit dE_i for the highly excited bound E_i pairs in block $\mathscr{E}$ of the complex of radius R_T is

$$\alpha_i(E_i<0,R_T) = [\pi R_T^2\tilde{n}_i(R_T)v_i(R_T)]P_i^A(E_i<0,R_T)$$

$$= \int_0^{R_T} d\mathbf{R}\left[\int_{V(R)}^0 C_{if}(R)P_f^S dE_f\right.$$

$$\left. - P_i^S\int_{V(R)}^\infty C_{if}(R)dE_f\right]. \tag{2.20}$$

As $R_T\to R_i$, the outermost turning point of E_i motion where $|E_i| = |V(R_i)|$, this rate (2.20) vanishes owing to the QSS requirement (1.8) of zero net gain of all E_i pairs with $R<R_i$ in block $\mathscr{E}$, a condition on which calculation of the stabilization probabilities P_i^S is based.

Strong collision and Thomson probabilities: The corresponding strong-collision association probability P_i^{ST} is given by Eq. (2.18) with $P_f^S = 1$, i.e., by the probability

$$P_i^{ST}(E_i>0,R_T) = [\pi R_T^2\tilde{n}_i(R_T)v_i(R_T)]^{-1}$$

$$\times \int_0^{R_T} d\mathbf{R}\int_{V(R)}^0 C_{if}(R)dE_f \tag{2.21}$$

for direct collisional formation of bound levels from a dissociated state of energy E_i. It overestimates the exact association probability by

$$P_i^{RD} \equiv P_i^{ST}(R_T) - P_i^{AE}(R_T)$$

$$= [\pi R_T^2\tilde{n}_i(R_T)v_i(R_T)]^{-1}$$

$$\times \int_0^{R_T} dR\int_{V(R)}^0 C_{if}(R)P_f^D dE_f \tag{2.22}$$

which in fact is the probability P_i^{RD} for subsequent redissociation of bound pairs formed with $R<R_T$ and which is inherently neglected by the strong-collision model. On defining the free path length[4] $\lambda_i(R)$ for continuum–bound transitions in A–M collisions during the (A–B) trajectory by

$$\lambda_i^{-1}(R) \equiv [\nu_i(R)/v_i]$$

$$= \left[\int_{V(R)}^0 C_{if}(R)dE_f\right]/[\tilde{n}_i(R)v_i(R)] \tag{2.23}$$

then the strong-collision probability (2.21) is redefined as in

$$\pi R_T^2[1 - V(R_T)/E_i]P_i^{ST}(R_T)$$

$$= \int_0^{R_T}[1 - V(R)/E_i]d\mathbf{R}/\lambda_i(R). \tag{2.24}$$

The corresponding strong collision rate (2.14) is now

$$\alpha_T(R_T) = \int_0^\infty G(E_i)dE_i$$

$$\times \int_0^{R_T} v_i[1 - V(R)/E_i)]^{1/2}d\mathbf{R}/\lambda_i(R), \tag{2.25}$$

where the (Boltzmann) distribution of internal energies $(E_i>0)$ is

$$G(E_i)dE_i = \frac{2}{\sqrt{\pi}}(E_i/kT)^{1/2}\exp(-E_i/kT)d(E_i/kT). \tag{2.26}$$

When λ_i is assumed to be λ, independent of R and E_i, as for hard-sphere collisions, and when $V(R)$ is neglected, Eq. (2.24) yields

$$P_T^A(R_T) = \tfrac{1}{2}R_T/\lambda \tag{2.27}$$

the Thomson probability[7] for (A–M) collisions during recti-

linear A–B relative motion within $R<R_T$. Also Eq. (2.25) yields

$$\alpha_T(R_T) = \tfrac{1}{3}\pi R_T^2(\bar{v}/\lambda) \tag{2.28}$$

the Thomson rate[7] in terms of $\bar{v}$, the mean (A–B) relative speed $(8kT/\pi M_{AB})^{1/2}$. All of the rates calculated here and previously[1-3] are however normalized (cf. Appendix) to

$$\tilde{\alpha}_T = \frac{4}{3}\frac{\pi}{\lambda}\left(\frac{2}{3}\frac{e^2}{kT}\right)^3\left(\frac{3kT}{M_{AB}}\right)^{1/2}, \tag{2.29}$$

where the root-mean-square speed rather than $\bar{v}$ has been customarily used, and where $\frac{2}{3}(e^2/kT)$ is assigned for R_T. Unless otherwise noted, all of the following calculations in the following sections (II C–II E) refer to symmetrical resonance charge-transfer ion–neutral collisions involving equal-mass species $M_A = M_B$ in an equal mass gas.

C. Calculated stabilization and disruption probabilities, and partial rates

The stabilization and disruption probabilities P_f^S and $P_f^D = 1 - P_f^S$ are the stochastic probabilities that (A–B) pairs initially in a bound level E_f of block $\mathscr{B}$, will either become fully associated or disrupted by multicollisions with the thermal gas. For a quasi-steady-state distribution of bound pairs in block $\mathscr{B}$, P_f^S are numerical solutions of the integral equation (1.8) and are illustrated in Fig. 4. The probabilities P_f^S increase from zero at the dissociation limit to near unity for binding energy $|E_f|>5kT$. Note that $P_f^S \simeq 1/2 \simeq P_f^D$ for $E_f \sim -2kT$, the bottleneck energy E^* (cf. Fig. 3) based on the assumption in Eq. (2.13) that P_f^S is zero for $E>E^*$ and unity for $E_i < -E^*$. The probabilities $P_f^D = (1 - P_f^S)$ for multistep collisional disruption of these pairs decrease fairly rapidly with binding energy $|E|$ and are negligible for binding $|E|>5\,kT$. Since block $\mathscr{S}$ of fully stabilized levels is characterized by unit P_f^S, Fig. 4 suggests that the block $\mathscr{S}$ is composed of all levels with binding $\gtrsim 10kT$. Since the deexcitation frequency ν_{if} from the continuum directly to the strongly bound levels with $E_f \lesssim -10kT$ of block $\mathscr{S}$ is vanishingly small, association given by Eq. (1.9) therefore occurs primarily via multistep transitions to the block $\mathscr{B}$ of levels E_f within the range $0>E_f> -10kT$, which are then connected stochastically with probability P_f^S to the fully associated block $\mathscr{S}$ via a Markov-element chain.[6]

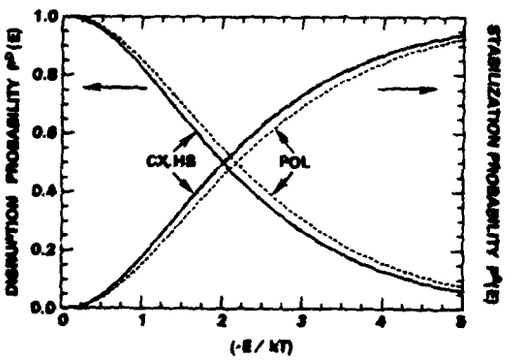

FIG. 4. Stabilization and disruption probabilities, solutions of Eq. (1.8) for equal mass components.

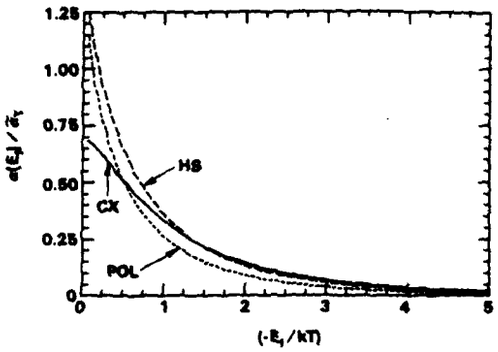

FIG. 5. Partial rates (2.30a) per final bound level $-E_f$ normalized to $\tilde{\alpha}_T$, the Thomson rate (2.29).

Figure 5 for the partial rate

$$\alpha(E_f)\tilde{N}_A\tilde{N}_B = \left(\int_0^\infty C_{if}\,dE_i\right)P_f^S(E_f) \equiv C_f P_f^S \tag{2.30a}$$

normalized to $\tilde{\alpha}_T$, which is the contribution per unit normalized interval (dE_f/kT) from level E_f to the full association rate of all dissociated pairs, illustrates that levels in general within kT of the dissociation limit, are mainly responsible for the association process. This is less so however for CX since deactivation by symmetrical resonance charge transfer involves larger energy reductions[1-3] than for the case of polarization and hard-sphere collisions. The very rapid increase of $\alpha(E_f)$ from zero at $E_f = 0$, not shown in Fig. 5, and subsequent decrease arises from the combination of the monotonic increase from zero of the stabilization probabilities P_f^S and the rapid decrease from infinity of C_f, the collisional rate from the continuum to a bound level f.

Figure 6 for the E_i-partial contribution

$$\alpha(E_i)\tilde{N}_A\tilde{N}_B = \int_{-D}^{0} C_{if}P_f^S\,dE_f \tag{2.30b}$$

to the exact rate for association of dissociated E_i pairs per unit interval (dE_i/kT) illustrates a monotonic increase as $E_i > 0$ approaches the dissociated limit at zero energy. This

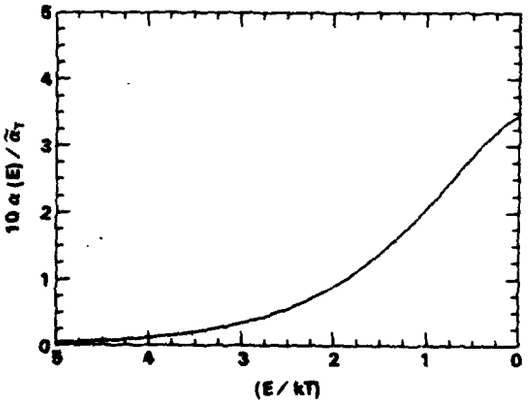

FIG. 6. Partial rate (2.30b) per initial continuum state E_i, normalized to $\tilde{\alpha}_T$, the Thomson rate (2.29).

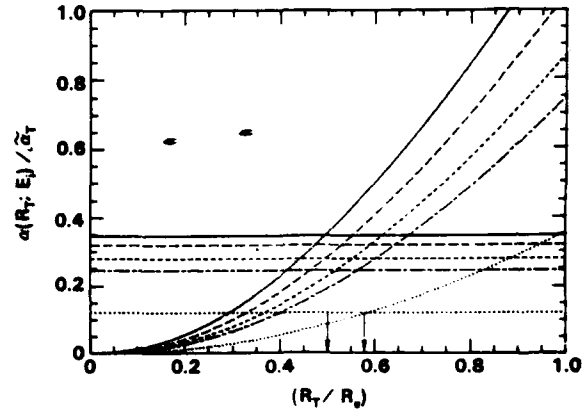

FIG. 7. Partial strong continuum rate $\alpha(R_T;E_i)$, Eq. (2.31), per initial continuum state E_i, normalized to $\bar{\alpha}_T$, the Thomson rate (2.29). Exact normalized partial rates are indicated by straight lines. $E_i/kT = 0, 0.26, 0.529, 0.734$, and 1.646 ordered sequentially from top to bottom.

is expected since C_{if} for a given bound level E_f increases quite rapidly as the energy difference $(E_i - E_f)$ is reduced. The full rate (1.9) is the E_i-integrated area of Fig. 6.

Variations of the partial E_i contributions

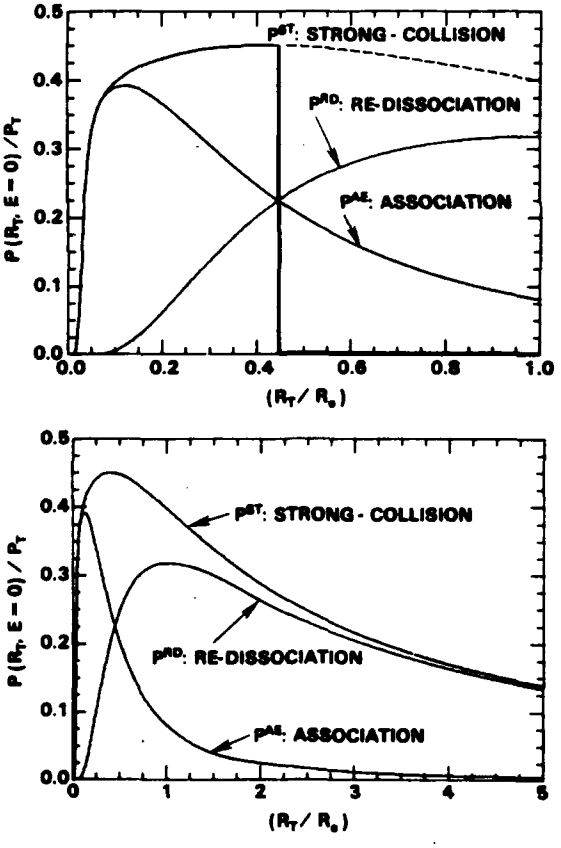

FIG. 8. (a),(b) Probabilities P^{ST}, P^{AE}, and P^{RD} for strong collisions (2.21), association (2.18), and redissociation (2.22) of (A–B) pairs with energy $E = 0$. Probabilities are normalized to the Thomson probability P_T, Eq. (2.27) and are presented as a function of R_T (normalized to $R_e = e^2/kT$).

$$\alpha(R_T;E_i)\tilde{N}_A\tilde{N}_B = \int_0^{R_T} d\mathbf{R} \int_{V(R)}^{0} C_{if}(R)\,dE_f \quad (2.31)$$

to the strong-collision rate (2.10) with R_T are displayed in Fig. 7. They intersect the corresponding exact partial rates (2.31a), represented as straight lines at R_T, in the range $0.5R_e < R_T < 0.6R$, a result consistent with the E_i-integrated rates of Fig. 2 where $R_T \sim 0.55R_e$.

D. R variation of calculated probabilities for multistep association

Figure 8 illustrates variation with R_T of P_l^{AE}, the exact probability (2.18) for multistep association via bound levels of $E_l = 0$ pairs with $R < R_T$, and of P_l^{ST}, the corresponding strong-collision probability (2.21). The probabilities are normalized to P_T, the Thomson probability (2.27). Also shown [Fig. 8(a)] is P_l^{RD}/P_T, the normalized probability (2.22) for redissociation of the bound pairs so formed with $R < R_T$. Figure 8(a) emphasizes that association dominates redissociation within smaller $R_T \ll (e^2/kt) \equiv R_e$ so that the exact and strong probabilities P_l^{AE} and P_l^{ST}, respectively, are equal. Figure 8(b) emphasizes that pairs within larger $R_T \gg R_e$ are mainly redissociated. The strong-collision probability P_l^{ST} accurately represents either P_l^{AE}, the association probability at small R_T, or P_l^{RD}, the redissociation probability at larger R_T, thereby providing the actual physical basis for Fig. 1.

Within radius $R_T \sim 0.45R_e$, there is as much association as redissociation [Fig. 8(a)] so that the strong rate is twice the exact rate for association of pairs with $R < 0.45R_e$. The contribution of pairs with $R > 0.45R_e$ to the exact rate is however equal to the contribution from $R < 0.45R_e$, so that the exact rate form all R and the strong rate from $R < 0.45R_e$ are fortuitously equal. This balance is the essential basis for agreement with the strong-collision model as previously illustrated by Figs. 2 and 7. Figure 8(a) also suggests that the R_T variation of the strong collision probability (2.21) is represented fairly well by P_T^A, the Thomson result (2.27), over the region $R < R_e$ important to association, although the magnitude is overestimated by a factor of $\lesssim 2.5$.

As the energy E_i of the dissociated pairs increases from

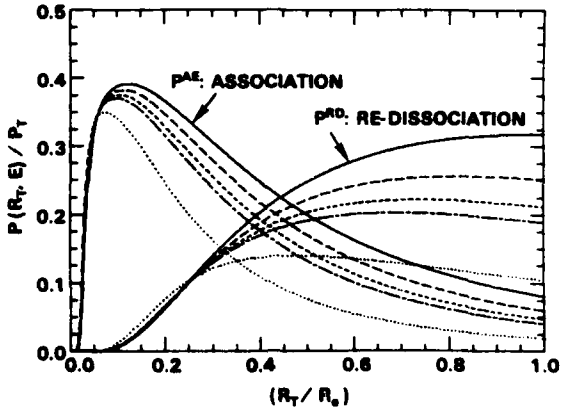

FIG. 9. As in Fig. 8 but for various continuum energies ($E/kT = 0, 0.529, 1.09, 1.56$, and 4.7 ordered sequentially from top to bottom).

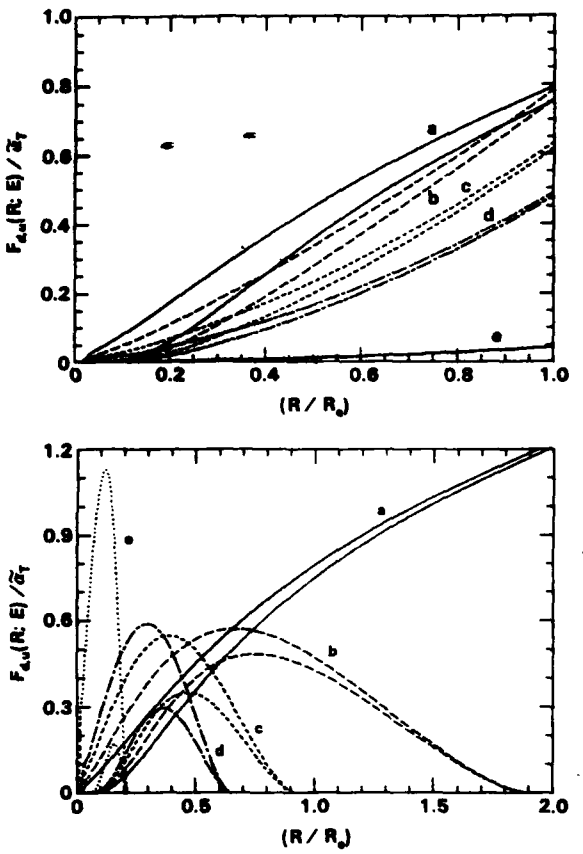

FIG. 10. R dependence of downward F_d and upward F_u normalized flux, Eqs. (2.32) and (2.33), upper and lower curves of each set, across various continuum energies [$E/kT = 0$, 0.529, 1.09, 1.56, and 4.7, (a)–(e), respectively] and across various bound energies [$-E/kT = 0$, 0.529, 1.09, 1.56, and 4.7, (a)–(e), respectively] in (b).

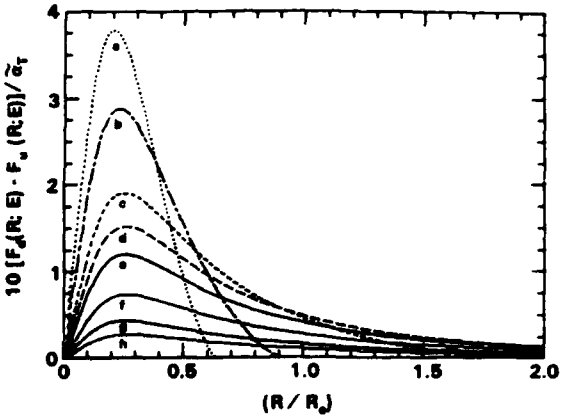

FIG. 11. R dependence of the net flux ($F_d - F_u$) downward across various continuum [$E/kT = 0$, 0.529, 1.09, 1.56; (e)–(h), respectively] and bound [$-E/kT = 0.26$, 0.529, 1.09, 1.56; (d)–(a), respectively] energy levels.

zero, Fig. 9 shows that the probabilities for association of these pairs and for subsequent redissociation decreases monotonically with E_i and that the R_T region over which association exceeds redissociation becomes somewhat smaller. As before, the strong collision probability P_i^{ST}, the sum ($P_i^{AE} + P_i^{RD}$) of each pair of curves, tends to P_i^{AE} at small R_T, to P_i^{RD} at large R_T. The sum is fairly constant for the range $0.2R_e < R_T < R_e$, as in Fig. 8(a).

E. (R,E) variation of calculated flux and rates

In Figs. 10(a) and 10(b) are shown the variation with R of the downward differential flux ($dF = FdR$),

$$F_d(R;E) = 4\pi R^2 \int_E^\infty (1 - P_i^S)dE_i \int_{V(R)}^E C_{if}(R)dE_f \tag{2.32}$$

per unit interval dR across various continuum [Fig. 10(a)] and bound [Fig. 10(b)] energy levels E, and of the corresponding upward flux

$$F_u(R;E) = 4\pi R^2 \int_E^\infty dE_i \int_{V(R)}^E (1 - P_f^S)C_{fi}(R)dE_f \tag{2.33}$$

with both normalized to the Thomson rate (2.29). For small $R < 0.3R_e$, F_d increases more rapidly from zero and remains greater for all R than F_u which eventually tends at large R to F_d from below. This limiting behavior at small and large R also elucidate the physical basis for the separate R regions in Fig. 1. For bound levels [Fig. 10(b)], both F_d and F_u across state (R,E) increase from zero to a maximum and then decrease as expected to zero at the turning points associated with energy E.

Variation with R in Fig. 11 of $F(R)$, the *net* differential flux ($F_d - F_u$) across both bound and continuum energy levels E exhibits a peak at roughly the same $R \sim (0.2\text{–}0.3)R_e$ for all E. As E decreases through the continuum the flux, and R-integrated flux, $\int_0^\infty F(R)dR$, increases. For bound E, the net flux increases and then decreases to zero at the classical turning points $R_i = e^2/|E|$. The net R-integrated flux across the highly excited bound levels remains constant, i.e., the area under each of the bound curves remains constant in accord with the QSS condition $[dn_i(t)/dt = 0]$ in block $\mathscr{E}$, so that the flux becomes constricted into more restricted R space as E decreases through the bound levels. The resulting increase exhibited in Fig. 11 of the net differential flux as E decreases is therefore expected. The E variation of the normalized R-integrated net flux

$$F(E) = \begin{cases} \int_0^\infty [F_d(R;E) - F_u(R;E)]dR, & E > 0 \\ \int_0^{R_i} [F_d(R;E) - F_u(R;E)]dR, & E < 0 \end{cases} \tag{2.34}$$

is illustrated in Fig. 12. That $F(E<0)$ is constant simply reflects the QSS condition or constant flux through the highly excited block $\mathscr{E}$.

Figure 13 illustrates the variation with R_T of α, the exact partial rates (2.19) and (2.20) for the association of dissociated pairs ($E_i > 0$) and of highly excited bound pairs ($E_i < 0$), respectively, within the sphere of radius R_T. The former rate increases with R_T and saturates fairly rapidly for large R_T to the exact rate for association which, in order to

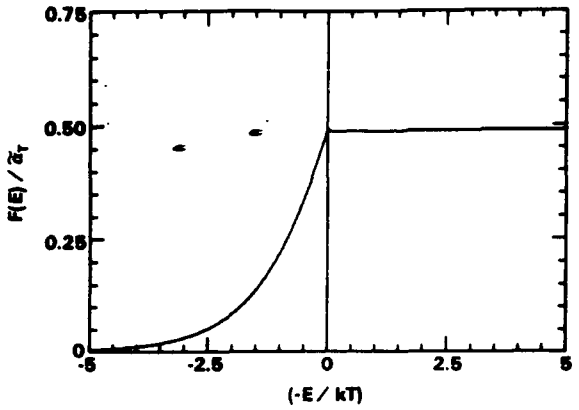

FIG. 12. Energy dependence of exact current, Eq. (2.34), normalized to $\tilde{\alpha}_T$, for the association of equal mass species under charge–transfer ion–neutral collisions. Exact rate is the constant current across bound levels.

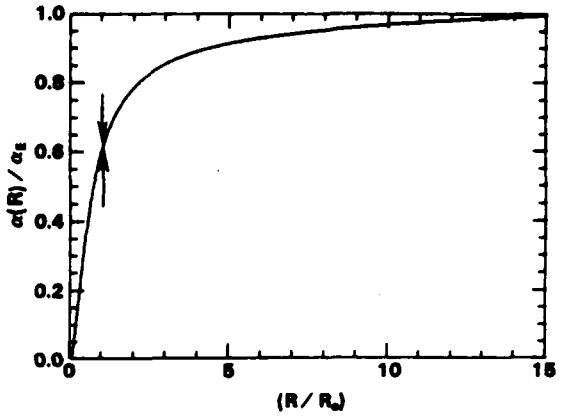

FIG. 14. Rate that fully dissociated pairs (with a Maxwellian energy distribution) recombine within a sphere of radius R. The exact rate is α_E.

maintain a steady-state $\mathscr{C}$ block, is the rate of generation of net inward E_i pairs with infinite separation.

The rates that bound E_i pairs are lost also increase with R_T due to continual downwards output, but reach a maximum when the upward input from other levels becomes competitive, and then decrease as a result to zero at the classical point R_i of classical motion. There is a net loss of bound E_i pairs with small R and a net gain of pairs with larger $R<R_i$ so that the R-integrated distribution (2.5b) remains constant in time. The zero rate at the apocenter R_i in Fig. 13 reflects the QSS condition (1.8) in Eq. (2.20) for no net loss or gain of R-integrated bound E_i pairs in block $\mathscr{E}$.

The rate $\alpha(R)$ of volume recombination within a sphere of radius R, the rates of Fig. 13 integrated over $E>0$ is given in Fig. 14 as a function of R. It is worth noting that 60% of the exact rate $\alpha_E = \alpha(R\to\infty)$ is achieved within the sphere of the natural (Onsager) radius $R_e = e^2/kT$ as designated by the arrows.

III. MASS EFFECT IN STRONG-COLLISION MODEL

Figures 2 and 7 illustrate the ratio of the strong collision result (2.10) to the exact result α_E for equal mass species recombining in an equal mass gas, i.e., a, the mass parameter (2.11), is (1/3). In Fig. 15 is displayed variation of the same ratio over the full range of a. Small $a\approx 10^{-3}$ implies heavy particle recombination in a vanishingly light gas, while electron–ion recombination in a normal gas is characterized by large $a\approx 10^3$. It is noted that the radius R^*_T, where $\alpha(R_T) = \alpha_E$ increases from $\sim 0.1R_e$ to $\sim 0.5R_e$ as the parameter a increases to unity, and then decreases back again as the parameter a further increases. For greatly mismatched species, i.e., in the limits of small and large a the energy-change collision dynamics is weak, and vanishingly small energy changes are involved particularly for deactivating transitions across the dissociation limit at $E_i = 0$. The stabilization probability P_f^S in Eq. (2.6) and Fig. 4 is therefore of prime significance. To invoke the strong-collision assumption (2.9) for these bound levels close to the dissociation limit and important at small and large a is therefore without validity. Although some physical significance can be attached to R^*_T, where $\alpha(R_T)$ and α_E are equal, for intermediate $a\sim 1$, as previously discussed in Sec. II, no such significance exists in the limits of small and large a. The essential reason why $R^*_T\sim 0.1R_e$ becomes unacceptably small at

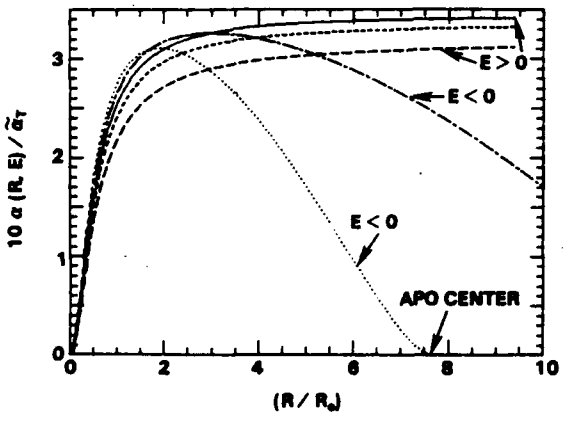

FIG. 13. Normalized rate equations (2.19) and (2.20) that pairs in continuum and bound energy levels E recombine within a sphere of radius R.

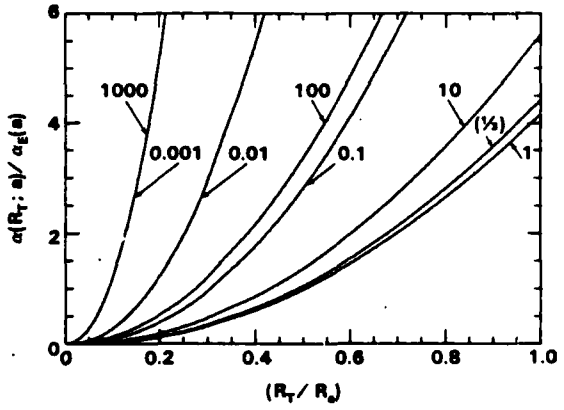

FIG. 15. Mass effect in strong-collision model: R_T variation of the strong-collision rate (2.31) normalized to the exact rate α_E, Eq. (1.6), for recombination of systems with various mass parameters a, Eq. (2.11).

these limits is that small R_T^* effectively (numerically) offsets the large addition to the inner integral of Eq. (2.10) entailed by the strong collision assumption ($P_f^S = 1$) in Eq. (2.6). The smaller exact values of P_f^S (cf. Fig. 4) are more appropriate to the important levels in the vicinity of the dissociation limit for large and small a.

IV. RECOMMENDED LOW-DENSITY TERMOLECULAR RATES

Due to the long-range Coulombic attraction and to the use of shorter-range ion–neutral interactions [charge–transfer (CX), polarization (POL), and hard sphere (HS)], rates for the termolecular ion–ion recombination,

$$A^+ + B^- + M \rightarrow AB + M \tag{4.1}$$

between general atomic species in a general atomic gas may be characterized[9] by a universal function of the mass parameter (2.11) and of the gas temperature T [cf. Eqs. (A40)–(A55)]. This universality does not extend to ion–atom association which, due to the closer interactions involves, demands individual calculations for specific systems. As previously mentioned, rates (1.6) or (1.9) or (1.10) have been obtained numerically from Eq. (A55) via the highly accurate numerical solutions P_f^S to the integral equation (1.8) for the stabilization probabilities. Converged probabilities for small and large mass parameters a in particular were obtained only when the integral equation (1.8b) was discretized into 100 algebraic equations via the efficient procedure of Ref. 3. Previous results[1–3] adopted 36 equations at most.

Recommended values of the ratio[1–3]

$$\mathcal{R}(a) = (M_A/M_{AB})[\alpha_E^{(A)}(a,T)/\bar{\alpha}_T(T)], \tag{4.2}$$

where $\alpha_E^{(i)}$ is the exact numerical rate (A55a) originating from $(i - M)$ collisions alone, are presented at closely spaced a in Table I. The exact low density rate can be represented to a high degree of accuracy by[9]

$$\alpha = \alpha_E^{(A)} + \alpha_E^{(B)}. \tag{4.3}$$

Although the partial rates $\alpha_E^{(i)}$ are tabulated here to four significant figures, the recombination rule (4.3) as previously tested was then shown to be accurate to three figures at best or two figures at worst. The test however relies on the accuracy of the solutions to the integral equations (1.8b) with C_{if} taken as $C_{if}^{(A)}, C_{if}^{(B)}$ and $[C_{if}^{(A)} + C_{if}^{(B)}]$ where $C_{if}^{(A),(B)}$ is the one-way equlibrium rate which results from individual A–M and B–M collisions, respectively. Since the present converged probabilities P_f^S have been determined by a numerical procedure[3] more accurate and efficient than that[9] previously used for the test, the accuracy of rule (4.3) is being updated.

TABLE I. Normalized partial rates $10\ (M_A/M_{AB})(\alpha_E^A/\bar{\alpha}_T)$ for termolecular recombination $A^+ + B^- + M \rightarrow AB + M$ as a function of mass parameter $a = M_A M_B/M_A(M_A + M_B + M_g)$ for various interactions (CX: symmetrical resonance charge transfer; HS: hard sphere; POL: polarization attraction) in collision between A and gas atoms of mass M_g.

a	CX[a]	HS[b]	POL[b]	a	HS[b]	POL[b]
0.0010	1.291	1.278	1.029	1.5000	9.452	6.751
0.0020	1.816	1.818	1.472	2.0000	8.593	6.044
0.0030	2.208	2.221	1.800	2.5000	7.877	5.472
0.0040	2.530	2.554	2.071	3.0000	7.276	5.003
0.0050	2.807	2.841	2.304	3.5000	6.766	4.611
0.0060	3.053	3.098	2.512	4.0000	6.328	4.280
0.0070	3.274	3.329	2.699	4.5000	5.947	3.994
0.0080	3.476	3.542	2.870	5.0000	5.613	3.746
0.0090	3.662	3.739	3.029	5.5000	5.317	3.529
0.0100	3.835	3.923	3.177	6.0000	5.053	3.336
0.0200	5.115	5.313	4.288	6.5000	4.815	3.164
0.0300	5.959	6.264	5.039	7.0000	4.601	3.010
0.0400	6.581	6.986	5.603	7.5000	4.406	2.871
0.0500	7.066	7.565	6.049	8.0000	4.228	2.744
0.0600	7.456	8.042	6.414	8.5000	4.065	2.629
0.0700	7.778	8.444	6.719	9.0000	3.914	2.523
0.0800	8.047	8.789	6.976	9.5000	3.775	2.426
0.0900	8.276	9.086	7.197	10.0000	3.646	2.336
0.1000	8.471	9.347	7.387	12.0000	3.212	2.036
0.2000	9.459	1.078, + 1	8.377	14.0000	2.875	1.806
0.3000	9.709	1.127, + 1	8.644	16.0000	2.604	1.624
0.3333	9.727	1.134, + 1	8.666	18.0000	2.382	1.476
0.4000	9.709	1.140, + 1	8.652	20.0000	2.196	1.353
0.5000	9.600	1.136, + 1	8.547	50.0000	1.029	6.064, − 1
0.6000	9.446	1.124, + 1	8.389	100.0000	5.535, − 1	3.177, − 1
0.7000	9.269	1.107, + 1	8.206	500.0000	1.195, − 1	6.582, − 2
0.8000	9.045	1.087, + 1	8.013	1000.0000	6.029, − 2	3.253, − 2
0.9000	8.860	1.067, + 1	7.818			
1.0000	8.678[c]	1.046, + 1	7.625			

[a] In CX small a implies $M_B \ll M_A = M_g$; $a = 1$ implies $M_B \gg M_A = M_g$.

[b] In HS and POL small a implies recombination in a vanishingly light gas and large a ($\simeq 10^3$) implies electron–ion recombination in a normal mass gas.

[c] For CX, the maximum value of a is 0.998.

The partial rates (4.2) are very insensitive to a realistic choice of either the level $-S(\lesssim -10kT)$, below which the stabilization probability P_f^S is calculated as unity, or the lowest level $-D$ since the one-way coupling C_{if} connecting the dissociated states i to any bound level f decreases extremely rapidly and is quite negligible for states with binding energies D as low as 30 kT, which is much smaller, in general, than dissociation energies of normal molecules.

The temperature dependence of $\alpha_E^{(i)}$ follows that of $\tilde{\alpha}_T$, the Thomson rate (A40) with Eqs. (A41)–(A44). Results of a recent diffusional treatment[5] are in close agreement with those of Table I.

In conclusion, via an exhaustive investigation of the strong-collision and bottleneck methods of the termolecular process (4.1), interesting underlying physics and dynamics of the basic process have been uncovered and studied. Highly accurate rates have been presented (Table I) for future use.

ACKNOWLEDGMENT

This research is supported by the U.S. Air Force of Scientific Research under Grant No. AFOSR-84-0233.

APPENDIX: ONE-WAY EQUILIBRIUM COLLISION KERNELS $C_{if}(R)$

The one-way equilibrium rate per unit interval $d\mathbf{R}\,dE_i\,dE_f$ for $E_i \to E_f$ transitions in the microscopic process,

$$(\text{A–B})_{E_i,R} + \text{M} \to (\text{A–B})_{E_f,R} + \text{M} \tag{A1}$$

at specified internal separation R of the pair AB is

$$C_{if}(R) = \tilde{n}_i(\mathbf{R})\nu_{if}(R) = \tilde{n}_i\left[\nu_{if}^{(1)}(R) + \nu_{if}^{(2)}(R)\right]. \tag{A2}$$

The equilibrium distribution $\tilde{n}_i(R)$ per unit interval $d\mathbf{R}$ of (A–B) pairs with internal energy E_i, internal kinetic energy T_{12}, and reduced mass M_{12} is

$$\frac{\tilde{n}_i(\mathbf{R})dE_i}{\tilde{N}_A\tilde{N}_B} = \frac{2}{\pi^{1/2}}\left(\frac{T_{12}}{kT}\right)^{1/2}\exp(-E_i/kT)d(T_{12}/kT) \tag{A3}$$

at temperature T. The frequency ν_{if} per unit interval dE_f for $E_i \to E_f$ transitions is assumed in Eq. (A2) to be the sum $\nu_{if}^{(1)} + \nu_{if}^{(2)}$ of the separate contributions $\nu_{if}^{(j)}$ that arise from (A–M), $j=1$, and (B–M), $j=2$, binary collisions at fixed $\mathbf{R}$. The species A, B, and M denoted by indices 1, 2, and 3, respectively, have masses M_i, reduced masses M_{ij} and velocities $\mathbf{v}_i$ and $\mathbf{v}_i'$ before and after the (1–3) elastic collision with differential cross section $\sigma(g,\psi)$ which changes the (1–3) relative velocity from $\mathbf{g}$ along the polar axis to $\mathbf{g}'(\psi,\phi)$. Hence the (1–3) energy-change collision frequency is

$$\nu_{if}^{(1)}(R)dE_f = \left[\int N_0(\mathbf{v}_3)d\mathbf{v}_3\int_{\psi^-}^{\psi^+} g\sigma(g,\psi)d(\cos\psi)\right]d\phi, \tag{A4}$$

where the integration is over the $(\mathbf{v}_3,\psi)$ region of velocity space accessible to $E_i \to E_f$ transitions. The velocity distribution of gas species with concentration N (cm^{-3}) over the kinetic energy

$$T_3 = \tfrac{1}{2}M_3v_3^2 \tag{A5}$$

of AB–M relative motion is the Maxwellian

$$N_0(\mathbf{v}_3)d\mathbf{v}_3 = NG(T_3)dT_3\left[\frac{1}{4\pi}d(\cos\theta_3)d\phi_3\right], \tag{A6}$$

where the distribution

$$G(T_3)dT_3 = \frac{2}{\sqrt{\pi}}(T_3/kT)^{1/2}\exp(-T_3/kT)d(T_3/kT) \tag{A7}$$

represents thermodynamic equilibrium at temperature T between 3 and the (1–2) center of mass.[14] The reduced mass of the AB–M system is

$$M_s = (M_1+M_2)M_3/(M_1+M_2+M_3) = aM = (1+a)M_{13}, \tag{A8}$$

where a convenient mass parameter[9] for (1–3) collisions is

$$a = M_2M_3/M_1(M_1+M_2+M_3). \tag{A9}$$

The (1–2) center of mass is at rest before the (1–3) collision which changes both the kinetic energy

$$T_{12} = \tfrac{1}{2}M_{12}(\mathbf{v}_1-\mathbf{v}_2)^2 = \tfrac{1}{2}\bar{M}v_1^2;\quad \bar{M} = M_1(1+M_1/M_2) \tag{A10}$$

of (1–2) relative motion to T_{12}' and the internal energy

$$E_i = \tfrac{1}{2}\bar{M}v_1^2 + V(R) \tag{A11}$$

at a fixed R by

$$\epsilon = T_{12}' - T_{12} = \tfrac{1}{2}M_{12}\left[(\mathbf{v}_1'-\mathbf{v}_2)^2 - (\mathbf{v}_1-\mathbf{v}_2)^2\right]. \tag{A12}$$

The (1–3) relative momentum is changed by

$$\mathbf{P} = M_{13}(\mathbf{g}'-\mathbf{g}) = M_1(\mathbf{v}_1'-\mathbf{v}_1) = M_3(\mathbf{v}_3-\mathbf{v}_3') \tag{A13}$$

and the (1–3) relative energy T_{13} remains $\tfrac{1}{2}M_{13}g^2$. On following from analysis in Ref. 15 it can be shown that the Jacobian J_2 in the angle-kinetic energy transformation

$$d(\cos\theta_3)d\phi = J_2\,dT_{13}\,dT_{12}' \tag{A14}$$

is given by

$$J_2(\psi,T_{13},T_3;\epsilon) = \frac{(1+a)^2}{2a}\left[(T_{12}T_3T_{13})\times(T_{12}+T_3-T_{13})(\mu^+-\mu)(\mu-\mu^-)\right]^{-1/2}. \tag{A15}$$

The scattering ψ region accessible at fixed T_{13}, T_3, and ϵ is the range $\mu^- < \cos\psi < \mu^+$, with limits

$$\mu^\pm = (1-\Gamma_i^2)^{1/2}(1-\Gamma_f^2)^{1/2} \pm \Gamma_i\Gamma_f, \tag{A16}$$

where

$$\Gamma_i^2 = \left[(T_{13}^+ - T_{13})(T_{13}-T_{13}^-)\right]/\left[4T_{13}(T_{12}+T_3-T_{13})\right] \tag{A17a}$$

and

$$\Gamma_f^2 = [(\tilde{T}_{13}^{+} - T_{13})(T_{13} - \tilde{T}_{13}^{-})]/ [4T_{13}(T_{12} + T_3 - T_{13})]. \quad \text{(A17b)}$$

The accessible T_{13} region accessible for fixed T_3 and ϵ is the range

$$T^- = \max(T_{13}^-, \tilde{T}_{13}^-) < T_{13} < \min(T_{13}^+, \tilde{T}_{13}^+) = T^+ \quad \text{(A18)}$$

which ensures real $\mu^{\pm}$, where

$$T_{13}^{\mp}(T_3;T_{12}) = (T_3^{1/2} \mp a^{1/2}T_{12}^{1/2})^2/(1+a) \quad \text{(A19a)}$$

is a function of the initial kinetic energies, and where

$$\tilde{T}_{13}^{\mp}(T_3';T_{12}') = (T_3'^{1/2} \mp a^{1/2}T_{12}'^{1/2})^2/(1+a) \quad \text{(A19b)}$$

is the same function of the final (1–2) and 3 kinetic energies

$$T_{12}' = T_{12} + \epsilon, \quad \text{(A20)}$$

$$T_3' = T_3 - \epsilon. \quad \text{(A21)}$$

Since

$$\frac{\tilde{n}_i(\mathbf{R})}{T_{12}^{1/2}} \frac{N_0(T_3)dT_3}{T_3^{1/2}} = \frac{4}{\pi} \frac{(\tilde{N}_A\tilde{N}_B)}{(kT)^2} \exp - (E/kT)d(E/kT), \quad \text{(A22)}$$

where

$$E = E_i + T_3 = (T_{12} + T_3) + V(R) = \tilde{T} + V(R) \quad \text{(A23)}$$

then the contribution to the one-way equilibrium rate (A2) from (1–3) collisions is

$$C_{if}^{(1)}(R) = \tilde{n}_i(\mathbf{R})\nu_{if}^{(1)}(R) = \frac{(1+a)^2}{a}\left(\frac{2}{M_{13}}\right)^{1/2} \times \frac{(\tilde{N}_A\tilde{N}_BN)}{\pi(kT)^2}\int_{E_0}^{\infty} \exp(-E/kT)d(E/kT) \times \int_{T^-}^{T^+} (\tilde{T} - T_{13})^{-1/2}dT_{13}\int_{\mu^-}^{\mu^+} \sigma(T_{13},\mu) \times [(\mu^+ - \mu)(\mu - \mu^-)]^{-1/2}\,d\mu, \quad \text{(A24)}$$

where T is $E - V(R)$, as defined in Eq. (A23), and where

$$E_0 = \min(E_i, E_f) \quad \text{(A25)}$$

ensures real T_3 and T_3' in Eq. (A18).

Case I: When the differential cross section σ is a function only of T_{13} as for spiralling ion–neutral collisions under pure polarization attraction when

$$\sigma(T_{13},\psi) = \left(\frac{\alpha_M e^2}{8T_{13}}\right)^{1/2}, \quad \text{(A26)}$$

where α_M is the polarizability of M, then

$$C_{if}^{(1)}(R) = \left(\frac{\alpha_M e^2}{M_{13}}\right)^{1/2} \times \frac{(1+a)^2(\tilde{N}_A\tilde{N}_BN)}{a(kT)^2}\int_{E_0}^{\infty} \exp(-E/kT) \times \left[\sin^{-1}\left(\frac{T^+}{\tilde{T}}\right)^{1/2} - \sin^{-1}\left(\frac{T^-}{\tilde{T}}\right)^{1/2}\right] \times d(E/kT), \quad \text{(A27)}$$

where $\tilde{T}$ is $T_{12} + T_3$ as in Eq. (A23). Integration over $\mathbf{R}$ yields an expression identical to that of Bates and Mendaš.[3]

Case II: For hard sphere collisions when

$$\sigma(T_{13},\psi) = \frac{\sigma_0}{4\pi} \quad \text{(A28)}$$

then[2]

$$C_{if}^{(1)}(R) = \frac{\sigma_0}{\pi} \frac{(\tilde{N}_A\tilde{N}_BN)}{(2M_{13})^{1/2}(kT)^2}\int_{E_0}^{\infty} \exp(-E/kT) \times [(\tilde{T} - T^-)^{1/2} - (\tilde{T} - T^+)^{1/2}]d(E/kT). \quad \text{(A29)}$$

Case III. When $\sigma(T_{13},\psi)$ is a function only of momentum change P as for the Born approximation or for pure Coulombic attraction when

$$\sigma(T_{13},\psi) = 4\epsilon^4 M_{13}^2/P^4 = \sigma(P) \quad \text{(A30)}$$

and by finding the Jacobean J_3 in

$$d(\cos\theta_3)\,d\phi\,d(\cos\psi) = J_3\,dT_{12}'\,dP\,dT_{13} \quad \text{(A31)}$$

then from previous analysis,[15] it can be shown that

$$C_{if}^{(1)}(R) = \frac{2^{1/2}(1+a)}{a^{1/2}M_{13}} \frac{(\tilde{N}_A\tilde{N}_BN)}{(kT)^2} \times \int_{E_0}^{\infty} \exp(-E/kT)d(E/kT)\int_{P^-}^{P^+} \sigma(P)dP, \quad \text{(A32)}$$

where the limits to the momentum change P for specified $v_1^{(1)}$, $v_3^{(1)}$, and ϵ are

$$P^-(v_1,v_3;\epsilon) = \max[M|v_1' - v_1|, M_s|v_3' - v_3|] \quad \text{(A33a)}$$

and

$$P^+(v_1,v_3;\epsilon) = \min[M(v_1' + v_1), M_s(v_3' + v_3)]. \quad \text{(A33b)}$$

Case IV. Symmetrical resonance charge–transfer (1–3) collisions

$$X^+ + X \rightarrow X + X^+ \quad \text{(A34)}$$

between an ion and its parent gas simply interchange $\mathbf{v}_1$ and $\mathbf{v}_3$. At thermal energies the integral cross section σ^x is essentially independent of relative speed g. It can then be shown that[1]

$$C_{if}^{(1)}(R) = \frac{[(1+c)/c]^{3/2}}{(2\pi M_{12})^{1/2}} \frac{(\tilde{N}_A\tilde{N}_BN)\sigma^x}{(kT)^{3/2}} \times \exp\left[-\frac{(1+c)}{(1+2c)}\frac{(E_i+E_f)}{kT}\right] \times \exp\left[-\frac{V(R)/kT}{(2c+1)}\right]\int_{E^-}^{E^+} G(E)dE, \quad \text{(A35)}$$

where

$$c = M_1/M_2$$

and where the fraction of Maxwell particles with energies E in the range $E^- < E < E^+$ with limits

$$E^{\pm} = [c(1+c)/(1+2c)][T_{12}^{1/2} \pm T_{12}'^{1/2}]^2 \quad \text{(A36)}$$

is

$$\int_{\mathcal{E}^-}^{\mathcal{E}^+} G(E)dE = \left[\operatorname{erfc}(E/kT)^{1/2} - \frac{2}{\sqrt{\pi}}(E/kT)^{1/2}\exp(-E/kT)\right]_{\mathcal{E}^-}^{\mathcal{E}^+}. \quad \text{(A37)}$$

The above rates (A24), (A27), (A29), (A32), and (A35) satisfy the detailed balance relation $C_{if}(R) = C_{fi}(R)$, and R integration of Eqs. (A27), (A29), and (A35) yields previous expressions.[1-3]

Computational equilibrium rates: C_{if} may be conveniently expressed for computational purposes in terms of dimensionless units,

$$\lambda = -E_i/kT, \quad \mu = -E_f/kT, \quad v(r) = -V(R)/kT, \quad r = R/R_e, \quad R_e = e^2/kT \quad \text{(A38)}$$

by

$$4\pi C_{if}(R)R^2\,dR\,|dE_i|dE_f| = \Gamma\tilde{\alpha}_T F(\lambda,\mu;r)r^2\,dr\,d\lambda\,du \ \ (\mathrm{cm^3\,s^{-1}}) \quad \text{(A39)}$$

in terms of specified mass factors Γ and the Thomson (low density) rates,

$$\tilde{\alpha}_T = \tfrac{8}{3}\pi(R_e/\beta)^3(3kT/M_{12})^{1/2}\sigma_0 N, \ \beta = 3/2, \quad \text{(A40)}$$

where σ_0 is the integral cross section for (1-3) collisions are relative energy $\frac{1}{2}kT$. The appropriate mass factors Γ in Eq. (A39) and cross section σ_0 in Eq. (A40) are

$$\Gamma^H = \left(\frac{3}{2}\right)^{1/2}\left(\frac{\beta^3}{\pi}\right)\frac{(1+a)^2}{a^{3/2}}\left(\frac{M_{12}}{M_1}\right); \quad \sigma_0 = \sigma_0^H \quad \text{(A41)}$$

for hard-sphere (1-3) collisions with integral cross section σ_0^H,

$$\Gamma^C = \frac{3a}{\pi(1+a)}\Gamma^H; \quad \sigma_0 = \sigma_0^C = \frac{1}{9}\pi R_e^2 \quad \text{(A42)}$$

for Coulomb (1-3) collisions with integral cross section σ_0^C which corresponds to Coulomb scattering by angles $\psi > \pi/2$, and to energy transfers $\epsilon > (3/2)kT$ for equal mass species. For (1-3) polarization attraction/core repulsion for collisions within the orbiting radius,

$$\Gamma^P = \left(\frac{3}{2}\right)\left(\frac{\beta^3}{\pi}\right)\frac{(1+a)^{5/2}}{a^{3/2}}\left(\frac{M_{12}}{M_1}\right); \quad \sigma_0 = \sigma_0^P = 2\pi(\alpha_M R_e/3)^{1/2} \quad \text{(A43)}$$

and σ_0^P adopted in Thomson's rate (A40) is the corresponding integral (elastic or momentum transfer) collisional cross section at $(3/2)kT$ relative energy. For (1-3) charge-transfer collisions,

$$\Gamma^X = \left(\frac{3}{2}\right)^{1/2}\left(\frac{\beta^3}{\pi}\right)\left(\frac{1+c}{c}\right)^{3/2}; \quad \sigma_0 = 2\sigma^X, \quad \text{(A44)}$$

where σ_0 in Eq. (A44) is the corresponding momentum-transfer cross section, taken as twice the cross section σ^X for charge transfer.[1]

The corresponding dimensionless functions F in Eq. (A39) are symmetric in λ and μ and are

$$F^H(\lambda,\mu;r) = \int_{Y_0}^{\infty}\exp(-Y)dY[\tilde{P}_+ - \tilde{P}_-]; \quad Y_0 = \max(-\lambda,-\mu) \quad \text{(A45)}$$

for hard-sphere (1-3) collisions with (dimensionless) momentum-change limits $\tilde{P}_+ > \tilde{P}_-$, given by

$$\tilde{P}_-(\lambda,\mu;r) = \max\{[v(r)-\lambda\,]^{1/2} - [v(r)-\mu]^{1/2}; a^{1/2}[(Y+\lambda)^{1/2} - (Y+\mu)^{1/2}]\} \quad \text{(A46a)}$$

and

$$\tilde{P}_+(\lambda,\mu;r) = \min\{[v(r)-\lambda\,]^{1/2} + [v(r)-\mu]^{1/2}; a^{1/2}[(Y+\lambda)^{1/2} + (Y+\mu)^{1/2}]\}. \quad \text{(A46b)}$$

For Coulomb (1-3) collisions,

$$F^C(\lambda,\mu;r) = \int_{Y_0}^{\infty}\exp(-Y)dY[\tilde{P}_-^{-3} - \tilde{P}_+^{-3}]. \quad \text{(A47)}$$

For polarization (1-3) collisions,

$$F^P(\lambda,\mu;r) = \int_{Y_0}^{\infty}\exp(-Y)dY \times[\sin^{-1}(G_2/A) - \sin^{-1}(G_1/A)], \quad \text{(A48)}$$

where

$$G_1(\lambda,\mu;r) = \max[|(Y+\lambda)^{1/2} - a^{1/2}[v(r)-\lambda\,]^{1/2}|; |(Y+\mu)^{1/2} - a^{1/2}[v(r)-\mu]^{1/2}|], \quad \text{(A49)}$$

$$G_2(\lambda,\mu;r) = \min[(Y+\lambda)^{1/2} - a^{1/2}[v(r)-\lambda\,]^{1/2}; (Y+\mu)^{1/2} - a^{1/2}[v(r)-\mu]^{1/2}],$$

and

$$A = (1+a)^{1/2}[v(r)+Y]^{1/2}. \quad \text{(A50)}$$

For charge-transfer (1-3) collisions

$$F^X(\lambda,\mu;r) = \exp\left[\left(\frac{1+c}{1+2c}\right)(\lambda+\mu)\right] \times\exp[-1/(1+2c)r] \times\left[\frac{\sqrt{\pi}}{2}\operatorname{erf} g - g\exp(-g^2)\right]_{g^-}^{g^+}, \quad \text{(A51)}$$

where

$$g_\pm^2(\lambda,\mu;r) = \frac{c(1+c)}{(1+2c)}\{[v(r)-\lambda\,]^{1/2} \pm [v(r)-\mu]^{1/2}\}^2. \quad \text{(A52)}$$

The universal expression (A39) is also valuable in that the one-way equilibrium current (rate) across an arbitrary bound level $v = -E/kT$ is simply

$$\alpha_{eq} = \Gamma\tilde{\alpha}_T\int_{-\infty}^{\nu}d\lambda\int_{\nu}^{\infty}F(\lambda,\mu)d\mu, \quad \text{(A53)}$$

where $\omega = -D/kT$ is the maximum binding energy in units of (kT) and where

$$F(\lambda,\mu) = \int_0^{r_m}F(\lambda,\mu;r)r^2\,dr, \quad r_m = 1/\max(\lambda,\mu). \quad \text{(A54)}$$

This equilibrium collisional rate displays a minimum at $v^* = (1\text{-}3)kT$, the location of a bottleneck (see Fig. 3). The QSS rates (1.9), (1.10), and (1.6) reduce simply to

$$\alpha = \Gamma\tilde{\alpha}_T \int_{-\infty}^{0} d\lambda \int_{0}^{\infty} F(\lambda,\mu) P^{S}(\mu) d\mu, \qquad \text{(A55a)}$$

$$\alpha = \Gamma\tilde{\alpha}_T \int_{0}^{\infty} d\lambda \int_{-\infty}^{\epsilon} F(\lambda,\mu) P^{D}(\mu) d\mu, \qquad \text{(A55b)}$$

$$= \Gamma\tilde{\alpha}_T \int_{-\infty}^{\nu} d\lambda \int_{\nu}^{\infty} [P^{S}(\mu) - P^{S}(\lambda)] F(\lambda,\mu) d\mu, \qquad \text{(A55c)}$$

where $\epsilon = -S/kT$.

Also various energy-change moments,

$$D_i^{(m)}(E_i) = \frac{1}{m!} \int_{-D}^{\infty} (E_f - E_i)^m C_{if}\, dE_f \qquad \text{(A56)}$$

are useful[5] in a Fokker–Planck reduction of the collision term (1.2). These can be expressed simply as

$$D_i^m(E_i) = \Gamma\tilde{\alpha}_T \tilde{N}_A \tilde{N}_B (kT)^{m-1} (-1)^m \mathscr{D}_i^{(m)}(\lambda), \qquad \text{(A57)}$$

where the dimensionless moments

$$\mathscr{D}_i^{(m)}(\lambda) = \frac{1}{m!} \int_{-\infty}^{\infty} (\mu - \lambda)^m F(\lambda,\mu) d\mu \qquad \text{(A58)}$$

are easily determined[5] on using one of the relevant expressions, (A45), (A47), (A48), or (A51), pertinent to the chosen binary A–M and B–M interactions of A and B with the gas M.

[1] M. R. Flannery, J. Phys. B 13, 3649 (1980).
[2] M. R. Flannery, J. Phys. B 14, 915 (1981).
[3] D. R. Bates and I. Mendaš, J. Phys. B 15, 1949 (1982).
[4] M. R. Flannery, J. Phys. B 18, L839 (1985).
[5] M. R. Flannery, J. Chem. Phys. 87, 6947 (1987).
[6] M. R. Flannery, Ann. Phys. (N.Y.) 67, 376 (1971).
[7] J. J. Thomson, Philos. Mag. 47, 337 (1924).
[8] P. J. Feibelman, J. Chem. Phys. 42, 2462 (1965).
[9] D. R. Bates and M. R. Flannery, Proc. R. Soc. London Ser. A 302, 367 (1968).
[10] M. R. Flannery, J. Phys. B. 20, 4929 (1987).
[11] M. R. Flannery and T. P. Yang, J. Chem. Phys. 73, 3239 (1980).
[12] M. R. Flannery, *Recent Studies of Atomic and Molecular Processes*, edited by A. E. Kingston (Plenum, New York, 1987).
[13] J. C. Keck, in *Advances in Atomic and Molecular Physics*, edited by D. R. Bates and I. Estermann (Academic, New York, 1972), Vol. 8; Adv. Chem. Phys. 13, 83 (1967).
[14] D. R. Bates, P. B. Hays, and D. Sprevak, J. Phys. B 4, 962 (1971).
[15] M. R. Flannery, Phys. Rev. A 22, 2408 (1980).

3.2 Variational Treatment.

Variational principle for termolecular recombination in a gas

M. R. Flannery
School of Physics, Georgia Institute of Technology, Atlanta, Georgia 30332-0430

(Received 29 February 1988; accepted 22 March 1988)

A variational principle for the rates of termolecular processes is proposed and then applied to recombination between atomic ions with excellent results. The variational expression when minimized with respect to stabilization probabilities is capable of providing rates identical to those determined from the quasi-steady-state solution of the full Master equation. Connection is made with electrical networks and with the principle of least dissipation.

I. INTRODUCTION

An important objective in chemical physics is the formulation of a variational theory of chemical reactions which is exact in the sense that the deduced variational expression will yield, upon variation of relevant parameters, the distributions n_i and rate constants which are identical with those obtained by direct solution of the exact Master equation for the particular process. The variational procedure of Wigner[1] and Keck[2] is "variational" in the sense that it yields a least upper bound to the rate of a chemical reaction as determined from a Master equation. The reaction is represented by the motion of a point (p,q) in multidimensional phase space across a trial surface S which separates a block $\mathscr{C}$ of initial reactant states i from a block $\mathscr{S}$ of final product states f. The one-way rate R that representative phase points flow (downward) across S—or flux of trajectories—is an upper limit to the actual rate since (a) upward reexcitation to states i above S is ignored and since (b) a representative point which passes through S more than once is repeatedly included at each pass. The additional use of an equilbrium density $\tilde{n}_i$ for the reacting states then provides a rigorous upper bound R_e to the reaction rate. A minimum—the least upper bound—to R_e is then obtained by variation of the trial surface S.

In termolecular electron-ion or ion-ion collisional recombination

$$A^+ + B^- + M \rightarrow AB + M \qquad (1.1)$$

at low gas densities, for example, the "surface", can be taken as some bound energy level $-E$ of the pair AB so that an upper bound to the two-body rate constant $\alpha(\mathrm{cm^3\,s^{-1}})$ for recombination (1.1) is

$$R_e(-E) = \int_{-E}^{\infty} dE_i \int_{-D}^{-E} C_{if}\, dE_f > \alpha \tilde{N}_A \tilde{N}_B , \quad (1.2)$$

where $\tilde{N}_A$ and $\tilde{N}_B$ are the equilibrium concentrations of A^+ and B^- and where C_{if} is the one-way equilibrium collisional rate per unit interval $dE_i\, dE_f$ for transitions between energy levels E_i and E_f of AB pairs. The level $-E$ separates the "reactant" block $\mathscr{C}$ of states i with energies E_i in the range $-E \leq E_i \leq \infty$ from the "product" block $\mathscr{S}$ of states f with energies E_f in the range $-E \geq E_f \geq -D$, where $-D$ is the lowest energy level of the AB pair relative to a dissociation limit at zero energy. A minimum to R_e occurs at $-E = -E^*$ which therefore acts as a bottleneck or transition state. States above $-E^*$ are more likely to be excited by collision and hence are unstable with respect to association, while those below $-E^*$ tend to be deexcited and are therefore considered as stable. For this one-dimensional surface, the Wigner–Keck treatment is then identical with the bottleneck method proposed by Byron *et al.*[3] for three-body electron–ion recombination.[4] For termolecular recombination of arbitrary mass ions in a gas, this variational treatment yields rates[5] which are higher by factors of 2 to 8 than the exact rates[6] obtained from a Master equation.

What is desirable is a variational method which will yield a rate identical to that determined from solution of the full Master equation. This search requires the addition, as illustrated by Fig. 1, of a block $\mathscr{B}$ of highly excited states i for which the reaction can go either way. The block is characterized by the overall probability P_i^S for stabilization via downward ($\mathscr{B} \rightarrow \mathscr{S}$) transitions or by the overall probability $P_i^D = (1 - P_i^S)$ for disruption via upward ($\mathscr{B} \rightarrow \mathscr{C}$) transitions. This block $\mathscr{B}$ lies intermediate between the reactant and product blocks $\mathscr{C}$ and $\mathscr{S}$ which are separately characterized by $P_i^S = 0$ and $P_i^S = 1$, respectively.

In this paper such a method is proposed and is then applied as a case study to the well-developed example[6] of termolecular ion–ion recombination (1.1) in a low density gas M. Connection is then made with the principle of least

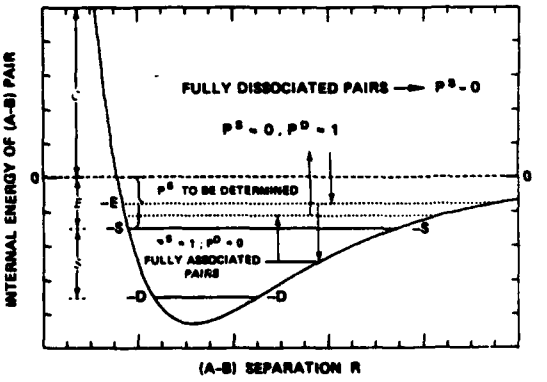

FIG. 1. Schematic diagram of energy blocks $\mathscr{C}$, $\mathscr{B}$, and $\mathscr{S}$ pertinent to recombination at low gas densities.

 0021-9606/88/130214-09$02.10

dissipation, well known in heat-conduction problems and in electrical networks. By analogy with this principle for a network of resistors, Bates[7] very perceptively postulated that a minimum would exist, with respect to variation in the normalized time-independent distributions $\gamma_i(E_i) = n_i/\tilde{n}_i$ in the time-independent measure:

$$\mathscr{M} = \int_{-D}^{\infty} dE_i \int_{-D}^{\infty} (\gamma_f - \gamma_i)^2 C_{if}\, dE_f \tag{1.3}$$

of the total rate of restoration to thermal equilibrium. Mendaš[8] then noted that minimum $\mathscr{M}$ is obtained for a quasi-steady-state distribution of excited levels determined by

$$\gamma_i \int_{-D}^{\infty} C_{if}\, dE_f = \int_{-D}^{\infty} \gamma_f\, C_{if}\, dE_f . \tag{1.4}$$

The present formulation permits the identification of this $\mathscr{M}$ so minimized with twice the actual (quasi-steady-state) rate constant

$$\alpha \tilde{N}_A\, \tilde{N}_B = \int_{-E}^{\infty} dE_i \int_{-D}^{-E} (\gamma_i - \gamma_f) C_{if}\, dE_f \tag{1.5}$$

which is the net downward constant energy-space current across any level $-E$, in the block $\mathscr{E}$ of excited levels in quasi-steady-state. A supplementary calculation of Eq. (1.5) with the variational result of Eq. (1.3) is then not required. Note that the upper bound [Eq. (1.2)] is recovered upon eliminating block $\mathscr{E}$ by assigning $\gamma_i(-E<E_i<\infty) = 1$ and $\gamma_f(-E>E_f>-D) = 0$ in either Eq. (1.3) or Eq. (1.5).

II. VARIATIONAL PRINCIPLE

The net rate for termolecular association

$$A + B + M \underset{k}{\overset{\alpha}{\rightleftarrows}} AB + M \tag{2.1}$$

between A and B in a gas M is[9]

$$R^A(t) = \int_{-D}^{\infty} P_i^S \left(\frac{dn_i}{dt}\right) dE_i \tag{2.2}$$

$$= \alpha N_A(t) N_B(t) - k\, n_s(t) , \tag{2.3}$$

where P_i^S is the stochastic probability that a pair AB with internal relative energy E_i is connected via a series of energy (state)-changing collisions to a sink $\mathscr{S}$ of fully associated AB pairs. The concentration $n_i(t)$ of AB pairs with internal energy E_i of relative motion in unit interval dE_i about E_i develops in time t according to the standard Master equation[9]

$$\frac{dn_i}{dt} = -\int_{-D}^{\infty} [n_i(t)\nu_{if} - n_f(t)\nu_{fi}]\, dE_f = -\frac{\partial J_i}{\partial E_i} , \tag{2.4}$$

where $-D$ is the energy of the lowest vibrational level of AB relative to the dissociation limit taken as zero energy.

The frequency per unit interval dE_f for $E_i \to E_f$ transitions in AB by collision with gas species M is ν_{if} which is linear in gas density N. At low gas densities, R^A is linear in N so that P_i^S is then only required to zero order in N. Over the range $0<E_i<\infty$ which defines the $\mathscr{E}$ block of fully dissociated reactant states, n_i at low N can then be taken in the collisional part of Eq. (2.4) as its thermodynamic equilibrium value $\tilde{n}_i$, so that $P_i^S \simeq 0$ for block $\mathscr{E}$. The effective two-body rate constant for the association of A and B with (cm^{-3}) concentrations $N_A(t)$ and $N_B(t)$ at time t is α ($cm^3\, s^{-1}$). The constant $k(s^{-1})$ is the frequency for dissociation of the tightly bound pairs in the product block $\mathscr{S}$ of levels with energies E_i in the range $-S>E_i>-D$, within which the stabilization probability P_i^S is unity. In the intermediate block $\mathscr{E}$ of "reacting" states with $0>E_i>-S$ in Fig. 1, the probabilities P_i^S must be determined. The net rate for termolecular dissociation in the closed system is

$$R^D(t) = \int_{-D}^{\infty} P_i^D \left(\frac{dn_i}{dt}\right) dE_i = -R^A(t) , \tag{2.5}$$

where $P_i^D = 1 - P_i^S$ is the probability that state i is collisionally connected to fully dissociated channels (at infinite A–B separation).

The proposed variational principle now asserts that the probabilities $P_i^{S,D}$ and densities n_i have energy distributions which ensure that $R^{A,D}(t)$ of Eqs. (2.2) and (2.5) are extrema at time t.

A. The quasi-steady-state deduction

Rewrite Eq. (2.2) as

$$R^A(t) = -\int_{-D}^{\infty} P_i^S \left(\frac{\partial J_i}{\partial E_i}\right) dE_i \tag{2.6}$$

in terms of the net downward collisional current

$$-J(E,t) = \int_{E}^{\infty} dE_i \int_{-D}^{E} [n_i(t)\nu_{if} - n_f(t)\nu_{fi}]\, dE_f \tag{2.7}$$

past level E. Since J_i vanishes as E_i tends to both $-D$ and ∞, the rate is then

$$R^A(t) = \int_{-D}^{\infty} J_i(E,t) \left(\frac{dP_i^S}{dE_i}\right) dE_i . \tag{2.8}$$

Since P_i^S is constant (0 and 1 in blocks $\mathscr{E}$ and $\mathscr{S}$, respectively), Eq. (2.8) further reduces to

$$R^A(t) = \int_{-S}^{0} J_i(E,t) \left(\frac{dP_i^S}{dE_i}\right) dE_i . \tag{2.9}$$

A necessary condition for the integral

$$I = \int_{x_1}^{x_2} F[y(x), \dot{y}(x); x]\, dx, \quad \dot{y} = dy/dx \tag{2.10}$$

to exhibit an extremum is given in the calculus of variations by the Euler–Lagrange equation[10]

$$\frac{d}{dx}\left(\frac{\partial F}{\partial \dot{y}_i}\right) - \frac{\partial F}{\partial y_i} = 0, \quad i = 1,2,\ldots,N , \tag{2.11}$$

the solution of which determines $y(x) \equiv [y_i(x)]$ over the fixed range $x_1<x<x_2$. Write $x \equiv E_i$, $y_i \equiv P_i^S$ and $F(\dot{y}(x); x) \equiv J(E_i)\,(dP_i^S/dE_i)$. The integral (2.9) is then an extremum provided

$$\frac{\partial J_i}{\partial E_i} = 0 = -\frac{dn_i}{dt}, \quad 0>E_i>-S \tag{2.12}$$

for each level i within block $\mathscr{B}$. This is the quasi-steady-state (QSS) condition for pairs in block $\mathscr{B}$ with $n_i(t)$ distributed so that J, the current (2.7), is constant over all energies $(-E)$ of block $\mathscr{B}$. The extremum rate, obtained from Eq. (2.12) in Eq. (2.9), is then the net downward current across bound level $-E$ of block $\mathscr{B}$:

$$R_*^A(t) = -J(-E,t) = \int_{-E}^{\infty} dE_i \times \int_{-D}^{-E} [n_i(t)\nu_{if} - n_f(t)\nu_{fi}]\, dE_f , \quad (2.13)$$

which depends on the probabilities P_i^S only implicitly via n_i. As E tends from above to the dissociation limit at $E=0$, $-J(E,t)$ increases monotonically to this rate.[5]

B. Analysis

From Eq. (2.4) the distribution

$$\gamma_i(t) = n_i(E_i,t)/\tilde{n}_i(E_i) \quad (2.14)$$

normalized to the distribution $\tilde{n}_i$ for full thermodynamic equilibrium satisfies

$$\frac{dn_i}{dt} = \tilde{n}_i \frac{d\gamma_i}{dt} = -\int_{-D}^{\infty} [\gamma_i(t) - \gamma_f(t)]\, C_{if}\, dE_f , \quad (2.15)$$

where the one-way equilibrium rate

$$C_{if} = \tilde{n}_i \nu_{if} = \tilde{n}_f \nu_{fi} = C_{fi} \quad (2.16)$$

satisfies detailed balance and is linear in gas density N. On introducing the implicit dependence of n_i on the probabilities $P_i^{S,D}$ via the separation[9]

$$\gamma_i(t) = P_i^D \gamma_c(t) + P_i^S \gamma_s(t) , \quad (2.17)$$

where

$$\gamma_c(t) = n_c(t)/\tilde{n}_c = N_A(t) N_B(t)/\tilde{N}_A \tilde{N}_B \quad (2.18a)$$

and

$$\gamma_s(t) = n_s(t)/\tilde{n}_s \quad (2.18b)$$

are the respective concentrations $n_c(t)$ and $n_s(t)$ of fully dissociated pairs with energies E_i in the range $0 \leqslant E_i < \infty$ of block $\mathscr{C}$ and of fully associated pairs of block $\mathscr{S}$ normalized to their respective equilibrium concentrations $\tilde{n}_c$ and $\tilde{n}_s$, then Eq. (2.15) separates as[9]

$$\frac{dn_i}{dt} = [\gamma_c(t) - \gamma_s(t)] \times \int_{-D}^{\infty} (P_i^S - P_f^S) C_{if}\, dE_f = -\frac{\partial J_i}{\partial E_i} . \quad (2.19)$$

Hence the macroscopic rate (2.3) is now

$$R^A(t) = \alpha \tilde{N}_A \tilde{N}_B [\gamma_c(t) - \gamma_s(t)] = -R^D(t) , \quad (2.20)$$

where the association rate in units of the time-dependent difference $(\gamma_c - \gamma_s)$ is the rate constant

$$\alpha \tilde{N}_A \tilde{N}_B = k\tilde{n}_s , \quad (2.21a)$$

$$= \int_{-D}^{\infty} P_i^S\, dE_i \int_{-D}^{\infty} (P_i^S - P_f^S)\, C_{if}\, dE_f , \quad (2.21b)$$

$$= \frac{1}{2} \int_{-D}^{\infty} dE_i \int_{-D}^{\infty} (P_i^S - P_f^S)^2\, C_{if}\, dE_f \quad (2.21c)$$

which is now time independent and is always positive. The upward current J past energy E in Eq. (2.19) separates similarly as[9]

$$J(E,t) = [\gamma_c(t) - \gamma_s(t)]\, j(E) , \quad (2.22)$$

where

$$j(E) = \int_{E}^{\infty} dE_i \int_{-D}^{E} (P_i^S - P_f^S)\, C_{if}\, dE_f . \quad (2.23)$$

Since Eq. (2.20) is an extremum provided the QSS condition (2.12) holds, i.e., Eq. (2.19) vanishes in block $\mathscr{B}$ where Eq. (2.23) is constant, then the probabilities P_i^S satisfy the standard integral equation[9]

$$P_i^S \int_{-D}^{\infty} C_{if}\, dE_f = \int_{-D}^{\infty} C_{if} P_f^S\, dE_f . \quad (2.24)$$

When inserted in Eq. (2.21) the solutions P_i^S yield after some reduction the extremum rate constant,

$$R_* = \alpha_* \tilde{N}_A \tilde{N}_B = \int_{-E}^{\infty} dE_i \int_{-D}^{-E} (P_f^S - P_i^S)\, C_{if}\, dE_f , \quad (2.25a)$$

$$= \int_{0}^{\infty} dE_i \int_{-D}^{0} C_{if} P_f^S\, dE_f , \quad (2.25b)$$

$$= \int_{-S}^{\infty} dE_f \int_{-D}^{S} C_{if} P_f^D\, dE_i , \quad (2.25c)$$

where $-E$ is any level in block $\mathscr{B}$, including the $\mathscr{C}$–$\mathscr{B}$ and $\mathscr{B}$–$\mathscr{S}$ boundaries at 0 and $-S$, respectively. This extremum simply confirms the identification in Eq. (2.13) of rate with current. The nature (maximum or minimum) of the extremum becomes apparent on performing independent variations δP_i^S to P_i^S for each level in block $\mathscr{B}$ subject to the constraints

$$P_i^S = 0; \quad 0 < E_i < \infty , \quad (2.26)$$
$$= 1; \quad -D < E_i < -S ,$$

associated with blocks $\mathscr{C}$ and $\mathscr{S}$, respectively. The resulting change in Eq. (2.20) is

$$\delta R^A(t) = 2[\gamma_c(t) - \gamma_s(t)] \times \left[\int_{-S}^{0} dE_i\, \delta P_i^S \left\{ \int_{-D}^{\infty} (P_i^S - P_f^S)\, C_{if}\, dE_f \right\} + \frac{1}{4} \int_{-D}^{\infty} dE_i \int_{-D}^{\infty} (\delta P_i^S - \delta P_f^S)^2\, C_{if}\, dE_f \right] \quad (2.27)$$

to second order in δP_i^S. For an extremum the change δR^A to first order in δP_i^S vanishes so that Eq. (2.24) is recovered from Eq. (2.27). The change to second order in δP_i^S is determined by the sign of $(\gamma_c - \gamma_s)$. When $\gamma_c(t) > \gamma_s(t)$ so that the overall direction, according to Eq. (2.20), is association, then the extremum to R^A is a minimum; and the dissociation rate R^D in Eq. (2.20) is a negative maximum. When $\gamma_s(t) > \gamma_c(t)$ so that the overall direction is dissociation, then R^A is a negative maximum; and R^D is a minimum. The proposed variational principle governing Eqs. (2.2) and (2.5) thus asserts that the rate R^A or R^D, whichever corresponds to the overall direction, always adjusts itself to a min-

imum, i.e., the probabilities P_i^S are so distributed that they tend to counteract the change so as to impede the progress towards full equilibrium (when $\gamma_c \to \gamma_s \to 1$). The rate R_* in Eq. (2.25) is a minimum to Eq. (2.21).

Rather than inserting the numerical solution of the QSS integral equation (2.23) in Eq. (2.25a) for the rate constant, an alternative procedure is therefore a direct search of a minimum in the rate (2.21) with respect to variation of P_i^S, a procedure similar to that noted by Mendaš with respect to variation of Eq. (1.3) with respect to γ_i. The present variational principle however provides a variational expression (2.21) for the actual QSS rate (2.25) obtained otherwise from the Master equation.

Although the present analysis has been developed with termolecular ion–ion recombination (1.1) in mind, it may be easily generalized to include ion–atom association

$$A^+ + B + M \to AB^+ + M \tag{2.28}$$

between atomic species in a low density gas M. Here quasibound levels (E_i, L_i^2) of AB^+ can be formed with $E_i > 0$ within the centrifugal barrier associated with internal relative angular momentum (squared) L_i^2. By adopting the ansatz [Eq. (5.2) of Ref. 5] for the distribution $n_i(E_i, L_i^2)$ of AB^+ pairs in terms of the stabilization probability $P_i^S(E_i, L_i^2)$ then expression (2.21), generalized to include relevant integrations over L_i^2 and L_f^2, is varied with respect to $P_i^S(E_i, L_i^2)$ so as to provide a minimum which is then the required QSS rate.

C. Application to termolecular recombination

Since dP_i^S/dE_i tends to zero as $E_i \to 0$ and as $E_i \to -S$ (taken now to be $-\infty$), the simplest one-parameter (λ^*) trial function is provided by

$$\frac{dP^S(\lambda;\lambda^*)}{d\lambda} = A\lambda\, e^{-(\lambda/\lambda^*)}, \tag{2.29}$$

where $\lambda = -E_i/kT$ is the binding energy in units of kT, the mean energy of the gas M, and where the variational parameter λ^* is the location of the maximum at $\lambda = \lambda^*$ of Eq. (2.29). Since $P(\infty)$–$P(0)$ is unity, then integration yields the normalization parameter A to be $(1/\lambda^*)^2$ and

$$P^S(\lambda;\lambda^*) = 1-(1+x)\exp(-x); x = \lambda/\lambda^*. \tag{2.30}$$

Consider, as a case study, the well-developed example of termolecular ion–ion recombination[6]

$$X^+ + X^- + X \to X_2 + X \tag{2.31}$$

between equal mass species. Necessary integrations of Eq. (2.21) and solution[6] of the integral equation (2.24) are performed by choosing 72 pivots each in blocks $\mathscr{G}$ and $\mathscr{F}$ according to the procedure outlined in Ref. 11. When Eq. (2.30) is inserted into Eq. (2.21) and when λ^* is varied, the long-dashed curve in Fig. 2 is obtained for the ratio

$$r = R(\lambda = \lambda^*)/R_*, \tag{2.32}$$

where R_* is the exact QSS rate (2.25) determined from the direct solution[6] of Eq. (2.24). Not only does the single parameter $\lambda^* = 1.1624$ provide a minimum to R but it also yields the exact result to 1% accuracy with $r = 1.011$. Introduction of a more sophisticated three parameter (λ^*, a, b) trial function

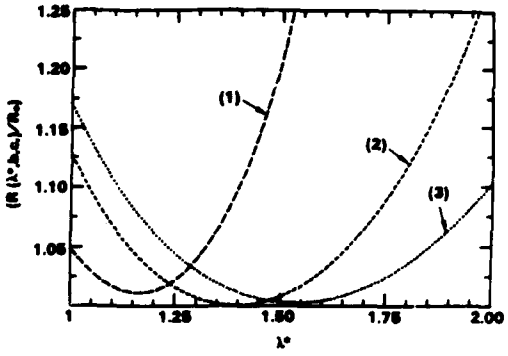

FIG. 2. Ratio of the variational rate (2.21) to the exact QSS rate (2.25) as a function of variational parameter λ^*. (1): One parameter function (2.30). (2) and (3): Two- and three-parameter functions (2.35) with $a = 1$, $b = 0$ and $a = 1$, $b = 0.7$, respectively.

$$dP^S(\lambda;\lambda^*,a,b)/d\lambda = A\lambda(1 + a\lambda + b\lambda^2)e^{-\lambda/\Lambda_*}, \tag{2.33}$$

where, in terms of the location at λ^* of the maximum to Eq. (2.33), Λ_* is the function

$$\Lambda(\lambda,a,b) = \lambda(1 + a\lambda + b\lambda^2)/(1 + 2a\lambda + 3b\lambda^2) \tag{2.34}$$

evaluated at $\lambda = \lambda^*$.

Integration of Eq. (2.33) subject to the constraints Eq. (2.26) determines the normalization factor A and yields

$$P^S(\lambda;\lambda^*,a,b) = 1 - [1 + x + x^2 g(x)^2]\exp(-x);$$
$$x = \lambda/\Lambda_*, \tag{2.35}$$

where

$$g(x;\Lambda_*,a,b) = \Lambda_*(a + 3b\Lambda_* + b\Lambda_* x)/$$
$$(1 + 2a\Lambda_* + 6b\Lambda_*^2). \tag{2.36}$$

The derivative is

$$\frac{dP^S(\lambda;\Lambda_*,a,b)}{d\lambda} = [(x + a\Lambda_* x^2 + b\Lambda_*^2 x^3)/$$
$$(1 + 2a\Lambda_* + 6b\Lambda_*^2)]\exp(-x). \tag{2.37}$$

Figure 2 illustrates that minima $r = 1.0008$ and $r = 1.0029$ are obtained for two-parameter ($\lambda^* = 1.3962$, $a = 1.0$, $b = 0$) and three-parameter ($\lambda^* = 1.5348$, $a = 1.0$, $b = 0.7$) trial functions, respectively, and that these minima agree with the calculation of the exact QSS rate (2.25). Comparison of the corresponding probabilities for all three variational cases with the exact QSS solution[6] of Eq. (2.24) is given in Fig. 3(a). The two-parameter function is graphically indistinguishable from the numerical QSS solution in Fig. 3(a). The agreement is in general very good for such simple variational functions, and could be easily improved at larger λ by insisting that $P_i^S \to 1$ as $E_i \to -S \simeq -(10\text{–}20)\,kT$ rather than as $E_i \to -\infty$ in Eq. (2.35). Although the two-parameter function provides a slightly better representation we note from Fig. 2 that the rate (2.21) is not overly sensitive to the small deviations in the probabilities.

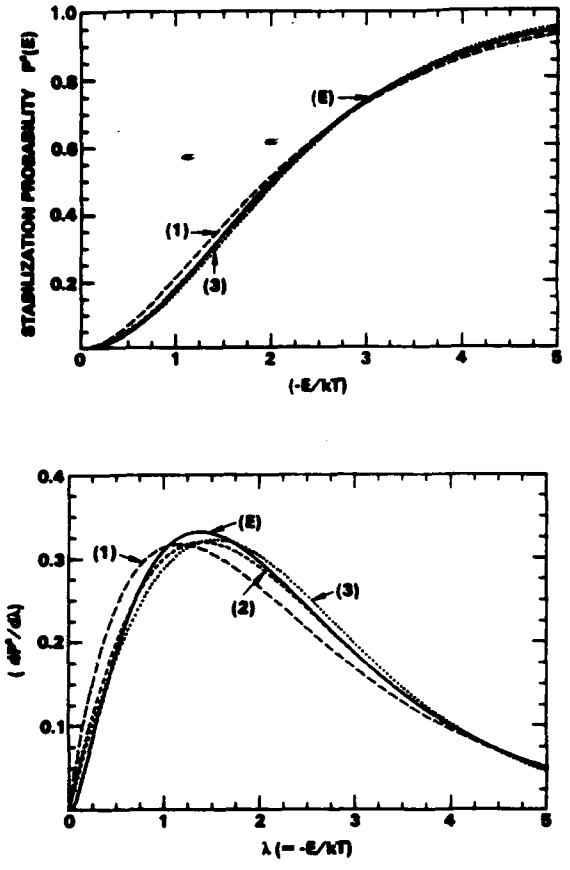

FIG. 3. (a) Variational probabilities (2.35), (1), (2), and (3) as a function of normalized bound energy ($-E/kT$). Parameters (λ^*,a,b) given by (1.1624,0,0), (1.3962,1,0), and (1.5348,1,0.7), respectively. Exact QSS probability (2.24):(E). (b) Corresponding derivatives.

A more sensitive test[5] is provided in Fig. 3(b) which displays the corresponding comparison of the derivatives. All of these variational curves and the direct QSS solution of Eq. (2.24) display maxima almost equal and located in the same neighborhood. This location has physical significance and is perhaps key to the overall success obtained. This is most easily illustrated by expanding

$$P_f^S = P_i^S + (E_f - E_i)\left[\frac{dP_i^S}{dE_i}\right] + \tfrac{1}{2}(E_f - E_i)^2\left[\frac{d^2P_i^S}{dE_i^2}\right] + \cdots \quad (2.38)$$

in powers of the energy difference $(E_f - E_i)$ so that Eq. (2.19) yields

$$-[\gamma_c(t) - \gamma_s(t)]^{-1}\frac{dn_i}{dt} = D_i^{(1)}\left[\frac{dP_i^S}{dE_i}\right] + D_i^{(2)}\left[\frac{d^2P_i^S}{dE_i^2}\right] \quad (2.39)$$

to second order in the energy-change moments[5]

$$D_i^{(m)}(E_i) = \frac{1}{m!}\int_{-D}^{\infty}(E_f - E_i)^m C_{if}\,dE_f. \quad (2.40)$$

For QSS of block $\mathscr{B}$,

$$\left(\frac{d^2P_i^S}{dE_i^2}\right)\Big/\left(\frac{dP_i^S}{dE_i}\right) = -D_i^{(1)}/D_i^{(2)} \equiv -\chi_i(E_i) \quad (2.41)$$

so that (dP_i^S/dE_i) exhibits a maximum where $D_i^{(1)}$, the average energy increase per second, passes through zero, which in general occurs[5] at $E_i^* = -(1\text{–}2)\,kT$. The above trial expressions (2.29) and (2.33) therefore implicitly acknowledge the physical tendency for collisions to excite those pairs with $E > E_i^*$ and to degrade those with $E < E_i^*$. Once λ_i^* has been variationally determined by the present procedure, it will only coincide with the actual location of the zero in $D_i^{(1)}$ to the extent that approximation (2.39) is valid. If so the expressions then imply that the ratio (kT) $D_i^{(1)}/D_i^{(2)}$ may be represented quite accurately either by the simple form $(1/\lambda - 1/\lambda^*)$ or by the more complicated form $(1/\Lambda - 1/\Lambda_*$, respectively. Both forms yield zero at $\lambda = \lambda^*$. Interestingly enough, the zero of $D_i^{(1)}$ for symmetrical resonance charge transfer collisions occur at $\lambda_i^* = 1.329$ in close agreement with the two-parameter variational and exact calculations [cf. Fig. 3(b)].

The solution of Eq. (2.41) subject to Eq. (2.26) is

$$P^S(-E) = \left[\int_{-E}^{0} dE_f \exp\left\{\int_{-E_f}^{0}\chi_i\,dE_i\right\}\right] \times\left[\int_{-S}^{0} dE_f \exp\left\{\int_{-E_f}^{0}\chi_i\,dE_i\right\}\right]^{-1} \quad (2.42)$$

in block $\mathscr{B}$. When the approximation[5]

$$D_i^{(1)} = \frac{dD_i^{(2)}}{dE_i} \quad (2.43)$$

between moments $D_i^{(1)}$ and $D_i^{(2)}$ can be invoked, then

$$\exp\left[\int_{-E_f}^{0}\chi_i\,dE_i\right] = D^{(2)}(0)/D^{(2)}(-E_f) \quad (2.44)$$

so that Eq. (2.42) reduces to

$$P_d^S(-E_i) = \left[\int_{-E}^{0} dE_f/D^{(2)}(-E_f)\right] \times\left[\int_{-S}^{0} dE_f/D^{(2)}(-E_f)\right]^{-1}. \quad (2.45)$$

This expression (2.45) has been used in Eq. (2.21c) to provide accurate rates α_D in a previous diffusional treatment.[5] The more basic expression (2.42) is currently being tested.[12]

There are now two accurate treatments which provide accurate *analytical* representations of the collisional stabilization and disruption probabilities—the previous diffusional method[5] and the present (two-parameter) variational method. These results D from Eq. (2.45) and V from Eq. (2.35) are compared in Fig. 4 with the exact numerical solution E of Eq. (2.24). Due to a more accurate evaluation of $D_i^{(1)}$, the present diffusional results differ somewhat from those previously reported.[5] The resulting rates

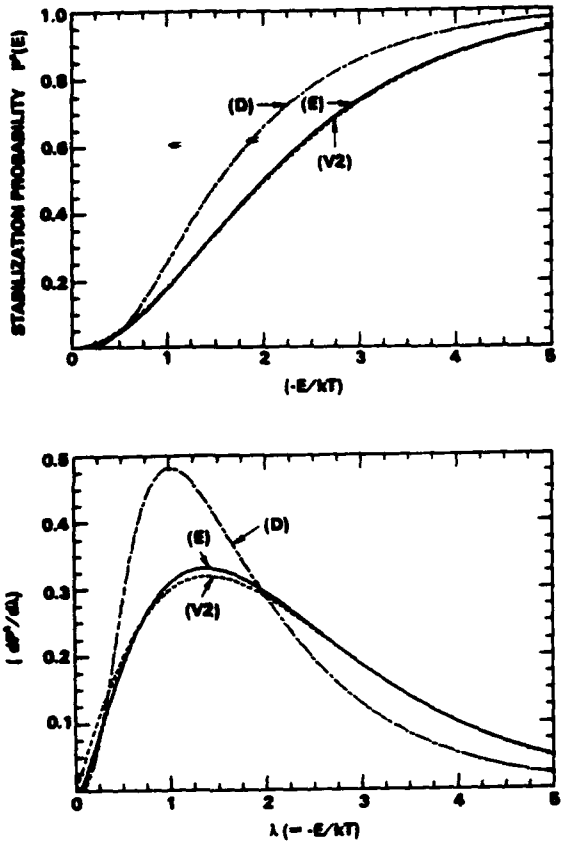

FIG. 4. (a) Probabilities and (b) corresponding derivatives in exact QSS (E), two-parameter ($\lambda^* = 1.3962$, $a = 1$) variational ($V2$), and diffusional (D) treatments, as a function of normalized bound energy ($-E/kT$).

($\alpha_D/\alpha_E = 1.08$, $\alpha_V/\alpha_E = 1$) are not that sensitive, as before, to the larger discrepancies in P_i^S resulting from the diffusional and variational treatments.

III. ANALOGY WITH (R,C) ELECTRICAL CIRCUIT AND WITH PRINCIPLE OF LEAST DISSIPATION

Bates[7] has already provided the interesting analogy with a network of resistors for the case when $\gamma_c(t) = 1 > \gamma_s(t)$ so that time dependencies can be omitted,[5] and has introduced the variational function $\mathscr{M}$, Eq. (1.3), as a measure of the restoration rate to thermodynamic equilibrium. Here capacitors are introduced (Sec. III A) so as to explicitly acknowledge time-dependent currents and voltages. The present approach allows us to identify (Sec. III B) the time-independent function $\mathscr{M}$ with $2\alpha\tilde{N}_A\,\tilde{N}_B$.

The Master equation (2.15) involves the internal energy E_f of relative (A–B) motion as a continuous variable since the spacing between bound levels are much smaller than the thermal energy (kT) of the thermal gas bath M. The discrete representation of Eq. (2.15) gives the net electrical current flowing outward from node i of a multimode system as

$$I_i(t) = -\frac{dn_i}{dt} = \sum_{f=-D}^{\infty} I_{if}(t)\,, \tag{3.1}$$

where the current in the $i \to f$ segment is

$$I_{if}(t) = [\gamma_i(t) - \gamma_f(t)]\, C_{if}\,. \tag{3.2}$$

This reduces under Eq. (2.16) to

$$I_{if}(t) = [\gamma_c(t) - \gamma_s(t)](P_f^S - P_i^S)\, C_{if} \tag{3.3}$$

$$\equiv [\gamma_c(t) - \gamma_s(t)]\, i_{if}\,.$$

The formal structure of Eqs. (3.1) and (3.2) is identical[7] to an electrical network where the current I_{if} along the line element e_{if} from junction i to junction f in the network is equivalent to the time-dependent voltage drop

$$V_{if}(t) = [\gamma_i(t) - \gamma_f(t)] \tag{3.4}$$

$$= [\gamma_c(t) - \gamma_s(t)](P_i^D - P_f^D) \tag{3.5}$$

times the conductivity $C_{if} = R_{if}^{-1}$ of the line element of resistance R_{if}.

Since, Eq. (3.2) is Ohm's law ($V_{if}(t) = I_{if}(t)\, R_{if}$)[7], a time-dependent potential

$$V_i(t) = \gamma_i(t) \tag{3.6}$$

can be associated with any level i. All states within the source block $\mathscr{C}$ are at equipotential $\gamma_c(t)$ and all levels within sink block $\mathscr{S}$ are at equipotential $\gamma_s(t)$. The potential γ_i of each $\mathscr{E}$ level i is below γ_c by an amount

$$V_{ci} = \gamma_c(t) - \gamma_i(t) = P_i^S\,[\gamma_c(t) - \gamma_s(t)] \tag{3.7}$$

or is above γ_s by an amount

$$V_{is} = \gamma_i(t) - \gamma_s(t) = P_i^D\,[\gamma_c(t) - \gamma_s(t)]\,. \tag{3.8}$$

Hence in units of $(\gamma_c - \gamma_s)$, P_i^S is the potential drop from $\mathscr{C}$ to i, P_i^D is the potential height of i above $\mathscr{S}$, and I_{if} is the current Eq. (3.3) along segment e_{if}. Since P_i^D within $\mathscr{E}$ increases with E_i continuously and monotonically from zero within $\mathscr{S}$ to unity within $\mathscr{C}$ then

$$\sum_{e_{if}} V_{if} = [\gamma_c(t) - \gamma_s(t)] \oint_{E_i}^{E_2} \left[\frac{dP_i^D}{dE_i}\right] dE_i = 0\,, \tag{3.9}$$

where the sum is over each segment e_{if} within any closed loop ($E_1 \to E_2 \to E_1$). Equation (3.9) as already noted,[7] is Kirchoff's voltage law (KVL) which is based on the uniqueness of the potential $\gamma_i(t)$ at a given time and which expresses *energy conservation* for any closed loop within the entire ($\mathscr{C}$, $\mathscr{E}$, $\mathscr{S}$) circuit at time t.

A. QSS simplification: (R,C) circuit

The QSS condition (2.12) for each level i of block $\mathscr{E}$ ($0 > E_i > -S$) is equivalent to

$$I_i(t) = \sum_{f=-D}^{\infty} I_{if}(t) = \sum_{f=-D}^{\infty} [\gamma_i(t) - \gamma_f(t)]\, C_{if} \tag{3.10a}$$

$$\equiv [\gamma_c(t) - \gamma_s(t)] \int_{-D}^{\infty} (P_f^S - P_i^S)\, C_{if}\, dE_f \tag{3.10b}$$

$$= 0, \quad i = 1, 2, N \tag{3.10c}$$

which[7] is Kirchoff's current law (KCL). The balance of currents I_{if} which exits and enters any junction i within block

$\mathscr{B}$ ($1<i<N$) to all junctions ($f=N+1, N+2,..\infty$, in block $\mathscr{C}$, $f=1,2,...,N$ in block $\mathscr{B}$ and $f=0,-1,...,-D$ in block $\mathscr{S}$) of the network is zero. This expresses *charge conservation* at junction i where there is no net buildup of density (charge) n_i. The ansatz (2.17) which enables the QSS condition (2.12) to be satiafied by a specified distribution P_i^S at all times provides the separation in Eqs. (3.3), (3.5), and (3.10b).

Under KCL or QSS, the voltages P_i^S satisfy

$$P_i^S \int_{-D}^{\infty} C_{if}\, dE_f = \int_{-D}^{0} C_{if}\, P_f^S\, dE_f . \tag{3.11}$$

The time-dependent $\mathscr{C}$ and $\mathscr{S}$ blocks of states are analogous to capacitors connected in parallel with their positive plates charged to

$$Q_1(t) = n_c(t) = \int_0^{\infty} n_i(t) dE_i \tag{3.12}$$

and

$$Q_2(t) = n_s(t) = \int_{-D}^{-S} n_i(t) dE_i , \tag{3.13}$$

at time t and held at voltages

$$V_1(t) = \gamma_c(t) \tag{3.14}$$

and

$$V_2(t) = \gamma_s(t) \tag{3.15}$$

above their negative plates. Since $Q = C/V$, their capacitances

$$C_1 = \tilde{n}_c = \int_0^{\infty} \tilde{n}_i\, dE_i \tag{3.16}$$

and

$$C_2 = \tilde{n}_s = \int_{-D}^{-S} \tilde{n}_i\, dE_i \tag{3.17}$$

are constant. The external capacitor $C_1 \equiv \mathscr{C}$ is connected to internal KCL node f (or energy level) by equivalent resis-

$$\frac{1}{R_{Cf}} = \sum_{i=N+1}^{\infty} \frac{1}{R_{if}} \equiv \int_0^{\infty} C_{if}\, dE_i = C_{Cf} \tag{3.18}$$

and directly to the external capacitor $C_2 \equiv \mathscr{S}$ by a resistance R_{CS} given by

$$\frac{1}{R_{CS}} = \sum_{i=N+1}^{\infty} \sum_{f=-D}^{0} \frac{1}{R_{if}} \equiv \int_0^{\infty} dE_i \int_{-D}^{-S} C_{if}\, dE_f = C_{CS} . \tag{3.19}$$

Each internal KCL node i of block $\mathscr{B}$ is coupled to internal node f by R_{if} and externally coupled to C_2 via R_{iS} given by

$$\frac{1}{R_{iS}} = \sum_{f=-D}^{0} \frac{1}{R_{if}} \equiv \int_{-D}^{-S} C_{if}\, dE_f = C_{iS} . \tag{3.20}$$

The above resistances R_{Cf}, R_{iS}, and R_{CS} are equivalent to a parallel network of resistances R_{if} connecting, respectively, all states $C(i=N+1,...,\infty)$ of block $\mathscr{C}$ to the specified $\mathscr{B}$-block state f, each $\mathscr{B}$-block state i to all states $S(f=0,-1,...,-D)$ of block $\mathscr{S}$ and all states C to all states S, respectively. The electrical network which corresponds to the Master equation (3.10) for association is illustrated by Fig. 5. A time-varying current $I(t)$ from capacitor C_1 with initial charge $Q_1(0) = n_c(0)$ is subdivided along mainline channels R_{Cn} to enter a KCL network with N nodes, composed entirely of resistors R_{nj} and internal currents $I_{nj}(t)$, and is then reconstituted at C_2 via mainline exit channels R_{fs}.

B. Principle of least dissipation

The network of resistances R_{CS}, R_{Cf}, R_{iS}, and R_{if} may now be replaced by an equivalent resistance R with throughput current $I(t)$ determined from the power loss

$$I(t)^2 R = [\gamma_c(t) - \gamma_s(t)] I(t) \tag{3.21}$$

$$= \sum_{n=-D}^{\infty} \sum_{f>n}^{\infty} I_{nf}^2 R_{nf} \tag{3.22}$$

to be

$$I(t) \equiv \frac{1}{2} [\gamma_c(t) - \gamma_s(t)] \times \int_{-D}^{\infty} dE_i \int_{-D}^{\infty} (P_i^S - P_f^S)^2\, C_{if}\, dE_f . \tag{3.23}$$

The summations include external junctions $C(n=N+1,N+2,...,\infty)$ and $S(n=-D,-D+1,...,0)$ at the source and sink capacitors and the internal junctions ($n=1,2,...,N$). By comparison with Eq. (2.20), the association rate $R^A(t)$ may now be identified with the electrical current $I(t)$ of Eq. (3.23), and the rate constant identified with

$$\alpha \tilde{N}_A\, \tilde{N}_B = \frac{1}{2} \int_{-D}^{\infty} dE_i \int_{-D}^{\infty} (P_i^S - P_f^S)^2\, C_{if}\, dE_f , \tag{3.24}$$

the effective conductivity R^{-1} of the network, or with the time-dependent electrical current $I(t)$, Eq. (3.23), per unit

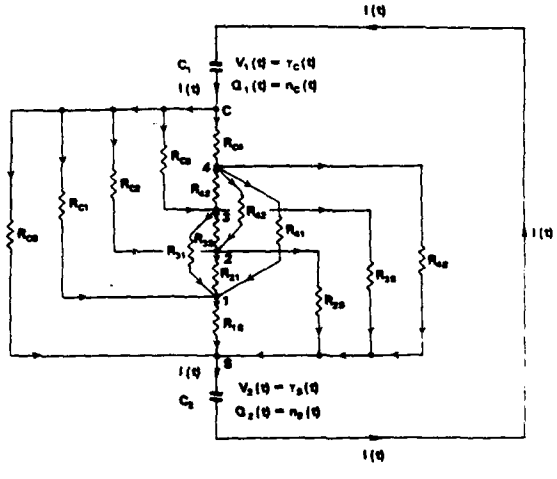

FIG. 5. (R,C) electrical diagram analogous to termolecular recombination.

voltage drop $[\gamma_c(t)-\gamma_s(t)]$. When the KCL condition (3.11) is used directly in Eq. (3.24) then the previous results (2.25) are obtained.

The power loss

$$I^2(t)R=[\gamma_c(t)-\gamma_s(t)]\,R^A(t)\geq 0 \tag{3.25}$$

is always positive. The present variational principle (VP) asserts that P_i^S, the voltage drop in units of $(\gamma_c-\gamma_s)$, are so distributed that the rate $R^A(t)$—the electrical current $I(t)$—is a minimum. When $\gamma_c(t)>\gamma_s(t)$, i.e., association occurs at positive rate $R^A(t)$, then VP implies that the power (3.25) dissipated by (A–B) and absorbed by the gas M is least. When R^A is negative, the net direction is dissociation which occurs at rate $R^D(t)=-R^A(t)$ when $\gamma_c<\gamma_s$, then VP implies that the power provided to AB *by* the gas M is least.

This principle of least dissipation is basic in many fields, e.g., thermodynamics, heat conduction, fluid mechanics. The principle for heat conduction was derived explicitly by Onsager.[13] For a current I entering a KVL and a KCL electrical network via R_{Cn} and exiting via R_{nS}, the currents within the KCL network are so distributed that the summed rate of dissipation of energy in the R_{Cn}, R_{nj}, and R_{nS} resistors is a minimum—Joule's law. With this law, Bates[7] postulated that a minimum would exist in the measure $\mathscr{M}$, Eq. (1.3) of the restoration rate of thermodynamic equilibrium by recombination in highly nonequilibrium systems [when $\gamma_c\gg\gamma_s$ and $\gamma_i=P_i^D$ in Eq. (2.17) so that explicit time dependences can be ignored[5]]. Mendaš[8] then noted that the distributions n_i associated with this minimum satisfy the QSS condition (1.4). From Eq. (3.23) it follows that this unnormalized time-independent measure $\mathscr{M}$ may now be uniquely identified as the rate $2\alpha\tilde{N}_A\tilde{N}_B$ so that the minimum of $\mathscr{M}$ yields the minimum rate (2.25a) directly, without the further need for substituting the final variational function $P_i^D=1-P_i^S$ in expression (2.23) for the current (2.25a) or in Eq. (1.5).

The present assertion that the rates (2.2) and (2.5) are extremum implies a principle of least dissipation for chemical reactions. The rates $R^{A,D}(t\to\infty)$ tend naturally to zero when thermodynamic equilibrium is obtained for the complete system. This is analogous to the electrical current I decaying to zero when the voltages across the capacitors C_1 and C_2 connected in series across R become equal.

C. Use of diagram

Various QSS results may be deduced rather readily from consideration of the electrical diagram (Fig. 5).

Result I: The mainline entrance current along R_{Cn} and entering KCL node n is

$$i_n^-=P_n^S\,C_{Cn} \tag{3.26}$$

in units of $(\gamma_c-\gamma_s)$. The total mainline current which enters all N nodes of KCL block $\mathscr{G}$ and node $n=0$ of block $\mathscr{S}$ from block $\mathscr{G}$ is

$$\alpha\tilde{N}_A\tilde{N}_B=\sum_{n=0}^{N}i_n^-\equiv\int_{-D}^{0}C_{Cf}\,P_f^S\,dE_f \tag{3.27}$$

which is the association rate $R^A(t)$ in units of $[\gamma_c(t)-\gamma_s(t)]$ in agreement with Eq. (2.25b).

Result II: The current which exits KCL node n along all the internal resistors R_{nf} and external resistors R_{nS} of Fig. 5. is

$$i_n^+=\sum_{f=0}^{N}(P_n^S-P_f^S)\,C_{nf}\,. \tag{3.28}$$

The total current exiting from all N-KCL nodes is then

$$\sum_{n=1}^{N}i_n^+=\sum_{n=1}^{N}(1-P_n^S)\,C_{nS}\equiv\int_{-S}^{0}C_{Sf}\,P_f^D\,dE_f \tag{3.29}$$

which when combined with the $\mathscr{G}$–$\mathscr{S}$ direct current, $i_0=C_{CS}$ yields

$$k\,\tilde{n}_s=\int_{-S}^{\infty}C_{Sf}\,P_f^D\,dE_f \tag{3.30}$$

in agreement with Eq. (2.25c). The KCL law, $I_n=i_n^+-i_n^-=0$, Eq. (3.10) applied to nodes $n=1,2,\ldots,N$ not only confirms the QSS condition (2.25) but also demands equality of Eqs. (3.27) and (3.30), which provides macroscopic detailed balance.

Result III: From Fig. 5, the total mainline entrance current to nodes below a designated KCL node N^*:

$$i_*^-(<N^*)=\sum_{n=0}^{N^*}i_n^-\equiv\int_{-D}^{-E}C_{Cf}\,P_f^S\,dE_f\,, \tag{3.31}$$

where the junction N^* is associated with energy level $-E$. The internal and mainline exit currents from nodes above N^* sum to

$$i_*^+(>N^*)=\sum_{n=N^*}^{N}i_n^+=\sum_{n=N^*}^{N}\sum_{f=0}^{N}(P_n^S-P_f^S)\,C_{nf} \tag{3.32}$$

$$\equiv\int_{-E}^{0}dE_i\int_{-D}^{0}(P_f^S-P_i^S)\,C_{if}\,dE_f \tag{3.33}$$

which reduces to

$$i_*^+=\int_{-E}^{0}dE_i\int_{-D}^{-E}(P_f^S-P_i^S)\,C_{if}\,dE_f\,. \tag{3.34}$$

Since $i_n^+=i_n^-$ for each KCL node the total current $(i_*^++i_*^-)$ in units of $[\gamma_c(t)-\gamma_s(t)]$ is

$$\alpha\tilde{N}_A\tilde{N}_B=\int_{-E}^{0}dE_i\int_{-D}^{-E}(P_f^S-P_i^S)\,C_{if}\,dE_f \tag{3.35}$$

in agreement with Eqs. (2.23) and (2.25).

Result IV: When C_1 with charge $Q_1(t)$ gains a charge dQ_1 and C_2 with charge $Q_2(t)$ gains a charge dQ_2 on their positive plates within time dt, the sum of the total electrostatic energy $(V_1dQ_1+V_2dQ_2)$ gained by the capacitors and the thermal energy (3.21) radiated must be zero. Since the charge

$$q_i=n_i(t)=n_i(0),\quad i=1,2,\ldots,N \tag{3.36}$$

at each junction i of the N junction KCL network remains constant then the total charge distributed among the capacitors of initial charges Q_{10} and Q_{20} is

$$Q_1(t)+Q_2(t)=Q_{10}+Q_{20} \tag{3.37}$$

and the discharging/charging current is

$$I=-\frac{dQ_1(t)}{dt}=\frac{dQ_2(t)}{dt}\,. \tag{3.38}$$

Hence the power equation is

$$(V_1 - V_2)\left[\frac{dQ_1}{dt}\right] + I^2R = 0 \tag{3.39}$$

which also follows from application of KVL, Eq. (3.9), to the (C_1,R,C_2) circuit at time t. Hence

$$R^{\mathcal{A}}(t) = -\frac{d\bar{Q}_1(t)}{dt} = \frac{dQ_2(t)}{dt}$$

$$= \frac{1}{R}\left[Q_1(t)/C_1 - Q_2(t)/C_2\right] \tag{3.40}$$

which is the analog of Eq. (2.20) with $R^{-1} = \alpha\tilde{N}_A\,\tilde{N}_B$, $\gamma_c = Q_1(t)/C_1$, and $\gamma_s = Q_2(t)/C_2$. The equation is linear (rather than quadratic) in Q_1 since Eq. (2.7) renders the basic equation (2.2) linear in the (pair) distribution (3.12) of dissociated species AB. The solution of Eq. (3.40) subject to C_1 being initially uncharged ($Q_{10} = 0$) is

$$Q_1(t) = Q_{20}(C/C_2)[1 - \exp - t/RC\,]$$

$$\overset{t\to\infty}{\to} \frac{C_1}{(C_1 + C_2)}\,Q_{20} \tag{3.41}$$

and

$$Q_2(t) = Q_{20}[1 - (C/C_2)(1 - \exp - t/RC\,)]$$

$$\overset{t\to\infty}{\to} \frac{C_2}{(C_1 + C_2)}\,Q_{20}\,, \tag{3.42}$$

where C is $C_1C_2/(C_1 + C_2)$. As $t \to \infty$, the voltages across each pair of plates, $\gamma_c = Q_1/C_1$ and $\gamma_s = Q_2/C_2$ are equal (and opposite), no current flows and charging is complete (corresponding to thermodynamic equilibrium). When C_1 has infinite capacity for absorbing charge, i.e., when $C_1 \gg C_2$ then $C \to C_2$ so that

$$Q_1(t) \to Q_{20}(1 - \exp - t/RC_2) \tag{3.43}$$

and

$$Q_2(t) \to Q_{20} \exp - t/RC_2\,, \tag{3.44}$$

so that the dissociation frequency k can be related to the time constant for discharging of C_2 and charging of C_1 by

$$k = 1/RC_2 \tag{3.45}$$

as expected (since $C_2 = \tilde{n}_s$ and $1/R = \alpha\tilde{N}_A\,\tilde{N}_B = k\tilde{n}_s$). This rate constant governs only the rate of approach to, but not the magnitude of, the asymptotic limits.

In summary, appeal to the network (Fig. 5) provides results (3.27), (3.30), and (3.35) which are exact under KCL condition (3.11). For voltages which do not satisfy this KCL condition, then Eq. (3.24) is used for the electrical current in units of $(\gamma_c - \gamma_s)$.

IV. SUMMARY

A variational principle based on the search for a minimum to the net rate $R^{\mathcal{A}}(t)$ for association with respect to variation of the stabilization probabilities P_i^S has been proposed. It is capable (Sec. II B) of providing probabilities P_i^S and rate coefficients α identical with those determined from direct QSS solutions of the Master equation. In this sense the developed expression (2.21) provides a variational expression for the QSS approximation. Good trial representations (Sec. II B) for P_i^S exhibit a maximum in $|dP_i^S/dE_i|$ near the location E_i^* of a physical bottleneck.

By introduction of the additional block $\mathscr{B}$ of highly excited levels i sandwiched between the reactant and product zones $\mathscr{C}$ and $\mathscr{S}$, respectively, and characterized by forward and reverse (variational) probabilities P_i^S and P_i^D, respectively, the present variational method is more detailed and complete than the least-upper-bound variational method of Wigner[1] and Keck[2] which ignores this block.

The minimum with respect to variation in n_i of function (1.3) postulated by Bates[7] via analogy with an electrical network is identified here with $2\alpha\tilde{N}_A\,\tilde{N}_B$ so that the supplementary explicit calculation of the rate (1.5) is not required. Electrical diagrams (as Fig. 5) may be utilized very effectively not only to analyze (Sec. III C) the detailed dynamics of termolecular processes but also to facilitate the ready construction of various simplified approximate schemes.[14]

ACKNOWLEDGMENT

This research is supported by the U. S. Air Force Office of Scientific Research under Grant No. AFOSR-84-0233.

[1]E. P. Wigner, J. Chem. Phys. 5, 720 (1937).
[2]J. C. Keck, J. Chem. Phys. 32, 1035 (1960).
[3]S. Byron, R. C. Stabler, and P. I. Bortz, Phys. Rev. Lett. 8, 376 (1962).
[4]B. Makin and J. C. Keck, Phys. Rev. Lett. 11, 281 (1963).
[5]M. R. Flannery, J. Chem. Phys. 87, 6947 (1987).
[6]M. R. Flannery and E. J. Mansky, J. Chem. Phys. 88, 4228 (1988), and Refs. 1–3 therein.
[7]D. R. Bates, Proc. R. Soc. London. Ser. A 337, 15 (1974).
[8]I. Mendaš, J. Phys. B 12, L209 (1979).
[9]M. R. Flannery, J. Phys. B 18, L839 (1985).
[10]See, for example, G. Arfken, *Mathematical Methods for Physicists*, 3rd ed. (Academic, New York, 1985), p. 937.
[11]D. R. Bates and I. Mendaš, J. Phys. B 15, 1949 (1982).
[12]M. R. Flannery and E. J. Mansky (work in progress).
[13]L. Onsager, Phys. Rev. 37, 405 (1931).
[14]M. R. Flannery and E. J. Mansky, J. Chem. Phys. (to be published).

3.3. Diffusional Treatment.

Diffusional theory of termolecular recombination and association of atomic species in a gas

M. R. Flannery
School of Physics, Georgia Institute of Technology, Atlanta, Georgia 30332

(Received 10 June 1987; accepted 10 September 1987)

A diffusional treatment of termolecular association of atomic species A and B in a low density gas is presented and applied to positive ion–negative ion recombination over the full range of masses of reactants for various classes of ion–neutral interactions. In contrast to rates given by the diffusional current, excellent results are obtained for general mass species *provided* a more basic expression for the association rate is introduced.

I. INTRODUCTION

The picture of electron–ion recombination, of termolecular positive ion–negative ion recombination, and of termolecular ion–atom association:

$$A + B + M \underset{k}{\overset{\alpha}{\rightleftarrows}} AB + M, \tag{1.1}$$

involving subsystems (A–B) associating in a thermal bath of dilute gas M as proceeding via diffusion in energy space has stimulated[1–7] a great deal of interest, in principle, valuable to elucidation of the dynamics of association processes and to many examples of decay of laser-produced plasmas, of reaction processes in flames, of shock wave propagation, etc. In a classic paper on electron–ion recombination, Pitaevskii[1] derived a rather elegant analytical expression for the two-body rate coefficient α ($cm^3\ s^{-1}$) in Eq. (1.1). Because of its inherent simplicity over more sophisticated and therefore time consuming procedures based on a collisional input–output Master equation,[8–12] the result has been applied to heavy-particle recombination[3–5] which proceeds three orders of magnitude faster than collisional electron–ion recombination[1,7] for which the result was originally intended. In spite of its attractive features, the diffusion picture as formulated[1–6] achieved remarkably disappointing results for heavy-particle termolecular ion–ion recombination.[3–6]

Apart from recognition that diffusion methods (based on a Fokker–Planck reduction of the input–output collision integral) are likely to be valid only when the collisional changes in energy are small, the basic intrinsic defect for application of the Pitaevskii expression to general mass sytems remains as yet undetected. Moreover, that a much less sophisticated "bottleneck" model[13] originally designed also for electron–ion recombination achieved much closer agreement[10] with the exact results of the Master equation[8–10] for ion–ion recombination presents a puzzle.

In this paper, the foundation of the diffusion approach as applied to processes (1.1) will be examined and the basic defect in previous applications will become apparent. The proposed theory is valid for termolecular ion–ion recombination[8–11] and ion–atom association[14] at low gas densities and as a case study will be applied here to ion–ion recombination. Association at rate coefficient α ($cm^3\ s^{-1}$) and dissociation at frequency k (s^{-1}) in Eq. (1.1) are treated in a unified way so that equilibrium can eventually be established.

II. RATES AND CURRENT

The distribution $n_i(E_i,t)$ per unit interval dE_i of pairs AB with internal energy E_i at time t is governed by the collisional input–output Master equation[2,8–11,15]

$$\frac{d}{dt} n_i(E_i,t) = -\int_{-D}^{\infty} S_{if}\, dE_f = -\int_{-D}^{\infty} [n_i(t)\nu_{if} - n_f(t)\nu_{fi}]\, dE_f, \tag{2.1}$$

where $-D$ is the energy of the lowest vibrational level of AB relative to the dissociation limit taken as zero energy, and where ν_{if} is the frequency per unit interval dE_f for $E_i \to E_f$ transitions by collisions between AB and M. For bound states $dn_i/dt = \partial n_i/\partial t$, and for dissociated states $dn_i/dt = (\partial n_i/\partial t + F_i)$ where F_i is the net flux of contracting E_i *pairs created with infinite separation*. A basic expression for the rate $R^A(t)$ of association has already been derived.[16] In the interests of elucidation and completeness of the present discussion (in Secs. III C and IV) and of direct comparison with the diffusional quasi-steady-state approach, the key steps therein are provided below. The first step involves writing the net rate for association as[16]

$$R^A(t) = \int_{-D}^{\infty} P_i^S \left(\frac{dn_i}{dt}\right) dE_i = \alpha N_A(t) N_B(t) - k n_s(t), \tag{2.2}$$

where P_i^S is the probability of stabilization of E_i pairs by subsequent multicollisions with M. The effective two-body rate constant for the association of A and B with (cm^{-3}) concentrations $N_A(t)$ and $N_B(t)$ is α ($cm^3\ s^{-1}$), and k (s^{-1}) is the frequency for dissociation of those tightly bound pairs of concentration $n_s(t)$ which are considered to be fully associated with energies E_i within a block of $\mathscr{S}$ of low lying levels in a range $-S > E_i > -D$ within which the stabilization probability P_i^S is calculated to be unity.

The separation between the energy levels of AB is sufficiently small compared to the thermal energy (kT) of the gas bath so that the levels form a quasicontinuum. Thus,

$$\frac{d}{dt} n_i(E_i,t) = -\frac{\partial}{\partial E_i} J(E_i,t), \tag{2.3}$$

so that the upward current past level E at time t is

$$J(E,t) = \int_E^\infty dE_i \int_{-D}^{E} S_{fi}(t) dE_f, \tag{2.4}$$

since J vanishes at the end points $(-D,\infty)$ and since $S_{if} + S_{fi} = 0$.

On introducing the normalized distribution

$$\gamma_i(t) = n_i(E_i,t)/\bar{n}_i(E_i), \tag{2.5}$$

where $\bar{n}_i$ is the pair distribution under full thermodynamic equilibrium with the gas, the Master equation (2.1) is

$$\frac{d}{dt} n_i(E_i,t) = -\int_D^\infty [\gamma_i(t) - \gamma_f(t)] C_{if}\, dE_f$$

$$= -\frac{\partial}{\partial E_i} J_i(E_i,t), \tag{2.6}$$

where the one-way equilibrium collisional rate

$$C_{if} = \bar{n}_i \nu_{if} = \bar{n}_f \nu_{fi} = C_{fi} \tag{2.7}$$

satisfied detailed balance. The second step is to introduce the ansatz[16]

$$\gamma_i(t) = P_i^D \left[\frac{N_A(t) N_B(t)}{\tilde{N}_A \tilde{N}_B}\right] + P_i^S \left[\frac{n_s(t)}{\bar{n}_s}\right]$$

$$\equiv P_i^D \gamma_c(t) + P_i^S \gamma_s(t) \overset{t\to\infty}{\to} 1, \tag{2.8}$$

which holds at low gas densities. The equilibrium concentrations of A and B are $\tilde{N}_A$ and $\tilde{N}_B$. The probability that state i is a stabilized state, or is a destabilized state with respect to association is P_i^S or $P_i^D = 1 - P_i^S$, respectively, and γ_c and γ_s are the normalized distribution of pairs in the fully dissociated (source) block $\mathscr{G}$, $0 < E_i < \infty$, where P_i^D is unity, and in the fully associated (sink) block $\mathscr{S}$, $-S > E_i > -D$, where P_i^S is unity. Hence, the Master equation (2.6), current (2.4), and rate (2.2) separate as[16]

$$\frac{dn_i}{dt} = [\gamma_c(t) - \gamma_s(t)]$$

$$\times \int_{-D}^{\infty} (P_i^S - P_f^S) C_{if}\, dE_f = -\frac{\partial J_i}{\partial E_i}, \tag{2.9}$$

$$J(-E,t) = [\gamma_c(t) - \gamma_s(t)]$$

$$\times \int_{-E}^{\infty} dE_i \int_{-D}^{-E} (P_f^S - P_i^S) C_{if}\, dE_f, \tag{2.10}$$

and

$$R^A(t) = [\gamma_c(t) - \gamma_s(t)]$$

$$\times \int_{-D}^{\infty} P_i^S\, dE_i \int_{-D}^{\infty} (P_i^S - P_f^S) C_{if}\, dE_f. \tag{2.11}$$

From Eq. (2.9), the loss rates of fully dissociated and of fully associated species of energy E_i are, respectively,

$$-\frac{dn_i}{dt} = [\gamma_c(t) - \gamma_s(t)]$$

$$\times \int_{-D}^{0} C_{if} P_f^S\, dE_f, \quad E_i > 0 \tag{2.12}$$

and

$$-\frac{dn_i}{dt} = [\gamma_s(t) - \gamma_c(t)]$$

$$\times \int_{-S}^{\infty} C_{if} P_f^D\, dE_f, \quad -S > E_i > -D, \tag{2.13}$$

which illustrate quite effectively the significance of both the stabilization and disruption probabilities P_f^S and P_f^D.

From Eqs. (2.9) and (2.10),

$$\frac{dn_i}{dt} = -[\gamma_c(t) - \gamma_s(t)] \left(\frac{\partial j_i}{\partial E_i}\right), \tag{2.14}$$

where the time-independent background current downward across E is

$$-j(-E) = \int_{-E}^{\infty} dE_i \int_{-D}^{-E} (P_f^S - P_i^S) C_{if}\, dE_f. \tag{2.15}$$

From Eq. (2.11) the time-independent macroscopic coefficients α and k for association and dissociation in Eq. (2.2) are, therefore, given by the basic expression,

$$\alpha \tilde{N}_A \tilde{N}_B = \int_{-D}^{\infty} P_i^S\, dE_i \int_{-D}^{\infty} (P_i^S - P_f^S) C_{if}\, dE_f = k\bar{n}, \tag{2.16}$$

and satisfy (macroscopic) detailed balance.

The expressions (2.10) and (2.11), or equivalently Eqs. (2.15) and (2.16) for the current j and rate coefficient α are in general not identical unless the following additional requirement is satisfied.

A. Quasi-steady-state (QSS)

As Eqs. (2.12) and (2.13) illustrate, the distribution of pairs in blocks $\mathscr{G}$ and $\mathscr{S}$ are time dependent, until full thermodynamic equilibrium is established when $\gamma_{c,s} \to 1$ from above and below, respectively. Since $dn_i/dt = \partial n_i/\partial t$ for the intermediate block $\mathscr{E}$ of highly excited levels with energy E_i in the range $0 > E > -S$ then quasi-steady-state (QSS) in block $\mathscr{E}$ requires

$$\frac{dn_i}{dt} = 0, \quad 0 > E_i > -S \tag{2.17}$$

so that the stabilization probabilities in Eq. (2.9) then rigorously satisfy the integral equation

$$P_i^S \int_{-D}^{\infty} C_{if}\, dE_f = \int_{-D}^{0} C_{if} P_f^S\, dE_f; \quad 0 > E_i > -S. \tag{2.18}$$

The stochastic probability for stabilization P_i^S of state i is therefore the fraction of all collisions which eventually result in association. Under this circumstance it readily follows that the rate (2.11) reduces to

$$R^A(t) = -J(-E,t), \tag{2.19}$$

the downward current (2.10), and that the rate coefficient (2.16) is given by

$$\alpha \tilde{N}_A \tilde{N}_B = -j(-E), \tag{2.20}$$

where E is an arbitrary energy level in block $\mathscr{E}$ $(0 > E > -S)$.

The rate of association (2.16) may be identified with the

current (2.15) only when the QSS-condition (2.17) for the probabilities is satisfied.[16] Use of Eq. (2.17) from the outset in Eq. (2.2) also illustrates this relation,

$$R^A(t) = \int_{-D}^{-S} \left(\frac{dn_i}{dt}\right) dE_i = -J(-S,t) = -J(-E,t), \tag{2.21}$$

although the basic expression (2.16) for α cannot then be deduced. An exact expression which emphasizes the role of the current J is obtained from Eqs. (2.2) and (2.3) to give

$$R^A(t) = -\int_{-D}^{\infty} P_i^S \left(\frac{\partial J_i(t)}{\partial E_i}\right) dE_i = \int_{-S}^{0} J_i(t) \left(\frac{\partial P_i^S}{\partial E_i}\right) dE_i, \tag{2.22}$$

since J_i vanishes as $E_i \to -D$ and ∞, and since P_i^S is constant (0 and 1 within blocks $\mathscr{C}$ and $\mathscr{S}$, respectively). Only when Eq. (2.10) for J is constant over block $\mathscr{E}$, i.e., when QSS Eq. (2.18) is satisfied, does Eq. (2.22) reduce to Eq. (2.19). It may be shown (work in progress) that the QSS-condition (2.18) corresponds to a minimum[18] in Eq. (2.16) for α. Any approximate P_i^S which does not rigorously satisfy Eq. (2.18) will therefore yield higher rates α.

The QSS (minimum) rate coefficients are therefore given by

$$\alpha_* \tilde{N}_A \tilde{N}_B = \int_{-E}^{\infty} dE_i \int_{-D}^{-E} (P_f^S - P_i^S) C_{if}\, dE_f = -j(-E) \tag{2.23}$$

$$= \int_{0}^{\infty} dE_i \int_{-D}^{0} C_{if} P_f^S\, dE_f = -j(0) \tag{2.24}$$

$$= \int_{-D}^{-S} dE_i \int_{-S}^{\infty} C_{if} P_f^D\, dE_f = -j(-S) = k_* \tilde{n}_s, \tag{2.25}$$

which are, in general, different from Eq. (2.16) *unless* the probabilities P_f^S *exactly* satisfy[16] the QSS-condition (2.18). Note that Eq. (2.24) is the QSS rate for association that would result from the full equilibrium concentration $\tilde{N}_A \tilde{N}_B$ of dissociated pairs and zero population of fully associated $\mathscr{S}$ pairs i.e., $\gamma_c = 1$ and $\gamma_s = 0$ in Eq. (2.8). Similarly, Eq. (2.25) is the QSS rate for dissociation which would result from an equilibrium population $\tilde{n}_s$ of associated $\mathscr{S}$ pairs and zero population of dissociated pairs, i.e., $\gamma_c = 0$ and $\gamma_s = 1$ in Eq. (2.8).

The aim is now to derive a simple analytic but approximate expression for $j(-E)$ by converting Eq. (2.15) from an integral representation to a differential representation so that approximate expressions for the probabilities P_i^S may be derived, in contrast to the exact numerical solutions of Eq. (2.18).

III. FOKKER–PLANCK REDUCTION FOR ION–ION RECOMBINATION AT LOW GAS DENSITIES

The conversion of the integral operator in Eq. (2.13) into a differential operator achieved by a Fokker–Planck analysis[1,2] is useful when the collision kernel C_{if} favors small changes in energy. Here the current J_i in Eq. (2.6) can be determined to fourth order, rather than to the customary second order.[2]

A. Fokker–Planck current to fourth order in energy-change moments

On introduction of an arbitrary but well-behaved function $\Phi_i(E_i)$ whose derivatives vanish at the end points $[\infty, -D]$, then, with the aid of Eq. (2.6),

$$\int_{-D}^{\infty} \Phi_i \frac{dn_i}{dt} dE_i = \int_{-D}^{\infty} \gamma_i\, dE_i \int_{-D}^{\infty} (\Phi_f - \Phi_i) C_{if}\, dE_f. \tag{3.1}$$

On expanding the difference

$$\Phi_f - \Phi_i = \sum_{n=1}^{\infty} \frac{1}{n!} (E_f - E_i)^n \left[\frac{\partial^n \Phi_i}{\partial E_i^n}\right] \tag{3.2}$$

as a Taylor series in energy change $(E_f - E_i)$, assumed small, and on integration by parts with the explicit recognition that $(\partial^n \Phi_i / \partial E_i^n) \to 0$ for $n > 1$ as $E_i \to [\infty, -D]$, then Eq. (3.1) can be expressed as

$$\int_{-D}^{\infty} \Phi_i \frac{dn_i}{dt} dE_i = [J_i \Phi_i]_{-D}^{\infty} - \int_{-D}^{\infty} \Phi_i \frac{\partial J_i}{\partial E_i} dE_i, \tag{3.3}$$

where the current is

$$J_i(E_i,t) = \sum_{n=0}^{\infty} (-1)^n \frac{\partial^n [\gamma_i D_i^{(n+1)}]}{\partial E_i^n} \tag{3.4}$$

in terms of the normalized distributions γ_i and the energy change moments[2-4]

$$D_i^{(m)}(E_i) = \frac{1}{m!} \int_{-D}^{\infty} (E_f - E_i)^m C_{if}\, dE_f, \tag{3.5}$$

with respect to the one-way equilibrium rate for $E_i \to E_f$ transitions. The number per second of all collisions with an equilibrium distribution of E_i pairs in unit interval dE_i and unit volume is $D_i^{(0)}$; and $D_i^{(1)}$ and $2D_i^{(2)}$ are the average energy change and average energy change squared *per second*, $d\langle \Delta E \rangle / dt$ and $d\langle \Delta E^2 \rangle / dt$, respectively. The ratios $D_i^{(1)}/D_i^{(0)}$ and $2D_i^{(2)}/D_i^{(0)}$ specify $\langle \Delta E_i \rangle$ and $\langle \Delta E_i^2 \rangle$ *per collision*, respectively.

Evaluation of these moments can be facilitated by adopting the expressions for C_{if} which correspond to various A–M and B–M binary interactions (symmetrical resonance charge–transfer,[8-10] hard-sphere,[10] polarization[11]). They can be collected under a universal form (work in progress). These moments are normalized[10] to the quantity $(-1)^m \Gamma \alpha_T (kT)^{m-1} \tilde{N}_A \tilde{N}_B$ where α_T is the Thomson rate [Eq. (4.1) below], where Γ is a dimensionless mass factor[10] and where T is the temperature of the gas bath.

Figures 1(a) and 1(b) illustrate the general trend of these moments calculated here for the specific case[8,10] where internal-energy changes in an ion pair (X^+–X^-) are due to symmetrical resonance charge–transfer ($X^\pm$–X) collisions with a parent gas X. In this case, the velocity vectors of the

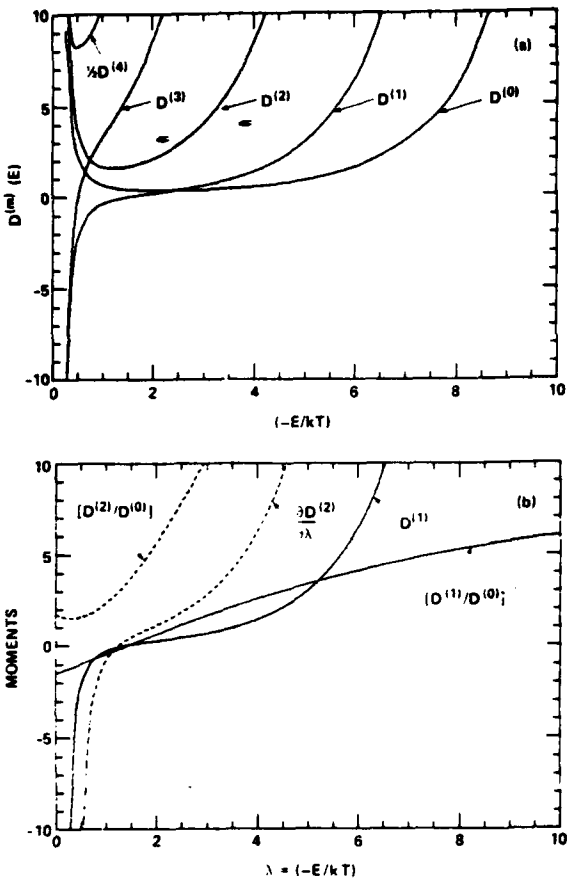

FIG. 1. (a) Normalized moments $D^{(m)}$ of energy change rate (energy^m s^{-1}), $m = 0$–4, as a function of internal energy $E_i = -\lambda(kT)$ of the bound ion pair. (b) Averaged energy change and energy-change squared $D^{(m)}/D^{(0)}$ per collision, $D^{(1)}$ and derivative of $D^{(2)}$. Equal-mass species and charge–transfer ion–neutral collisions are assumed and moments are normalized to the quantity $(-1)^m \Gamma \alpha_T (kT)^{m-1} \tilde{N}_A \tilde{N}_B$.

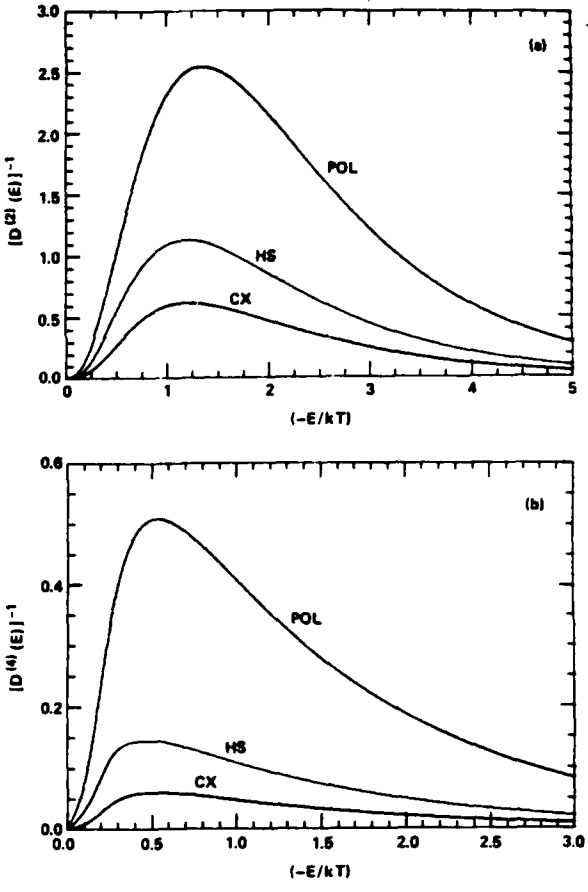

FIG. 2. Inverses of moments (a) $D^{(2)}(\lambda)$ and (b) $D^{(4)}(\lambda)$ as a function of internal energy $E_i = -\lambda kT$ of the ion pair for various ion–neutral interactions: POL (polarization), HS (hard-sphere), CX (charge–transfer). Equal mass species are assumed.

(fast) ion X^+ and the (thermal) neutral X are interchanged.[8] Large transfers of energy are therefore involved, as is confirmed by $D_i^{(2)}$, the averaged energy change squared $\langle \Delta E_i^2 \rangle$ *per second* shown in Fig. 1(a). This case will therefore provide a most stringent test of the weak-collision (diffusion) procedure adopted here.

As the binding energy $-E_i$ decreases from the dissociation limit (at zero energy), the equilibrium density $\tilde{n}(E_i) \sim |E_i|^{-5/2} \exp(-E_i/kT)$ per unit interval dE_i decreases from infinity, reaches a minimum at $E_i = -2.5kT$ and then increases exponentially.[10] Since the energy change frequency ν_{if} for each pair decreases rapidly with increase of binding, the overall shapes of the equilibrium moments $D_i^{(m)}$ in Figs. 1(a) and 1(b) reflect the variation of the product $\tilde{n}_i \nu_{if}$. Note that the equilibrium collisional rate $D_i^{(0)}$ is relatively constant in the range (1.8–4)kT of binding. Also $D_i^{(1)} \approx d/dt \langle \Delta E \rangle$ is positive for $E_i > -1.4kT = E^*$, so that these pairs on average become less tightly bound upon collision. Pairs with $E_i < -1.4kT$ become more tightly bound upon collision (since $D_i^{(1)} < 0$). This critical energy specifies the location of E^* of a bottleneck where the averaged energy change vanishes and where the region $E_i > E^*$ where excitation is greater is separated from the region $E_i < E^*$ where deexcitation is greater. Note also that the even moments $D_i^{(m)}$ display minima which become sharper with increase of m, as expected, and that the minimum in $D_i^{(2)} \simeq \frac{1}{2} d/dt \langle \Delta E_i^2 \rangle$ coincides with the zero of $D_i^{(1)} \sim d/dt \langle \Delta E_i \rangle$ at E^*, as is clearly shown in Fig. 1(b). These features are quite general for the various ion–neutral interactions and are utilized below.

Figures 2(a) and 2(b) illustrate the variation of $[D_i^{(2)}]^{-1}$ and $[D_i^{(4)}]^{-1}$ for different interactions of A and B with M (charge–transfer CX, hard-sphere HS, and polarization POL). The bottleneck to $D_i^{(2)}$ occurs where the $\langle \Delta E_i^2 \rangle$ rate is least and in roughly in the same location ($E_i \sim 1.25kT$) for all the interactions. The $\langle \Delta E_i^2 \rangle$ rate is greatest for the charge–transfer interaction and weakest for the polarization attraction, as expected. The moment $D_i^{(4)}$ exhibits similar but more rapidly varying behavior.

Since C_{if} is symmetrical in i and f—the detailed-balance

relation (2.7)—then C_{if}, when expressed as a function of the energy-mean $\bar{E} = \frac{1}{2}(E_f + E_i)$ and the energy change $\Delta = E_f - E_i$, is such that $C_{if} = C_{if}(\bar{E}, |\Delta|)$ as previously noted by Keck and Carrier.[2] On expanding C_{if} about E_i in terms of the expansion parameter Δ, which is assumed small, then

$$C_{if}(\bar{E} = E_i + \tfrac{1}{2}\Delta, |\Delta|) = \sum_{n=0}^{\infty} \frac{\Delta^n}{n!}\left(\frac{1}{2}\right)^n \left(\frac{\partial^n C_i}{\partial E_i^n}\right), \tag{3.6}$$

where C_i is $C_{if}(\bar{E} = E_i, |\Delta|)$. The general moments (3.5) are therefore determined from

$$m! D_i^{(m)}(E_i) = \sum_{n=1,3,5}^{\text{odd}} (2^n n!)^{-1} \left[\frac{\partial^n F_i^{(m+n)}}{\partial E_i^n}\right]; \quad m \text{ odd}, \tag{3.7a}$$

$$= \sum_{n=0,2,4}^{\text{even}} (2^n n!)^{-1} \left[\frac{\partial^n F_i^{(m+n)}}{\partial E_i^n}\right]; \quad m \text{ even}, \tag{3.7b}$$

which involves only the terms

$$F_i^{(s)}(E_i) \doteq \int_{-D}^{\infty} \Delta^s C_i(E_i, |\Delta|) dE_f, \tag{3.8}$$

with s even. Terms with s odd vanish since D is effectively infinite (~ 5 eV).

For equilibrium, γ_i in Eq. (3.4) is unity and the equilibrium current can then be expressed, with the aid of Eq. (3.7) as

$$\tilde{J}_i = \sum_{n=0}^{\infty} (-1)^n \left[\frac{\partial^n D_i^{(n+1)}}{\partial E_i^n}\right] = \sum_{n=0,2}^{\text{even}} \sum_{j=0,2}^{\text{even}} (n-2j)[2^{j+1}(n+2)!(j+1)!]^{-1} \times \frac{\partial^{j+n+1} F_i^{(j+n+2)}}{\partial E_i^{j+n+1}}. \tag{3.9}$$

This new form clearly shows that the coefficient of its first term $\partial F_i^{(2)}/\partial E_i$, which arises from the leading term of the expansion (3.7) for both $D_i^{(1)}$ and $\partial D_i^{(2)}/\partial E_i$, is identically zero. The coefficient of the second term $\partial^3 F_i^{(4)}/\partial E_i^3$, which is the net balance of the second term in the expansion (3.7) for both $D_i^{(1)}$ and $\partial D_i^{(2)}/\partial E_i$ and of the leading term in the expansion (3.7) for both $\partial^2 D_i^{(3)}/\partial E_i^2$ and $\partial^3 D_i^{(4)}/\partial E_i^3$, is also zero. The leading nonvanishing contribution to Eq. (3.9) is $[-\frac{1}{576}\partial^5 F_i^{(6)}/\partial E_i^5]$ which is the net balance of the third terms in the expansion (3.7) for both $D_i^{(1)}$ and $\partial D_i^{(2)}/\partial E_i$ and of the second terms in the expansion (3.7) for both $\partial^2 D_i^{(3)}/\partial E_i^2$ and $\partial^3 D_i^{(4)}/\partial E_i^3$. The consistent neglect of $\partial^4 D_i^{(5)}/\partial E_i^4 \sim \partial^5 F_i^{(6)}/\partial E_i^5$ and higher-order derivatives demands both the neglect in Eq. (3.4) of terms with $n > 4$ and the neglect in Eqs. (3.7a) and (3.7b) of terms with $n > 5$ and $n > 4$, respectively. Hence, the equilibrium current

$$\tilde{J}_i \approx D_i^{(1)} - \frac{\partial D_i^{(2)}}{\partial E_i} + \frac{\partial^2 D_i^{(3)}}{\partial E_i^2} - \frac{\partial^3 D_i^{(4)}}{\partial E_i^3} \equiv 0 \tag{3.10}$$

is exact to fourth order in the moments and is identically zero! Relationships between even and odd moments can be obtained from Eq. (3.7) by neglecting $F_i^{(6)}$ and higher terms, i.e., $D_i^{(5)}$ and higher moments, to give

$$D_i^{(1)} = \frac{\partial}{\partial E_i}\left[D_i^{(2)} - \frac{\partial^2 D_i^{(4)}}{\partial E_i^2}\right] \tag{3.11a}$$

and

$$D_i^{(3)} = 2\frac{\partial}{\partial E_i} D_i^{(4)}, \tag{3.11b}$$

which also ensure zero equilibrium current. In view of Eq. (3.11) note that equilibrium ($\tilde{J}_i = 0$) is obtained only when the current (3.4) is expanded to even order.

With the aid of Eq. (3.10), the nonequilibrium current (3.4) to fourth order in moments $D_i^{(m)}$ is

$$J_i^{(4)}(E_i,t) = -\left[D_i^{(2)} - 2\frac{\partial D_i^{(3)}}{\partial E_i} + 3\frac{\partial^2 D_i^{(4)}}{\partial E_i^2}\right]\left[\frac{\partial \gamma_i}{\partial E_i}\right] + \left[D_i^{(3)} - 3\frac{\partial D_i^{(4)}}{\partial E_i}\right]\left[\frac{\partial^2 \gamma_i}{\partial E_i^2}\right] - D_i^{(4)}\left[\frac{\partial^3 \gamma_i}{\partial E_i^3}\right] \tag{3.12}$$

which is the differential representation (up to and including the fourth-order moment $D_i^{(4)}$) of the double integral

$$J(E,t) = \int_E^{\infty} dE_i \int_{-D}^{E} [\gamma_f(t) - \gamma_i(t)] C_{if}\, dE_f \tag{3.13}$$

for the exact current (2.4). The differential form (3.12) is the Fokker–Planck current to fourth order since the general Fokker–Planck expansion can be employed for any variable whose changes are small in comparison with averaged characteristic values, e.g., the collisional energy change Δ here is assumed small relative to the thermal energy kT of the gas bath.

Upon use of the approximations (3.11), which are internally consistent to neglect of moments higher than $D_i^{(4)}$, Eq. (3.12) reduces to

$$J_i^{(4)}(E_i,t) = -\left[D_i^{(2)} - \frac{\partial^2 D_i^{(4)}}{\partial E_i^2}\right]\left[\frac{\partial \gamma_i}{\partial E_i}\right] - \frac{1}{2} D_i^{(3)}\left[\frac{\partial^2 \gamma_i}{\partial E_i^2}\right] - D_i^{(4)}\left[\frac{\partial^3 \gamma_i}{\partial E_i^3}\right]. \tag{3.14}$$

Inserting the ansatz (2.8) in Eq. (3.12), then Eq. (2.6) with Eq. (3.12) yields

$$\frac{dn_i(E_i,t)}{dt} = -[\gamma_c(t) - \gamma_s(t)]\frac{\partial j_i(E_i)}{\partial E_i}, \tag{3.15}$$

where in terms of the stochastic probability P_i^D that state i dissociates, the time-independent background current to fourth order is

$$j_i^{(4)}(E_i) = -\left[D_i^{(2)} - 2\frac{\partial D_i^{(3)}}{\partial E_i} + 3\frac{\partial^2 D_i^{(4)}}{\partial E_i^2}\right]\left[\frac{\partial^3 P_i^D}{\partial E_i}\right] + \left[D_i^{(3)} - 3\frac{\partial D_i^{(4)}}{\partial E_i}\right]\left[\frac{\partial^2 P_i^D}{\partial E_i^2}\right] - D_i^{(4)}\left[\frac{\partial^3 P_i^D}{\partial E_i^3}\right]. \tag{3.16}$$

B. Diffusion equation and current for termolecular recombination

On ignoring moments $D_i^{(3)}$ and higher, the (diffusional) current (3.16) is

$$j_d(E_i) = -D_i^{(2)}\frac{\partial \bar{P}_i^D}{\partial E_i} = D_i^{(2)}\frac{\partial P_i^S}{\partial E_i}, \tag{3.17}$$

so that Eq. (3.15) is

$$\frac{dn_i(E_i,t)}{dt} = [\gamma_c(t) - \gamma_s(t)]\frac{\partial}{\partial E_i}\left[D_i^{(2)}\frac{\partial P_i^D}{\partial E_i}\right], \tag{3.18}$$

which is a diffusion equation in energy space. The moment $D_i^{(2)} = \frac{1}{2}d/dt\ \langle \Delta E_i^2 \rangle$ is the diffusion coefficient (energy^2 s^{-1}) in energy space. This type of streaming equation has been previously derived via other techniques by Pitaevskii[1] for electron–ion recombination under highly nonequilibrium conditions when $\gamma_c \gg \gamma_s$ so that $\gamma_i = P_i^D\gamma_c$ in Eq. (2.6), and by Keck and Carrier[2] for heavy-particle association/dissociation. It has been investigated by Landon and Keck,[3] by Mahan[5], and by Bates and Zundi[6] for highly nonequilibrium ($\gamma_c \gg \gamma_s$) termolecular ion–ion recombination. By explicitly including here the factor $(\gamma_c - \gamma_s)$ via the ansatz (2.8), Eqs. (3.15) and (3.18) for all $\gamma_{c,s}$ help to emphasize the evolution via termolecular recombination and dissociation (into ion products) of the subsystems (A–B) towards thermodynamic equilibrium with the gas M, attained when $\gamma_c \to \gamma_s \to 1$.

Another advantage of the ansatz (2.8) is that the intermediate block of highly excited levels can be taken to be in quasi-steady-state (QSS), i.e., $\partial n_i/\partial t \approx 0$ in either Eq. (2.9) or (3.18), *for all times*. The QSS-diffusional current (3.17) is constant over $\mathscr{E}$, so that the solution of Eq. (3.17) subject to conditions,

$$P_i^D(-S) = 0, \quad P_i^S(-S) = 1 \tag{3.19}$$

is

$$P_d^D(E_i) = -j_d\left[\int_{-S}^{E_i} dE/D^{(2)}(E)\right] = 1 - P_d^S(E_i), \tag{3.20}$$

where the subscript d denotes quantities associated with the diffusion equation (3.18). Various levels of approximation readily follow:

(a) Since

$$P_i^D(0) = 1, \quad P_i^S(0) = 0, \tag{3.21}$$

then Eq. (3.20) yields

$$-j_d^{(\rho)} = \left[\int_{-S}^{0} dE/D^{(2)}(E)\right]^{-1} = \alpha_\rho \tilde{N}_A \tilde{N}_B \tag{3.22}$$

for the downward diffusional current which, when compared with Eq. (2.20) provides the recombination rate α_ρ of Pitaevskii,[1] adopted for ion–ion recombination by Landon and Keck[3] and by Mahan.[5] Note that the current (3.22) is the inverse of the area under the curves in Fig. 2(a), and that Eq. (3.20) for the stabilization and disruption probabilities $P_i^{S,D}$ at energy E_i are the respective ratios of the areas which correspond to the energy ranges $(0 \to E_i)$ and $(E_i \to -S)$ to the total area.

(b) Rather than requiring Eq. (3.21) for the probabilities, j_d in Eq. (3.20) can be fixed by inserting Eq. (3.20) directly into Eq. (2.24) for $j(0)$ to give

$$-j(0) = \int_0^\infty dE_i \int_{-D}^{0} C_{if}\,dE_f + j_d \int_0^\infty dE_i \times \int_{-D}^{0} C_{if}\,dE_f \left\{\int_{-S}^{E_f} dE/D^2(E)\right\}. \tag{3.23}$$

On equating the exact current $j(0)$ in Eq. (3.23) with the diffusional current j_d, then

$$-j_d^{(k)}(0) = \left[\int_0^\infty dE_i \int_{-D}^{0} C_{if}\,dE_f\right]\left\{1 + \int_0^\infty dE_i \times \int_{-D}^{0} C_{if}\,dE_f \int_{-S}^{E_f} dE/D^{(2)}(E)\right\}^{-1} = \alpha_K \tilde{N}_A \tilde{N}_B, \tag{3.24}$$

which yields the expression of Keck[4] for α. The term in braces, $\{\ \}^{-1}$ is simply the ratio of the downward diffusional current to the one-way equilibrium current across the dissociation neck.

(c) Another possibility in similar vein to (b) is to insert Eq. (3.20) directly into Eq. (2.25) for $j(-S)$ to give

$$j_d(-S) = \left[\int_{-D}^{-S} dE_i \int_{-S}^{\infty} C_{if}\,dE_f\right] \times \left\{1 + \int_{-D}^{-S} dE_i \int_{-S}^{0} C_{if}\,dE_f \times \int_{-S}^{E_f} dE/D^2(E)\right\}^{-1} = \alpha_K \tilde{N}_A \tilde{N}_B, \tag{3.25}$$

where the term in braces, $\{\ \}^{-1}$, is simply the ratio of the upward diffusional current across $-S$ to the one-way equilibrium current upward across $-S$.

The feature common to all the above procedures (a)–(c) is that the required current (3.17) depends upon the accuracy of the gradient (dP_i^D/dE_i) which, due to the neglect of higher derivatives in Eq. (3.16), is described by the diffusion equation (3.18) less precisely than are the actual diffusion QSS solutions, i.e., Eq. (3.18) may furnish accurate P_i^D but relatively inaccurate derivatives. More importantly, however, is that Eq. (2.20), which is valid only under exact QSS-condition (2.18) of the exact Master equation (2.19) has been invoked for the diffusional currents $j_d^{(\rho)}$ of Eq. (3.22) and $j_d^{(k)}$ of Eq. (3.24) which are QSS solutions of the different and approximate diffusional equation (3.18).

The QSS solution of Eq. (3.18) subject to both constraints (3.19) and (3.21) is

$$P_d^S(E_i) = \left\{\int_{E_i}^{0} dE/D^{(2)}(E)\right\}\left\{\int_{-S}^{0} dE/D^{(2)}(E)\right\}^{-1} \tag{3.27}$$

for the probability that any level E_i in block $\mathscr{E}$, once accessed by collision, has "associative" character. The probability that level E_i has "dissociative" character is the complementary function

$$P_d^D(E_i) = \left\{\int_{-S}^{E_i} dE/D^{(2)}(E)\right\}\left\{\int_{-S}^{0} dE/D^{(2)}(E)\right\}^{-1}. \tag{3.28}$$

Thus, both functions are constrained to vary monotonically between zero and unity as does the exact numerical solution to the integral equation (2.18) so that, when compared with the exact numerical values, will involve less error than their corresponding derivatives

$$\frac{\partial P_i^{A,D}}{\partial E_i} = \mp \{D_i^{(2)}(E_i)\}^{-1} j_d^{(p),k} \tag{3.29}$$

appropriate to currents (3.22) and (3.24) in schemes (a) and (b) above.

C. Calculations for termolecular recombination at low N

The well developed case[9-12] of termolecular ion–ion recombination

$$A^+ + B^- + M \rightarrow AB + M \tag{3.30}$$

serves as a case study for assessing the accuracy of the diffusion approaches of Secs. III A and III B. The recombination coefficient α has previously been represented[9,17] very accurately by the sum

$$\alpha = \alpha_1 + \alpha_2 \tag{3.31}$$

of coefficients α_i obtained by considering separate contributions from (A^+–M) and (B^-–M) *binary* collisions ($i = 1$ and 2, respectively). The exact numerical rates α_i are obtained by inserting the exact numerical solution of the integral equation (2.18), the QSS condition into Eq. (2.32) for the current $j(-E_i)$. The rates α_i have been tabulated[9-11] as a function of the mass-ratio parameter:

$$a_i = M_j M_3 / M_i (M_1 + M_2 + M_3), \tag{3.32}$$

where M_i are the masses of species A^+, B^-, and M, $i = 1, 2$, and 3, respectively and where the set (i, j) is equal to (1,2) or (2,1) for $(1-3)$ or $(2-3)$ collisions, respectively.

Expressions for the equilibrium rate C_{if} appropriate to the three classes—polarization,[11] charge–transfer,[8,10] and hard-sphere[10]—of ion–neutral interactions have been previously derived.[9-11] Calculations have been performed here for the exact QSS-rates α_E that rise from 1–3 collisions and for the corresponding diffusional rates, (3.22) for α_P and (3.24) for α_K of Pitaevskii[1] and Keck,[4] respectively. Little discernable difference was found between α_P and α_K which may now be simply called the diffusional rates α_D obtained when the diffusional current (3.17) is inserted in Eq. (2.20). Previous results[9-11] were based on the solution of, at most, 36 coupled algebraic equations, the discretized equivalent representation of Eq. (2.18). Present calculations solve 100 coupled equations required for convergence in α for small and large mass parameters (3.32).

Table I provides present values of the ratio α_D/α_E for the various interactions over the full range of mass parameter a_1. Small $a \approx 10^{-3}$ corresponds to collisional recombination of heavy ions ($M_1 \approx M_2 \gg M_3$) in a much lighter (electron) gas, intermediate $a(=1/3$ for $M_1 = M_2 = M_3)$ corresponds to normal mass components, and large $a = 10^3$ for $M_1 \ll M_2 \approx M_3$ corresponds to electron–ion recombination in an ambient gas. The cases of small and large a involve energy transfers which are very much less than the energy kT of the gas so that the diffusional (weak collision) approach is likely then to be valid.

As Table I shows, the diffusional rates are reliable, as expected, only for recombination in a vanishingly light gas ($a \approx 10^{-3}$) or for electron–ion recombination ($a \approx 10^3$) in a general gas, the case for which Pitaevskii[1] designed his diffusional treatment. The diffusional rates are higher by between a factor of 3–9 for intermediate $a \sim 1$. As the ion–neutral interaction varies from polarization attraction to hard-sphere repulsion and then to charge–transfer interaction, the energy change in the ion–neutral collision becomes progressively larger [see Fig. 2(a) and 2(b)] so that the diffusional rates (based on weak collisions) become less accurate, as shown directly by the variation of entries in Table I for a specified mass parameter a.

Since Eq. (3.17) predicts zero current in both the fully dissociated and fully associated blocks, $\mathscr{C}$ and $\mathscr{S}$, respectively, the diffusional current (3.17) is therefore discontinuous, zero in $\mathscr{C}$, j_d in $\mathscr{E}$ and zero in $\mathscr{S}$. The diffusion rates (3.22) of Pitaevskii and (3.24) of Keck are therefore expected to be valid only in the limit of vanishingly small currents and rates α of recombination. This is confirmed in Table I for

TABLE I. Variation of the ratio (α_D/α_E) and (α_{BN}/α_E) with mass-ratio parameter a for 1–3 collisions and with the various 1–3 interactions: polarization (POL), hard-sphere (HS), and symmetrical resonance charge–transfer (CX). The exact, diffusional, and bottleneck rates are α_E, α_D, and α_{BN}, respectively.

	α_D/α_E			α_{BN}/α_E		
a	POL[a]	HS[a]	CX[b]	POL	HS	CX
0.001	1.001	1.013	1.030	32.447	25.782	16.996
0.01	1.163	1.222	1.321	8.369	7.336	5.513
0.1	2.131	2.739	3.522	3.354	2.939	2.384
1/3	3.360	4.967	6.840	2.541	2.215	1.865
1.0	4.060	6.604	9.272	2.333	2.015	1.722
10.0	2.131	3.510	⋯	3.354	2.746	⋯
100.0	1.163	1.455	⋯	8.369	6.302	⋯
1000.0	1.001	1.093	⋯	32.447	20.233	⋯

[a] In POL and HS, small a implies ion–ion recombination in a vanishingly light gas and large a ($\sim 10^3$) implies electron–ion recombination in a normal-mass gas.
[b] In CX small a implies $M_2 \ll M_1 = M_3$ and $a = 1$ implies $M_2 \gg M_1 = M_3$.

the limiting cases of small and large a. Then the actual rate for electron–ion collisional recombination in a gas is[7] $\alpha_E \sim 10^{-9}\,\mathrm{cm^3\,s^{-1}}$ at STP, which is three orders of magnitude less than the rate $\alpha_E \sim 10^{-6}\,\mathrm{cm^3\,s^{-1}}$ at STP (cf. Ref. 19) for ion–ion recombination a similar mass gas.

Another reason for the inadequacy of the diffusion approach as previously applied to general-mass cases is also apparent. As Figs. 3(a) and 3(b) show, the diffusion equation (3.18) in general furnishes fairly accurate probabilities $P_l^{A,D}$, Eqs. (3.29) and (3.30), but less reliable gradients $dP_l^{A,D}/dE_l$.

In an effort to assess the relative importance between using relatively accurate distributions P_l^S within the integral (2.23) or differential (3.17) forms of the collision integral of the Master equation, assume that the intermediate block $\mathscr{B}$ between blocks $\mathscr{G}$ and $\mathscr{S}$ is absent, i.e.,

$$P^S(E_l) = \begin{cases} 0, & -E < E_l < \infty \\ 1, & -D < E_l < -E' \end{cases} \tag{3.33}$$

where $-E$ is some bound energy level. The current (2.15) then reduces to

$$-j_{BN}(-E) = \int_{-E}^{\infty} dE_i \int_{-D}^{-E} C_{if}\, dE_f = \alpha_{BN}(E)\tilde{N}_A\tilde{N}_B, \tag{3.34}$$

which is the one-way equilibrium downward current across level $-E$. As $-E$ is varied, this current achieves a minimum[10] at energy $-E^*$ ($\simeq -2kT$) which therefore acts as a bottleneck[13] to the recombination which proceeds at rate $\alpha_{BN}(E^*)$. The ratio of α_{BN} at the bottleneck E^* to the exact numerical rate α_E is displayed in Table I for the various interactions. The bottleneck method fails quite markedly for small and large mass parameters a, where the diffusion current is by contrast successful, and becomes much more reliable than the diffusion approach at intermediate $a(\simeq 1)$. For a given a, less error is involved for stronger collisions in harmony with Eq. (3.34) being a strong collision approximation. Since Eq. (3.33) assumes the least possible knowledge of the probabilities P_l^S(subject to the constraints) but an integral form (3.34) to the collision rate, it follows that fairly accurate distributions are required at small and large a where the collision rate and dynamics are weak, so that the discontinuous integral form (2.23) does reduce indeed to the continuous streaming form (3.17). For intermediate a when the energy changes are certainly not weak, inclusion of the integral form (2.22) is apparently more important than the use of fairly accurate distributions (which in any event are constrained to vary between unity and zero at the boundaries of block $\mathscr{B}$). Note also that the diffusional and bottleneck results are always greater than the exact QSS rates, in accord with predictions of the variational principle recently proposed.[18] The bottleneck method provides the *least* of the one-way equilibrium rates—the least upper limit—across a bound level. The diffusion method incorporates the effect of the net downward–upward collisional transitions.

The closeness exhibited in Fig. 3(a) between the diffusional probabilities, (3.27) and (3.28), and the exact numerical probabilities may be utilized in two ways. First, an

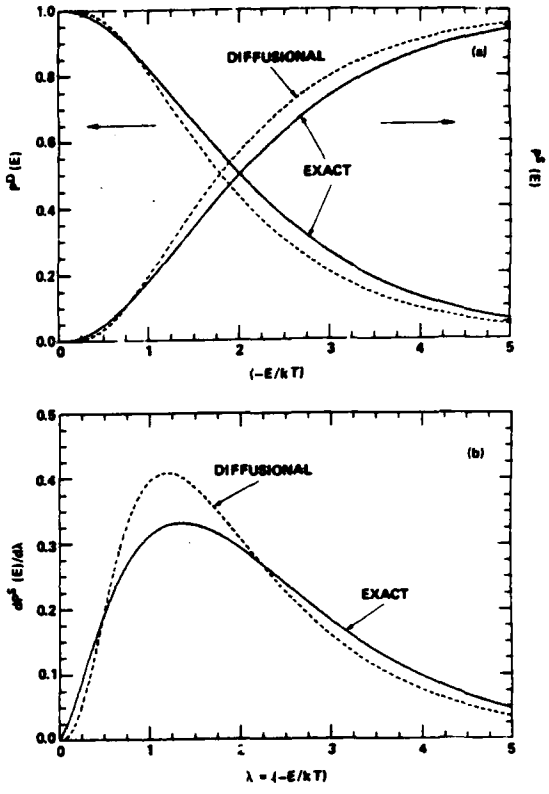

FIG. 3. (a) Probabilities $P^{S,D}$ for stabilization and dissociation of an ion-pair bound with energy $E_l = -\lambda kT$. Equal-mass species and charge-transfer ion–neutral collisions are assumed. —: Exact QSS solution of Eq. (2.18). - - -: Diffusional approximation, Eqs. (3.27) and (3.28). (b) Derivatives $(dP^S/d\lambda)$ of stabilization probability P^S. From numerical solution of Eq. (2.18) and from diffusional approximation, Eq. (3.29).

iterative procedure[4]

$$P^{(n+1)}(E_l)\int_{-D}^{\infty} C_{lf}\, dE_f = \int_{-D}^{\infty} P^{(n)}(E_f) C_{lf}\, dE_f \tag{3.37}$$

to the solution of the integral equation (2.18) can be developed by using the diffusional analytical probabilities (3.27) as the starting ($n = 0$) solution. It is found here that convergence to within 1% of the exact solution can be in general achieved after five iterations, so that accurate rates can then be determined from Eqs. (2.23)–(2.25) since the QSS-condition (2.18) is satisfied.

Since the diffusional probabilities (3.27) and (3.28) are reasonably accurate, a second possibility is to insert them directly into the current (2.23). This procedure, at first sight attractive, is however inconsistent, in that the diffusional probabilities while satisfying quasi-steady-state (QSS) of the diffusional equation (3.18) in block $\mathscr{B}$, *do not* satisfy the condition (2.18) for QSS of the Master equation (2.9) on which Eq. (2.23) relies. The resulting current (2.15) will therefore not be a constant in block $\mathscr{B}$. This is demonstrated by Fig. 4 which compares the exact downward current $-j_E(E_l)$ past level E_l obtained from the solution of Eq.

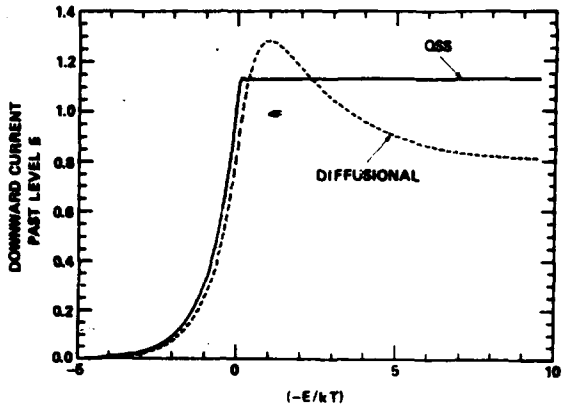

FIG. 4. Comparison of currents, Eq. (2.15), past energy level $-E=-\lambda kT$, obtained (—) from exact solution of Eq. (2.18) and from (- - -) diffusion probabilities Eq. (3.27). Equal-mass species and hard-sphere ion–neutral collisions are assumed. The current is normalized to $(2\alpha_T \bar{N}_A \bar{N}_B)$ where α_T is the Thomson rate, Eq. (4.1).

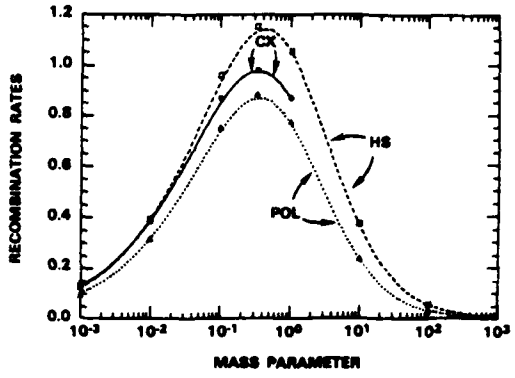

FIG. 5. Normalized rates R_T, Eq. (4.2), for ion–ion recombination in a dilute gas as a function of mass parameter a, Eq. (3.32) for various ion–neutral interactions: HS (hard-sphere), CX (charge–transfer) and POL (polarization). —: exact rates. □, ○, Δ: rates obtained with diffusional probabilities, Eq. (3.27), in basic Eq. (2.16) for HS, CX, and POL interactions.

(2.18) in Eq. (2.23) with the approximate downward current $-j_A(E_l)$ obtained by inserting Eq. (3.27) in Eq. (2.23). The diffusional current through the bound levels is far from constant over the block $\mathcal{E}$ of highly excited levels and hence, Eq. (2.20) cannot be used for steady-state rates. The figure also shows that assignment of a bound level E_l for determination of α from Eq. (2.23) is uncertain. Since the current $j(-E)$ exhibits a very rapid variation in the neighborhood of the dissociation limit (at zero energy), use of Eq. (2.24) for $j(0)$ is therefore a risky procedure, the exact value of $j(0)$ being $\sim 50\%$ higher than the approximate $j(0)$. Some defense can be made by calculating Eq. (2.23) at the bottleneck energy $E^* \sim -2kT$ where the diffusional and exact currents agree. This adoption is however not firmly based.

The basic reason for the inconsistency of using the diffusional probabilities (3.27) in Eq. (2.23) is not that the diffusional probabilities are not sufficiently accurate for useful application, but is that the expression (2.23) based on identifying the association rate with the current is not appropriate for the use of approximate probabilities, which do not satisfy the basic condition (2.18) for such identification.

IV. BASIC RATE WITH DIFFUSIONAL PROBABILITIES

The exact rates α_E obtained in Sec. III C from Eq. (2.18) in Eq. (2.23) for the various ion–neutral interactions are normalized[10,11] to the corresponding Thomson rate

$$\alpha_T = \tfrac{4}{3}\pi(R_e/\beta)^3(3kT/M_{12})^{1/2}\sigma_0 N, \quad \beta = 3/2, \quad (4.1)$$

where R_e is the natural unit (e^2/kT) for Coulombic attraction between the ions 1 and 2. The integral cross section σ_0 for 1–3 elastic collisions at relative energy $(\frac{1}{2}kT)$ is taken in Eq. (4.1) to be $2\sigma^x$, $2\pi(pR_e/3)^{1/2}$, and σ_0^H, respectively for symmetrical resonance charge–transfer collisions with cross section σ^x, for polarization (orbiting) collisions in terms of the polarizability p of the gas M, and for hard-sphere collisions with cross section σ_0^H.

Approximate rates α_A may now be determined by inserting P_l^S, the diffusional (approximate) probabilities (3.27) into the basic expression (2.16) which does not rely on the use of exact (QSS) P_l^S. Figure 5 displays a comparison of the corresponding ratios,

$$R_T = (M_1/M_{12})(\alpha/\alpha_T), \quad (4.2)$$

where α is taken as the exact rate α_E or the approximate rate α_A, which arises from 1–3 collisions. The exact rates reproduce those previously presented.[10,11] The present study adopts a 100-point quadrature throughout, rather than 36 and 18 used in Refs. 10 and 11, respectively, in order to obtain convergence at small and large a.

Excellent agreement between α_E and α_A is obtained over the full range of the mass parameter a, Eq. (3.32) for a_1 all the way, from $a \approx 10^{-3}$ for association of heavy ions in a light (electron) gas, to intermediate $a \approx 1/3$ for equal mass species and up to large $a \approx 10^3$ which corresponds to electron–ion recombination in a gas. As expected, greatest departures occur for the case of equal mass which involves the largest energy transfer so that the diffusional probabilities would also show their greatest departure from the exact probabilities as in Fig. 3(a). For this case $(a = 1/3)$, the diffusional result corresponding to hard-sphere collisions, which in turn involve largest energy transfers (cf. Fig. 2), exhibit the largest of small departures. The present diffusional treatment is also excellent over all of the various classes of 1–3 interaction considered.

V. ION–ATOM ASSOCIATION AT LOW GAS DENSITIES

The above theory may now be suitably modified to cover ion–atom association

$$A^+ + B + M \underset{k}{\overset{\alpha}{\rightleftarrows}} AB^+ + M \quad (5.1)$$

of atomic species A^+ and B in a low density gas M. In contrast to ion–ion recombination (3.30) where an equilibrium distribution over internal angular momentum L_l is established[12] the A^+–B attraction can support centrifugal barriers so that nonequilibrium distributions $n_l(E_l, L_l^2; t)$ over

both E_i and L_i^2 must be acknowledged. Thus, the ansatz (2.8) is replaced by

$$\gamma_i(E_i,L_i^2;t) = \frac{n_i(E_i,L_i^2;t)}{\bar{n}_i(E_i,L_i^2)} = P_i^D(E_i,L_i^2)\gamma_c(t) + P_i^S(E_i,L_i^2)\gamma_s(t) \overset{t\to\infty}{\to} 1, \quad (5.2)$$

where $P_i^S = 1 - P_i^D$, the probability of stabilization of (E_i,L_i^2) pairs by subsequent multicollisions, is zero for dissociated pairs and unity for fully associated pairs.

Bates and McKibbin[14] found that a delta function approximation $\delta(L_i^2 - L_f^2)$ for $(E_i,L_i^2 \to E_f,L_f^2)$ transitions was quite satisfactory. The above analysis in Secs. III A and III B for energy change alone can then be immediately modified to yield corresponding results for the stabilization probabilities $P_i^S(E_i,L_i^2)$ for quasibound and bound states. Thus, the diffusion approximation for the bound and quasibound level yields

$$P_d^S(E_i,L_i^2) = \left[\int_{E_i}^{U_i} dE/D^{(2)}(E,L_i^2)\right] \times \left[\int_{-S}^{U_i} dE/D^{(2)}(E,L_i^2)\right]^{-1}, \quad (5.3)$$

where $U_i(L_i^2)$ is the energy at the top of the centrifugal barrier of the effective interaction

$$V_i(R) = V(R) + L_i^2/2mR^2. \quad (5.4)$$

In terms of C_{if} the one way equilibrium rate per unit $dE_i\,dL_i^2\,dE_f\,dL_f^2$ for $(E_i,L_i^2 \to E_f,L_f^2)$ collisional transitions, the diffusion coefficient is

$$D^{(2)}(E_i,L_i^2) = \frac{1}{2}\int_{-D}^{\infty}(E_f - E_i)^2\,dE_f \times \int_0^{L_{0f}^2} C_{if}(E_i,L_i^2;E_f,L_f^2)dL_f^2, \quad (5.5)$$

where L_{0f} is the maximum angular momentum for fixed E_f. For dissociated levels P_d^S is zero. The association rate corresponding to the basic rate (2.16) is then given by

$$\alpha\tilde{N}_A\tilde{N}_B = \int_{-D}^{\infty} dE_i \int_0^{L_{0i}^2} P_i^S\,dL_i^2 \int_{-D}^{\infty} dE_f \times \int_0^{L_{0f}^2}(P_i^S - P_f^S)C_{if}\,dL_f^2, \quad (5.6)$$

where the stabilization probabilities P_i^S are given by Eq. (5.3).

VI. SUMMARY

On introduction of stochastic probabilities $P_i^{S,D}(E_i)$ that ion pairs A–B with internal energy E_i will be stabilized or disrupted by collisions with a thermal bath of gas M, and upon the use of the ansatz (2.8) for their normalized distributions $\gamma_i(t)$ at time t, the basic Master equation (2.1), rate (2.2) and current (2.4) has been transformed into corresponding equations (2.9)–(2.11) which are separable in E_i and t. The diffusional equation (3.18), yields, for systems of general mass, accurate probabilities $P_i^{S,D}$ but very inaccurate currents (3.22)–(3.25) (cf. Fig. 3 and Table I). Identification as in Eq. (2.20) of association rates α with current, is valid only under QSS quasi-steady-state condition (2.18), appropriate to the original Master equation (2.9). Since the diffusional probabilities do not satisfy this condition, the diffusional current in general, may not be identified with the rate α. As Table I shows, the resulting diffusional rates (3.22)–(3.25), are therefore not reliable[2–6] except for those cases in which the current is relatively small, i.e., for collision electron–ion recombination[1] in a gas and for ion–ion recombination in a vanishingly light gas.

A new expression (2.11) or (2.16) derived[16] for the rates, is more appropriate for use under general conditions, as when QSS is not satisfied. When QSS is satisfied, Eq. (2.16) reduces to the current (2.23). The QSS rates are minimum (Ref. 18 and work in progress). The rate (2.16) is required when approximate probabilities are used, as here.

The diffusional probabilities can also be used in an iterative solution[4] of the QSS-condition (2.18) to provide highly accurate probabilities (to within 1%) after a few iterations and hence accurate QSS-rates (2.23)–(2.25).

Application of the diffusional equation (3.18) to general systems represents an accurate procedure provided the solutions $P_i^{S,D}$ are inserted in the appropriate and more basic expression (2.16) for the rate, rather than into the derived expressions (3.17) or (2.13) for the diffusional or exact currents. Excellent agreement with the exact numerical QSS results for various classes of ion–neutral interactions over the full range of mass parameters for general systems has been obtained.

Finally, generalization (Sec. V) of the above analysis Secs. II and III to cover the distributions $n(E_i,L_i^2,t)$ of A–B pairs over their internal energy E_i and angular momentum L_i is straightforward. The resulting equations are appropriate to consideration of ion–atom association of atomic species in a gas.

ACKNOWLEDGMENT

This research is supported by the U.S. Air Force of Scientific Research under Grant No. AFOSR-84-0233.

[1] L. P. Pitaevskii, Sov. Phys.–DETP 15, 919 (1962); E. M. Lifshitz and L. P. Pitaevskii, in *Physical Kinetics* (Pergamon, Oxford, 1981), Chap. 2, pp. 89 and 102.
[2] J. C. Keck and G. Carrier, J. Chem. Phys. 43, 2284 (1965).
[3] S. A. Landon and J. C. Keck, J. Chem. Phys. 48, 374 (1968).
[4] J. C. Keck, in *Advances in Atomic and Molecular Physics*, edited by D. R. Bates and I. Estermann (Academic, New York, 1972) Vol. 8, p. 39.
[5] B. H. Mahan, J. Chem. Phys. 48, 2629 (1968).
[6] D. R. Bates and Z. Jundi, J. Phys. B 1, 1145 (1968).
[7] D. R. Bates and S. P. Khare, Proc. Phys. Soc. 85, 231 (1965).
[8] D. R. Bates and R. J. Moffett, Proc. Soc. London Ser. A 291, 1 (1966).
[9] D. R. Bates and M. R. Flannery, Proc. Soc. London Ser. A 302, 367 (1968).
[10] M. R. Flannery, J. Phys. B 13, 3649 (1980); 14, 915 (1981).
[11] D. R. Bates and I. Mendaš, J. Phys. B 15, 1949 (1982).
[12] D. R. Bates and I. Mendaš, J. Phys. B 8, 1770 (1975).
[13] S. B. Byron, R. C. Stabler, and P. I. Bortz, Phys. Rev. Lett. 8, 376 (1962).
[14] D. R. Bates and C. S. McKibbin, Proc. R. Soc. London Ser. A 339, 13 (1974).
[15] M. R. Flannery, J. Phys. B 20, 4929 (1987).
[16] M. R. Flannery, J. Phys. B 18, L 839 (1985).
[17] M. R. Flannery and T. P. Yang, J. Chem. Phys. 73, 3239 (1980).
[18] M. R. Flannery, in *Recent Studies in Atomic and Molecular Processes*, edited by A. E. Kingston (Plenum, New York, 1987), p. 167.
[19] M. R. Flannery, in *Applied Atomic Collision Physics*, edited by E. W. McDaniel and W. L. Nighan (Academic, New York, 1982), Vol. 3, p. 141.

3.4 Coupled Nearest-Neighbor and Uncoupled Intermediate Level Methods.

Termolecular recombination: Coupled nearest-neighbor limit and uncoupled intermediate levels limit

M. R. Flannery and E. J. Mansky
School of Physics, Georgia Institute of Technology, Atlanta, Georgia 30332

(Received 18 April 1988; accepted 15 June 1988)

Two extreme limits of collisional coupling in termolecular recombination are investigated. The coupled nearest neighbor (CNN) limit includes only couplings between neighboring excited energy levels of the associating species AB^*, while the uncoupled intermediate levels (UIL) limit includes only couplings between the fully dissociated reactants A^+ and B^- and each of the (assumed uncoupled) excited levels of AB^*, which are then coupled to the fully associated products AB. Comparison is made with results of previous exact and diffusion treatments.

I. INTRODUCTION

Analogy with a mathematically equivalent electrical network provides an effective framework whereby not only can the complicated multilevel collisional dynamics intrinsic to a master equation treatment of termolecular recombination

$$A^+ + B^- + M \rightarrow AB + M \qquad (1.1)$$

between atomic species A^+ and B^- in a gas M be analyzed in a different light[1,2] but also physically appealing models may be readily constructed. In previous reports,[2-4] the (exact) quasi-steady-state (QSS) master equation method,[3] the corresponding variational method,[2] and an approximate diffusional method[4] were considered. In this paper, two simple models prompted by considering the analogous electrical diagram (Fig. 1)are investigated. So as to emphasize the importance of collisional couplings between many excited levels in a realistic treatment of process (1.1), two extreme limits will be tested. The *coupled nearest-neighbor limit* includes only the coupling of a given excited level n with its lower neighboring level $n-1$. The limit of *uncoupled intermediate levels* includes only couplings from the (external) source block $\mathscr{C}$ of fully dissociated states of the reactants A^+ and B^- to each of the excited levels n assumed to be *uncoupled* within the (internal) block $\mathscr{E}$ and then the coupling from each of these uncoupled n to the (external) sink block $\mathscr{S}$ of fully associated levels of the products AB (cf. Fig. 1). The "*intermediate*" levels comprise block $\mathscr{E}$ which is *intermediate* between blocks $\mathscr{C}$ and $\mathscr{S}$.

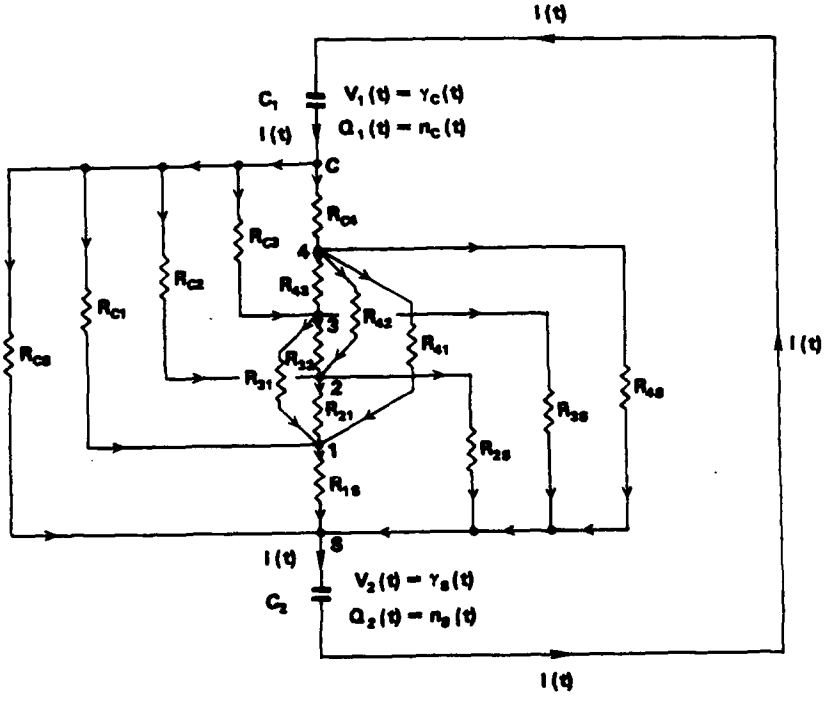

FIG. 1. (R, C) Electrical diagram (Ref. 2) appropriate to analysis of termolecular recombination, involving as an example, four excited levels ($n = 1,2,3,4$).

 0021-9606/88/194086-06$02.10

II. CONSTRUCTION

Termolecular recombination (1.1) may be described[4] via a *time-independent* treatment wherein equilibrium concentrations $\tilde{N}_A$ and $\tilde{N}_B$ of the fully dissociated atomic species A and B with relative energies E_i in the range $0 \leq E_i < \infty$, the reactant $\mathscr{C}$ block, are associated (a) by direct collisions into the product block $\mathscr{S}$ of fully associated molecular levels in the range $-S \geq E_i \geq -D$ maintained at zero population and (b) by a series of indirect transitions via the intermediate energy block $\mathscr{I}$ $(0 \geq E_i \geq -S)$ of highly excited levels. The indirect mechanism $\mathscr{C} \rightarrow \mathscr{I} \rightarrow \mathscr{S}$ is the most important[2-4] at thermal energies since the rate of the large energy transfers involved with direct $\mathscr{C} \rightarrow \mathscr{S}$ transitions is vanishingly small, by comparison. The lowest energy level of AB is $-D$, relative to the dissociated limit at zero energy, and $-S$ is a bound level below which the probability P_i^S of collisional stabilization of pairs in level E_i is by definition unity. The two key quantities are P_i^S which is unknown and the one-way equilibrium rate C_{if} which is given[3] in terms of the equilibrium number density of $\tilde{n}_i$ of levels of energy E_i per unit interval dE_i and the frequency ν_{if} for $E_i \rightarrow E_f$ transitions per unit interval dE_f by $\tilde{n}_i\, \nu_{if}$.

A hierarchy of approximate schemes are apparent via consideration[2] of process (1.1) in terms of the analogous electrical diagram displayed in Fig. 1. Here N discrete junctions ($\mathscr{I}$-block levels) n are at time-independent potentials P_n^S *below* the $\mathscr{C}$ block junctions C, all maintained at unit equipotential (due to the assumed equilibrium concentrations of A and B), or equivalently are at potentials $P_n^D = 1 - P_n^S$ *above* the zero potential of the $\mathscr{S}$ block junctions S (due to assumed zero concentration of AB). In terms of these voltages and of the conductances $C_{if} = R_{if}^{-1}$ of each element of resistance R_{if}, the rate constant deduced[2] from the power equation is then the effective conductance R^{-1} of the mathematically equivalent network. It follows from consideration of the power loss in the circuit that[2]

$$\alpha \tilde{N}_A \tilde{N}_B = \frac{1}{2} \int_{-D}^{\infty} dE_i \int_{-D}^{\infty} (P_i^S - P_f^S)^2 C_{if}\, dE_f \equiv R^{-1} . \tag{2.1}$$

Since the overall voltage drop is unity in the time-independent treatment, Eq. (2.1) is also the throughput electrical current. Only when the N nodes i in block $\mathscr{I}$ obey the Kirchoff current law, (KCL), or the following quasi-steady-state (QSS) equivalent condition for excited pairs:

$$P_i^S \int_{-D}^{\infty} C_{if}\, dE_f = \int_{-D}^{0} C_{if} P_f^S\, dE_f \tag{2.2}$$

does Eq. (2.1) reduce to $-j(0)$, the energy-space current

$$\alpha(0) \tilde{N}_A \tilde{N}_B = \int_0^{\infty} dE_i \int_{-D}^{0} C_{if} P_f^S\, dE_f = -j(0) \tag{2.3a}$$

across the dissociation limit at zero internal energy, or in general to

$$\alpha(-E) \tilde{N}_A \tilde{N}_B = \int_{-E}^{\infty} dE_i \int_{-D}^{-E} (P_f^S - P_i^S) C_{if}\, dE_f = -j(-E) , \tag{2.3b}$$

the constant energy-space downward current $-j(-E)$, across any arbitrary level of energy $-E$ in block $\mathscr{I}$. Two extreme limits may now be constructed.

(A) *Uncoupled intermediate levels (UIL) limit*: When the mainline entrance and exit channels of resistances R_{Cn} and R_{nS} defined in terms of collisional couplings by

$$R_{Cn}^{-1} = \int_0^{\infty} C_{in}\, dE_i \equiv C_{Cn} \tag{2.4}$$

and

$$R_{nS}^{-1} = \int_{-D}^{-S} C_{nf}\, dE_f \equiv C_{nS} , \tag{2.5}$$

respectively, are only included in the network for indirect passage between the reactant and product blocks $\mathscr{C}$ and $\mathscr{S}$ via junction n, the current I_n flowing past any of the uncoupled junctions n is given by

$$I_n [R_{Cn} + R_{nS}] = 1 , \tag{2.6}$$

since the voltage drop ($\mathscr{C} \rightarrow \mathscr{S}$) is unity and since n is not coupled to any other junction n' of intermediate block $\mathscr{I}$. The direct ($\mathscr{C} \rightarrow \mathscr{S}$) current

$$I_0 = R_{CS}^{-1} = \int_0^{\infty} dE_i \int_{-D}^{-S} C_{if}\, dE_f \tag{2.7}$$

is normally negligible but can be given by expression (2.6) since R_{fS} vanish for all nodes f in block $\mathscr{S}$. The voltage drop between junctions C and each isolated n is then

$$P_n^S = I_n R_{Cn} = \frac{C_{nS}}{C_{Cn} + C_{nS}} , \tag{2.8}$$

to be used in the basic power expression (2.1) for the rate constant.

Although expression (2.8) violates the KCL condition (2.2) required for reduction of Eq. (2.1) to Eq. (2.3), the QSS rate (2.3a) nonetheless provides the rate

$$\alpha_1(0) \tilde{N}_A \tilde{N}_B = \int_{-D}^{0} \left[\frac{C_{Cf} C_{fS}}{(C_{Cf} + C_{fS})} \right] dE_f \tag{2.9a}$$

$$= \left[\int_{-D}^{0} \alpha_f\, dE_f \right] \tilde{N}_A \tilde{N}_B \tag{2.9b}$$

which has several exemplary features. This rate is also the effective conductance obtained from the total electrical current $\Sigma_{n=0}^{N} I_n$ flowing between nodes C and S maintained at unit potential difference. Although invalid when compared to Eq. (2.8) in Eq. (2.1), expression (2.9) illustrates quite effectively (a) that the partial rate α_f of a reaction which proceeds via the series sequence $\mathscr{C} \rightarrow f$ and $f \rightarrow \mathscr{S}$ of transitions is given by the conductance

$$C_f = R_f^{-1} = [R_{Cf} + R_{fS}]^{-1} = \frac{C_{Cf} C_{fS}}{C_{Cf} + C_{fS}} \tag{2.10}$$

due to resistances R_{Cf} and R_{fS} connected in series and (b) that the overall rate α_1 of the reaction which proceeds via the parallel sequence involving each f is given by the conductance

$$C = R^{-1} = \sum_{f=0}^{N} R_f^{-1} = \sum_{f=0}^{N} C_f \tag{2.11}$$

of the effective network with resistances R_f $(f = 1,2,\ldots,N)$ connected in parallel. The resistance, $R_0 = R_{CS}$, of the $\mathscr{C}-$

$\mathscr{S}$ direct connection is included in Eq. (2.11). Expressions (2.9) provide illustrations of the theorem due to Bates.[1] The approximate QSS rate $\alpha_1(-E)$ as a function of $\mathscr{E}$ block energy $-E$ is obtained by inserting Eq. (2.8) in Eq. (2.3b). The first rate under test is given by the probability (2.8) inserted in the power expression (2.1).

(*B*) *Coupled nearest-neighbor* (*CNN*) *limit*: When resistors $R_{n,n-1}$ are only included in block $\mathscr{E}$, the throughput current I is given by

$$I=\left[R_{\mathrm{CN}}+\sum_{n=1}^{N} R_{n,n-1}\right]^{-1}, \tag{2.12}$$

where junctions in block $\mathscr{S}$ are again denoted by $n=0$. As the highest excited bound level $N\to\infty$, R_{CN} vanishes, and the voltage drop between junctions C and f is then

$$P_f^s = I\sum_{n=f+1}^{\infty} R_{n,n-1} = \left[\sum_{n=f+1}^{\infty} C_{n,n-1}^{-1}\right]\left[\sum_{n=1}^{\infty} C_{n,n-1}^{-1}\right]^{-1}, \tag{2.13}$$

which, when inserted in the power equation (2.1) yields the second rate under investigation. A simplified rate given by the effective conductance (or electrical current) in Eq. (2.12) is

$$\alpha_2\tilde{N}_A\tilde{N}_B = R^{-1}=\left[\sum_{n=1}^{\infty} C_{n,n-1}^{-1}\right]^{-1}, \tag{2.14}$$

which again illustrates the reaction-in-series principle of Bates.[1] The approximation (2.14) has been previously obtained for $(e\text{-}A^+)+e$ recombination.[5] In contrast to Eq. (2.9), the result (2.14) cannot be obtained from the energy-space current (2.3a) since connections between C and the various n are ignored.

Note that the key approximations CNN, Eq. (2.13), and UIL, Eq. (2.8), satisfy the correct boundary conditions

$$P_l^s(E_l=0)=0,$$
$$P_l^s(E_l=-S)=1 \tag{2.15}$$

for the probability P_l^s.

III. RESULTS

As a test of the above approximations the case of termolecular ion–ion recombination (1.1) is adopted since the association (exact) rate α_E has been well studied (cf. Ref. 3) over full variation of the mass parameter

$$a=\frac{M_B M_E}{M_A(M_A+M_B+M_E)} \tag{3.1}$$

pertinent to A^+–M collisions and over the following model (A^+–M) interactions: symmetrical resonance charge transfer (CX), polarization attraction (POL), and hard-sphere repulsion (HS). The masses of A^+, B^-, and M are M_A, M_B, and M_E, respectively.

The approximate probabilities labeled UIL and CNN are calculated from the limit (2.8) for uncoupled-intermediate levels and the limit (2.13) for coupled-nearest-neighbor, respectively. They are compared in Fig. 2(a) with the exact quasi-steady-state (QSS) solution of Eq. (2.2). The results, which pertain to termolecular recombination of equal mass species ($a=\frac{1}{3}$) for A^+–M collisions under polarization attraction (POL), are quite representative of other cases. Closer agreement of CNN with the exact results indicates that association tends to proceed via a sequence of small energy-changing transitions down the ladder of intermediate levels n, as expected, rather than via the indirect ($\mathscr{E}\to n\to\mathscr{S}$) larger energy-changing transitions of UIL, which involves each intermediate level n presumed uncoupled from one another. Moreover, both approximations appear robust with respect both to the number N ($=36$ and 72) of intermediate levels n adopted in block $\mathscr{E}$ and to the consequent decrease in spacing between the levels. The N pivots and spacings are selected by the highly accurate method prescribed in Ref. 6.

Since both approximations CNN and UIL are seen to satisfy the correct constraints (2.15), the overall agreement in Fig. 2(a) may however mask certain deficiencies. A more sensitive quantity of greater significance to recombination is the gradient (dP_l/dE_l), since, in the limit of small energy transfers, the energy-space current (2.3b) across $\mathscr{E}$ block level $-E$ reduces[4] to the diffusional current

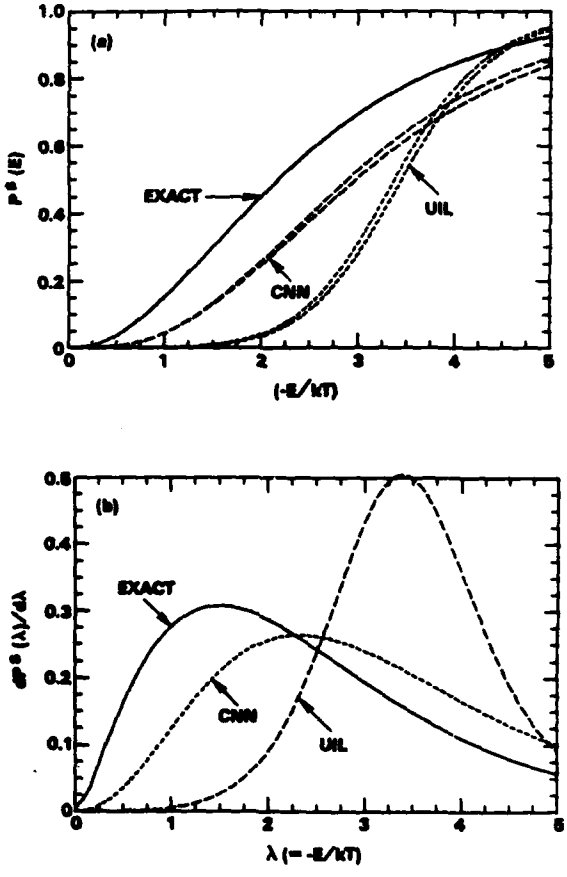

FIG. 2. (a) Stabilization probabilities (voltage drops) as a function of binding energy ($-E/kT$): EXACT [Eq. (2.2)]; CNN [Eq. (2.13)]; and UIL [Eq. (2.8)] with 72 pivots (upper curve) and 36 pivots (lower curve). (b) Corresponding derivatives.

$$j_d(-E) = D_i^{(2)}\left[\frac{dP_i^S}{dE_i}\right], \tag{3.2}$$

where the second-order energy-change moment is

$$D_i^{(2)}(E_i) = \frac{1}{2}\int_{-D}^{\infty}(E_f - E_i)^2 C_{if}\, dE_f . \tag{3.3}$$

The gradients shown in Fig. 2(b) are therefore expected to provide more reliable indicators of the extent of expected agreement between the corresponding rates.

This sensitivity is indeed confirmed in Figs. 3(a) and 3(b) which illustrate the quite different shapes for the variations with E of $-j(-E)$, the downward energy-space current (2.3b), obtained from both approximations. The currents (2.3b) are normalized to the exact QSS rate calculated from the numerical solution of Eq. (2.2) in Eq. (2.3b). Although α_E is then by definition, constant with respect to E variation, the E variation of the rate (2.3b) with the approximate probabilities (2.8) and (2.13) indicates the severe breakdown of QSS, due to the differences displayed in Figs. 2(a) and 2(b). The following points may now be noted.

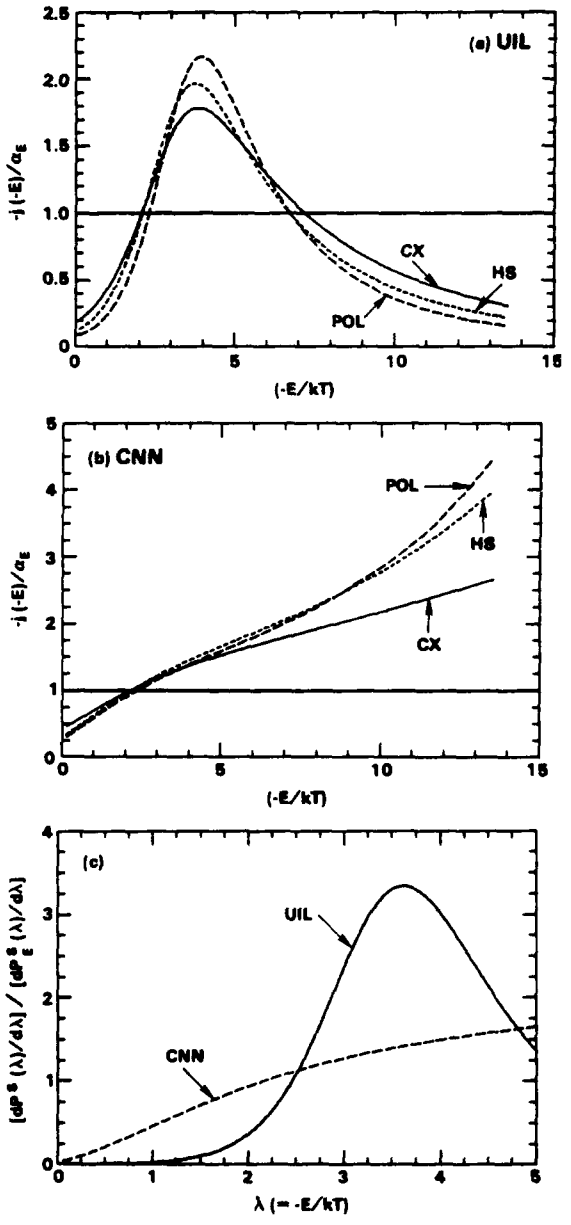

FIG. 3. Energy-space currents (2.3b), normalized to exact QSS rate α_E [Eq. (2.3b) with (2.2)] per unit $\bar{N}_A\bar{N}_B$ across bound energies ($-E/kT$): for model A–M interactions POL, HS, and CX. (a) UIL, with Eq. (2.8); (b) CNN, with Eq. (2.13); (c) ratio of approximate to exact derivatives, Eq. (3.4).

First, assigning the rate either at the dissociation limit $E = 0$ (the $\mathscr{C}$–$\mathscr{S}$ interface) or at the lower association limit $-S$ (the $\mathscr{E}$–$\mathscr{S}$ interface) represents a highly inaccurate procedure for the case of non-QSS probabilities, as previously noted[4] for the diffusional results. Choosing the rate at $\sim 2kT$ below the dissociation limit yields the exact QSS rate for both approximations, a coincidence mainly due to the agreement in Fig. 2(b) of the derivatives (dP_i^S/dE_i) at $E_i \sim -2kT$.

Second, the different shape of Fig. 3(a) from that in Fig. 3(b) can be explained with the aid of Fig. 2(b). From Eq. (3.2), the ratio of the downward energy-space current to the exact rate is

$$-j_d^{(A)}(E_i)/\alpha_E \approx \left[\frac{dP^S}{d\lambda}\right]_A \left[\frac{dP^S}{d\lambda}\right]_E^{-1}, \tag{3.4}$$

where A and E label approximate and exact quantities, respectively. As $\lambda = -E_i/kT$ increases to 2, Fig. 3(c) shows that the ratio (3.4) increases to unity for both CNN and UIL. With further increase of λ, the CNN ratio continues to increase while the UIL ratio increases until λ approaches ~ 3.5 and then falls below unity past $\lambda \sim 7$. The different shapes in Figs. 3(a) and 3(b) are a direct reflection of the variation for each approximation of the ratio (3.4) and confirms the physical importance and significance of the gradients (dP_i^S/dE_i).

In spite of its attractive illustrative features, the UIL energy current (2.9) yields rates which are much smaller than α_E by factors ranging from ~ 10 to $\sim 10^4$ as the mass parameter a of Eq. (3.1) varies from (1/3) for equal masses to $10^{\pm 3}$. The simplified CNN result (2.14) varies from a factor of 3 higher for $a = 10^{-2}$, to a factor of 10 smaller at $a = 1/3$, to a factor of 17 higher at $a = 10^3$, the limit for e-ion recombination in a gas.

As previously noted, the power expression (2.1), rather than Eq. (2.3), must be used when approximate (non-QSS) probabilities as Eq. (2.8) and (2.13) are adopted. Since the QSS probabilities provided[2] a minimum α_E to Eq. (2.1), all other approximate rates must be higher than α_E. This is indeed confirmed by Figs. 4(a) and 4(b), which also show that the CNN rates are much closer to α_E than the UIL rates, as expected from the closer gradients in Fig. 2(b). The maximum deviation occurs at $a = 1/3$ where the CNN rates are only $\sim 25\%$ higher than the exact QSS rates α_E. All of the rates are normalized to the Thomson rate $\tilde{\alpha}_T$, as defined in the previous reports.[3,4]

In addition to the exact QSS treatment, there are now three accurate methods available for termolecular rates: (a) the previous variational procedure[2] which provides, in fact, an alternative route to the QSS rates; (b) the previous diffu-

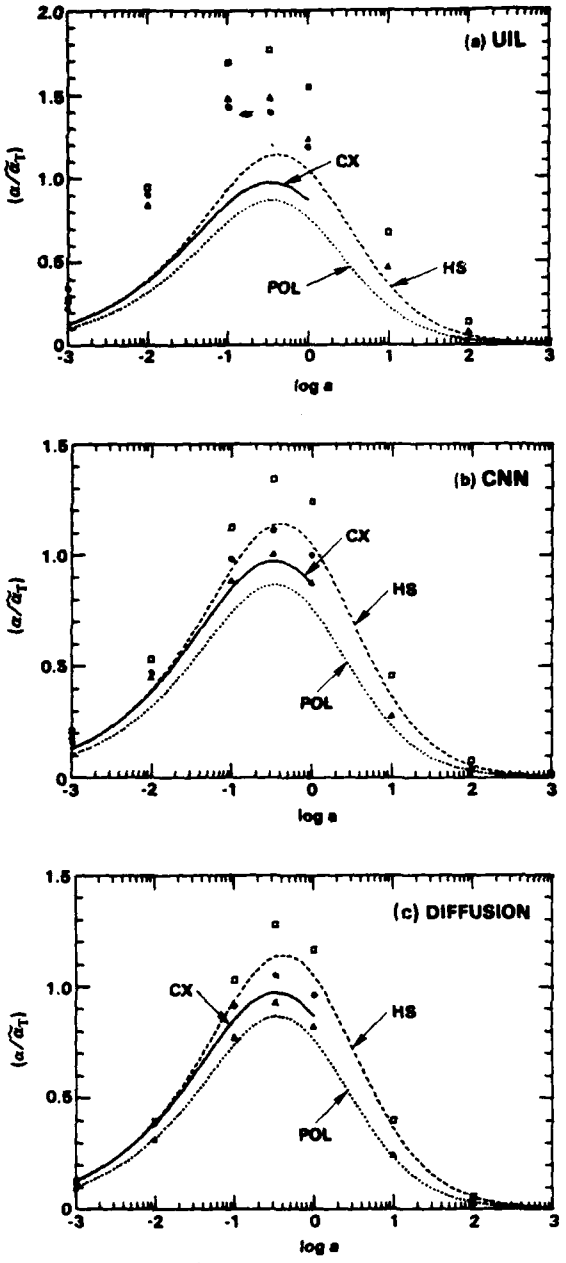

FIG. 4. Normalized partial rates $(M_A/M_{AB})(\bar{\alpha}/\alpha_T)$ for termolecular recombination $A^+ + B^- + M \rightarrow AB + M$ resulting from $(A^+\text{–}M)$ collisions as a function of mass parameter a for various model interactions (CX and ○: symmetrical resonance charge transfer; HS and □: hard-sphere; POL and Δ: polarization attraction). (a) UIL, Eq. (2.1) with (2.8); (b) CNN, Eq. (2.1) with Eq. (2.13); (c) diffusion method, Eq. (2.1) with Eq. (3.6).

sional method[4] D; and (c) the present CNN method. Methods CNN and D are in effect similar in spirit in that CNN also includes upward and downward transitions, and also emphasizes the role of small energy changes between neighboring levels. The diffusion method, however, does not impose, as does CNN, an immediate cutoff to transitions which involve larger energy changes. The CNN probability (2.13) relies only on evaluation of the collision kernel $C_{n,n-1}$ via the relation

$$P_n^S = P_{n+1}^S + C_{n+1,n}^{-1}\left[\sum_{n=0}^{\infty} C_{n+1,n}^{-1}\right] \tag{3.5}$$

which is simpler to implement than the diffusion method,[4] for which

$$P_f^S(E_f) = P_i^S(E_i) + \left[\int_{E_i}^{E_f} \frac{dE}{D^{(2)}(E)}\right]\left[\int_{-S}^{0} \frac{dE}{D^{(2)}(E)}\right]^{-1} \tag{3.6}$$

which requires highly accurate[2] evaluation of the energy-change moment $D^{(2)}(E)$ given by Eq. (3.3).

Figure 4(c) shows the rates of the diffusion method obtained from calculations of $D_i^{(2)}$ which are more accurate than those previously determined in Ref. 4. Comparison between Figs. 4(b) and 4(c) indicates that comparable rates are achieved by the diffusion and CNN methods. The more sophisticated diffusion method, however, is, in principle, more accurate in the limits of small and large mass parameters a where the collision dynamics is weak so that the rates are then more sensitive to the stabilization probabilities P_i^S near the dissociation limit. The diffusion method is also more accurate for intermediate $a \sim 1/3$ since the larger energy transfers tend to be more influential and are included. In spite of these shortcomings, the CNN method yields rates, just slightly less good than the diffusion treatment.

IV. SUMMARY AND CONCLUSION

With the aid of an electrical diagram (Fig. 1) two extreme limits of collisional coupling are investigated in order to elucidate the role of various classes of transitions. A given level n is directly coupled only to its neighbor in CNN while, in UIL, each n is assumed coupled only to the fully dissociated and fully associated states of the reactant $\mathscr{C}$ and product $\mathscr{S}$ channels, respectively. The CNN approximation furnishes closer stabilization probabilities P_i^S and association rates α, thereby indicating that recombination tends to proceed more down an energy ladder of coupled levels than by larger energy jumps $\mathscr{C} \rightarrow n \rightarrow \mathscr{S}$ involving each intermediate level n. As in the case for all approximate P_i^S, the power equation (2.1) furnishes[7] the required rate (which is always higher than the exact QSS rate), rather than $j(-E_i)$ the energy-space current (2.3b) which holds[7] only for quasi-steady-state probabilities (2.2). The E_i variation of the energy-space currents $j(-E_i)$ deduced from non-QSS probabilities P_i^S is mainly determined by the derivatives (dP_i^S/dE_i), as in Eq. (3.4). When assessing via comparison with the exact QSS rate the effectiveness of the underlying physical mechanism in each approximate model (CNN, UIL, or diffusion) it is important to use the power expression (2.1). Otherwise, use of Eq. (2.9b), (2.14), or even of the energy-space currents (2.3b) as in Figs. 3(a) and 3(b) can lead to incorrect conclusions regarding the efficacy of the basic physical assumption.

In conclusion, the nearest-neighbor limit CNN appears to be a satisfactory approximation for termolecular ion–ion recombination over the full range of mass parameter and

interactions associated with (A^+–M) collisions. It is similar in spirit to the more sophisticated diffusion method, yields comparable rates, and yet it is much simpler to implement.

ACKNOWLEDGMENT

This research is supported by the U.S. Air Force Office of Scientific Research under Grant No. AFOSR-84-0233.

[1]D. R. Bates, Proc. R. Soc. London Ser. A 337, 15 (1974).
[2]M. R. Flannery, J. Chem. Phys. 89, 214 (1988).
[3]M. R. Flannery and E. J. Mansky, J. Chem. Phys. 88, 4228 (1988).
[4]M. R. Flannery, J. Chem. Phys. 87, 6947 (1987).
[5]D. R. Bates and A. E. Kingston, Proc. Phys. Soc. 83, 43 (1964).
[6]D. R. Bates and I. Mendaš, J. Phys. B 5, 1949 (1982).
[7]M. R. Flannery, J. Phys. B 18, L839 (1985).

Appendix A

Recombination Processes

M. R. Flannery

School of Physics

Georgia Institute of Technology

Atlanta, Georgia 30332-0430

U. S. A.

CONTENTS

1. SCOPE

The aim here is to survey the mechanisms basic to various types of recombination processes and provide some recent results. Most assume significance in astrophysics (interstellar medium, stellar and planetary atmospheres) and some in laboratory (Tokamak) fusion plasmas and in various types of lasers. They span a wide range in physical conditions e.g., the ranges $10 \leq T \lesssim 10^6$ in temperature T (^oK) and $1 \lesssim N \leq 10^{20}$ in particle density N (cm^{-3}). Recombination includes here not only electron-ion and ion-ion processes but also ion-atom (molecule) association. Most of the processes below may be characterized by the mechanism responsible for stabilization of an intermediate resonant collision complex. Typical two-body rates $k(cm^3\ s^{-1})$ for simple atomic and diatomic systems are indicated in parenthesis beside each process.

For *Termolecular Association* (TA)

$$A^+ + B + M \rightleftarrows (AB^+)^* + M \rightarrow AB^+ + M, \quad (10^{-28}\text{-}10^{-32})\ N\ cm^3 s^{-1} \qquad (1)$$

in a gas M of density N, stabilization of AB^* occurs via AB^* - M collisions at a quenching frequency $\nu_q \lesssim 10^{-9}\ N\ s^{-1}$, while *Radiative Association* (RA),

$$A^+ + B \rightleftarrows (AB^+)^* \rightarrow AB + h\nu\ , \quad (10^{-9}\text{-}10^{-17})\ cm^3 s^{-1} \qquad (2)$$

occurs via photon emission (vibrational and electronic) at a radiative rate $\nu_r \sim (10^3\text{-}10^6)\ s^{-1}$ depending on the type (vibrational or electronic) of stabilizing transition.

For *Dissociative Recombination* (DR),

$$e + AB^+ \rightleftarrows AB^* \rightarrow A^* + B\ , \quad (10^{-6}\text{-}10^{-7})\ cm^3 s^{-1} \qquad (3)$$

stabilization of AB^* occurs by quantal predissociation onto repulsive covalent excited molecular states at a dissociative frequency $\nu_d \sim 10^{15}\ s^{-1}$.

Emission of radiation provides the required stabilization in *Dielectronic Recombination* (DIR)

$$e + A^{z+}(i) \rightleftarrows [A^{z+}(k) - e]_{n',\ell'} \rightarrow A^{(z-1)}(j;n\ell) + h\upsilon \ , \ (10^{-11}\ cm^3\ s^{-1}) \qquad (4)$$

which occurs at (resonant) electron energies much higher than the lower threshold energies for which the direct (non-resonant) *Radiative Recombination* (RR)

$$e + A^{z+}(i) \rightarrow A^{(z-1)+}\ (i;n\ell) + h\upsilon \ , \ (10^{-12}\ cm^3\ s^{-1}) \qquad (5)$$

is more important. In contrast to the above formation of intermediate long lived scattering resonances in (1)-(4), *Termolecular Ion-Ion Recombination* (TR)

$$A^+ + B^- + M \rightarrow AB + M \ , \qquad (10^{-24}\text{-}10^{-25})\ N\ cm^3 s^{-1} \qquad (6)$$

of simple systems proceeds by non-resonant scattering since the Coulomb attraction cannot accomodate quasi-bound levels. The rates are fast since the third body M effectively utilizes the many (A^+-B^-) Coulombic superthermal encounters, which occur at large ion-ion separations $R \leq 3\ 70$ Å at room temperature. Elastic A^+-M and B^--M collisions are very efficient in removing most of the energy gained by A^+ and B^- from the Coulomb field so that the highly excited bound levels of AB so formed are then destroyed by multistep collisional cascades to stable levels. In parallel to the resonant scattering in (1), TA can also proceed via non-resonant (A^+-M) collisions which change the energy and angular-momentum of (A^+-B) relative motion.

Termolecular Electron-Ion Recombination

$$e + A^{+} + M \rightarrow A(n) + M, \quad (10^{-26}\text{-}10^{-29})\ N\ cm^{3}s^{-1} \tag{7}$$

also proceeds via collisions with the gas M, but at a much smaller rate, since elastic electron-atom M collisions cause only a small fraction (~2m/M) of energy to be transferred to M. Rates become larger for molecular M which absorb a much larger fraction of energy via rotational and vibrational excitation, and for molecular ions when dissociative recombination involving bound electrons can provide substantial enhancement.

As is well known, *Mutual Neutralization* (MN)

$$A^{+} + B^{-} \rightarrow A^{*} + B\ , \qquad (10^{-7}\text{-}10^{-8})\ cm^{3}\ s^{-1} \tag{8}$$

proceeds by direct coupling of the diabatic ionic potential energy curve with the covalent curves, which however involve much smaller ion-ion separations $R \sim (10\text{-}50)$ Å to yield rates an order of magnitude smaller than for (6). The fact that the Coulombic interaction between the ions is strong at large separations where the (Landau-Zener) probability for curve crossing is weak ensures the dominance of termolecular process (6) over bimolecular process (8), even at modest pressures. Since collisions with M can form bound $(A^{+}\text{-}B^{-})$ states which in turn promote more efficient curve crossing, MN can be considerably enhanced by an ambient gas. It does not occur parallel to TR (6) so that the effective rate for neutralization is then not simply the sum $(k_{TR} + k_{MN})$ of the individual rates.

In an electron-ion plasma of intermediate density $n_e \sim 10^{11}\ cm^{-3}$, recombination

$$e + A^{+} + e \rightarrow A(n) + e + h\nu \tag{9}$$

proceeds by collisions into high n-levels, which become de-excited by e-A(n) collisions and radiative emission. State-to-states rates for DIR (4), RR (5), DR (3), and NSR (7) would all be relevant. *Collisional-radiative recombination* (CRR) then yields the familiar set of quasi-equilibrium (input = output) Master Equations to be solved for the individual excited state populations N_n in terms of the concentration of free electrons, ions and recombined atoms in the lowest stabilized states.

1.1 *CURRENT STATUS OF RECOMBINATION*

The present state of recombination is that theory (with reliable results) for most of the above processes involving simple atomic or diatomic systems is reaching maturity and is approaching a well defined Hi-Tech State. In particular the recent theoretical developments[1-3] of DIR indicate that DIR cross sections may be calculated to within the same degree of accuracy (~10%) as electron-ion inelastic collisions. Termolecular ion-ion recombination[4-6] of simple ion systems in a gas has been solved as a universal function of mass species, and gas density and temperature. Results for simple systems of general mass are available at low density. Dissociative recombination[8] of simple diatomic systems is in principle well known but lack of relevant molecular potential energy curves and branching ratios to final products prohibit rigorous quantal calculation. Ion-neutral reactions and termolecular electron-ion recombination for complex systems remain by comparision in a more exploratory condition, although substantial progress[9,10] has recently occurred.

Reliable experiments[8,11-13] exist for DR, TA and MN which proceed with measurable rates (10^{-7}-10^{-9} cm^3s^{-1}). Technical breakthroughs have recently permitted measurements on DIR[14,15] and RA[16] which proceed at much slower rates (10^{-10}-10^{-15}) cm^3s^{-1}, respectively. The influence of electric fields in the experiments is important, particularly for DIR and to a lesser extent for

DR. Theories of recombination in external fields are currently under development.

Although TR (6) is now well understood theoretically and proceeds at the largest rate of any recombination processes involving simple systems, reliable experimental measurement, apart from some historical data,[17] is as yet not forthcoming although some activity has recently emerged.[18] There are at present no measurements from a given laboratory which span the full range of gas pressures studied theoretically and which monitor the identity of ions as the pressure changes. The task is difficult in that the ions may well be clustered to high orders.

1.2 GENERIC KINETIC AND RESONANT-SCATTERING TREATMENT

Identify the interacting species in (1)-(9) as A, B and M with concentrations n_A, n_B and N, respectively. The two stage sequence common to TA(1), RA(2), DIR(3) and DR(5) is the formation of a long-lived unstable collision complex AB^*, or scattering resonance, followed by an irreversible stabilization mechanism, whether radiative as in RA and DIR, collisional as in TA or dissociative as in DR. The complex with energy degenerate to and lying within the continuum of dissociated A(i) + B(j) states is formed when the excess energy and angular momenta of internal and relative motion of A and B become redistributed among the internal degrees of freedom of AB^*. Following large perturbations in (A-B) close encounters, a quasi-equilibrium of these excited states of AB^* is established. Thus processes RA(1), TA(2), DR(3) and DIR(4) above may be conveniently analyzed in terms of the macroscopic two stage sequence

$$A + B \underset{\nu_d}{\overset{k^*}{\rightleftarrows}} AB^* \xrightarrow{\nu_s} \text{products} \qquad (10)$$

which involves the stabilization at frequency ν_s of quasi-bound resonant scattering states of AB^* formed at rate k^* ($cm^3 s^{-1}$) before AB^* can

redissociate (or autoionize) back to the initial or any other dissociated channel at frequency ν_d. For a quasi-steady-state density n^*_{AB} of the AB^*, the overall process then proceeds at a rate (cm^3s^{-1})

$$k = n^*_{AB}\nu_s = \left[\frac{\nu_s}{\nu_d+\Sigma\nu_s}\right] k^* \equiv P_s\, k^* \qquad (11)$$

where P_s is the probability of routing to a particular pair of stabilized products s. A negative temperature T dependence is anticipated for k since ν_d increases with T. As the density N of the gas M is raised, (11) for collisional association TA predicts an initial linear variation of k with N (when $\nu_d >> \nu_s \sim k_s N$) increasing towards a saturation value k^* (when $\nu_s >> \nu_d$) times the branching ratio $[\nu_s/\Sigma_s\nu_s]$ for that particular pair of products.

The reaction volume (cm^3)

$$K = n^*_{AB}/n_An_B = k^*/\nu_d \qquad (12)$$

is pivotal in determining the T-dependence of the overall rate

$$k = \left[\frac{\nu_s K(T)}{k^*+\Sigma_s\nu_s K(T)}\right] k^* = K(T)\left[\frac{\nu_s\nu_d}{\Sigma_s\nu_s+\nu_d}\right] \qquad (13)$$

Note that K is not an equilibrium constant in the usual sense since AB^* is distributed only among those states satisfying energy and angular momentum conservation above the dissociation limit. It is given in usual notation by

$$K(T) = \frac{h^3}{(2\pi M_{AB}kT)^{3/2}}\,\frac{q(AB^*)}{q(A)q(B)}\,\frac{\omega_{AB}}{\omega_A\omega_B} \qquad (14)$$

where q is the internal partition function, or the number of quantum states available at temperature $T \sim \sum_i \exp(-E_i/kT)$, and where ω is the electronic statistical weight, associated with each reactant A and B and with the activated complex AB^* of reduced mass M_{AB}. While q(A) and q(B) are generally known, $q(AB^*)$ must include only those rotational-vibrational-electronic states of AB^* accessible at energies above the dissociation threshold of AB. It also includes states which satisfy conservation of total angular momentum produced from the orbital angular momentum for (A-B) relative motion and the combined internal angular momentum of the individual reactants.

The key quantities which characterize the T-dependence and rate limiting step of each of RA, TA, DIR and DR are therefore K(T) and the stabilization frequency ν_s. For polyatomic species, not only is calculation of K difficult but ν_s is uncertain to the extent that the type of transition (vibration or electronic) may not be established. This lack can involve at least two orders of magnitude difference in the rates.[10]

For cases RA, DIR, DR and TA, a microscopic state-to-state generalization, (phase-space or multichannel) of the basic premise underlying (11) can be written down in terms of all the relevant electronic, vibrational and rotational quantum numbers for the internal degrees of freedom i and j of A(i) and B(j), for the translational energy and angular momentum of A-B relative motion and for the total conserved angular momentum and energy. The simplified expression (11) however not only serves as a guide to experimentalists in elucidating the role, and extracting the rate peculiar to various stabilization mechanisms but is also capable of providing order-of-magnitude rates and the associated dependence on temperature T fairly reliably.

The intimate connection of (11), standard in chemical kinetics, with scattering theory is instructive. When the redissociation or autoionization channels in (1)-(5) are considered as a series of non-overlapping resonances

and when the non resonant background scattering is neglected, then Breit-Wigner resonance scattering theory with explicit inclusion of all multi-channels, consistent with energy and angular momentum conservation, can be applied. In order to preserve a simple notation to isolate the key connection, and to illustrate the essential technique, let AB^* exhibit only relative motion scattering resonances (quasi bound states) at (A-B) relative energies $E = E_r^*$. The cross section for the resonant reaction of A and B with internal energies $E_{A,B}$ is

$$\sigma(E;E_A,E_B) = \frac{\pi}{E}\left[\frac{h^2}{2M_{AB}}\right]\frac{\omega(AB^*)}{\omega(A)\omega(B)}\sum_r \frac{\Gamma_a\,\Gamma_s}{[(E_T-E_r^*)^2+\frac{1}{4}\Gamma^2]} \qquad (15)$$

where the total energy of the system is $E_T = E_A + E_B + E$, where the energy widths for stabilization and re-dissociation (autoionization) are related to the corresponding frequencies by

$$\Gamma_s = h\,\nu_s, \qquad \Gamma_d = h\,\nu_d \qquad (16)$$

where Γ is the total width $(\sum_d \Gamma_d + \sum_s \Gamma_s)$ for all dissociative (d) and stabilization channels (s). The electronic statistical weight of species X is $\omega(X)$. The rate of recombination for a Maxwellian distribution of relative energies E at temperature T is

$$k(T) = \left[\frac{8kT}{\pi M_{AB}}\right]^{1/2}\int_0^\infty \epsilon\,\sigma(\epsilon)\,\exp(-\epsilon)d\epsilon \;;\quad \epsilon = E/kT \qquad (17)$$

where M_{AB} is the reduced mass of (A-B). Since the Dirac delta function $\delta(x)$

is $\pi^{-1} \lim_{h\to o} h(x^2+h^2)^{-1}$, the rate (17) for sharp resonances $\Gamma << (E_T - E_r^*)$ then reduces to

$$k(T,E_A,E_B) = \frac{h^3}{(2\pi M_{AB} kT)^{3/2}} \frac{\omega_{AB}}{\omega_A \omega_B} \left[\sum_r \frac{\upsilon_d \upsilon_s}{(\Sigma \upsilon_s + \upsilon_d)} \exp -(E_r^*/kT) \right] \exp(E_A+E_B)/kT \quad (18)$$

On assuming that the frequencies are independent of the resonance positions E_r^*, then $\sum_r \exp(-E_r^*/kT)$ is then simply the partition function $q(AB^*)$ arising from all the resonance states of AB^*. On averaging over all internal states i and j of A and B and with the use of detailed balance, (12), (11) and (14) are then recovered since $\sum_{i,j} \exp(-E_A/kT) \exp(-E_B/kT)$ is the product $q(A)q(B)$ of the reactant partition functions. This connection provides a basis for (11) or (14) more quantitative than the earlier steady-state kinetic rate argument. The extension to include all multichannels directly is straight- forward, but the case of overlapping resonances existing in various polyatomic systems requires attention, and may well under approximation provide the rate (13) in current use.

Because of the long range Coulombic attraction in the entrance channels the remaining related processes (TR, TER), as indicated earlier, do not proceed via the resonating tight complex but rather by energy-changing collisions between M and $(A^+ - B^-)$ pairs. The collisions are effective for those pairs with separation $R \lesssim R_T = e^2/kT \sim 370$ Å at room temperature, which in a sense can be regarded to form an extremely large loose non-resonating complex with reaction volume $K = \frac{4}{3} \pi R_T^3$. At low gas density N, (13) predicts

$$k_{TR} \sim \frac{4}{3} \pi R_T^3 \upsilon_s = \frac{4\pi}{3} R_T^3 \langle v_{AB} \rangle N \sigma \quad (19)$$

where σ is the cross section for free-bound energy-changing $(A^+-B^-)-M$ collisions, and emphasizes the characteristic linear N and the $T^{-5/2}$-T^{-3} dependencies. At high N, however, the rate does not converge to the saturation value k^* predicted by (13). The rate of approach of A^+ and B^- to R_T is limited by the transport rate, which decreases as N^{-1} and which becomes comparable to the reaction rate (19) within R_T at about ~1 atm. For TA(1) however the transport rate always remains much higher than the rate limiting step of reaction so that saturation to the thermal rate k^* is eventually obtained.

2. RADIATIVE AND TERMOLECULAR ASSOCIATION

2.1 *SIMPLE SYSTEMS*: The underlying physics of *Radiative Recombination* of simple system as

$$C^+(^2P_{1/2}) + H(^2S) \rightarrow CH^+(A\,^1\Pi) \rightarrow CH^+(X\,^1\Sigma) + h\nu \tag{20}$$

becomes transparent in a semiclassical treatment,[19] where the cross section is

$$\sigma(E) = 2\pi \int_0^\infty P_r(E,\rho)\rho\, d\rho \tag{21}$$

at relative energy E. The probability of radiative emission during a collision at impact parameter ρ is

$$P_r(E,\rho) = \int_{-\infty}^{\infty} G(t)A(t)dt = \oint_R^\infty G(R)A(R)dR/v_R \tag{22}$$

where the radial speed at relative separation R is v_R with turning point R_T, and where G(R) is the probab lity that CH^+ during the collision is in state i ($A\,^1\Pi$), which radiates at a local rate

$$A(R) = \frac{4}{3} h^4 c^3 \, |M(R)|^2 \, \Delta E^3(R) \tag{23}$$

to the stabilized state f($X\,^1\Sigma$). The molecular states, with wavefunctions $\Psi_{i,f}$ and energy separation $\Delta E(R) = V_f(R) - V_i(R)$, are connected via the dipole

matrix element $M(R) = \langle \Psi_f(\underset{\sim}{r},R) | e\underset{\sim}{r} | \Psi_i(\underset{\sim}{r},R) \rangle$. Rates $k_{RA} = 1.3\ 10^{-17}\ cm^3\ s^{-1}$ obtained[19] for (20) over the temperature range $20 \leq T\ (^oK) \leq 1000$ do not, however, satisfactorily explain the discrepancy between the observed and theoretically deduced abundances of the radical CH^+ in diffuse interstellar clouds. A quantal treatment can in addition acknowledge the discrete vibrational levels of the intermediate electronic state $i(A\,^1\Pi)$ and can include quasi-bound resonances formed within the centrifugal barrier. These effects enhance[20] the semiclassical rates for (20) by ~ 25%, mainly at lower T. Also state i may support predissociating levels between the fine structure state $C^+\ (^2P_{1/2})$ and $C^+\ (^2P_{3/2})$ of the reactants. No full treatment has as yet been performed.

Termolecular Association

$$A^+ + B + M \rightarrow AB^+ + M \qquad (24)$$

for formation of simple diatomics as He_2^+, Ne_2^+, etc. can be considered[21] as proceeding via a multistep series of collisions between $(A^+\text{-}B)$ pairs and M which change both the energy E and angular momentum L of relative $(He^+\text{-}He)$ motion to such an extent that bound stabilized levels are formed. At lower energies E there is an additional contribution from quasi-bound resonances[22] formed at positive E within the centrifugal barrier.

A multichannel generalization of (13) to simple (structureless) atomic systems yields the termolecular association rate[23]

$$k_{TA} = \int_0^\infty dE \int_0^{L^2_{max}} dL^2 \left[\frac{k_i^s K_i N}{k_i^* + k_i^s K_i N} \right] k_i^* \qquad (25)$$

where subscripted-i rates refer to specific energy E and angular momentum L of A-B relative motion, where L_{max} is the maximum L of the complex at fixed E,

and where

$$k_i^s N n_i^* = \int_{R_i^-}^{R_o} n_i(R)\, \upsilon_i(R) d\underset{\sim}{R} \tag{26}$$

is the overall frequency for stabilization of all the $(A\text{-}B)_i$-pairs with internal separation R between the innermost turning point R_i^- of radial motion and the radial boundary $R_o(E,L)$ of the complex. The pair-distribution per unit interval $d\underset{\sim}{R}\, dE\, dL_i^2$ is $n_i(R)$, and $\upsilon_i(R) = k_q N$ is the frequency of $(A\text{-}B)_R^*$ - M quenching collisions with rate k_q at fixed (R, E_i, L_i^2). At low gas densities N this distribution can be taken as its equilibrium value $\tilde{n}_i$, since υ_i in (26) is already linear in N. When the quenching coefficient k_q is constant, and equal to some fraction β of the constant Langevin limiting rate for spiralling $(AB^*\text{-}M)$ collisions

$$k_L = 2\pi e(\alpha_M/M_s)^{1/2} \tag{27}$$

where α_M is the polarizability of M and M_s is the reduced mass of the $(AB^*\text{-}M)$ system, it then follows that

$$n^* = \int_0^\infty dE \int_0^{R_o(E)} d\underset{\sim}{R} \int_0^{R^2p^2} \tilde{n}_i(R) dL^2$$

$$= \frac{2}{\sqrt{\pi}} (kT)^{-3/2} \int_0^\infty \exp(-E/kT) dE \int_0^{R_o(E)} [E-V(R)]^{1/2}\, d\underset{\sim}{R} \tag{28}$$

For polarization attraction $V(R) \sim (\alpha_B e^2/2R^4)$ between A^+ and B of polarizability α_B and orbiting radius $R_o(E) = (\alpha_B e^2/2E)^{1/4}$, (28) yields

$$n^* = \frac{4}{3}\pi R_L^3 \frac{8}{\sqrt{\pi}} \tag{29}$$

where R_L is $(\alpha_B e^2/2kT)^{1/4}$ and $(8/\sqrt{\pi})$ arises from both the focusing effect and the enhancement of R_o at small E. The association rate at low N is then

$$k_{TA} = n^*[\beta(T,N)k_L]N \sim (10^{-28} - 10^{-31})N \text{ cm}^3 \text{ s}^{-1} \tag{30}$$

which exhibits the temperature dependence $\beta(T)\ T^{-3/4}$. The efficiency $\beta \sim 1$, but for He^+ - He charge transfer collisions the quenching rate $k_q \sim \langle v_{AM}\sigma_{AM}\rangle$ involves an additional $(kT)^{1/2}$ factor from v_{AM} and a factor $(kT)^{-1}$ from focusing effects so that $k_A \sim T^{-5/4}$ at low temperature.

2.2 *COMPLEX SYSTEMS*: Here, rates are much higher due to increase in the physical size and in the number of internal modes of the intermediate complex. For triatomic ionic systems as

$$C^+ + H_2 \underset{\nu_d}{\overset{k^*}{\rightleftarrows}} (CH_2^+)^* \overset{\nu_r}{\rightarrow} CH_2^+ + h\nu \tag{31a}$$

which initiates carbon phase chemistry in diffuse and dense interstellar clouds,[24] and for polyatomic complexes as in either

$$CH_3^+ + H_2 \rightleftarrows (CH_5^+)^* \rightarrow CH_5^+ + h\nu \tag{31b}$$

which is a precursor[9] to the formation of methane (CH_4), or in

$$CH_3^+ + H_2O \underset{\nu_d}{\overset{k^*}{\rightleftarrows}} (CH_3^+ \cdot H_2O)^* \overset{\nu_r}{\rightarrow} CH_3^+ \cdot H_2O + h\nu \tag{31c}$$

which can be photodissociated[24] to produce methanol (CH_3OH) in the interstellar medium, the "kinetic chemical" approach is as yet the only viable method. The collision duration is much longer than that for simple systems as (20) and there are simply too many degrees of freedom in the intermediate complex to consider in a full quantal state-to-state fashion. Moreover the complex offers a near continuum of closely spaced vibrational (and electronic) energies, overlapping resonances and many intramolecular processes so that a state-to-state method could not be considered as providing the most efficient or realistic description.

In order to isolate radiative association (RA) from termolecular association (TA) extremely low neutral densities $\lesssim 10^{10}$ cm^{-3} and temperatures T ($10^{o}K$-$30^{o}K$) are required. The mechanisms often proceed in parallel so that, in the coupled sequence,

$$A + B + (M) \underset{\upsilon_d}{\overset{k^*}{\rightleftarrows}} AB^+ \xrightarrow{\upsilon_r} AB + h\upsilon \tag{32}$$

$$\underset{\upsilon_d}{\overset{k^*}{\rightleftarrows}} AB^* \xrightarrow{\upsilon_q} AB + M \tag{33}$$

radiative association occurs at the rate

$$k_{RA} = n^*_{AB}\, \upsilon_r = \left[\frac{\upsilon_r}{\upsilon_d+\upsilon_s}\right] k^* \tag{34}$$

and termolecular association at the rate

$$k_{TA} = n^*_{AB}\, \upsilon_q = \left[\frac{k_q M}{\upsilon_d+\upsilon_s}\right] k^* . \tag{35}$$

The frequency of stabilization of the complex, against *both* natural and collisional disruption at frequency ν_d, is

$$\nu_s = \nu_r + k_q N \quad , \tag{36}$$

the sum of the radiative decay frequency ν_r, and the frequency $k_q N$ for collisional quenching. At low densities $N(H_2,He) \sim (10^3\text{-}10^{10})$ cm^{-3} in interstellar clouds, $\nu_s = \nu_r << \nu_a$, so that the overall association is radiative controlled proceeding at rate

$$k_A = k_{RA} = K \nu_r \tag{37}$$

where the reaction volume is given by (14). At intermediate densities $(10^{10}\text{-}10^{16})$ cm^{-3}, ν_s still remains $<< \nu_a$, and association proceeds at rate

$$k_A = k_{RA} + k_{TA} = K (\nu_r + k_q N) \tag{38}$$

which increases with gas density N, until it saturates to the limiting rate $k_{TA} = k^*$ of collisional formation of the original complex. The rate (38) is determined by the character of the interaction between the transition channels within the complex and differences in temperature dependence are mainly controlled by the T-variation of the reaction volume K(T). Radiative stabilization rates ν_r for complex systems are also uncertain, but are expected to be $\nu_r \sim 10^3$ s^{-1} for vibrational transitions and $\nu_r \sim 10^5\text{-}10^6$ s^{-1} for electronic transitions. The larger electronic rates ν_r permits association in interstellar clouds to proceed faster than originally supposed.[9]

Typical values for the relevant rates are the Langevin limit $k^* \sim 10^{-9}$ cm^3 s^{-1}, $\nu_a \sim 10^7$ s^{-1}, $\nu_r \sim 10^3\text{-}10^5$ s^{-1} and the Langevin limit $\nu_q \sim 10^{-9}$N s^{-1}.

Radiative rates $k_{RA} \sim (10^{-13}\text{-}10^{-11})$ cm^3 s^{-1} and termolecular rates $k_{TA} \sim 10^{-25}$ N cm^3 s^{-1} are then expected for complex systems at low gas densities N. Termolecular association therefore begin to compete with RA for $N \sim 10^{12}$ cm^{-3} while at higher $N \gtrsim 10^{15}$ cm^{-3}, TA becomes dominant.

Few experiments exist on RA, mainly due to the smallness of the rate $\sim 10^{-13}$ cm^3 s^{-1} and difficulty in achieving low temperatures ($T \sim 10^{o}K$) and densities ($N \lesssim 10^{9}$ cm^{-3}) needed for isolation of RA. The TRAP technique of Dunn and associates[16] represents a spirited effort while at higher $N \sim 10^{11}$ - 10^{13} cm^{-3}, the ICR (ion-cyclotron resonance)-experiment[25] measures the RA and TA combination (21). By contrast, many TA experimental studies at yet higher $N \gtrsim 10^{15}$ cm^{-3} exist for atmospheric species - the SIFT (selected ion flow tube) technique[12] being the major contributor. For TA, reasonable (order-of-magnitude) agreement exist with theory, particularly in the temperature variation. For RA, the few measurements of (24) and (25) do not agree with available theory and do not furnish information on the type (vibrational or electronic) of radiative stabilization. Interesting discrepancies between experiment and theory based on (42) and (43) for polyatomic species are discussed by Bates and Herbst.[10]

3. DISSOCIATIVE RECOMBINATION

3.1 *DIRECT PROCESS*

In the direct two stage mechanism (Fig. 1a)

$$e + AB^{+}(v_i) \underset{\upsilon_a}{\overset{k^{*}}{\rightleftarrows}} (AB^{**})_r \xrightarrow{\upsilon_s} A^{*}+B, \quad k_{DR} \sim (300/T)^{1/2}\ 10^{-7}\ cm^3\ s^{-1} \qquad (39)$$

the electron of energy ϵ excites an electron of the ion-core AB^{*} and is then resonantly captured via a Franck-Condon (FC) vertical transition onto the repulsive state r of the double excited molecule (AB^{**}). Competition between reverse autoionization at nonlocal frequency υ_a and predissociation at

nonlocal frequency ν_s continue until the electronically excited neutral fragments accelerate past the stabilization point R_s. Beyond R_s the increasing energy of relative separation has reduced the total electronic energy to such an extent that autoionization is essentially precluded and the neutralization is then rendered permanent. The kinetic energy of the electron (in the field of AB^+) is effectively transferred here to motion of the nuclei not by direct collision but via a rearrangement in (39) of the whole electronic cloud. DR is a "*reactive*" process in the sense that the reactants and products involve different collision partners.

The autoionization character of AB^* for $R < R_s$ makes resonant capture originally possible, and the covalent repulsive character for $R > R_s$ makes neutralization finally permanent. For reasonable capture over a range of ϵ, the autoionization width $\Gamma_a \sim h \nu_a$ must not be too small, while large stabilization probabilities P_s demand small widths. The requirement of resonant capture without any energy transfer between electronic and nuclear motion is that the vertical difference in the potential-energy curves (PE^+ and PE^*) for XY^+ and XY^* equals ϵ (Fig. 1a). For thermal-energy electrons this requirement is best fulfilled when PE^* crosses PE^+ on the right side of its minimum (cf. Fig. 1a), as for most cases of doubly excited electronic states with more than four electrons. This energy-matching can consequently occur over the full range of ϵ.

Large capture rates depend therefore on good electron-electron communication (correlation) and on good vibrational overlap between the AB^+ bound and AB^*-continuum nuclear wavefunctions, an overlap which is sensitive to the initial vibrational level v_i of the ion and to the crossing of PE^* and PE^+. When the only crossings in Fig. 1a are provided by the upper repulsive PE^* curves, then the capture probability remains small for $v_i=0$ ions and thermal electrons, and becomes large only when these curves are accessed by more

energetic electrons $\epsilon \gtrsim 0.5$ eV, which imply however smaller Coulomb focused scattering cross sections $\sigma \sim \epsilon^{-1}$. This is the situation with H_2^+ (v_i=0) and He_2^+. Conversely, the overlap of AB^+ (v_i=2) in Fig. 1(a) with the lower PE^* is poor, relative to the much larger overlap with the upper curves. Note ϵ is measured from R on PE^+.

In keeping with (11), the recombination cross section for simple systems may be factored as

$$\sigma_{DR}(\epsilon) = \sigma_c(\epsilon)\ P_s(\epsilon) \tag{40}$$

where the cross section for capture at R_c is[26]

$$\sigma_c(\epsilon) = \frac{C}{\epsilon} |V(R_c)|^2 |\psi_v^+(R_c)|^2 [dR/d(PE^*)]_{R_c} \tag{41}$$

Here V(R) is the electronically-averaged interaction coupling the initial and intermediate molecular systems, ψ_v^+ is the vibrational wavefunction for $AB^+(v)$ and C is $(2\pi^3/m\ h)[\omega(AB)/\omega(AB^+)]$. The stabilization probability is given as in (11) by $\nu_s/(\nu_a+\Sigma_s \nu_s)$. By analogy with dissociative attachment, it may also be approximated by,[26]

$$P_s(\epsilon) = \exp[-\int_{t_c}^{t_s} [\Gamma_a(R)/h]dt] \tag{42}$$

where $\Gamma_a(R)$ is a *local* autoionization width (so that $\Gamma_a = h\ \nu_a$ is the probability of electron ejection per unit time) and where the integration is over the interval from the time t_c at formation of AB^* at R_c to the time t_s when stabilization at R_s is rendered permanent. This interval depends on the total energy and slope of PE^*. Although the *local* $\Gamma_a(R)$ in (42) is not strictly

appropriate to recombination at thermal ϵ, (43) remains useful as an estimate of the influence of autoionization. Thus P_s is reduced by an increase in number of open bound vibrational channels over which autoionization proceeds when electrons are emitted not only at energy $\epsilon_a = \epsilon$ but also at $\epsilon_a \neq \epsilon$ when the energy imbalance is absorbed by vibrational motion. It is enhanced not only by a reduction in the time interval, but also by an increase in the density of intermediate complexes and product channels, as with ion-clusters. The ϵ^{-1}-dependence of σ_c results in recombination rates (11) which decreases as $T_e^{-0.5}$. For typical diatomic molecular ions as Ne_2^+ or NO^+, dissociation occurs at frequencies $\nu_a \sim 10^{15}\ s^{-1}$, large compared with $\nu_a \sim 10^{14}\ s^{-1}$ for autoionization, so that P_s is close to unity. At thermal energies Coulomb focusing dominates the capture so that $\sigma_c \sim \epsilon^{-1} \gtrsim 10^{-14}\ cm^2$. Rates $k_{DR}\ (Ne_2^+) \sim 2\ 10^{-7}\ (300/T)^{0.5}\ cm^3\ s^{-1}$ are then quite typical, As one proceeds through an ion sequence ($Ne_2^+ \rightarrow Xe_2^+$), the natural increase in σ_c is due both to the stronger interactions and larger vibrational amplitudes and P_s remains substantial. Owing to the increasing steepness of $PE^{\#}$, it generally increases. Continued increase in σ_c however implies a corresponding increase in autoionization width so that P_s will eventually decrease, until it becomes limited to (ν_s/ν_a) as for the case of polyatomic systems.

3.2 *INDIRECT PROCESS*

In the following indirect additional mechanism for DR,[26]

$$e + AB^+(v) \rightleftarrows [AB^*(n,v)]_a \rightleftarrows (AB^*)_r \rightarrow A^* + B \qquad (43)$$

the electron is captured into attractive (a) vibrationally excited (v') Rydberg states (n) of AB^* which converge to the initial electronic state of AB^+ (Fig. 1b) and which are then coupled by configuration interaction to the dissociative channels. The first stage involves energy transfer from the

electron directly to vibrational excitation of the nuclei. In contrast to the broad ϵ-range enjoyed by the direct process (31), only selected energies ϵ' close to the Rydberg level (Fig. 1b) contribute to the indirect process which is therefore characterized by a series of narrow resonances (enhancements or dips) in the overall recombination cross section at the low electron energies $\epsilon \leq 1$ eV favored by this process.

The formal multichannel quantum theory of DR via the direct and indirect mechanisms can be constructed.[8] For full quantal calculations the following information is required as input: (a) identification and calculation of the relevant PE^+ and PE^* curves for the capture cross section including those for the vibrationally excited Rydberg state, (b) the quantum coupling between the autoionization and dissociation channels for the widths Γ_a and Γ_s and (c) the branching ratios to all possible products of dissociation. Since the coupling (b) appears as a resonance in the asymptotic phase of the electronic wavefunction the widths may be obtained either from direct electron-ion scattering calculations or from extrapolation of the properties of the Rydberg and valence bound states across the ionization threshold. The main theoretical problems are associated with the uncertainty of the role of the vibrationally excited Rydberg states and with the branching ratios which in turn involves solution of a set of coupled equations incorporating the interactions between the various products of dissociation. The "reactive" DR process combines therefore both electron-ion, ion-ion and neutral-neutral scattering technologies. Because of the sensitivity (as indicated above) of k_{DR} on the slopes, shapes and relative positions of PE^+ and PE^* and the lack of accurate PE curves for most systems, rigorous calculation has been confined mainly[27,28] to H_2^+ and to some diatomic ions (N_2^+, O_2^+ and NO^+) of atmospheric significance.[8]

DR for even the simplest diatomic system $e+H_2^+$, although not quite typical, is instructive. The sole candidate in the direct process for $e-H_2^+(X^2\Sigma_g^+,v)$ recombination at low energies $\epsilon \leq 1$ eV is the lowest doubly excited $^1\Sigma_g\ (2p\sigma_u)^2$ state of H_2 which crosses the $^1\Sigma_g^+$ ion state in the vicinity of the v = 2 level, and which dissociates into ionic fragments $H^+ + H^-$. Because of the propensity rule $\Delta v' = 1$ for vibrational autoionization in (43), the recombination can be actively hindered by the higher vibrational levels v' of Rydberg states $(1s\sigma_g n\ell m)$ with intermediate $n \leq 8$, and the contribution from these levels is weak. However, the sequence, coupling the direct and indirect processes,

$$e + H_2^+ (v=0) \rightarrow H_2^{**} \rightarrow H_2\ (n,v\geq 2) \rightarrow H_2^{**} \rightarrow H_2^+ + e\ ,$$

does interfere destructively[27,28] with the direct process. The resulting resonant dips in the cross section have just been observed.[29] Rates for $e + H_2^+(v)$ can be given as $k_o\ (300/T)^\gamma\ 10^{-9}\ cm^3\ s^{-1}$ where (k_o,γ) have just been calculated[28] as (0.8,0.3), (6,0.5), (0.45,0.66), (0.66,0.32) and (1.1,0.77) for v = 0, 1, 2, 3 and 4, respectively.

The DR-rate for CH^+ (v=o) at 120°K was also calculated[28] to be ~ $1.12\ 10^{-7}\ cm^3\ s^{-1}$ in good agreement with a merged beam experiment.[8]

Even though measured DR rates for many ions of planetary and astrochemical interest can be used with reasonable confidence, severe disagreement exists for the simplest triatomic H_3^+ important to the Jovian atmosphere and to interstellar chemistry. The rate is expected to be small since the $^2A_1$ repulsive part of the PE^* curve of H_3 intersects the $^1A_1$ state of H_3^+ at 1 eV above the v=o level. Recent measurements[30] which vary from $2\ 10^{-8}\ cm^3\ s^{-1}$ at 100°K to $1\ 10^{-8}\ cm^3\ s^{-1}$ at 1000 K for v=o and 1 ions are orders of magnitude higher than the revised upper-limit rate[31] of $2\ 10^{-11}\ cm^3\ s^{-1}$ at

300 K. The merged beam experiment[30] detects the neutral products while the Flowing Afterglow Langmuir Probe (FALP) experiment[31] measures the loss of H_3^+ ions, and this may well be the source of the discrepancy.

Polyatomic ions and clusters offer many more additional degrees of freedom for capture of the electron, in both mechanisms. With increasing ion complexity, the multiplicity of readily excited internal modes of small energy separation makes the near resonant energy condition of the indirect process easier to attain by presenting a near continuum of closely spaced vibrational energies and trapping becomes more efficient over a broad range of ϵ'. This is confirmed by the large rates $k_{DR} \sim 2\ 10^{-6}\ (300/T)^{0.4}$ for dimer complexes $N_2^+ \cdot N_2$, $O_2^+ \cdot O_2$ and $CO^+ \cdot CO$, important in atmospheric chemistry. That polar clusters $H_3O^+ \cdot (H_2O)_n$ and $NH_4^+ \cdot NH_3$ with rates $k_{DR} \sim 3\ 10^{-6}$ cm^3 s^{-1} appear fairly insensitive to T, has as yet not been satisfactorily explained.

As systems become more complex ($Ne_2^+ \rightarrow Xe_2^+$), the resulting increase in the capture cross sections σ_c tends to be offset by a corresponding decrease in the stabilization probability P_s from near unity until stabilization becomes the rate limiting step. The rate from (11) is then

$$k_{RA} = K(T)\ \upsilon_s \tag{44}$$

where the reaction volume has now the interesting form[9]

$$K(T) = \frac{h^3}{(2\pi mkT)^{3/2}} \frac{\omega(AB^*)}{2\omega(AB^+)} \left[\int |\psi_v(R)|^2 \left[\frac{dR}{d(PE^*)}\right] \exp(-E/kT)dE \right] \tag{45}$$

which contains an effective Franck-Condon factor which essentially selects only that portion of the full internal partition function of AB^* that contributes to the capture by the vertical transition at $R = R_c$. Polyatomic systems relevant to interstellar cloud chemistry have recently been discussed by Bates.[9]

4. DIELECTRONIC AND RADIATIVE RECOMBINATION

Dielectronic recombination (DIR) at high temperatures ($\sim 10^6$K)

$$e(\epsilon\ell) + A^{Z+}(i) \underset{\upsilon_a}{\overset{k^*}{\rightleftarrows}} [A^{(z-1)+}(k)-e]_{n\ell} \xrightarrow{\upsilon_r} A^{(z-1)+}_{n\ell}(j) + h\upsilon \qquad (46)$$

is a resonant capture process into doubly excited Rydberg levels subsequently stabilized by radiative emission at frequency υ adjacent to, and usually on the lower frequency side of, the resonance transition

$$A^{Z+}(k) \rightarrow A^{Z+}(j) + h\upsilon_R \qquad (47)$$

of the recombining ion of charge Ze. These satellite lines are observed in solar and in high temperature fusion plasmas and provide valuable diagnosis of electron temperature, electron density and the various stages of ionization. The frequency shift which originates from core perturbation by the $n\ell$-electron is small for high Rydberg $n\ell$-levels but would be quite large for low-lying n levels. Since the product ion may be subsequently re-ionized by interaction with its environment the stabilization mechanism is not quite as secure as that for dissociative recombination.

Although stabilization of the high Rydberg ion mainly occurs at high electron temperatures T_e, by the inner-core transition (47) with the captured electron as a spectator, stabilization can also occur by a radiative transition $n\ell \rightarrow n'\ell'$ of the outer electron. This mechanism tends to be effective mainly at much lower temperatures ($\lesssim 10^{4}$°K) characteristic of planetary nebulae. It is also effective for ions with low lying metastable levels, as in

$$e + O^{+}\ (^{4}S) \rightarrow O^{*}\ [2p^{3}(^{2}D)n'\ell'] \rightarrow O^{*}(^{2}D, n\ell) + h\nu \qquad (48)$$

The rate for dielectronic recombination (DIR) for an initial state i of the ion is, in the isolated resonance approximation (IRA), given by (16) as

$$k_{DIR}(T;i) = \left[\frac{h^3}{(2\pi mkT)^{3/2}}\right] \frac{1}{2g_i} \sum_d \sum_f g_d \left[\frac{\nu_a(d\rightarrow i)\nu_r(d\rightarrow f)}{\nu_r(d)+\nu_a(d)}\right] \exp(-E_d^{*}/kT) \qquad (49)$$

where g_i and g_d $(=2(2\ell+1))$ are the electronic statistical weights for state i of the recombining ion and for intermediate resonant state d $(=n\ell)$ at energy E_d^{*} above state i. Each resonant state d may autoionize back (via an Auger transition) to state i with frequency ν_a (d→i) or radiate with frequency ν_r (d→f) to bound levels f. The total radiative and Auger rates from d to all states are $\nu_r(d)$ and $\nu_a(d)$, respectively. The total DIR rate is obtained by summing over all possible initial states i, intermediate states d and final bound states f. Note that the factor $h^3/(2\pi mkT)^{3/2}$ in (49) is $(4\pi I_A/kT)^{3/2}$ $a_o^3 = 4.1212\ 10^{-16}\ T^{-3/2}\ cm^3$.

DIR within the past three years has been subjected to intense theoretical[3] and experimental[15] study. The existing calculations are based on either the Coulombic model, the distorted wave method and the relativistic configuration interaction method. For example, Chen[31] in a series of excellent papers has used the multiconfiguration Dirac-Fock model to evaluate the detailed transition energies and Auger and radiative rates. The calculations not only include the Coulomb r_{12}^{-1} interaction but also the Breit interaction and other quantum-electrodynamic corrections. A considerable amount of theoretical data has now been accumulated[3] for many different isoelectronic sequences - for cases when the number N of electrons in the initial ion is N = 1-5, 8-12, 18 and 19).

The autoionization frequency decreases with (n,ℓ) as $\nu_a \sim n^{-3} \exp(-a\ell^2)$ owing to a decrease in communication between the core and Rydberg electrons, and is independent of Z. The radiative frequency is $\nu_r \sim \alpha^3 Z^p$ for core decay ($p = 4$ or 1 with or without a change in core principal quantum number) and $\nu_r \sim \alpha^3 Z/n^3$ for outer electron decay. For small $n << 50$ and low ℓ, $\nu_r << \nu_a$ so that (49) is radiatively limited. At nebular temperatures $T \sim 10^4$ K the exponential in (49) restricts the summation to levels within ~ 0.15 eV of the ionization limit and ν_r is determined by outer electron decay. Since $\nu_a << \nu_r$ for large n, convergence can be obtained. Rates $k_{DIR} \sim (12\text{-}7)\ 10^{12}$ cm^3 s^{-1} for C^{2+}, N^{3+}, O^{4+} recombination at $T \sim 10^4$K which exceed the direct radiative contribution are typical.[3]

At high T ($\sim 10^7$ ^oK) ~ 1 keV characteristic of the solar corona, the full Rydberg series of autoionization levels must be included and core relaxation is the main radiative decay. For $n >> 50$, $\nu_a << \nu_r$ so that (49) is limited by autoionization. While the number of resonances increases as $2n^2$, only the low ℓ fraction are effective. Electric fields can however mix high ℓ-states with low ℓ-states so that DIR could be significantly enhanced. Typical rates[32] are ~ 3 10^{-11} cm^3 s^{-1} at 1 keV for F-like Se^{25+} - an X-ray laser candidate.

The separation ΔE (a.u.) between resonances of Rydberg series is $\sim Z^2/n^3$ which can become less than the radiative width $\Gamma_r = h\,\nu_r$. The detailed resonance structure is then smeared out by interaction with the radiation field and IRA breaks down. Bell and Seaton[2] have solved this problem by quantum defect theory which because of its close connection with Rydberg series is ideally suited to DIR. Thus DIR-cross sections can in principle be calculated to the same accuracy as electron-ion scattering cross sections (to within 10%).

For ions with low Z, Coster-Kronig (CK) channels, such as $1s2pn\ell \rightarrow 1s2s + e$ for He-like ions, become energetically accessible for large n.

This effect of autoionization to excited states of the recombining ion has generally been neglected in the fluorescence yield υ_r (d→f) $[\upsilon_r(d) + \upsilon_a(d)]^{-1}$ in all calculations of (49) until only recently. For example, the onset of the above CK transition for Be^{3+} ion is at $n^* = 3$, and n^* increases with Z (e.g., $n^* = 9$ for F^{7+}). Inclusion of CK transitions reduce[32] the peak values of the total DIR-rates for B^{3+}, N^{5+} and F^{7+} by 60%, 13% and 4%, respectively. This trend is correct since the relative contributions to DIR from high n-state (important at low Z) decrease with n, while the onset of CK-transitions occurs at higher n as Z increases. The CK-effects are not, of course, included in the largely historical semi-empirical formulae of Burgess[33] (for core decay $\Delta n = 0$) and of Merts et al.[34] (for $\Delta n = 1$). These formulae, although used quite generally by astrophysicists, overestimate[32] small Z-rates by a factor of 3 and underestimate large Z-rates by as much as a factor of 2.

In addition to CK-transitions for low Z, some remaining problems appear to be (a) effects of external fields on DIR, (b) three-body density effects on k_{DIR} and (c) fine structure effects. For (c), fine structure states of the excited ion-core provide two Rydberg series of autoionization channels which can mutually interfere (as in the decay $3p_{3/2}\,(n\ell) \rightarrow 3p_{1/2}(\epsilon_1\ell) + 3s_{1/2}(\epsilon_2\ell)$ in Mg^+). A problem which appears to be solved is the coupling between resonant DIR and the following non-resonant radiative recombination (RR) which, while negligible for ions with low Z, becomes appreciable at high Z.

The subsequent chain of atomic processes in astrophysics was initiated by the basic (e-H^+) Radiative Recombination (RR) process

$$e + A^{Z+}(i) \rightarrow A^{(Z-1)}(n\ell) + h\upsilon \qquad (50)$$

into level $(n\ell)$. Since RR is a direct inverse of photoionization with cross section $\sigma_I^{n\ell}(h\upsilon)$, the RR rate by detailed balance is

$$k_R^{n\ell}(T) = \left(\frac{8kT}{\pi m}\right)^{1/2}\left(\frac{kT}{mc^2}\right)\left(\frac{g_{n\ell}}{2g_i}\right)\exp(I_{n\ell}/kT)\int_{I_{n\ell}/kT}^{\infty}\left(\frac{h\nu}{kT}\right)^2\sigma_I^{n\ell}(h\nu)\exp(-h\nu/kT)d(h\nu/kT) \tag{51}$$

where g_i and $g_{n\ell}$ are the electronic statistical weights of the initial ion and the recombined ion in level $n\ell$ with ionization potential $I_{n\ell}$. Various analytical forms for σ_I can be adopted e.g., when $(h\nu)^3\,\sigma_I(h\nu)$ equals its value $I_n^3\,\sigma_o^{n\ell}(I_n)$ at threshold then the rate is

$$k_R^{n\ell}(T) = 1.5\ 10^{-13}\left(\frac{300}{T}\right)^{1/2}\left(\frac{I_n}{I_H}\right)^2\left(\frac{g_{n\ell}}{2g_i}\right)\bar{\sigma}_o^{n\ell}(T)\ \text{cm}^3\ \text{s}^{-1} \tag{52}$$

where, in terms of the exponential integral E_1, the averaged cross section is

$$\bar{\sigma}_I^{n\ell}(T) = \sigma_o^{n\ell}\,[x_n \exp x_n]E_1(x_n), \quad x_n = I_n/kT \tag{53}$$

which reduces at low temperatures $kT \ll I_n$ to

$$\bar{\sigma}_I^{n\ell}(T) = \sigma_o^{n\ell}\,[1-(kT/I_n) + 2(kT/I_n)^2 - 6(kT/I_n)^3 + \ldots\,] \tag{54}$$

The quantal cross section for photoionization of hydrogenic ions of charge Z by radiation of scaled energy $\omega(=h\nu/I_n)$ is

$$\sigma_I^{n\ell}(h\nu) = \sigma_K^n(\omega)\,G_{n\ell}(\omega) \rightarrow \begin{cases} \omega^{-3}, & h\nu \rightarrow I_n \\ \omega^{-\ell-7/2}, & h\nu \gg I_n \end{cases} \tag{55}$$

The departure from the (Kramer) semiclassical (high n and ℓ averaged) photoionization cross section[35]

$$\sigma_K^n(\omega) = \frac{2^6 a}{3\sqrt{3}} \left[\frac{n}{Z^2}\right] \left[\frac{I_n}{h\nu}\right]^3 \pi a_o^2 = 7.9\ n^2 Z^4 \omega^{-3}(\text{Mb}) \qquad (56)$$

where α is the fine structure constant (e^2/hc) is given by the bound-free Gaunt factor $G_{n\ell}$. The rate (14) is then

$$k_R^{n\ell}(Z,T) = \left[\frac{8kT}{\pi m}\right]^{1/2} \left[\frac{I_n}{kT}\right] \frac{1}{n} \left[\frac{2^S}{3\sqrt{3}}\right] (\alpha^3 \pi a_o^2) \left[\frac{g_{n\ell}}{2g_1}\right] F_{n\ell}(T^*) \qquad (57)$$

Departures of (57) from the above standard ($Z^2\ n^{-3}\ T^{-1/2}$) low temperature rule is provided by the function

$$F_{n\ell}(T^*) = \frac{1}{T^*} \exp(1/T^*) \int_1^\infty \frac{G_{n\ell}(\omega)}{\omega} \exp(-\omega/T^*) d\omega \qquad (58)$$

which decreases monotonically from $G_{n\ell}(1)$ as the scaled temperature T^* ($=kT/I_n$) increases. For interstellar clouds $kT \ll I_n$ and $F_{n\ell}(T^* \ll 1)$ tends to $G_{n\ell}(1)$ the threshold Gaunt factor. Note that (57) also provides the universal scaling law

$$k_R^{n\ell}(Z,T) = Z k_R^{n\ell}(1, T/Z^2) \qquad (59)$$

Recombination rates are greatest into low n levels and the $\omega^{-\ell-1/2}$ variation of $G_{n\ell}$ in (58) preferentially populates states with low $\ell \sim 2$-5. Highly accurate analytical fits for $G_{n\ell}(\omega)$ have been obtained[36] for $n \leq 20$ so that (57) is expressed in terms of known functions of fit parameters. This procedure (which does not violate the S_2 sum rule) has been extended[36] to non-hydrogen systems of neon-like Fe XVII, where $\sigma_I^{n\ell}(\omega)$ is a monotonically

decreasing function of ω.

Variation of the ℓ-averaged values, $n^{-2} \sum_{\ell=o}^{n-1} (2\ell+1)F_{n\ell}(T^*)$, is close[36] in both shape and magnitude with the corresponding semi-classical function $S(T^*)$ i.e., (58) with $G_{n\ell}(\omega) = 1$. Hence the ℓ-averaged recombination rate is

$$k_R^n(Z,T) \approx 1.1932\ 10^{-12} \left[\frac{300}{T}\right]^{1/2} \left[\frac{Z^2}{n}\right] F_n(T^*)\ \text{cm}^3\ \text{s}^{-1} \qquad (60)$$

where F_n can be calculated directly from (58) or be approximated as $G_n(1)$ $S(T^*)$. A computer program based on a three term expansion of G_n is also available.[37]

Tables exist[38] for the effective rate

$$k_E^{n\ell}(T) = \sum_{n'=n}^{\infty} \sum_{\ell'=o}^{n-1} k_R^{n'\ell'}\ C_{n'\ell',n\ell} \qquad (61)$$

of populating levels $n\ell$ of hydrogen by radiative recombination rate all levels $n' \geq n$ followed with probability $C_{i,f}$ for subsequent radiative cascade ($i \to f$) via all possible intermediate paths. Tables[38] also exist for the total rate

$$k_R^N = \sum_{n=N}^{\infty} n^{-2} \sum_{\ell=o}^{n-1} k_R^{n\ell} \qquad (62)$$

of recombination of levels N and above of hydrogen. They are useful in deducing time scales radiative of recombination and rates from (59) for complex ions.

When effective at higher temperatures, dielectronic recombination proceeds in general faster than RR. Since $k_R \sim Z^2$, RR can however become

competitive for highly charged ions. A unified treatment of DIR and RR has recently been presented.[39] The mutual interference of the corresponding amplitudes and continuum-continuum coupling is expected to be most important for individual transitions involving low-lying auto-ionization levels and is probably negligible for DIR arising from highly excited levels. If the photoionization cross section $\sigma_I^{n\ell}(h\upsilon)$ already includes the effects of autoionizing resonances, no further correction for DIR to RR may be necessary.

5. MUTUAL NEUTRALIZATION (MN)

Until fairly recently (1984), lack of agreement of various curve-crossing and Landau-Zener type theories with experiment for such a simple system as

$$H^+ + H^- \rightarrow H^*(n) + H \qquad (63)$$

remained embarassing, and agreement between the two main experiments remained very good. Then a 1983-theory[40] which included couplings (neglected in previous theories) to the n = 3 level still did not agree with measurement, until new experiments[41,42] were performed in 1984 and 1985. The process (63) is now apparently well understood, but careful quantum mechanics and experiment is required.

In dense interstellar clouds, MN of complex systems can be important and can produce qualitative changes[24] in the chemistry sequence. For example, when polycyclic aromatic hydrocarbons (PAH) exist in high abundance, the negative charge is carried not by electrons but by PAH^- so that MN, as in $C^+ + PAH^- \rightarrow C + PAH$, replaces dissociative recombination (DR) so that the C-abundance is enhanced.[24]

6. TERMOLECULAR RECOMBINATION

6.1 *ION-ION*:

The theory of termolecular ion-ion recombination and

$$A^+ + B^- + M \underset{k}{\overset{\alpha}{\rightleftarrows}} AB + M \tag{64}$$

of positive and negative atomic ions of concentrations $N_{A,B}(t)$ at time t in a gas M is also well established,[43] and is also suitable as a case study. The effective two-body association rate $\alpha(N,T)$ cm^3 s^{-1} and the dissociation frequency $k(N,T)$ s^{-1} are functions of gas density and are given by[43]

$$\alpha \tilde{N}_A \tilde{N}_B = \int_{-D}^{\infty} P_i^S \, dE_i \int_{-D}^{\infty} (P_i^S - P_f^S) \, C_{if} \, dE_f = k \tilde{n}_s \tag{65}$$

where P_i^S, which measures the departure from equilibrium, is the stochastic probability that a pair (A^+-B^-) with energy-distribution n_i over internal relative energy E_i of the pair is connected via a multistep series of energy (state)-changing collisions to a stabilized sink $\mathcal{S}$ of low lying fully associated pairs of concentration n_s (cf. Fig. 2). The sink $\mathcal{S}$ extends over the energy range $-S \geq E_i \geq -D$ where -D is the lowest energy level and where -S is that bound level below which P_i^S is unity. The one-way equilibrium rate C_{if} for $E_i \to E_f$ collisional transitions per unit interval $dE_i dE_f$ is $\tilde{n}_i \upsilon_{if}$, and the distribution n_i satisfies the input-output collisional Master Equation[43]

$$\frac{dn_i}{dt} = [\tau_c(t) - \tau_s(t)] \int_{-D}^{\infty} (P_i^S - P_f^S) \, C_{if} \, dE_f \tag{66}$$

where the departures from their steady equilibrium (tilda) values of the total

time-dependent concentrations of fully dissociated pairs (in block $\mathscr{C}$, $0 \leq E_i \leq \infty$ where $P_i^S \tilde{\simeq} 0$) and of fully associated pairs (in block $\mathscr{S}$ where $P_i^S \tilde{\simeq} 1$) are

$$\tau_c(t) = N_A(t)N_B(t)/\tilde{N}_A\tilde{N}_B \; ; \quad \tau_s(t) = n_s(t)/\tilde{n}_s \tag{67}$$

respectively. For quasi-steady-state (QSS) of the intermediate block $\mathscr{E}$ ($0 \geq E_i \geq -S$) of highly excited levels at time t, (66) vanishes so that (64) reduces to

$$\alpha \tilde{N}_A\tilde{N}_A = \int_{-E}^{\infty} dE_i \int_{-D}^{-E} (P_f^S - P_i^S)\, C_{if}\, dE_f \; , \tag{68}$$

for arbitrary energy -E in block $\mathscr{E}$.

6.1.1 *VARIATIONAL PRINCIPLE*: It has been recently proposed[44] that P_i^S are so distributed that the rate (65) is a minimum. This distribution leads exactly to the QSS-distribution given by (66) set to zero. Thus (65) provides a variational expression for the QSS condition, so that P_i^S may be determined (Fig. 3) variationally or from the direct solution of the integral equation (66). The Variational[44] and QSS[43] rates obtained are of course identical.

6.1.2 *DIFFUSION METHOD.* By performing a Fokker-Planck conversion of the integral equation (66), the resulting (but approximate) differential equation is identical with a diffusion equation in energy space which can be solved analytically for P_i^S (Fig. 3). Insertion in (65) yields a proposed diffusional method[45] which is highly accurate (Fig. 4).

6.1.3 *BOTTLENECK LIMIT.* On assuming that pairs above and below a bound level -E are in equilibrium with the fully dissociated and associated (blocks C and S, respectively (i.e., $P_i^S = 0$ for $E_i > -E$ and $P_i^S = 1$ for $E_i < -E$) then either (64) or (68) yield,

$$\alpha(-E)\ \tilde{N}_A\tilde{N}_B = \int_{-E}^{\infty} dE_i \int_{-D}^{-E} C_{if}\ dE_f \tag{69}$$

the one-way equilibrium collisional rate across -E, which is then an upper limit to the exact rate. Variation of α with -E yields the least-upper-limit at the bottleneck energy E^* (see refs. [23] and [43]).

Other approximations such as Coupled Nearest-Neighbor (CNN) limit and Uncoupled Intermediate ℓ-block Levels (UIL), based on analogy of (65) and (66) with electrical networks recently proposed,[46] have also elucidated the modes of energy reduction.

6.1.4 *GAS DENSITY*

As the gas density N is raised non-equilibrium effects in internal separation R of A^+ and B^- must be considered. The appropriate input-output collisional-transport Master Equation satisfied by the distribution $n_i(\underset{\sim}{R})$ of $(A^+\text{-}B^-)$ pairs per unit interval $d\underset{\sim}{R}\ dE_i$ has been shown to satisfy the continuity equation[47]

$$\frac{d}{dt}\, n_i(R,t) = \frac{\partial n_i}{\partial t} + \frac{1}{R^2}\frac{\partial}{\partial R}\,[R^2 j_i^d(R)]_{E_i}$$

$$= -\int_{V(R)}^{\infty} [n_i(R)v_{if}(R) - n_f(R)v_{fi}(R)]dE_f \tag{70}$$

where $j_i^d(R)$ $(= j_i^+ - j_i^-)$ is the net outward transport current of pairs expanding at R, where $\nu_{if}(R)$ is the frequency per unit interval $d\underset{\sim}{R}\ dE_i\ dE_f$ for $E_i \to E_f$ collisional transitions for ions at fixed separation R and where V(R) is the energy of interaction between A and B. Integration of (70) over all accessible R yields the standard Master Equation (66).

The question of reproducing the cumulative effects of multistep

energy-changing collisions by an accumulative strong collision within a loose collision complex of radial extent R_T can now be examined.[43] The rate of recombination within a sphere of radius R_T and the overall probability $P_i^A(R_T)$ of association within R_T are related by low gas density by

$$\alpha(R_T)\ \tilde{N}_A\tilde{N}_B = \int_0^\infty [4\pi R_T^2 \tilde{j}_i^-(R_T)]P_i^A(R_T)dE_i \quad , \tag{71}$$

which is expressed via (70) in terms of the stabilization probabilities P_f^S by[43]

$$\alpha(R_T)\ \tilde{N}_A\tilde{N}_B = \int_0^\infty dE_i \int_0^{R_T} d\underline{R} \int_{V(R)}^0 C_{if}\ P_f^S\ dE_f \tag{72}$$

A strong-collision (or classical) treatment refers to the assignment $P_f^S = 1$ in (72).

Fig. 5 illustrates the ratio of the effective strong-collision rate, to α_E, the exact rate α ($R_T \to \infty$). Agreement can be obtained by assigning (de-facto) $R_T \tilde{\sim} 0.5\ R_e$. The underlying reason becomes apparent from Fig. 6. The exact probability P_i^{AE} that (E_i=0) dissociated pairs ultimately associate dominates the probability P_i^{RD} for ultimate redissociation (after bound levels are formed) for smaller $R_T << R_e = e^2/kT$, so that P_i^{AE} and the strong-collision probability P_i^{ST} (from (72) with $P_f^S = 1$) are essentially equal. Pairs with larger $R_T >> R_e$ are however mainly redissociated (Fig. 6). The strong collision rate at $R_T \sim 0.45$ is then twice the rate $\alpha(R_T)$ of (72). The remaining contribution from $R \geq R_T$ to the exact rate provides agreement with the strong collision rates.[43]

The concept of the above loose reaction complex is useful in showing[23] with the aid of (70) that the variation of recombination with gas density yields the familiar result

$$\alpha(N) = \frac{\alpha_{RN}\ \alpha_{TR}}{\alpha_{RN}+\alpha_{TR}} \tag{73}$$

where $\alpha_{TR}(N)$, the known rate for transport of pairs by diffusional-drift to within separation R_T, decreases as N^{-1}. The reaction rate α_{RN} by collision with M within $R \leq R_T$ increases initially linearly with N and saturates at higher N (~ 1 atm). The magnitude and density variation of (73), with accompanying theoretical procedures, agree with Monte-Carlo Computer Simulations for the recombination of rare gas-halide systems.[4,6] No benchmark measurements are available, but the two historical measurements at low and high N respectively in general agree[17] with (73).

6.2 Electron-Ion: The trapping radius concept is also useful to obtain classical rates (i.e., (72) with $P_f^S = 1$) not only for termolecular recombination (64) but also for electron and neutral stabilized electron-ion collisional recombination (9) and (7) respectively. The frequency $\nu_i(R) = \int_{V(R)}^{o} \nu_{if}(R)dE_f$ for formation of bound pairs is $v_{12}(R)\sigma N$, where v_{12} is the speed of $A^+ + B^-$ relative motion and σ is the cross section for AB^*-M deactivating collisions. On assuming constant cross section σ_o for such collisions, (72) reduces (with $P_f^S = 1$) exactly to

$$\alpha \tilde{N}_A \tilde{N}_B = \left[\int_o^\infty dE_i \int_o^{R_o} \tilde{n}_i(R)\, v_{12}(R)dR \right](\sigma_o N) \qquad (74)$$

$$= \left(\frac{8kT}{\pi M_{AB}}\right)^{1/2} \left[\frac{4}{3} \pi R_o^3 \right] \left[1 + \frac{3}{2} \frac{R_e}{R_o} \right] \sigma_o N \qquad (75)$$

where R_e is e^2/kT. A classical version of the semiquantal bottleneck treatment (§ 6.1.3 above) yields, a priori, the trapping radius to be $R_o = 0.41\ R_e$. The rates α of termolecular recombination (64), and of e-e collisional recombination ($e + A^+ + e$) at electron temperature T_e and electron density n_e

are therefore,

$$\alpha_{TR}(T) = 0.32 \left[\frac{8kT}{\pi M_{AB}}\right]^{1/2} \left[\frac{4}{3}\pi R_e^3\right] (\sigma_o N) \sim 2.3\ 10^{-25}\ (300/T)^{2.5}\ N(cm^3\ s^{-1}) \quad (76)$$

and

$$\alpha_{ee}(T) = 0.32 \left[\frac{8kT}{\pi m}\right]^{1/2} \left[\frac{4}{3}\pi R_e^3\right] (\frac{1}{9}\pi R_e^2) n_e \sim 2.7\ 10^{-20}\ (300/T)^{4.5}\ n_e(cm^3 s^{-1}) \quad (77)$$

respectively. In (77), σ_o for electron-electron collisions is taken as the Coulomb cross section ($\frac{1}{9}\pi R_e^2$) for energy changes $\geq \frac{3}{2}$ kT. These expressions provide the correct order of magnitude and temperature dependence, and, in general, agree with experiment. In particular (76) agrees with the expression of Mansbach and Keck[48] derived from more elaborate analysis. At higher T_e and lower n_e, the highly excited levels collisionally formed within kT of the ionization limit become increasingly stabilized by radiative transitions. The resulting rate for collisional-radiative recombination can then be approximated as[49]

$$\alpha_{CR} = [3.8\ 10^{-9}\ T_e^{-4.5}\ n_e + 1.55\ 10^{-10}\ T_e^{-0.63} + 6\ 10^{-9}\ T_e^{-2.98}\ n_e^{0.37}]cm^3 s^{-1} \quad (78)$$

where the first term is (77), the second term is the radiative correction and the third term arises from collisional-radiative coupling. This expression agrees with the experimental data[49] to within 10% for a Lyman optically thick plasma with n_e and T_e in the range $10^9 \leq n_e\ (cm^{-3}) \leq 10^{13}$ and $2.50 \leq T_e\ (^oK) \leq 4000K$.

For termolecular ($e + A^+ + B$) collisional recombination only a small fraction $\delta = 2m/M_B$ can be transferred in e-B elastic collisions so that the

E_i-integration in (74) must be so restricted to give

$$\alpha_{eB}(T_e) = \left(\frac{8kT}{\pi m}\right)^{1/2} 4\pi R_o^3 (\sigma_o N) \int_o^{r_o} r^2 dr \int_o^{\delta/r} \left(1 + \frac{1}{r\epsilon}\right) \epsilon e^{-\epsilon} d\epsilon \qquad (79)$$

with $R = r R_e$ and $\epsilon = E_i/kT$. Hence

$$\alpha_{eB}(T_e) = 4\pi\delta \left(\frac{8kT_e}{\pi m}\right)^{1/2} R_e^2 R_o (\sigma_o N) \sim [10^{-26}/M_C(AMU)] (300/T)^{2.5} N \qquad (80)$$

which agrees exactly with the diffusion result of Pitaevskii[50] and which is linear[51] in the trapping radius R_o. This result ($\sim 10^{-28}$ cm^3 s^{-1}) is in general agreement with experimental data for ($e + He^+ + Cs$) but is much smaller than that ($\sim 10^{-26}$) for ($e + He^+ + He$), which proceeds far more effectively[52] via formation of an intermediate complex He_2^* which then dissociates into neutral fragments.

The rate for ($e + A^+ + B$) is greatly increased[51] for a molecular gas B where energy reductions are effected mainly by rotational and vibrational transitions. Allowance for the discreteness of (e-A^+) Rydberg levels reduces α_{eM} and produces a sharper decrease with temperature.[53] When A^+ is a molecular ion XY^+ a dissociative recombination channel opens. Here the (e-XY^+) pairs formed in highly excited Rydberg molecular levels XY^* by collision with M, in addition to being collisionally and radiatively quenched to stable bound states of AB, may predissociate along repulsive curves X^*+Y i.e., by dissociative recombination involving bound electrons - the second half of the indirect mechanism.[43] The contribution from this *collisional dissociative recombination*[53] can dominate the contribution from direct collisional relaxation. That quantal curve-crossing is involved makes it

similar to the enhancement[6] of mutual neutralization ($A^+ + B^-$) by third bodies. In the limit of high gas density N, the recombination rate α_{eM} becomes transport limited, as in (73) for ion-ion recombination and decreases as N^{-1}. Because of the higher electron mobilities, its onset however occurs at much higher N. Between the linear low density region and the transport limited N^{-1} region only Monte Carlo simulations have been performed.[54] For ($e + A^+ + M$) recombination in a molecular gas the rotational and vibrational cross sections of Takayanagi[55] and of Takayanagi and Itikawa[56] and the recommended molecular constants[56] are invaluable.

Acknowledgements: This research is supported by the U.S. Air Force Office of Scientific Research under Grant No. AFOSR-84-0233.

REFERENCES

1. M. J. Seaton and P. J. Storey, in: Atomic Processes and Applications (P. G. Burke and B. L. Moiseivitsch, eds.), pp. 133-197, North-Holland, Amsterdam (1976).
2. R. H. Bell and M. J. Seaton, J. Phys. B 18, 1589-1629 (1985).
3. Y. Hahn and K. J. LaGattuta, Physics Reports 166, 195-268 (1988).
4. M. R. Flannery, in: Applied Atomic Collision Physics (E. W. McDaniel and W. L. Nighan, eds.), Vol. 3, pp. 141-172, Academic, New York (1982).
5. M. R. Flannery, Phil. Trans. R. Soc. London. Ser. A 304, 447-497 (1982).
6. D. R. Bates, in: Advances in Atomic and Molecular Physics (D. R. Bates and B. Bederson, eds.) Vol. 20, pp. 1-40, Academic, New York (1985).
7. M. R. Flannery, J. Chem. Phys. 88, 4228-4241 (1988).
8. See Contributions in: Proc. Intern. Workshop on Dissociative Recombination: Theory, Experiment and Applications (J. B. A. Mitchell and S. Guberman, eds.), World Scientific, New Jersey (1988).
9. D. R. Bates, in: Recent Studies in Atomic and Molecular Processes (A. E. Kingston, ed.), pp. 1-27, Plenum, New York (1987).
10. D. R. Bates and E. Herbst, in Reaction Rate Coefficients in Astrophysics (T. J. Miller and D. A. Williams, eds.) in press, Kluver, Dordrecht (1989).
11. J. B. A. Mitchell, in: Atomic Processes in Electron-Ion and Ion-Ion Collisions (F. Brouillard, ed.), pp. 185-222, Plenum, New York (1986).
12. D. Smith, in: Advances in Atomic and Molecular Physics (D. R. Bates and B. Bederson, eds.) Vol. 24, pp. 1-49, Academic, New York (1988).
13. K. Dolder and B. Peart, in: Advances in Atomic and Molecular Physics (D. R. Bates and B. Bederson, eds.) Vol. 22, Academic, New York (1986).
14. G. H. Dunn, in: Atomic Processes in Electron-Ion and Ion-Ion Collisions (F. Brouillard, ed.) pp. 93-116, Plenum, New York (1986).

15. See contributions in: Atomic Excitation and Recombination in External Fields (M. H. Hayfeh and C. W. Clark, eds.) pp. 439-452, Gordon and Breach, New York (1985).

16. S. E. Barlow, G. H. Dunn and K. Schauer, Phys. Rev. Letts. 52, 902-905; 53, 1610 (1984).

17. M. R. Flannery, in: Atomic Processes and Applications (P. G. Burke and B. L. Moiseiwitsch, eds.), pp. 407-466, North Holland, Amsterdam (1976).

18. H. S. Lee and R. Johnsen, Bull. Amer. Phys. Soc. 33(2), 149 (1988).

19. A. Gusti-Sugor, E. Roueff and H. van Regemorter, J. Phys. B 9, 1021-1034 (1976).

20. H. Abgrall, A. Giusti-Sugor and E. Roueff, Astrophys. Jour. 207, L69-L72 (1976).

21. D. R. Bates and C. S. McKibbin, Proc. Roy. Soc. A 33, 13-28 (1974).

22. A. D. Dickinson, R. E. Roberts and R. B. Bernstein, J. Phys. B 5, 355-365 (1976).

23. M. R. Flannery, in: Recent Studies in Atomic and Molecular Processes (A. E. Kingston, ed.) pp. 167-197, Plenum, New York (1987).

24. A. Dalgarno, in: Recent Studies in Atomic and Molecular Processes (A. E. Kingston, ed.) pp. 51-61, Plenum, New York (1987).

25. B. G. Anicich and W. T. Huntress, Jr., Astrophys. Jour. Supplem. Ser. 62, 553-672 (1986).

26. J. N. Bardsley and M. A. Biondi, in: Advances in Atomic and Molecular Physics (D. R. Bates and I. Esterman, eds.) Vol. 6, pp. 1-57, Academic, New York (1970).

27. A. Gusti-Sugor, J. N. Bardsley and C. Derkits, Phys. Rev. A 28, 682-691 (1983).

28. H. Nakamura, H. Takagi and K. Nakashima, in: reference 8.

29. H. Hus, F. Yousif, C. Noren, A. Sen and J. B. A. Mitchell, Phys. Rev. Letts. 60, 1006-1009 (1988).

30. H. Hus, F. Yousif, A. Sen and J. B. A. Mitchell, Phys. Rev. 38, 658-663 (1988).

31. D. Smith and N. G. Adams, J. Chem. Soc. Far. Trans. 2, 83 (1987); 2, 149 (1987).

32. M. H. Chen, Phys. Rev. A 34, 1079-1083 (1986).

33. A. Burgess, Astrophys. Journ. 141, 1588-1590 (1965).

34. A. L. Merts, R. D. Cowan and N. H. Magee, Los Alamos Scientific Laboratory Report No. LA-6220-MS, 1976.

35. H. A. Bethe and E. E. Salpeter, Quantum Mechanics of One- and Two-Electron Atoms, pp. 308-322, Plenum, New York (1977).

36. B. F. Rozsmyai and V. L. Jacobs, Astrophys. Jour. 327, 485-501 (1988).

37. D. R. Flower and M. J. Seaton, Computer Physics Communications 1, 31-34 (1969).

38. P. G. Martin, Astrophys. Jour. Supplem, 66, 125-138 (1988).

39. V. L. Jacobs, J. Cooper and S. L. Haan, Phys. Rev. A 36, 1093-1113 (1987).

40. V. Sidis, C. Kubach and D. Fussen, Phys. Rev. A 27, 2431-2446 (1983).

41. S. Szucs, M. Karema, M. Terao and F. Brouillard, J. Phys. B 17, 1613-1622 (1984).

42. B. Peart, M. A. Bennett and K. Dolder, J. Phys. B 18, L439-L444 (1985).

43. M. R. Flannery and E. J. Mansky, J. Chem. Phys. 88, 4228-4241 (1988).

44. M. R. Flannery, J. Chem. Phys. 89, 214-222 (1988).

45. M. R. Flannery, J. Chem. Phys. 87, 6947-6956 (1987).

46. M. R. Flannery, J. Chem. Phys. 89, 4086-4091 (1988).

47. M. R. Flannery, J. Phys. B 20, 3929-4938 (1987).

48. P. Mansbach and J. Keck, Phys. Rev. 181, 275-289 (1965).

49. J. Stevefelt, J. Boulmer and J. F. Delpech, Phys. Rev. A 12, 1246-1251 (1975).

50. L. P. Pitaevskii, Sov. Phys. - JETP 15, 919-921 (1962).

51. D. R. Bates, J. Phys. B 13. 2587-2599 (1980).

52. D. R. Bates, J. Phys. B 12, L35-L38 (1979).

53. D. R. Bates, J. Phys. B 14, 3525-3534 (1981).

54. W. L. Morgan, in: Recent Studies in Atomic and Molecular Processes (A. E. Kingston, ed.) pp. 149-166, Plenum, New York (1987).

55. K. Takayanagi, in: Advances in Atomic and Molecular Physics (D. R. Bates and I. Esterman, eds.), Vol. 1, pp. 149-194, Academic, New York (1965).

56. K. Takayanagi and Y. Itikawa, in: Advances in Atomic and Molecular Physics (D. R. Bates and I. Esterman, eds.), Vol. 6, pp. 105-153, Academic, New York (1970).

Figure Captions

Figure 1. Schematic representation of potential energy curves for dissociative recombination, $e + AB^+ \rightarrow A^{**} + B$, (a) via the direct (vertical transition) mechanism and (b) via the indirect (Rydberg) mechanism.

Figure 2. Schematic Diagram of energy blocks $\mathscr{C}$, $\mathscr{E}$ and $\mathscr{S}$ pertinent to recombination at low gas densities.

Figure 3. Stabilization probabilities: (E): quasi-steady-state[43] (V2): two-parameter Variational.[44] (D): Diffusion.[45]

Figure 4. $(A^+ + B^- + M)$ partial recombination rates $\left[\frac{M_A}{M_{AB}}\right] \alpha(a)$ normalized to Thomson's rate $\alpha_T(a)$ as a function of mass parameter $a = M_B M_g / M_A(M_A+M_B+M_g)$ for various (A^+-M) or (B^-M) interactions (CX: symmetrical resonance charge transfer; HS: hard-sphere; POL: polarization attraction). The full rates are $\alpha(a)\alpha_T(a) + \alpha(b)\alpha_T(b)$ where $b = (M_A/M_B)^2 a$ and where Thomson's rate is $\alpha_T(a) = \frac{4}{3}\pi R_e^3 (3\ kT/M_{AB})^{1/2} \sigma_{AM} N$. (Ref. 43.)

Figure 5. Variation of $\alpha(R_T)$, eq. (72) with $P_f^S = 1$, to exact rate, eq. (72) with $R_T \rightarrow \infty$, for ion-ion recombination of equal-mass species under various (A^+-M) interactions (cf. Fig. 4).

Figure 6. Probability for eventual association and re-dissociation of (A^+-B^-) pairs with zero internal energy. P^{AE} and P^{RD}: exact association and redissociation. P^{ST}: strong collision. The probabilities are normalized to Thomson's low density probability $P_T = R_T (\sigma_{AM} N)$. (Ref. 43).

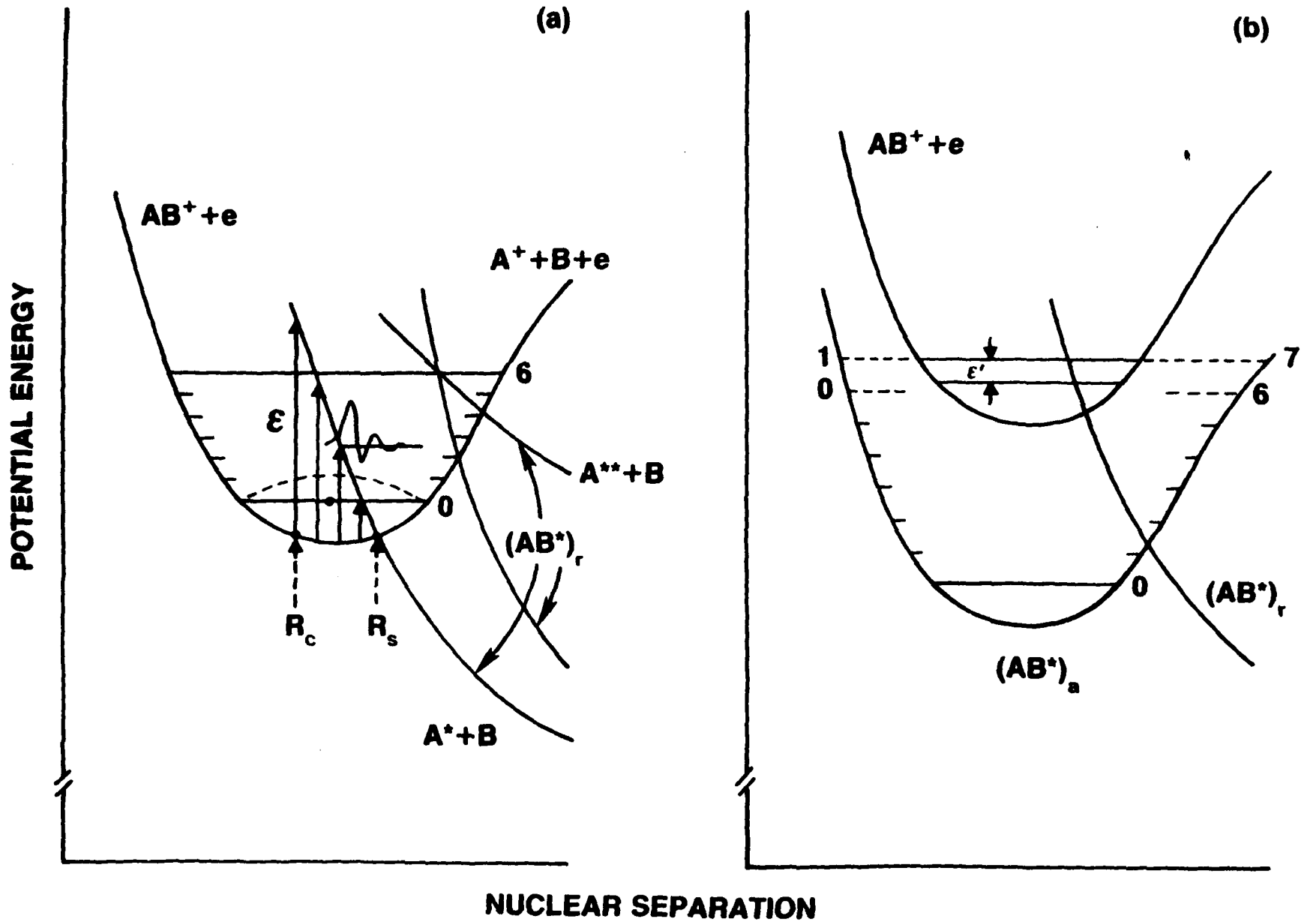
(a)
(b)
POTENTIAL ENERGY
NUCLEAR SEPARATION
AB+ +e
A+ +B+e
A** +B
A* +B
(AB*)r
(AB*)a
ε
ε'
R_c
R_s
6
0
1
7

FIG. 1

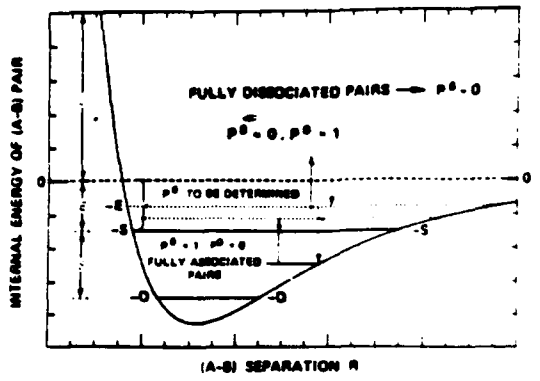

FIG. 2.

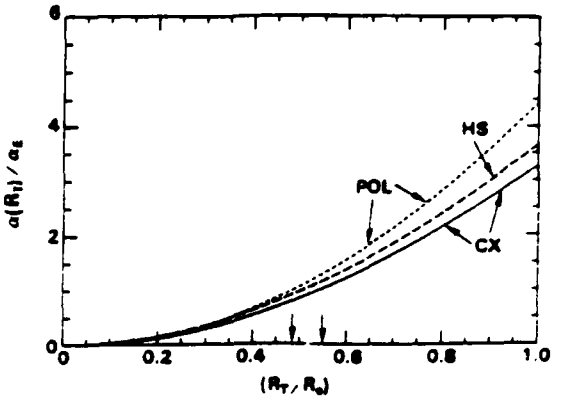

FIG. 5.

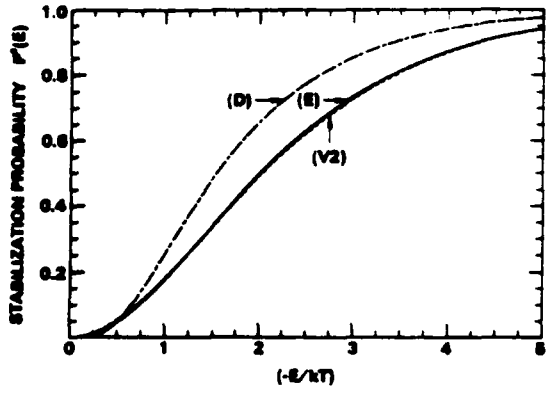

FIG. 3.

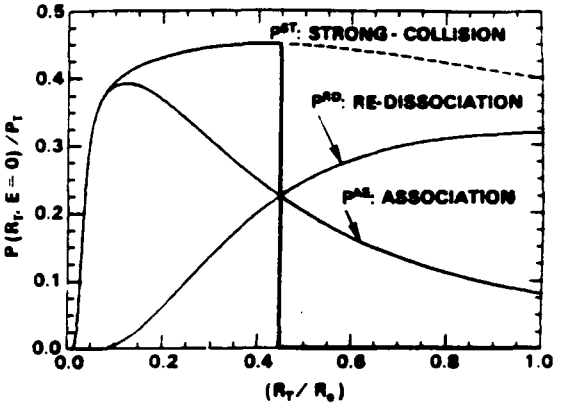

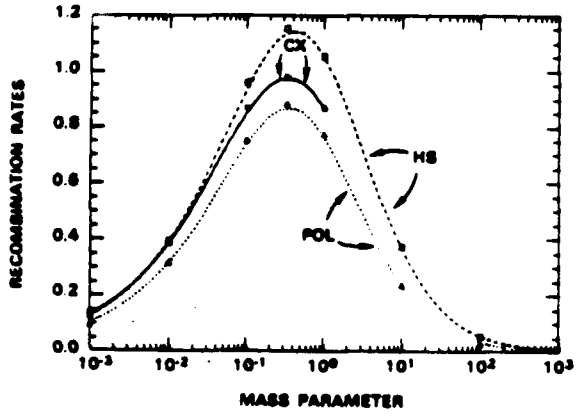

FIG. 4.

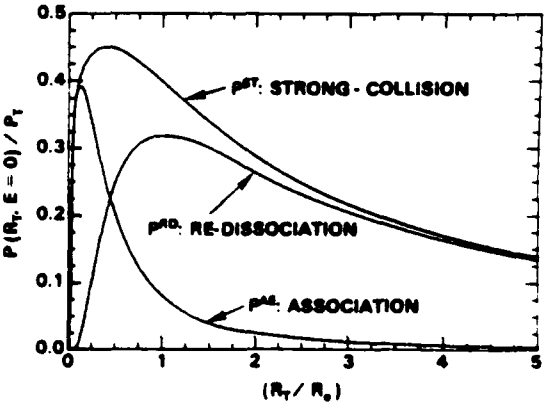

FIG. 6.

Appendix B

ELECTRON COLLISION CROSS SECTIONS INVOLVING EXCITED STATES

E. J. Mansky

School of Physics
Georgia Institute of Technology
Atlanta, Georgia 30332-0430 U.S.A.

Knowledge of the integral cross sections for the electron-impact excitation of atoms initially in a metastable state is of fundamental importance not only in determining the number densities of atoms in various excited states, but also in understanding the overall collision dynamics of energy transfer and excited-state diagnostics in partially ionized gases. Recently, the study of transitions between metastable states of He has been revitalized by experimental measurements at Kaiserslautern (Müller-Fiedler et al. 1984) of the differential cross sections, and at Madison (Rall et al. 1989) of the integral cross sections for the $2^3S \rightarrow 3^3L$ electronic excitations in helium. This signals a new era in experiments involving metastable states in that much more detailed information can now be obtained by modern measurements than was possible in the pioneering work of Phelps (1955). This has also marked a resurgence in theoretical activity in this area as well with recent distorted wave calculations (Mathur et al., 1987) and optical potential calculations (Vučić et al. 1987). In this note we will briefly summarize the original multichannel eikonal theory of Flannery and McCann (1974a,b,c, 1975a,b), together with the correction needed to account for the influence that distant trajectories have on the scattering amplitude for states dipole-coupled via an optically-allowed transition to the initial state (Mansky and Flannery 1989a). In particular, attention will be focused on the results for the $2^3S \rightarrow 3^3L$ transitions in He due to the recent experimental data which has become available.

The basic expression in the multichannel eikonal theory (MET) for the complex scattering amplitude for the transition $i \rightarrow n$ is (Flannery and McCann 1975a,c)

$$f_{ni}(\theta) = -(i)^{\Delta+1} \int_0^\infty J_\Delta(q'\rho) \, [I_1(\rho,\gamma(\theta)) - i \, I_2(\rho,\gamma(\theta))\rho \, d\rho \qquad (1)$$

where the integrals I_1 and I_2 are defined,

$$I_1(\rho,\tau(\theta)) = \int_{-\infty}^{\infty} dz\ \kappa_n(\rho,z)\ \frac{\partial C_n(\rho,z)}{\partial z}\ \exp[i\tau(\theta)z] \qquad (2a)$$

$$I_2(\rho,\tau(\theta)) = \int_{-\infty}^{\infty} dz\ [\kappa_n(\kappa_n-k_n) + \frac{\mu}{\hbar^2} V_{nn}]C_n(\rho,z)\ \exp[i\tau(\theta)z] \qquad (2b)$$

The other terms in equations (1) and (2) are: $q' = k_n \sin\theta$; $\tau(\theta) = k_n(1-\cos\theta)$; $\Delta \equiv m_i - m_n$, where $m_i(m_n)$ is the magnetic quantum number of state i(n); J_Δ is an ordinary Bessel function of order Δ; $\kappa_n^2 = k_n^2 - \frac{2\mu}{\hbar^2} V_{nn}$. The complex amplitude functions $C_n(\rho,z)$ in equation (2) are solutions of the following set of coupled first-order partial differential equations,

$$i\frac{\hbar^2}{\mu}\kappa_n \frac{\partial C_n(\rho,z)}{\partial z} + [\frac{\hbar^2}{\mu}\kappa_n(\kappa_n-k_n)+V_{nn}]C_n(\rho,z) = \sum_{j=1}^{N} V_{nj}C_j\ \exp[i(k_j-k_n)z] \quad (3)$$

which are solved subject to the asymptotic boundary condition condition, $C_n(\rho,z\to-\infty) = \delta_{ni}$ for the N states in the basis set (n = 1,2,...,N). For definitions of the remaining terms in equations (1-3) and a complete derivation of these equations see the original MET papers of Flannery and McCann (1974a,b,c, 1975a,b).

The main assumptions made in the derivation of (3) is that the trajectory for the relative motion of the electron in channel n is accurately characterized by a straight-line, and that the contribution of exchange to the inelastic integral cross section for channel n is negligible. The assumption of a straight-line trajectory for the relative motion of the projectile electron in $e^- + A^*$ collisions should be reliable due to the dominant nature of the long range part of the projectile-target electrostatic interaction in these collisions. However, in heavy particle collisions account must be taken of the curvature of the trajectory in order for accurate inelastic integral cross sections to be obtained. This has been done within the MET for applications in heavy particle collisions by McCann and Flannery (1975,1978).

Similarly, in electron-metastable atom collisions the neglect of electron exchange effects should not introduce a great deal of error (Vučić et al. 1987). This is due to the increased size of the target atom when the incident state is an excited state. Recall that for hydrogen (Bethe and Salpeter 1977), the mean value of r, the electron-nucleus distance, scales with n as, $\langle r\rangle = [3n^2 - \ell(\ell+1)]/2Z$. This increase results in a concomitant decrease in the electronic charge density $\rho(r)$ of the target atom, which results in a lowering of the probability of overlap of the projectile electron's wavefunction with that of the bound electron, thereby decreasing the importance of electron exchange when compared to the case of scattering from ground state targets (i.e., target atoms initially in the ground state).

In actual calculations the coupled PDE's (3) are solved over a finite 2-dimensional grid: $0 \le \rho \le \rho_{max}$, $-z_{max} \le z \le z_{max}$. The subsequent ρ-integration in (1) is then from $\rho = 0$ to $\rho = \rho_{max}$. Typical values of

z_{max} for ground state targets is 100-120 a_o, while for metastable targets (i.e., target atoms initially in a metastable state) z_{max} ranges from 250-300 a_o. The typical values of ρ_{max} range from 11 to 35 a_o for ground state targets, while for metastable targets the corresponding range is from 48 to 207 a_o. These ranges on z_{max} and ρ_{max} refer to 10-channel eikonal theory results for hydrogen and helium (Mansky and Flannery 1989a,b). While the above values of z_{max} and ρ_{max} for ground state targets is sufficient to insure convergence of the inelastic integral cross section to the corresponding Born value at high energy, in the case of metastable targets this is not the case. The contribution that trajectories, with impact parameters ρ in the range $\rho_{max} \leq \rho < \infty$, make to the scattering amplitude for metastable transitions (e.g., $2^3S \rightarrow 3^3L$, L = S,P,D) is not negligible at high energies. This is particularly true of metastable states dipole-coupled to the initial state via an optically-allowed transition. The correction to the scattering amplitude needed to account for these distant trajectories is given by (Mansky and Flannery 1989a),

$$f_{ni}^{(DMET)}(\theta) = \Gamma \int_0^{\rho_{max}} J_\Delta(q'\rho)[I_1(\rho,\gamma) - i\, I_2(\rho,\gamma)]\rho\, d\rho + f_{ni}^{(dipole)}(\theta)$$

$$= f_{ni}^{(MET)}(\theta) + f_{ni}^{(dipole)}(\theta), \text{ dipole-coupled transitions} \quad (4a)$$

$$= f_{ni}^{(MET)}(\theta) \quad , \text{ all other transitions} \quad (4b)$$

where,

$$f_{ni}^{(dipole)}(\theta) = \Gamma(i)^{\Delta+1} \frac{2\mu d'_{ni}}{\hbar^2} \frac{\alpha'}{q'^2+\alpha'^2} [x_1 J_{\Delta+1}(x_1)K_\Delta(x_1) - x_2 J_\Delta(x_2)K_{\Delta+1}(x_2)] \quad (5)$$

and $\Gamma = -(i)^{\Delta+1}$, $\alpha' = \gamma(\theta)-\alpha$, $\alpha = 2\mu(\epsilon_n-\epsilon_i)/\hbar^2(k_i+k_n)$, $d'_{ni} = \sqrt{3/4\pi}\, d_{ni}$, with d_{ni} denoting the dipole moment for the transition $i \rightarrow n$, and $x_1 = q'\rho_{max}$, $x_2 = \alpha'\rho_{max}$. The eigenenergies of the target atom are denoted ϵ_n, while $K_m(x)$ is a modified Bessel function of order m.

In this note the dipole correction (5) has been applied only to the $2^3S \rightarrow 2^3P_{o,\pm1}$ and $2^3S \rightarrow 3^3P_{o,\pm1}$ (Δ = 0,1) transitions within a 9-channel basis (2^3S, $2^3P_{o,\pm1}$, 3^3S, $3^3P_{o,\pm1}$ and $3^3D_{o,\pm1,\pm2}$). The present multichannel eikonal theory results for these transitions are hereafter denoted DMET. However, to avoid confusion with Flannery and McCann's (1975) original MET results, the present results for the remaining triplet transitions will also be denoted DMET (with equations (4a) and (4b) in mind this should cause little confusion).

In figure 1 the present DMET results for the differential cross sections for the $2^3S \rightarrow 2^3P$ and $2^3S \rightarrow 3^3L$ (L = S,P,D) transitions at E = 20 eV

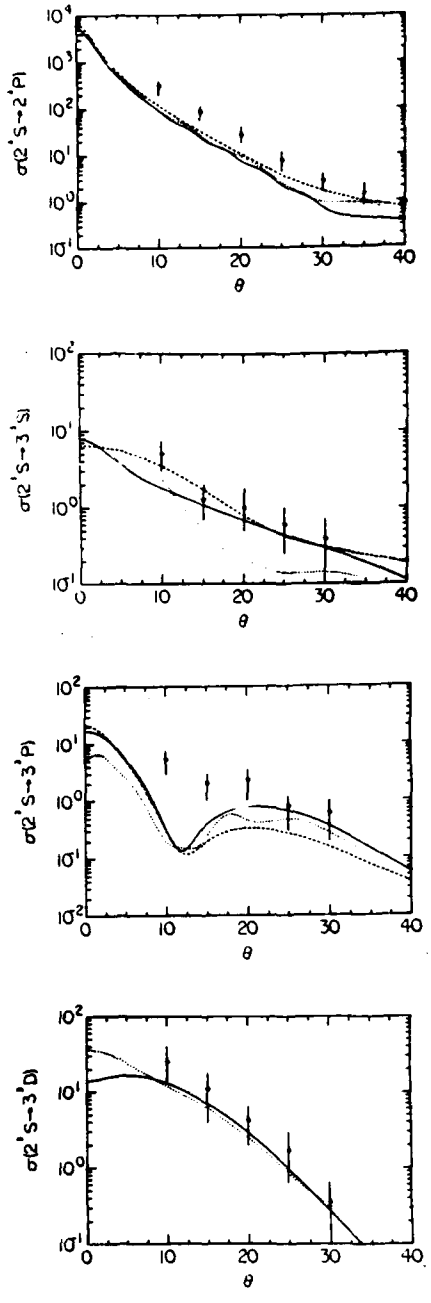

Figure 1. $e^- + He(2^3S \rightarrow n^3L)$ differential cross sections (πa_0^2/str.) at E = 20 eV; ___, present DMET results; -----, DW results (Mathur et al. 1987), ..., original MET results (Flannery and McCann, 1975b); o, experimental data (Muller-Fiedler et al. 1984).

are compared with the experimental data of Müller-Fiedler et al. (1984), the original MET results of Flannery and McCann (1975b) and (where available) the distorted-wave (DW) results of Mathur et al. (1987). The present DMET results for the $2^3S \rightarrow 3^3S$ and $2^3S \rightarrow 3^3D$ optically-forbidden transitions are clearly in excellent agreement with the experimental data. In particular, the agreement of the DMET results with experiment for the former transition is a direct result of the improved numerical solution of (3) used in the present results compared to that used in the original MET results. For the optically allowed $2^3S \rightarrow 2^3P$ and $2^3S \rightarrow 3^3P$ transitions, the present DMET results are seen to be underestimating the experimental data of Müller-Fiedler et al. This is also the case with the original MET results and the DW results. Interestingly however, all three theoretical results predict the existence of a deep diffractive minimum at about 12^o in the $2^3S \rightarrow 3^3P$ DCS. No such behavior is seen however in the experimental data, leading one to question the theoretical results. While the DW results of Mathur et al. (1987) includes electron exchange within the primary, $2^3S \rightarrow 3^3P$, transition (with no couplings to other states), both the original MET results and the present DMET results neglect exchange but include couplings up to the 3^3D state. These points, taken together with the DCS experimental data for the n=4 triplet states (cf. Table 1), seem to indicate that the major physical mechanism missing from the theoretical results shown in figure 1 is coupling to the n=4 triplet states of helium. At least both dipole ($2^3S \rightarrow 4^3P$) and quadrupole ($2^3S \rightarrow 4^3S$, 4^3D) couplings should be included in a theoretical calculation in light of the relative magnitudes observed in the Kaiserslautern experiment between the DCS for the 3^3P state and the n=4 triplet states.

TABLE 1. Experimental Differential Cross Sections for $e^- + He(2^3S \rightarrow n^3L)$ (πa_o^2/str.) (Müller-Fiedler et al. 1984).

θ	2^3P	3^3S	3^3P	3^3D	$4^3S+4^3P+4^3D+4^3F$
10	300	4.9	5	25	10
15	85	1.4	1.9	10	6
20	26	.99	2.1	4	1.8
25	7.5	.60	.78	1.7	.78
30	2.8	.38	.58	.37	.50
35	1.6				
40	.82				

The DMET integral cross sections for the 2^3P and 3^3L (L=S,P,D) states are compared in figure 2 with the Born results of Flannery et al. (1975), the original MET results of Flannery and McCann (1975b) and (where available) the distorted-wave results of Mathur et al. (1987). Also, for the 2^3P and 3^3S states, the 5-state R-matrix results of Fon et al. (1981) and the Glauber theory results of Khayrallah et al. (1978) are shown, respectively. The above theoretical results are compared in figure 2 with the recent experimental data of Rall et al. (1989) for the 3^3S, 3^3P and 3^3D states. In the case of the 3^3S and the 3^3D states the experimental results are absolute apparent cross sections, so a direct comparison with theory will require the subtraction of the cascade contribution from the apparent measurements. Only the 3^3P results of Rall et al. (1989) are direct measurements. These were determined from the optical cross sections for

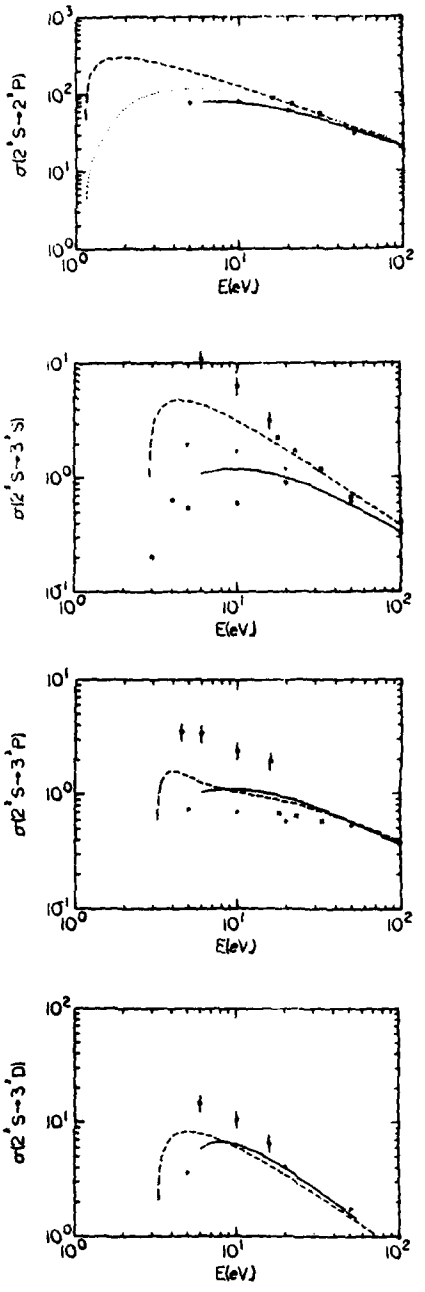

Figure 2. $e^- + He(2^3S \rightarrow n^3L)$ integral cross sections (πa_o^2). ---, Born results (Flannery et al. 1975); ___, present DMET results; +, original MET results (Flannery and McCann 1975b); x, DW results (Mathur et al. 1987); *, Glauber results (Khayrallah et al. 1978); ....., R-matrix results (Fon et al. 1981); o, experimental data (Rall et al. 1989).

the 2^3P and 3^3P and Einstein A coefficients (see Rall et al. (1989) for details). Clearly, further theoretical work will be required in order to convert the remaining apparent cross section measurements of Rall et al. to direct cross sections. However, the measurements of Rall et al. do confirm the basic trend, seen in both the MET and DMET, of the optically-forbidden $2^3S \rightarrow 3^3D$ cross section being larger than the optically-allowed $2^3S \rightarrow 3^3P$ cross section in the intermediate energy region.

ACKNOWLEDGEMENTS

This research is supported by AFOSR Grant No. 84-0233. Additional support from NATO and the Georgia Tech Research Corporation is also gratefully acknowledged.

REFERENCES

Bethe, H. A. and Salpeter E. E.,, 1977, Quantum Mechanics of One- and Two-Electron Atoms, Plenum Press (N.Y.)

Flannery, M. R. and McCann, K. J., 1974a, J. Phys. B: At. Mol. Phys. 7, L223-7

- 1974b, J. Phys. B: At. Mol. Phys. 7, 2518-32
- 1974c, J. Phys. B: At. Mol. Phys. 7, L522-7
- 1975a, J. Phys. B: At. Mol. Phys. 8, 1716-33
- 1975b, Phys. Rev. A 12, 846-55

Flannery, M. R., Morrison, W. F. and Richmond, B. L., 1975, J. Appl. Phys. 46, 1186-90

Fon, W. C., Berrington, K. A., Burke, P. G. and Kingston, A. E., 1981, J. Phys. B: At. Mol. Phys. 14, 2921-34

Khayrallah, G. A., Chen, S. T. and Rumble, J. R., 1978, Phys. Rev. A 17, 513-22

Mansky, E. J. and Flannery, M. R., 1989a, "The Multichannel Eikonal Theory of Electron-Hydrogen Collisions I. Excitation of H(1s)", to be submitted

- 1989b, "The Multichannel Eikonal Theory of Electron-Helium Collisions I. Excitation of He(1^1S)", to be submitted

Mathur, K. C., McEachran, R. P., Parcell, L. A. and Stauffer, A. D., 1987, J. Phys. B: At. Mol. Phys. 20, 1599-1608

McCann, K. J. and Flannery, M. R., 1975, J. Chem. Phys. 63, 4695-4707

- 1978, J. Chem. Phys. 69, 5275-87

Müller-Fiedler, R., Schlemmer, P., Jung, K., Hotop, H. and Ehrhardt, H., 1984, J. Phys. B: At. Mol. Phys. 17, 259-68

Phelps, A. V., 1955, Phys. Rev. 99, 1307-13

Rall, D. L. A., Sharpton, F. A., Schulman, M. B., Anderson, L. W., Lawler, J. E. and Lin, C. C., 1989, Phys. Rev. Lett. 62, 2253-6

Vučić, S., Potvliege, R. M. and Joachain, C. J., 1987, J. Phys. B: At. Mol. Phys. 20, 3157-70

Appendix C

THE NUMERICAL SOLUTION OF PARTIAL DIFFERENTIAL EQUATIONS IN ATOMIC SCATTERING THEORY

E. J. Mansky
School of Physics
Georgia Institute of Technology
Atlanta, Georgia 30332

ABSTRACT

The numerical solution of coupled partial and ordinary differential equations in electron-atom scattering theory are compared. In particular, a case study is made of the transition H(1s → 2s,2p) excited by electrons in the intermediate energy region. The results of the multichannel eikonal theory (MET) and the close coupling theory (CC) for this transition are compared and contrasted with experiment and each other. The principle conclusion is that the configuration space and angular momentum representations employed by the two theories provides information about the excitation process which is complementary. Specifically, the contrasting differences between the MET and CC results at small and large scattering angles for the modulus and phase angle of the complex scattering amplitudes $f_{ni}(\theta)$ sheds new light on the computational problems that need to be solved in order for the λ, R and I problem to be resolved.

I. INTRODUCTION

In this lecture the numerical solution of partial differential equations in electron-atom scattering theory will be discussed and contrasted with the problem of solving ordinary differential equations in scattering theory. In particular, the results obtained by the multichannel eikonal and close coupling theories for the electron impact excitation of hydrogen will be examined in detail. In Section II the partial differential equations of the multichannel eikonal theory are presented together with the ordinary differential equations of the close coupling theory. The advantages and limitations inherent in the representations employed by both theories is also discussed. In addition, the paralleli-

zability of the algorithms used in the numerical solution of the PDE's and the ODE's in the two theories is discussed in Section II. Section III contains a discussion of the results of the two theories for the integral and differential cross sections and the complex scattering amplitudes for the electron impact excitation of hydrogen. The conclusions are presented in Section IV together with a list of general references.

II. THEORY

Here we are concerned with the scattering of a structureless projectile B at a distance $\vec{R}$ from a target atom A with electronic coordinate $\vec{r}$. In this case, the time-independent Schrödinger equation is,

$$\mathcal{H}_i \psi_i = E_i \psi_i \tag{1}$$

where the Hamiltonian operator $\mathcal{H}_i$ is given by,

$$\mathcal{H}_i = \frac{-\hbar^2}{2m_A} \nabla_A^2 - \frac{\hbar^2}{2m_B} \nabla_B^2 - \frac{\hbar^2}{2m_e} \nabla_e^2 + V_{AB} + V_{Ae} + V_{Be} \tag{2a}$$

$$= \frac{-\hbar^2}{2m_T} \nabla_{CM}^2 - \frac{\hbar^2}{2\mu} \nabla_{AB}^2 - \frac{\hbar^2}{2m} \nabla_r^2 + V_{AB} + V_{Ae} + V_{Be} \tag{2b}$$

$$\equiv \mathcal{H}_{CM} + \mathcal{H}_i' \tag{2c}$$

In equation (2a) the first three terms on the right-hand side of the equation are the kinetic energy operators for the indicated particles, while in equations (2b,c) the separation into center-of-mass (CM) and relative motion terms are shown. As is well known, the separability of the CM and relative motion terms in this case allows one to write the system wavefunction ψ_i as a product of a plane wave with a wavefunction ψ_i for the relative motion of projectile B in the field of force of target A. The target atom A in the present case is assumed to be hydrogenic, generalization to other cases is straightforward. The masses

in (2b) are defined as $m = m_e(m_A+m_B)/m_T$, $\mu = m_A m_B/(m_A+m_B)$ and $m_T = m_A + m_B + m_e$.

Therefore, Schrödinger's equation (1) now becomes,

$$\mathcal{H}'\psi_i = E'\psi_i \tag{3}$$

To solve (3) one generally expands the wavefunction ψ_i in a sum over eigenstates χ_n of the target A,

$$\psi_i = \sum_n F_n(\vec{r}_{AB})\ \chi_n(\vec{r}_{AB},\vec{r}) \tag{4}$$

where F_n is the (unknown) wavefunction for the relative motion of projectile B a distance $\vec{r}_{AB}$ from target A (in channel n). In this lecture we are primarily concerned with contrasting the numerical solution of PDE's and ODE's in atomic scattering theory and hence the expansion given by (4) will be sufficient. However, if one is interested in resolving the spin structure of the target atom A, or the resonances in the cross section near threshold, additional terms (antisymmetrization, correlation, etc.) need to be added to (4). These additional terms will ultimately result in a larger set of coupled equations to be solved, but will not change in a material way our basic discussion of the numerical solution of coupled partial and ordinary differential equations in electron-atom scattering. References to calculations which do include the above effects are given in Section III.

Substitution of (4) into (3) results in the following set of coupled ordinary differential equations,

$$-\frac{\hbar^2}{2\mu}\nabla^2_{AB} F_n + \frac{\hbar^2 k_n^2}{2\mu} F_n - V_{nn} F_n = \sum_m{}' V_{nm}(\vec{r}_{AB})F_m$$

$$-\sum_m \frac{\hbar^2}{2\mu}\left[F_m(\chi_n,\ \nabla^2_{AB}\chi_m) + 2\,\vec{\nabla}_{AB}F_m\,(\chi_n,\ \vec{\nabla}_{AB}\chi_m)\right] \tag{5}$$

where the prime on the summation sign indicates omission of the term n=m, and the inner product (f,g) is defined.

$$(f,g) = \int f(\vec{r})\, g(\vec{r}) d\vec{r}$$

To convert (5) into a set of PDE's, write $F_n(\vec{r}_{AB}) = A_n(\vec{r}_{AB}) \exp[iS_n(\vec{r}_{AB})]$ and note that $r_{AB}^2 = \rho^2 + z^2$ with ρ, z, ϕ the usual cylindrical coordinates centered at A. This yields the following set of equations,

$$\Lambda_n \nabla_{AB}^2 A_n + 2 \vec{\nabla}_{AB} \Lambda_n \cdot \vec{\nabla}_{AB} A_n + \left\{ \nabla_{AB}^2 \Lambda_n + \left(k_n^2 - \frac{2\mu}{\hbar^2} V_{nn}\right) \Lambda_n \right\} A_n$$

$$= \sum_m{}' \frac{2\mu}{\hbar^2} V_{nm} \Lambda_m A_m - \sum_m \frac{2\mu}{\hbar^2} \vec{\beta}_{nm} \cdot \vec{\nabla}_{AB}(A_m \Lambda_m) \qquad (6)$$

with $\Lambda_n \equiv \exp[i S_n(\vec{r}_{AB})]$ and $\vec{\beta}_{nm} \equiv (\chi_n, \vec{\nabla}_{AB} \chi_m)$. After writing the gradient and Laplacian operators in (6) in terms of cylindrical coordinates, the coupled Hamilton-Jacobi partial differential equations are solved for the amplitude functions $A_n(\vec{r}_{AB})$. In these equations the eikonal phase $S_n(\vec{r}_{AB})$ is assumed to be known exactly. To obtain an equation for S_n set the term inside the curly brackets in (6) equal to zero,

$$\nabla_{AB}^2 \Lambda_n(\vec{r}_{AB}) + \left(k_n^2 - \frac{2\mu}{\hbar^2} V_{nn}\right) \Lambda_n(\vec{r}_{AB}) = 0 \qquad (7)$$

where the V_{nm} in (6) are the instantaneous electrostatic interaction between the projectile and target i.e., $V_{nm} = V_{nm}(\vec{r}_{AB}) = (\chi_n, V(\vec{r}_{AB}, \vec{r})\chi_m)$. Defining the local wavenumber $\kappa_n(\vec{r}_{AB}) \equiv k_n^2 - (2\mu/\hbar^2) V_{nn}$ and writing the Laplacian in (7) in spherical coordinates yields,

$$\frac{1}{r_{AB}^2} \frac{\partial}{\partial r_{AB}} \left[r_{AB}^2 \frac{\partial}{\partial r_{AB}} e^{iS_n(r_{AB})} \right] + \left[\frac{L_{AB}^2}{r_{AB}^2} + \kappa_n^2 \right] e^{iS_n(r_{AB})} = 0$$

$$\rightarrow i S_n'' + i \frac{2}{r} S_n' - (S_n')^2 + \omega_n^2 = 0 \qquad (8)$$

where the primes denote differentiation with respect to r_{AB} and L_{AB}^2 is the eigenvalue of the relative angular momentum operator $\vec{L}_{AB} = (\hbar/i)\, \vec{r}_{AB} \times \vec{\nabla}_{AB}$. The 'frequency' ω_n is defined, $\omega_n^2 \equiv (L_{AB}^2/r_{AB}^2) + \kappa_n^2$. Here we are interested in electron-atom collisions where the relative motion of the electron to a good approximation is a straight line. That is, we assume that the eikonal phase factor $S_n(\vec{r}_{AB})$ is a slowly varying function of $\vec{r}_{AB}$; or, equivalently, that the density of the classical ensemble of particles varies sufficiently slowly along the classical trajectory such that $S_n'' \sim 0$, and the L_{AB}^2 term in (8) can be ignored. In this case, the real part of (8) is integrated to give,

$$S_n(r_{AB}) \equiv S_n(\rho,z) = k_n z + \int_{-\infty}^{z} \left[[k_n^2 - \frac{2\mu}{\hbar^2} V_{nn}(\rho,z')]^{1/2} - k_n \right] dz' \qquad (9)$$

In the case of heavy particle collisions the curvature of the trajectory of the projectile must be included in the eikonal phase. An example of this type of calculation, for ion-molecule collisions, is the work of McCann and Flannery [26,27]. With the choice of (9) for the eikonal phase the coupled equations (6) are independent of A_n on the left-hand-side. In order to further simplify these 2nd-order partial differential equations for A_n, we in addition assume that the term $\nabla_{AB}^2 A_n$ is small and that the eigenstates χ_n are independent of $\vec{r}_{AB}$. The latter condition insures that the second summation on the RHS of (6) vanishes and is consistent with our omission of electron correlation effects in the wave-function expansion. These terms become important when there is significant configuration mixing in the target atom.

With the above approximations, the coupled equations (6) reduce to a set of first-order partial differential equations,

$$i\frac{\hbar^2}{\mu}\kappa_n\frac{\partial C_n(\rho,z)}{\partial z} + \left[\frac{\hbar^2}{\mu}\kappa_n(\kappa_n-k_n) + V_{nn}\right]C_n = \sum_j V_{nj}\,C_j\,\exp[i(k_j-k_n)z] \quad (10)$$

where $A_n(\rho,z) = C_n(\rho,z)\,e^{i\Delta_{in}\phi}\exp\{-i\int_{-\infty}^{z}(\kappa_n-k_n)dz'\}$, and $\Delta_{in} \equiv m_i-m_n$.

These equations are solved subject to the boundary condition $C_n(\rho,-\infty) = \delta_{ni}$. The coupled equations (10) are the basis of the multichannel eikonal theory (MET) of Flannery and McCann [11-16]. The three principal advantages of the semiclassical equations (10) are:

(i) The equations are first-order in z, hence the numerical techniques used for ordinary differential equations can be used to solve (10). This also means that no matrix diagonalization needs to be done in the numerical solution of (10), as is the case with 2nd-order ODE's.

(ii) The second variable ρ (the projectile's impact parameter) appears in (10) only as a parameter. This indicates that the coupled PDE's (10) will be readily parallelizable. While no calculations have yet been performed with (10) solved on a parallelizable machine, when this is done, a great deal of time should be saved. This is important since the numerical solution of (10) is the principle bottleneck in the MET calculations.

(iii) The memory and time required to solve (10) is a linear function of the number of eigenstates χ_n used in the basis set (4). This is in contrast to the case of 2nd-order ODE's where the time required for the matrix diagonalization is a cubic function of the number of elements in the matrix to be diagonalized. This in turn is a result of the direct methods used for the matrix diagonalization, and hence represents a major hurdle to the use of large basis sets in the solution of 2nd-order ODE's. The ultimate reason behind the difficulty in using large basis sets in solving 2nd-order ODE's by matrix techniques lies in the use of an angular momentum representation for the wavefunctions F_n rather than a

coordinate (i.e., configuration space) representation.

The main disadvantage of solving the 1st-order partial differential equations (10) is the fact that they must be solved over a 2-dimensional grid rather than a one-dimensional grid as is necessary in the solution of 2nd-order ODE's. A consequence of this is that the memory requirements are an order of magnitude larger for the former calculation as compared to the latter.

The close coupling 2nd-order ODE's which arise from using an angular momentum representation for $F_n(\vec{r}_{AB})$ in (4), are,

$$\left[\frac{d^2}{dr_{AB}^2} - \frac{\ell_i(\ell_i+1)}{r_{AB}^2} + \frac{2Z}{r_{AB}} + k_i^2\right] F_i(r_{AB})$$

$$= 2\sum_j V_{ij}(r_{AB})\, F_j(r_{AB}) + \int_0^\infty W_{ij}(r_{AB},r')\, F_j(r')dr'$$

$$+ \sum_{n\ell} \lambda_{n\ell}^{(i)}\, P_{n\ell}(r_{AB})\delta_{\ell\ell i} \qquad (11)$$

where ℓ_i is the orbital angular momentum quantum number of the projectile electron in state i, and the $\lambda_{n\ell}^{(i)}$ are Lagrange multipliers chosen such that the target orbitals $P_{n\ell}$ are orthogonal to the F_i. The matrix elements V_{ij} are the same as those defined previously, while the W_{ij} are the electrostatic matrix elements arising from inclusion of electron exchange (i.e., antisymmetrization) terms and correlation terms in the wavefunction expansion (4). The close coupling equations (11) are well known in the literature, hence their derivation need not be repeated here. However, attention is drawn to the following papers and reviews for those interested in further details [2,5-7,29].

Technically, the close coupling equations (11) are Fredholm ordinary integro-differential equations which, using the technique of Marriott [25], can be cast in the form of a larger set of purely ordinary differential equations. Then, after discretization of the Laplacian in (11), the problem is converted into one of matrix diagonalization.

The advantage of using the close coupling equations (11) is that very accurate inelastic cross sections can be obtained close to threshold - especially the resonance structure between the inelastic threshold and the threshold for ionization. However, as the energy crosses the ionization threshold (where the number of open channels becomes infinite), or in the case of transitions between excited states, the close coupling equations (11) become increasingly difficult to solve via matrix techniques due to the large number of basis states and partial waves ℓ_i required for convergence. This problem can partly be alleviated through the use of pseudo-states. Another way around the bottleneck of basis set size in the solution of (11) is through the use of multi-tasking on the CRAY-XMP. Important recent work in this regard is that of Sawey et al. [30]. Clearly further work on the numerical solution of (11), both by matrix diagonalization techniques and by solving the equivalent partial differential equations, is needed.

In this lecture we are interested in contrasting the numerical solutions of the coupled PDE's (10) with the ODE's (11). Hence we will only discuss the techniques used to solve numerically the PDE's (10), the techniques used to solve the close coupling equations (11) having been thoroughly described in [2,5,7]. In particular we will end Section II with a brief review of extrapolation methods used to solve 1st-order ordinary differential equations. A more complete discussion of the numerical solution of (10) including Runge-Kutta and predictor-corrector methods will be given in a forthcoming paper [22].

Extrapolation methods for ODE's

Consider the 1st-order ODE, $dy(t)/dt = F(t,y(t))$. When this is integrated for sufficiently small step sizes h, the solution of $y(t+h)$ can be written as a power series in h,

$$y(t+h) = y(t) + \sum_{i=1}^{m} \tau_i(t)h^i + \sigma(h^{m+1}) \qquad (13)$$

The goal of extrapolation methods is to eliminate the power series in h in (13) above by integrating the differential equation for a sequence of

step sizes $h_o, h_1, \ldots, h_m$, and then extrapolating the results to $h \to 0$. That is, the power series $\sum_i \tau_i(t)h^i$ is approximated by functions $R_m(t,h_i)$ which have m+1 unknowns. These unknowns are determined by the condition $R_m(t,h_j) = y(t+h_j)$, $j = 0,1,\ldots,m$. Hence the solution of the ODE y(t) is approximated by $R_m(t,0)$.

The two principle extrapolation methods are by polynomials and by rational functions. In polynomial extrapolation the function $R_m(t,h_i) \equiv R_m^{(i)}(h)$ is an mth degree polynomial in h and is computed recursively by,

$$R_m^{(i)} = R_m^{(i+1)} + \frac{R_{m-1}^{(i+1)} - R_{m-1}^{(i)}}{(h_i/h_{i+m})-1}$$

In rational function extrapolation the $R_m^{(i)} = P_m(h)/Q_m(h)$ where $P_m(h)$ and $Q_m(h)$ are polynomials in h of degree μ and ν, respectively. The $R_m^{(i)}(h)$ are computed in this case recursively via

$$R_{-1}^{(i)} = 0, \quad R_o^{(i)} = y(t+h_i)$$

$$R_m^{(i)} = R_{m-1}^{(i+1)} + \frac{R_{m-1}^{(i+1)} - R_{m-1}^{(i)}}{(h_i/h_{i+m})^2 \left[1 - \dfrac{R_{m-1}^{(i+1)} - R_{m-1}^{(i)}}{R_{m-1}^{i+1} - R_{m-2}^{i+1}}\right] - 1}, \quad m \geq 1$$

The MET results discussed in Section III were obtained by solving the coupled 1st-order PDE's (10) using Bulirsch and Stoer's [4] method of rational extrapolation for ODE's. A full discussion of extrapolation techniques can be gound in Gear [17] and Dahlquist and Bjorck [10].

III. RESULTS

Before comparing the MET results obtained by solving the PDE's (10) with the close coupling equations (11) a short discussion on the practical numerical methods used to solve (10) are in order. To do this we quote the final expression used in the multichannel eikonal theory for

the complex scattering amplitude for the transition $i \to n$,

$$f_{ni}(\theta) = -(i)^{\Delta_{in}+1} \int_0^\infty J_{\Delta_{in}}(q'\rho)\,[I_1(\rho,\gamma(\theta)) - i\, I_2(\rho,\gamma(\theta))]\rho d\rho \qquad (14)$$

where the integrals I_1 and I_2 are defined,

$$I_1(\rho,\gamma) = \int_{-\infty}^{\infty} dz\, \kappa_n(\rho,z)\, \frac{\partial C_n(\rho,z)}{\partial z} \exp[i\gamma(\theta)z] \qquad (15a)$$

$$I_2(\rho,\gamma) = \int_{-\infty}^{\infty} dz\, [\kappa_n(\kappa_n - k_n) + \frac{\mu}{h^2} V_{nn}] C_n(\rho,z) \exp[i\gamma(\theta)z] \qquad (15b)$$

and refer the reader to the original literature [12,13,16] for the details. In equations (14,15) $q' = k_n \sin\theta$ and $\gamma(\theta) = k_n(1-\cos\theta)$ and $\Delta_{in} = m_i - m_n$. The 1st-order PDE's (10) are solved using Burlisch and Stoer's rational extrapolation technique for ODE's over a finite 2-dimensional grid: $o \le \rho \le \rho_{max}$, $-z_{max} \le z \le z_{max}$ for the amplitude functions $C_n(\rho,z)$. The values of ρ_{max} and z_{max} are varied until the cross section,

$$\int_0^{\rho_{max}} |C_n(\rho,z_{max})|^2 \rho d\rho \qquad (16)$$

is computed to within a tolerence ϵ (i.e., until subsequent evaluations change by less than an amount ϵ (%)). An additional criterion for the selection of optimal values of ρ_{max} and z_{max} is that the MET integral cross section, computed from the scattering amplitude (14) should converge to the 1st Born approximation at high incident energies. For this to be achieved it was found necessary to solve (20) using a non-linear grid in z in order that the rapid variation of C_n and $\partial C_n/\partial z$ near $z = 0$ be accurately represented. This was needed so that the subsequent evaluations of I_1, I_2 were accurate. The nonlinear grid in z used was:

$z_i = 3\tan(i\delta)$, $i = -N_z,\ldots,N_z$ with $\delta = \tan^{-1}(z_{max}/3)/N_z$. However, since I_1 and I_2 must be evaluated numerically from the tabulated solution of the coupled equations (10), the most efficient way of solving (10) is to make the grid points z_i used to solve (10) and the pivots used in the evaluation of I_1, I_2 *identical*. This avoids the need to interpolate w.r.t. z in the quadrature of I_1 and I_2 (interpolation w.r.t. ρ must still be done however). In the MET calculations discussed below, integrals I_1, I_2 were evaluated using Simpson's rule with the nonlinear pivots z_i chosen above and with weights $\omega_i = r_i\delta\ \sec^2(i\delta)$, where r_i are the usual Simpson's rule weights and N_z is the number of points used to discretize the z-range $[o,z_{max}]$. Hence while the number of points required for an accurate evaluation of I_1, I_2 is much larger using Simpson's rule as compared with using a higher-order quadrature method, the amount of time saved by eliminating the need to interpolate w.r.t. z more than makes up for the increased number of grid/ pivot points z_i required.

In figure 1 the real and imaginary parts of the amplitude function $C_n(\rho,z)$ for the 1s state of hydrogen are shown as an example of the type of behavior exhibited by the solutions of equation (10). For a more extensive exhibition of the solutions of the semiclassical equations (10) see [22].

In the remainder of Section III an overview of the MET results for e^-+H collisions will be given. This will include differential and integral cross sections as well as the complex scattering amplitudes. For a complete update and discussion of the present MET see Mansky and Flannery [23,24]. It should be clear that by comparing the results obtained for a wide range of physical observables, from the solution of equations (10) and (11), one not only gets an idea of the success or failure of a particular theory over a wider range of physical conditions, but also insight into the accuracy of the numerical solution of the coupled equations underlying a given theory. That is, by varying z_{max} and ρ_{max} in the semiclassical equations (10) until the integral cross sections computed from (14), for all states in the basis set, have

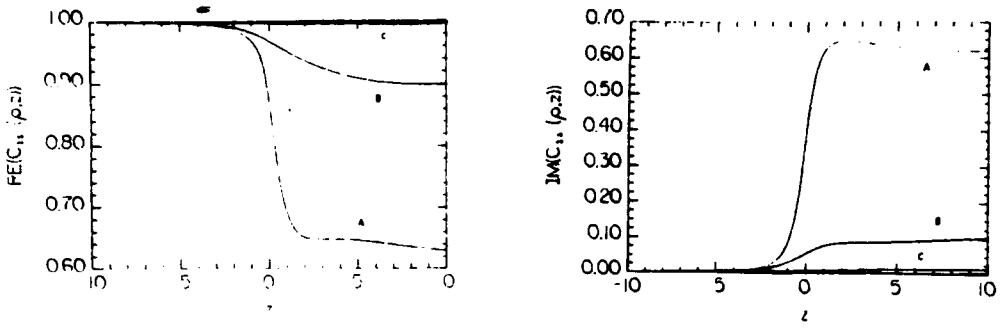

Figure 1: Real and imaginary parts of the MET amplitude function $C_{1s}(\rho,z)$ versus $z(a_o)$ for e^-+H collisions at E = 54.40 eV.

converged to their corresponding 1st Born approximation values in the limit of high energy, one obtains an idea of the minimum size 2-dimensional grid required to solve the coupled PDE's (10). These values of ρ_{max}, z_{max} can then be used to solve (10) for all other energies of interest. Note that a similar argument can be made about the numerical solution of the coupled ODE's (11) where the appropriate parameters are r_{max} and ℓ_{max} - the maximum value of the independent variable r_{AB} and the largest partial wave ℓ_i retained in the expansion.

The MET differential and integral cross sections are defined as,

$$\sigma_n(\theta) = \frac{k_n}{k_i} |f_{ni}(\theta)|^2 \qquad (17a)$$

$$\sigma_n = \int_0^{2\pi} d\phi \int_0^{\pi} \sin\theta \, d\theta \, \sigma_n(\theta) = 2\pi \int_0^{\pi} \sigma_n(\theta) \sin(\theta) d\theta \qquad (17b)$$

where the complex scattering amplitude for the transition i → n is given by (14). In figures 2,3 the integral and differential cross sections for

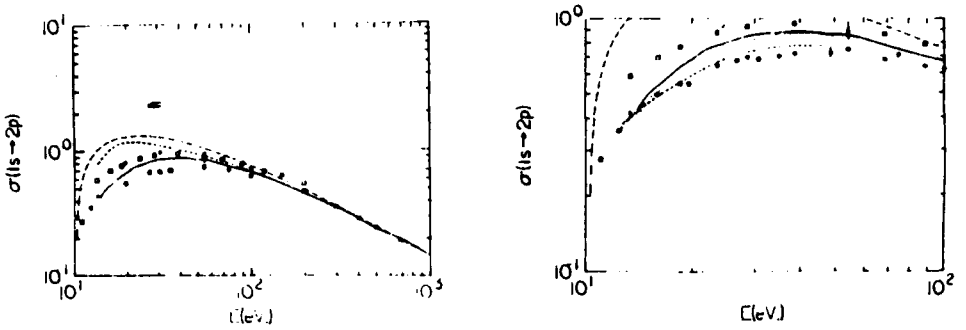

Figure 2a: Integral cross section σ_{2p} in units of πa_o^2 versus E (eV.). 1st Born (- - -), MET [23] (___), 3-state close coupling [18] (-----), DWSBA [20] (X), AVCC-18 state [9] (*), unitarized Born [31] (+), experimental data of Long et al. [21] as renormalized by Bransden and McDowell [3] (□), experimental data of Long et al. [21] as renormalized by van Wyngaarden and Walters [34] (O), experimental data of Williams [32] (Δ).

Figure 2b: Same as Fig. 2a except with AVCC-11 state (.....) [8].

e^-+H(1s → 2p) collisions are shown (results for other transitions in hydrogen are given in [23]). The MET results are in good overall agreement with experiment in figure 2, and clearly converge to the Born cross section at high energy. In particular, the agreement (cf. figure 2b) with the absolute measurement of Williams [32] at 54.40 eV is noteworthy. The differences between the original algebraic variational close coupling results of Callaway [8], and the same results as renormalized by van Wyngaarden and Walters [34], is a choice of normalization (i.e., normalization to experiment at 11 eV versus the pseudostate close coupling calculations of van Wyngaarden and Walters [35] at 350 eV). On the other hand, the differences between the 3-state close coupling results of Kingston, Fon and Burke [18] (cf. figure 2a) and the MET results is an indication of the lack of convergence w.r.t. basis set size in the former calculation. The importance of basis set size is evident in comparing the 3-state close coupling results of Kingston, Fon and Burke and the 18-state AVCC results of Callaway et al. [9] (cf. figure 2b). While the MET results are in good agreement with the results of Callaway et al. for energies E $\geq$ 70 eV, the differences observed in figure 2 at lower energies is due to the neglect of electron exchange terms in the MET. This is also evident in figure 3 by the rapid decrease of the MET

differential cross sections $\sigma_{2s}(\theta)$, $\sigma_{2p}(\theta)$ at scattering angles $\theta > 40^{o}$ when compared to the close coupling results of Kingston, Fon and Burke [18] and van Wyngaarden and Walters [34]. The agreement between the MET and the experimental data of Williams [32] for $\theta \leq 20^{o}$ in figure 3 also indicates that the choices for z_{max} and ρ_{max} in the solution of (10) were correct.

From figure 3 one would conclude that electron exchange effects are only important at large scattering angles. This is incorrect. While a definitive calculation has not yet been done, the ongoing problem of theory to reproduce the experimental data for the λ, R and I parameters indicates that theory is still not handling adequately the numerical solution of the coupled equations (10) or (11). In figure 4 we show the λ, R and I parameters for $e^{-}+H(1s \rightarrow 2p)$ collisions at E = 54.40 eV and scattering angles $\theta \leq 50^{o}$. Clearly the MET results accurately reproduce the experimental data of Williams [32] only for $\theta \leq 20^{o}$, while at the level of $\sigma_{2p}(\theta)$ the corresponding angular range was $\theta \leq 40^{o}$. In contrast, the two close coupling results shown in figure 4 are in good agreement with experiment out to approximately 40^{o}. However, at larger scattering angles ($\theta \geq 60^{o}$) the close coupling results fail to reproduce the second experimental minimum in the λ parameter observed around 100^{o} and the magnitude of the R parameter in the range $70^{o} \leq \theta \leq 120^{o}$. These facts taken together indicate that while the values of z_{max}, ρ_{max} used to solve (10) in the MET are adequate at the level of differential and integral cross sections, the small z behavior of the amplitude functions still needs refinement for physical observables directly dependent on the complex scattering amplitude $f_{n1}(\theta)$. For completeness, the λ, R and I parameters are defined,

$$\lambda = |f_{o}|^{2}/[|f_{o}|^{2} + 2|f_{+1}|^{2}] \qquad (18a)$$

$$R = \sqrt{[\lambda(1-\lambda)/2]}\,\cos(\beta_{1} - \beta_{o}) \qquad (18b)$$

$$I = \sqrt{[\lambda(1-\lambda)/2]}\,\sin(\beta_{1} - \beta_{o}) \qquad (18c)$$

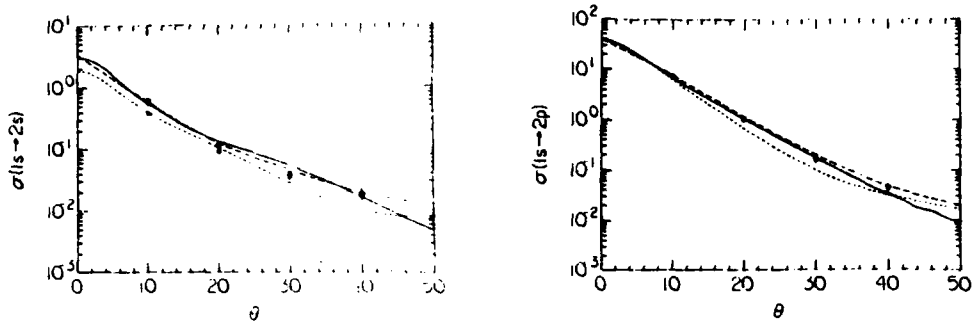

Figure 3: Differential cross sections $\sigma_{2s}(\theta)$, $\sigma_{2p}(\theta)$ in a_o^2/str. vs. θ for E = 54.40 eV. MET [23] (___), 3-state close coupling [18] (---), pseudostate close coupling [35] (----), experimental data of Williams [23] O (via sum), □ via ratio).

where $f_m(\theta) = |f_m(\theta)| \exp[i\beta_m(\theta)]$ and $f_m(\theta)$ denotes the complex scattering amplitude for $2p_m$ magnetic substate. For a complete discussion of the angular correlation and polarization correlation parameters in electron-atom scattering see Andersen et al. [1]. For more on the problem of the λ, R and I parameters in e^-+H collisions see Morgan [28].

To better understand what part of the solution of the PDE's (10) needs improvement, in regards to the λ, R and I problem discussed above, and where the electron exchange terms in (11) become important, we show the MET results for the scattering amplitudes $f_{2p_o}(\theta)$ and $f_{2p_1}(\theta)$ at E = 54.40 eV in figures 5 and 6, respectively. These are compared in figures 5,6 with the close coupling results of Kingston, Liew and Burke [19]. Two things are evident in these figures. First, that the electron exchange terms in the close coupling equations (11) manifest themselves quite differently in the modulus and phase angle of the scattering amplitude. For example, the phase angles for the singlet and triplet spin channels for the $f_{2p_o}(\theta)$ scattering amplitude differ from each other appreciably for $\theta \geq 30^o$, while for the $f_{2p_1}(\theta)$ they don't begin to differ greatly until $\theta \geq 40^o$. On the other hand, the modulii for the singlet

and triplet spin channels of the $f_{2p_o}(\theta)$, $f_{2p_1}(\theta)$ scattering amplitudes only differ appreciably for $\theta \leq 20^o$, $\theta \leq 30^o$, respectively. That is, electron exchange terms are important at small scattering angles for the moduli of scattering amplitudes, while for the corresponding phase angles, they are important only at large scattering angles. This indicates that unraveling the relative contributions that direct and exchange terms make to a given scattering amplitude at a specific angle will be difficult.

The second point to note from figure 5 is that the MET results for the $f_{2p_o}(\theta)$ amplitude agrees quite closely at all angles with the triplet spin channel results of Kingston, Liew and Burke. On the other hand in figure 6 the MET results only agree with the singlet spin channel results over a limited angular range. In particular the MET results exceed both the singlet and triplet spin channel results for $|f_{2p_1}(\theta)|$

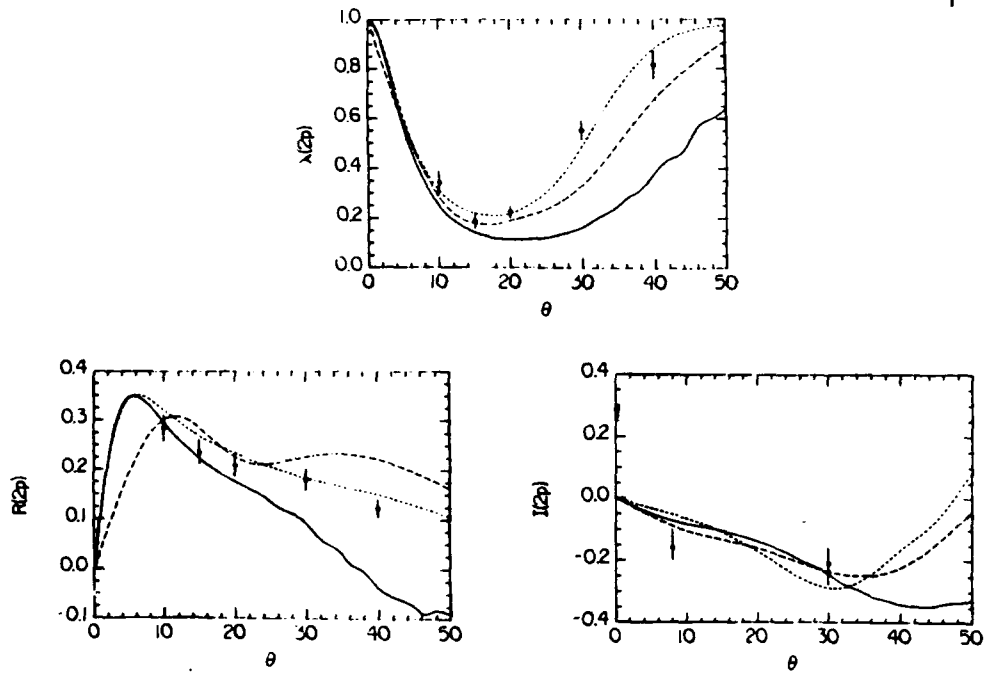

Figure 4: λ, R and I parameters for the 2p state at E = 54.40 eV. MET [23] (___), 3 state close coupling [18] (---), pseudostate close coupling [35] (-----), experimental data of Williams [32,33] O (λ, R from [32], I from [33]).

for $\theta \leq 20^{o}$. Note that we should not expect to see the MET results in figures 5,6 lying between the singlet and triplet spin channel results of Kingston, Liew and Burke. Rather, the observed behavior of the modulii and phase angles of the MET scattering amplitudes in figures 5,6 is a direct result of a complicated interplay between the z-behavior of the amplitude functions $C_n(\rho,z)$ and eikonal phases $S_n(\rho,z)$. A detailed discussion of these topics is beyond the scope of this lecture, but will be the subject of a forthcoming paper.

IV. CONCLUSIONS AND GENERAL REFERENCES

In this lecture we have contrasted solving coupled PDE's with ODE's in electron-atom collision theory. The principle conclusion of this lecture is that the solutions of (10) and (11) are complementary. That is, the configuration space representation employed by the MET, and the angular momentum representation employed by close coupling theories, complement one another, both in terms of information they provide about the scattering event, and in the energy ranges over which they are valid. This is important since it means that by solving (10) and (11) one gains additional insight into a particular excitation process that would not be obtained otherwise. This proved useful for example in the discussion of

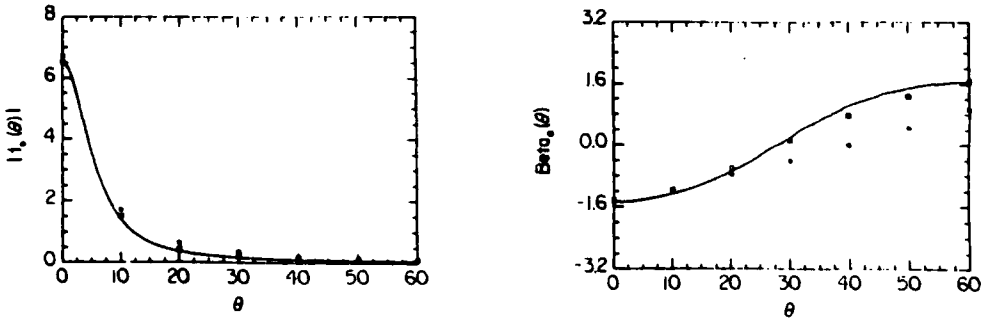

Figure 5: Modulus $|f_o|$ (in a_o) and phase angle β_o (in radians) for $f_{2p}(\theta)$ vs. θ for E = 54.40 eV. MET [23] (___), 3 state close coupling [19] O (singlet) □ (triplet).

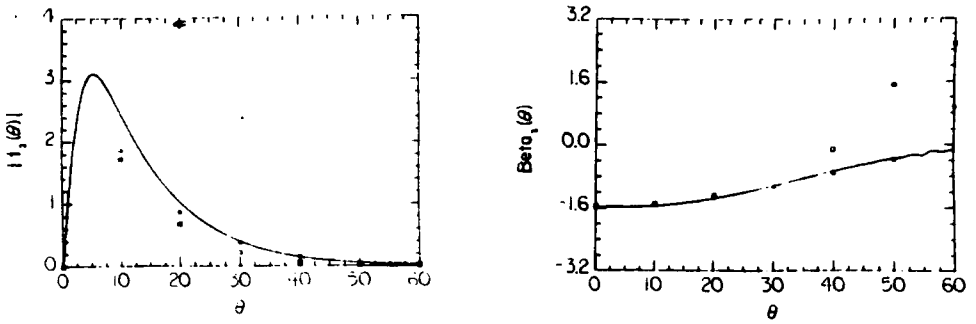

Figure 6: Same as Fig. 5 except for $f_{2p_1}(\theta)$.

the λ, R and I problem in Section III. We end this lecture with a short list of general references which we have found useful on the subject of coupled ordinary and partial differential equations.

- Collatz, L., 1960, The Numerical Treatment of Differential Equations 3rd ed., Springer-Verlag.
- Dahlquist, G., 1956, Math. Scandinavica 4 33-50, 1959, Trans. Roy. Inst. Tech., Stockholm, No. 130.
- Dahlquist, G., and Bjorck, A., 1974, Numerical Methods, Prentice Hall.
- Gear, C. W., 1971, Numerical Initial Value Problems in Ordering Differential Equations, Prentice-Hall.
- Henrici, P., 1962, Discrete Variable Methods for Ordinary Differential Equations, Wiley.
- Ince, E. L., 1956, Ordinary Differential Equations, Dover.
- Olver, P. J., 1986, Applications of Lie Groups to Differential Equations, Springer-Verlag.

Acknowledgements

This work is supported by AFOSR under grant no. 84-0233. The invitation to lecture, and the partial support received from Oak Ridge National Laboratory are also gratefully acknowledged.

References

1. Anderson, N., Gallagher, J. W., and Hertel, I. V., 1988, Phys. Rep. 165, 1-188.
2. Berrington, K. A., Burke, P. G., Le Dourneuf, M., Robb, W. D., Taylor, K. T. and Lan Vo Ky, 1978, Comp. Phys. Comm. 14, 367-412.
3. Bransden, B. H., and McDowell, M. R. C., 1978, Phys. Rep. 46, 249-394.
4. Bulirsch, R., and Stoer, J., 1966, Numer. Math. 8, 1-13.
5. Burke, P. G., and Eissner, W. B., 1983, Chapter 1 (p. 1-54) in Atoms in Astrophysics, Plenum Press (Burke, P. G., Eissner, W. B., Hummer, D. G. and Percival, I. C., eds.).
6. Burke, P. G., and Robb, W. D., 1971, Adv. Atom. Mol. Phys. 11, 143-214.
7. Burke, P. G., and Seaton, M. J., 1971, Methods in Comput. Phys. 10, 1-80.
8. Callaway, J., 1985, Phys. Rev. A 32, 775-83.
9. Callaway, J., Unnikrishnam, K., and Oza, D. H., 1987, Phys. Rev. A 36, 2576-84.
10. Dahlquist, G., and Bjorck, A., 1974, Numerical Methods, Prentice-Hall.
11. Flannery, M. R., and McCann, K. J., 1974, J. Phys. B: At. Mol. Phys. 7, L223-7.
12. ibid., J. Phys. B: At. Mol. Phys. 7, 2518-32.
13. ibid., J. Phys. B: At. Mol. Phys. 7, L522-7.
14. ibid., Phys. Rev. A 10, 2264-72.
15. ibid., 1975, J. Phys. B: At. Mol. Phys. 8, 1716-33.
16. ibid., Phys. Rev. A 12, 846-55.
17. Gear, C. W., 1971, Numerical Initial Value Problems in Ordinary Differential Equations, Prentice-Hall.
18. Kingston, A. E., Fon, W. C., and Burke, P. G., 1976, J. Phys. B: At. Mol. Phys. 9, 605-18.
19. Kingston, A. E., Liew, Y. C., and Burke, P. G., 1982, J. Phys. B: At. Mol. Phys. 15, 2755-66.
20. Kingston, A. E., and Walters, H. R. J., 1980, J. Phys. B: At. Mol. Phys. 13, 4633-62.

21. Long, R. L., Cox, D. M., and Smith, S. J., 1968, J. Res. NBS A 72, 521-35.
22. Mansky, E. J., 1989, J. Comput. Phys., to be submitted.
23. Mansky, E. J., and Flannery, M. R., 1989, "The Multichannel Eikonal Theory of Electron-Hydrogen Collisions I. Excitation of H(1s)", J. Phys. B, to be submitted.
24. ibid., "The Multichannel Eikonal Theory of Electron-Helium Collisions I. Excitation of He(1^1S)", J. Phys. B, to be submitted.
25. Marriott, R., 1958, Proc. Phys. Soc. (Lon.) 72, 121-9.
26. McCann, K. J., and Flannery, M. R., 1975, J. Chem. Phys. 63, 4695-4707.
27. ibid., 1978, J. Chem. Phys. 69, 5275-87.
28. Morgan, L. A., 1982, J. Phys. B: At. Mol. Phys. 15, 4247-57.
29. Percival, I. C., and Seaton, M. J., 1957, Proc. Camb. Phil. Soc. 53, 654-62.
30. Sawey, P. M. J., Berrington, K. A., Burke, P. G., and Kingston, A. E., 1989, 16th Int. Conf. on the Phys. of Electronic and Atom. Coll. (N.Y.) Abstracts of contrib. papers 214.
31. Somerville, W. B., 1963, Proc. Phys. Soc. (Lon.) 82, 446-55.
32. Williams, J. F., 1981, J. Phys. B: At. Mol. Phys. 14, 1197-1217.
33. ibid., 1986, Aust. J. Phys. 39, 621-32.
34. van Wyngaarden, W. L., and Walters, H. R. J., 1986, J. Phys. B: At. Mol. Phys. 19, L53-8.
35. ibid., J. Phys. B: At. Mol. Phys. 19, 929-68.

Appendix D

ITERATIVE SOLUTION OF LARGE LINEAR SYSTEMS AND HEAVY PARTICLE COLLISIONS: ION-ION RECOMBINATION

E. J. Mansky
School of Physics
Georgia Institute of Technology
Atlanta, Georgia 30332

ABSTRACT

The solution of large sparse linear systems of algebraic equations arising from the discretization of coupled Boltzmann partial integro-differential equations, which model ion-ion recombination processes in dense gases, is discussed. The advantages and limitations of various representations of these equations is provided. A detailed analysis is given of the derivation and structure of the coefficient matrix $\mathcal{A}$ of the resultant algebraic equations. The need for preconditioning the algebraic equations through the calculation of the condition number of the matrix $\mathcal{A}$ is highlighted. Approximate methods of computing termolecular recombination rate coefficients via the Debye-Smoluchowski equation and diffusion models in energy space are also briefly discussed.

I. INTRODUCTION

In this lecture the numerical solution of large sets of linear algebraic equations by iterative methods will be discussed with particular application to problems in heavy particle collisions. The physical problem specifically addressed is that of ion-ion recombination at arbitrary gas densities. The determination of the rate of recombination is governed by the solution of a pair of coupled Boltzmann-like integro-differential equations (IDE's). The derivation of these coupled Boltzmann equations from a more basic perspective involving the BBGKY hierarchy of equations is reviewed in Section II. The solution of these coupled IDE's provides a general framework for discussing the problem of computing chemical reaction rates in dense plasmas. This is provided in

Section II along with a detailed discussion of the advantages and limitations of transforming the IDE's into a set composed solely of differential equations (DE's) or integral equations (IE's). In all three representations the problem of numerically solving the coupled Boltzmann equations reduces to one of solving a set of simultaneous linear algebraic equations composed of a large, sparse, real, positive definite, non-symmetric, ill-conditioned matrix. The solution of these algebraic equations by iterative techniques is highlighted in Section II.

Historically, until the advent of supercomputers, the direct solution of the coupled Boltzmann equations was generally avoided through the use of simplifying approximations because of the difficulty in solving large sets of algebraic equations. In Section III the link between the coupled Boltzmann equations and it's approximations is given. In particular the formulation of the problem in terms of diffusion equations (in energy space) and Debye-Smoluchowski equations is accentuated in Section III. The conclusions of this lecture and a list of general references is given in Section IV.

II. BOLTZMANN EQUATION TREATMENT OF IONIC RECOMBINATION

The overall goal of the type of calculations described in this lecture is the prediction from a microscopic viewpoint, of the rate of chemical reactions in dense gases. The proto-type chemical reaction we are primarily interested in is that of ion-ion recombination at arbitrary gas densities,

$$X^+ + Y^- + Z \xrightarrow{\alpha} [XY]^* + Z \qquad (1)$$

whereby free ions (X^+,Y^-) are converted into diatomic molecules XY (usually in some metastable state denoted by *). We will assume that the number density of third bodies Z is arbitrary, but that the free ion number densities is sufficiently low so that the interaction potential between ions is strictly Coulombic. This will necessarily exclude from discussion dynamic screening effects in dense plasmas. We will also not discuss the related problem of ion-atom association,

$$X^+ + Y + Z \rightarrow [XY^+]^* + Z$$

which is an important mechanism by which molecular ions are formed in interstellar media and in laboratory plasmas. To solve both problems from a microscopic standpoint will require a great deal of information on the full three-body sector of phase space which is beyond the scope of this lecture to provide. Anyway, before the latter two problems can be solved, a complete understanding of the solution of the termolecular recombination rate in the limit of low ionic density and arbitrary gas density will be needed.

We are interested in computing in this lecture microscopic reaction rates which the reader should take to mean that the reaction rates will be expressed in terms of the phase space distribution functions f_N for the N particles comprising the three component plasma (positively and negatively charged particles as well as neutral species) undergoing termolecular recombination. Our starting point is the BBGKY hierarchy of equations,

$$\frac{\partial f_s}{\partial t} = -\mathcal{H}_s f_s + n\mathcal{L}_s f_{s+1} \qquad s = 1,2,3,\ldots,N-1 \tag{2}$$

which is a set of coupled equations for the s-particle reduced distribution functions $f_s = f_s(x_1,x_2,\ldots,x_s;t) = V^{-(N-s)} \int dx_{s+1} \int dx_{s+2} \ldots \int dx_N\, f_N(x_1,\ldots,x_N;t)$ with V denoting the total volume of phase space and $x_i:(\vec{r}_i,\vec{p}_i)$ denotes the 6-dimensional phase space point for particle i. In equation (2), the Hamiltonian operator for s particles of equal mass m is defined,

$$\mathcal{H}_s = \sum_{i=1}^{s} \frac{\vec{p}_i}{m} \vec{\nabla}_{\vec{r}_i} + \frac{\vec{\mathcal{F}}_i}{m} \cdot \vec{\nabla}_{\vec{p}_i} - \sum_{1\leq i<j\leq s} \theta_{ij} \tag{3}$$

where $\vec{\mathcal{F}}_i$ is the external force on particle i, and the interaction operator between particles i and j, is

$$\theta_{ij} = \frac{\partial \phi_{ij}}{\partial \vec{r}_i} \cdot \vec{\nabla}_{\vec{p}_i} + \frac{\partial \phi_{ij}}{\partial \vec{r}_j} \cdot \vec{\nabla}_{\vec{p}_j} \tag{4}$$

with the interaction potential between particles i and j denoted ϕ_{ij}. The phase-mixing operator $\mathscr{L}_s$ in the BBGKY equations (2) is defined,

$$\mathscr{L}_s = \sum_{i=1}^{s} \int dx_{s+1}\, \theta_{i,s+1} \tag{5}$$

and the number density n in (2) is $n = N/V$. For a detailed derivation of the BBGKY hierarchy (2) the reader is referred to the statistical mechanical literature (Akhiezer et al. [1], Balescu [3,4], Chapman and Cowling [13], Ferziger and Kaper [18] and Tolman [41]).

Since in ionic recombination we are interested in the formation of diatomic molecules, it is natural to assume that the most important reduced distribution functions in the three component plasma are those for one and two particles. Hence we will truncate the BBGKY hierarchy of equations at f_3 and concentrate on the equations for f_1, f_2. Also, since we are interested only in the recombination of positively and negatively charged particles to form neutral diatomic molecules, it follows that the main determining factor in computing α, the rate of reaction (1) will be the pair correlation function $g_2^{(+-)}$ between X^+ and Y^-. From this we conclude that a separate BBGKY hierarchy (2) will be required for each component of the plasma. These hierarchies for the three component plasma are,

$$\mathscr{D}f_1^{(+)} = -\mathscr{K}_1^{(+)} f_1^{(+)} + \mathscr{L}_1^{(++)} f_2^{(++)} + \mathscr{L}_1^{(+-)} f_2^{(+-)} + \mathscr{L}_1^{(+n)} f_2^{(+n)} \tag{6a}$$

$$\mathscr{D}f_1^{(-)} = -\mathscr{K}_1^{(-)} f_1^{(-)} + \mathscr{L}_1^{(-+)} f_2^{(-+)} + \mathscr{L}_1^{(--)} f_2^{(--)} + \mathscr{L}_1^{(-n)} f_2^{(-n)} \tag{6b}$$

$$\mathscr{D}f_1^{(n)} = -\mathscr{K}_1^{(n)} f_1^{(n)} + \mathscr{L}_1^{(n+)} f_2^{(n+)} + \mathscr{L}_1^{(n-)} f_2^{(n-)} + \mathscr{L}_1^{(nn)} f_2^{(nn)} \tag{6c}$$

$$\dot{f}_2^{(++)} = -\mathcal{H}_2^{(++)} f_2^{(++)} + \mathcal{L}_2^{(+++)} f_3^{(+++)} + \mathcal{L}_2^{(++-)} f_3^{(++-)} + \mathcal{L}_2^{(++n)} f_3^{(++n)} \quad (7a)$$

$$\dot{f}_2^{(+-)} = -\mathcal{H}_2^{(+-)} f_2^{(+-)} + \mathcal{L}_2^{(+-+)} f_3^{(+-+)} + \mathcal{L}_2^{(+--)} f_3^{(+--)} + \mathcal{L}_2^{(+-n)} f_3^{(+-n)} \quad (7b)$$

$$\dot{f}_2^{(+n)} = -\mathcal{H}_2^{(+n)} f_2^{(+n)} + \mathcal{L}_2^{(+n+)} f_3^{(+n+)} + \mathcal{L}_2^{(+n-)} f_3^{(+n-)} + \mathcal{L}_2^{(+nn)} f_3^{(+nn)} \quad (7c)$$

$$\dot{f}_2^{(--)} = -\mathcal{H}_2^{(--)} f_2^{(--)} + \mathcal{L}_2^{(--+)} f_3^{(--+)} + \mathcal{L}_2^{(---)} f_3^{(---)} + \mathcal{L}_2^{(--n)} f_3^{(--n)} \quad (7d)$$

$$\dot{f}_2^{(-n)} = -\mathcal{H}_2^{(-n)} f_2^{(-n)} + \mathcal{L}_2^{(-n+)} f_3^{(-n+)} + \mathcal{L}_2^{(-n-)} f_3^{(-n-)} + \mathcal{L}_2^{(-nn)} f_3^{(-nn)} \quad (7e)$$

$$\dot{f}_2^{(nn)} = -\mathcal{H}_2^{(nn)} f_2^{(nn)} + \mathcal{L}_2^{(nn+)} f_3^{(nn+)} + \mathcal{L}_2^{(nn-)} f_3^{(nn-)} + \mathcal{L}_2^{(nnn)} f_3^{(nnn)} \quad (7f)$$

where the superscripts +, -, n indicates a positively or negatively charged particle or a neutral species, respectively, and the dots indicate differentiation w.r.t. time.

The set of coupled equations (6,7) are closed by use of the cluster expansion (Ferziger and Kaper [18]) wherein the 3 particle distributions f_3 are written as functionals of the 1 and 2-particle distribution functions. The latter functions are written in turn as functionals of f_1 thereby closing the set of equations (6,7). For a detailed derivation of these equations see Mansky [35] and Flannery and Mansky [28]. Since we are primarily interested in the numerical aspects of the problem of computing ionic recombination rates α in this lecture, we will omit the details of the subsequent reduction of the coupled equations (6,7) to the working equations (8), but refer the reader to the above two references as well as two earlier important papers of Flannery's [24,25].

Therefore, after reduction, the final steady state working equations are

$$\left[\frac{1}{r} - \lambda\right] \frac{\partial \rho^+(r,\lambda)}{\partial r} + \frac{1}{r}\left[\frac{1}{r} - 2\lambda\right][\rho^+(r,\lambda) - \rho^-(r,\lambda)] = \Gamma' \int_{-\infty}^{1/r} \rho^+(r,\mu) F(\lambda,\mu;r)\, d\mu - \Gamma' \rho^+(r,\lambda) \mathcal{F}(r,\lambda) \quad (8a)$$

$$-\left[\frac{1}{r} - \lambda\right] \frac{\partial \rho^-(r,\lambda)}{\partial r} = \Gamma' \int_{-\infty}^{1/r} \rho^-(r,\mu) F(\lambda,\mu;r)\, d\mu - \Gamma' \rho^-(r,\lambda) \mathcal{F}(r,\lambda) \quad (8b)$$

$$\left[\frac{1}{r} - \lambda\right] \frac{\partial \rho^{+}(r,\lambda)}{\partial r} = \Gamma' \int_{-\infty}^{1/r} \rho^{+}(r,\mu) F(\lambda,\mu;r)\, d\mu - \Gamma'\, \rho^{+}(r,\lambda)\, \mathcal{F}(r,\lambda) \quad (8c)$$

$$-\left[\frac{1}{r} - \lambda\right] \frac{\partial \rho^{-}(r,\lambda)}{\partial r} - \frac{1}{r}\left|\frac{1}{r} - 2\lambda\right| [\rho^{+}(r,\lambda) - \rho^{-}(r,\lambda)] = \Gamma' \int_{-\infty}^{1/r} \rho^{-}(r,\mu) F(\lambda,\mu;r)\, d\mu - \Gamma'\, \rho^{-}(r,\lambda)\, \mathcal{F}(r,\lambda) \quad (8d)$$

where equations (8a,b) are valid for region I: $-\infty < \lambda \leq \frac{1}{2r}$ and (8c,d) are valid for region II: $\frac{1}{2r} \leq \lambda \leq \frac{1}{r}$ (see figure 1). The functions $\rho^{(\pm)}(r,\lambda)$ represented the number density of ion-pairs expanding (+) and contracting (-) at a given relative separation r and internal energy λ in phase space. The ρ's are just the ratio of the number density of ion-pairs undergoing recombination to the equilibrium number density (i.e., $\rho^{(\pm)}(r,\lambda) = n^{(\pm)}(r,\lambda)/n_{eq}$). *The working equations (8) are written* in terms of dimensionless natural variables which are defined,

$$r = r_{12}/R_e, \qquad \lambda = -E_i/kT, \qquad \mu = -E_f/kT$$

where $R_e = e^2/kT$ and $\Gamma' \equiv \Gamma\, e^{-\lambda}$, $\Gamma = \frac{\Lambda_{mfp}}{2\sqrt{\pi}}\, \Gamma_o$, $\Lambda_{mfp} = R_e/\lambda_{mfp}$, $\lambda_{mfp} = (N(Z)Q^D)^{-1}$. Hence the dependence on gas density in (8) is contained in the constant Γ, which also depends on the masses via,

$$\Gamma_o \equiv \begin{cases} [(1+c)/c]^{3/2} & \text{, charge transfer} \\ (1+a)^2/a^{3/2} & \text{, hard sphere} \\ \sqrt{3/2}\ (1+a)^{5/2}/a^{3/2} & \text{, polarization} \end{cases}$$

and,

$$\mathcal{F}(r,\lambda) \equiv \int_{-\infty}^{1/r} F(\lambda,\mu;r)\, d\mu$$

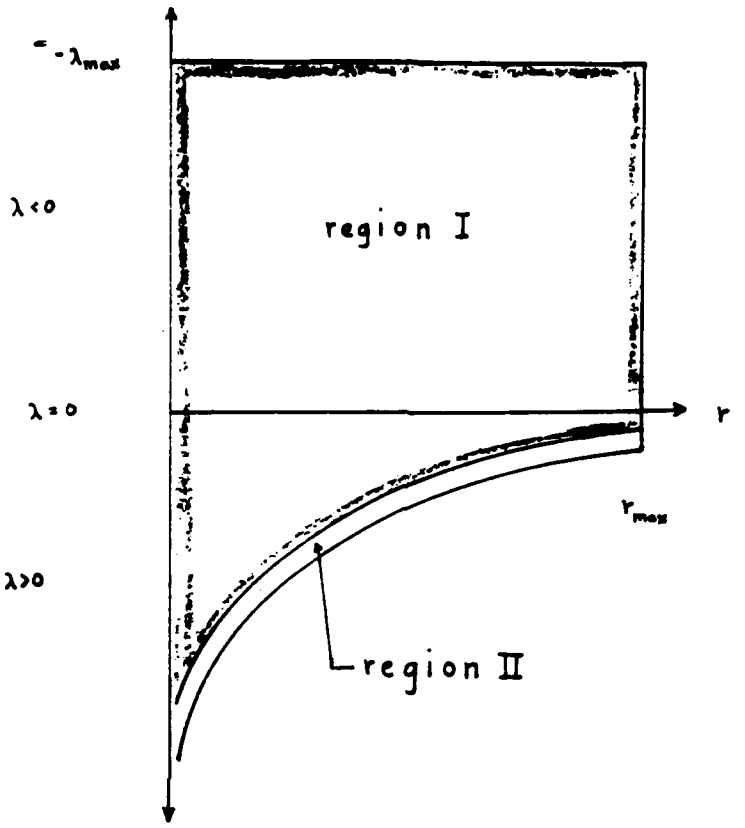

Figure 1: Illustration of λ, r phase space domain of equation (8).

The detailed formulae for the energy-change rate coefficients $F(\lambda,\mu;r)$ for the energy transfer mechanisms of charge-transfer, hard sphere and polarization collisions need not concern us here, but can be found in the original literature Flannery [21-23] and Flannery and Mansky [27]). In the definition of Γ_o the mass ratio parameters are defined,

$$a = m_2 m_3 / m_1 (m_1+m_2+m_3)$$

$$c = m_1/m_2$$

where m_2, m_2 and m_3 are the masses of X^+, Y^- and Z, respectively.

The functions $\rho^{\pm}(r,\lambda)$ are not completely determined by the working equations (8) until their associated boundary conditions are specified,

$$\rho^{\pm}(r,\lambda\to-\infty) = 1 \tag{9a}$$

$$\rho^{\pm}(r\to\infty,\lambda) = 1 \quad \text{for } \lambda \leq 0 \tag{9b}$$

$$\rho^{+}(r=o,\lambda) = \rho^{-}(r=o,\lambda) \tag{9c}$$

$$\rho^{+}(r,\tfrac{1}{r}) = \rho^{-}(r,\tfrac{1}{r}) \tag{9d}$$

Before we convert the working equations (8) into a set of practical, numerical equations we will discuss the relative computational merits of transforming the integro-differential equations (8) into equivalent differential equations or integral equations.

Technically, the working equations (8) are coupled Volterra partial integro-differential equations (PIDE's). They are 1^{st}-order in r and 1-dimensional in λ meaning that the highest derivative in r appearing in (8) is the first, while only single integrals w.r.t. λ appear. To convert (8) into a set of PDE's define the functions $\tilde{\rho}^{\pm}(r,\lambda)$ by

$$\rho^{\pm}(r,\lambda) = \frac{1}{F(\mu,\lambda;r)} \frac{\partial\tilde{\rho}^{\pm}(r,\lambda)}{\partial\lambda} \tag{10}$$

yielding,

$$(\tfrac{1}{r}-\lambda)\frac{\partial}{\partial r}\left[\frac{1}{F(\mu,\lambda;r)}\frac{\partial\tilde{\rho}^{+}(r,\lambda)}{\partial\lambda}\right] + \frac{\frac{1}{r}\left[\frac{1}{r}-2\lambda\right]}{F(\mu,\lambda;r)}\left[\frac{\partial\tilde{\rho}^{+}(r,\lambda)}{\partial\lambda} - \frac{\partial\tilde{\rho}^{-}(r,\lambda)}{\partial\lambda}\right]$$

$$+ \Gamma'\frac{\mathcal{F}(r,\lambda)}{F(\mu,\lambda;r)}\frac{\partial\tilde{\rho}^{+}(r,\lambda)}{\partial\lambda} = \Gamma'[\tilde{\rho}^{+}(r,\tfrac{1}{r}) - \tilde{\rho}^{+}(r,-\infty)] \tag{11a}$$

$$-(\tfrac{1}{r}-\lambda)\frac{\partial}{\partial r}\left[\frac{1}{F(\mu,\lambda;r)}\frac{\partial\tilde{\rho}^{-}(r,\lambda)}{\partial\lambda}\right] + \Gamma'\frac{\mathcal{F}(r,\lambda)}{F(\mu,\lambda;r)}\frac{\partial\tilde{\rho}^{-}(r,\lambda)}{\partial\lambda} = \Gamma'[\tilde{\rho}^{-}(r,\tfrac{1}{r})-\tilde{\rho}^{-}(r,-\infty)] \tag{11b}$$

$$(\tfrac{1}{r}-\lambda)\frac{\partial}{\partial r}\left[\frac{1}{F(\mu,\lambda;r)}\frac{\partial\tilde{\rho}^{+}(r,\lambda)}{\partial\lambda}\right] + \Gamma'\frac{\mathcal{F}(r,\lambda)}{F(\mu,\lambda;r)}\frac{\partial\tilde{\rho}^{+}(r,\lambda)}{\partial\lambda} = \Gamma'[\tilde{\rho}^{+}(r,\tfrac{1}{r})-\tilde{\rho}^{-}(r,-\infty)] \tag{11c}$$

$$-\left(\frac{1}{r}-\lambda\right)\frac{\partial}{\partial r}\left[\frac{1^{*}}{F(\mu,\lambda;r)}\frac{\partial\tilde{\rho}^{-}(r,\lambda)}{\partial\lambda}\right]+\Gamma'\frac{\mathcal{F}(r,\lambda)}{F(\mu,\lambda;r)}\frac{\partial\tilde{\rho}^{-}(r,\lambda)}{\partial\lambda}-\frac{\frac{1}{r}\left|\frac{1}{r}-2\lambda\right|}{F(\mu,\lambda;r)}\left[\frac{\partial\tilde{\rho}^{+}}{\partial\lambda}-\frac{\partial\tilde{\rho}^{-}}{\partial\lambda}\right]$$

$$=\Gamma'[\tilde{\rho}^{-}(\cdot,\tfrac{1}{r})-\tilde{\rho}^{-}(r,-\infty)] \qquad (11d)$$

Performing the indicated differentiation w.r.t. r and rearranging terms results in the following set of coupled hyperbolic 2nd-order partial differential equations,

$$\frac{\left[\frac{1}{r}-\lambda\right]}{F(\mu,\lambda;r)}\frac{\partial^{2}\tilde{\rho}^{+}(r,\lambda)}{\partial r\partial\lambda}+\left[\frac{\frac{1}{r}\left[\frac{1}{r}-2\lambda\right]}{F(\mu,\lambda;r)}-\frac{\left[\frac{1}{r}-\lambda\right]F'(\mu,\lambda;r)}{(F(\mu,\lambda,;r))^{2}}+\frac{\Gamma'\mathcal{F}(r,\lambda)}{F(\mu,\lambda;r)}\right]\frac{\partial\tilde{\rho}^{+}(r,\lambda)}{\partial\lambda}$$

$$-\frac{\frac{1}{r}\left[\frac{1}{r}-2\lambda\right]}{F(\mu,\lambda;r)}\frac{\partial\tilde{\rho}^{-}(r,\lambda)}{\partial\lambda}=\Gamma'[\tilde{\rho}^{+}(r,\tfrac{1}{r})-\tilde{\rho}^{+}(r,-\infty)] \qquad (12a)$$

$$-\frac{\left[\frac{1}{r}-\lambda\right]}{F(\mu,\lambda;r)}\frac{\partial^{2}\tilde{\rho}^{-}(r,\lambda)}{\partial r\partial\lambda}+\left[\frac{\Gamma'\mathcal{F}(r,\lambda)}{F(\mu,\lambda;r)}+\frac{\left[\frac{1}{r}-\lambda\right]F'(\mu,\lambda;r)}{(F(\mu,\lambda,;r))^{2}}\right]\frac{\partial\tilde{\rho}^{-}(r,\lambda)}{\partial\lambda}$$

$$=\Gamma'[\tilde{\rho}^{-}(r,\tfrac{1}{r})-\tilde{\rho}^{-}(r,-\infty)] \qquad (12b)$$

$$\frac{\left[\frac{1}{r}-\lambda\right]}{F(\mu,\lambda;r)}\frac{\partial^{2}\tilde{\rho}^{+}(r,\lambda)}{\partial r\partial\lambda}+\left[\frac{\Gamma'\mathcal{F}(r,\lambda)}{F(\mu,\lambda;r)}-\frac{\left[\frac{1}{r}-\lambda\right]F'(\mu,\lambda;r)}{(F(\mu,\lambda,;r))^{2}}\right]\frac{\partial\tilde{\rho}^{+}(r,\lambda)}{\partial\lambda}$$

$$=\Gamma'[\tilde{\rho}^{+}(r,\tfrac{1}{r})-\tilde{\rho}^{+}(r,-\infty)] \qquad (12c)$$

$$-\frac{\left[\frac{1}{r}-\lambda\right]}{F(\mu,\lambda;r)}\frac{\partial^{2}\tilde{\rho}^{-}(r,\lambda)}{\partial r\partial\lambda}+\left[\frac{\frac{1}{r}\left|\frac{1}{r}-2\lambda\right|}{F(\mu,\lambda;r)}+\frac{\left[\frac{1}{r}-\lambda\right]F'(\mu,\lambda;r)}{(F(\mu,\lambda,;r))^{2}}+\frac{\Gamma'\mathcal{F}(r,\lambda)}{F(\mu,\lambda;r)}\right]\frac{\partial\tilde{\rho}^{-}(r,\lambda)}{\partial\lambda}$$

$$- \frac{\frac{1}{r}\left|\frac{1}{r} - 2\lambda\right|}{F(\mu,\lambda;r)} \frac{\partial \tilde{\rho}^{+}(r,\lambda)}{\partial \lambda} = \Gamma'[\tilde{\rho}^{-}(r,\tfrac{1}{r}) - \tilde{\rho}^{-}(r,-\infty)] \qquad (12d)$$

with the boundary conditions at the turning point ($\lambda = 1/r$) and in the continuum ($\lambda \to -\infty$) incorporated into the RHS of (12). Equations (12a,b) are valid only in region I, while (12c,d) are valid only in region II. Note that primes on $F(\mu,\lambda;r)$ in (12) denote differentiation w.r.t. r, and that $F(\mu,\lambda;r) = F(\lambda,\mu;r)$.

To convert (8) into an analogous set of coupled integral equations, define the functions $\bar{\rho}^{\pm}(r,\lambda)$ by,

$$\rho^{\pm}(r,\lambda) = \int_0^r \bar{\rho}^{\pm}(r',\lambda)dr' \qquad (13)$$

yielding,

$$\left(\frac{1}{r} - \lambda\right)[\bar{\rho}^{+}(r,\lambda) - \bar{\rho}^{+}(o,\lambda)] + \frac{1}{r}\left(\frac{1}{r} - 2\lambda\right)\int_0^r [\bar{\rho}^{+}(r',\lambda) - \bar{\rho}^{-}(r',\lambda)]dr'$$

$$= \Gamma' \int_{-\infty}^{1/r} d\mu\, F(\lambda,\mu;r) \int_0^r \bar{\rho}^{+}(r',\mu)dr' - \Gamma' \mathcal{F}(r,\lambda) \int_0^r \bar{\rho}^{+}(r',\lambda)dr' \qquad (13a)$$

$$-\left(\frac{1}{r} - \lambda\right)[\bar{\rho}^{-}(r,\lambda) - \bar{\rho}^{-}(o,\lambda)] = \Gamma' \int_{-\infty}^{1/r} d\mu F(\lambda,\mu;r) \int_0^r \bar{\rho}^{-}(r',\mu)dr'$$

$$- \Gamma' \mathcal{F}(r,\lambda) \int_0^r \bar{\rho}^{-}(r',\lambda)dr' \qquad (13b)$$

$$\left(\frac{1}{r} - \lambda\right)[\bar{\rho}^{+}(r,\lambda) - \bar{\rho}^{+}(o,\lambda)] = \Gamma' \int_{-\infty}^{1/r} d\mu\, F(\lambda,\mu;r) \int_0^r \bar{\rho}^{+}(r',\mu)dr'$$

$$- \Gamma' \mathcal{F}(r,\lambda) \int_0^r \bar{\rho}^{+}(r',\lambda)dr' \qquad (13c)$$

$$-\left(\frac{1}{r}-\lambda\right)\left[\bar{\rho}^{-}(r,\lambda)-\bar{\rho}^{-}(o,\lambda)\right]-\frac{1}{r}\left|\frac{1}{r}-2\lambda\right|\int_{o}^{r}\left[\bar{\rho}^{+}(r',\lambda)-\bar{\rho}^{-}(r',\lambda)\right]dr'$$

$$=\Gamma'\int_{-\infty}^{1/r}d\mu\ F(\lambda,\mu;r)\int_{o}^{r}\bar{\rho}^{-}(r',\mu)dr'-\Gamma'\,\mathcal{F}(r,\lambda)\int_{o}^{r}\bar{\rho}^{-}(r',\lambda)dr' \quad (13d)$$

Rearranging terms in (13) to show the couplings present between the integral equations gives,

$$\left(\frac{1}{r}-\lambda\right)\bar{\rho}^{+}(r,\lambda)+\left[\frac{1}{r}\left(\frac{1}{r}-2\lambda\right)+\Gamma'\,\mathcal{F}(r,\lambda)\right]\int_{o}^{r}\bar{\rho}^{+}(r',\lambda)dr'$$

$$-\Gamma'\int_{-\infty}^{1/r}d\mu\ F(\lambda,\mu;r)\int_{o}^{r}\bar{\rho}^{+}(r',\mu)dr'-\frac{1}{r}\left(\frac{1}{r}-2\lambda\right)\int_{o}^{r}\bar{\rho}^{-}(r',\lambda)dr'$$

$$=\left(\frac{1}{r}-\lambda\right)\bar{\rho}^{+}(o,\lambda) \quad (14a)$$

$$-\left(\frac{1}{r}-\lambda\right)\bar{\rho}^{-}(r,\lambda)+\Gamma'\,\mathcal{F}(r,\lambda)\int_{o}^{r}\bar{\rho}^{-}(r',\lambda)dr'$$

$$-\Gamma'\int_{-\infty}^{1/r}d\mu\ F(\lambda,\mu;r)\int_{o}^{r}\bar{\rho}^{-}(r',\mu)dr'=-\left(\frac{1}{r}-\lambda\right)\bar{\rho}^{-}(o,\lambda) \quad (14b)$$

$$\left(\frac{1}{r}-\lambda\right)\bar{\rho}^{+}(r,\lambda)+\Gamma'\,\mathcal{F}(r,\lambda)\int_{o}^{r}\bar{\rho}^{+}(r',\lambda)dr'$$

$$-\Gamma'\int_{-\infty}^{1/r}d\mu\ F(\lambda,\mu;r)\int_{o}^{r}\bar{\rho}^{+}(r',\mu)dr'=\left(\frac{1}{r}-\lambda\right)\bar{\rho}^{+}(o,\lambda) \quad (14c)$$

$$-\left(\frac{1}{r}-\lambda\right)\bar{\rho}^{-}(r,\lambda)+\left[\frac{1}{r}\left|\frac{1}{r}-2\lambda\right|+\Gamma'\,\mathcal{F}(r,\lambda)\right]\int_{o}^{r}\bar{\rho}^{-}(r',\lambda)dr'$$

$$-\Gamma'\int_{-\infty}^{1/r}d\mu\ F(\lambda,\mu;r)\int_{o}^{r}\bar{\rho}^{-}(r',\mu)dr'-\frac{1}{r}\left|\frac{1}{r}-2\lambda\right|\int_{o}^{r}\bar{\rho}^{+}(r',\lambda)dr'$$

$$=-\left(\frac{1}{r}-\lambda\right)\bar{\rho}^{-}(o,\lambda) \quad (14d)$$

where the boundary condition at r = o has been incorporated into the RHS of (14). The three representations of the coupled Boltzmann equations (equations (8), (12) and (14)) all require the same number of quadratures to obtain a solution - namely two each for $\rho^{+}(r,\lambda)$ and $\rho^{-}(r,\lambda)$. However, our reason for giving the details of the transformation between representations (cf. equations (10), (13)) is to highlight the different types of boundary conditions required in each case. In the case of the PDE's (12), it is clear from (10) that the required boundary conditions on $\tilde{\rho}^{\pm}(r,\lambda)$ should be global in energy and local in r, while in the case of (14) the boundary conditions on $\bar{\rho}^{\pm}(r,\lambda)$ should be local in energy and global in r. We use the word global to indicate that the integrand of an integral w.r.t. the specified degree of freedom is required as a boundary condition. Otherwise it is called a local boundary condition (e.g., equation (9) is local in both r and λ). Therefore, from (10) and (13) it is clear that the boundary conditions for the PDE and IE representations are of a mixed nature, and will be difficult to implement numerically. It should be clear however that in all three cases (eqs. (8), (12) and (14)), after discretization, the basic problem numerically is the same - namely one of solving a set of simulataneous algebraic equations for the PIDE representation (8) (these are the practical equations mentioned earlier), and leave it to the reader to write down the corresponding sets of equations for the other representations (12), (14).

Numerical Solution of PIDE's

To convert the coupled PIDE's (8) into algebraic equations, four steps need to be taken:

(i) Replace all derivatives with finite differences. If the PIDE is part of an initial value problem, the choice of either forward or backward differences will depend on the boundary conditions.

(ii) Replace all integrals with quadrature sums. The choice of quadrature rule is crucial in determining the overall stability and convergence rate of the resulting algorithm. The type of quadrature rule chosen in turn depends on the global behavior of the

integrand over all of phase space. Hence, for a multidimensional kernal, this step can easily be the most time consuming one in preparing for the full solution.

(iii) Impose all boundary conditions on the algebraic equations resulting from steps (i) and (ii). Make sure that the boundary conditions used lead to a well-posed problem with a non-singular coefficient matrix.

(iv) Finally, choose a technique for solving the resultant set of algebraic equations which takes advantage as much as possible of the structure of the coefficient matrix. Compute the condition number of the coefficient matrix and determine whether the algebraic equations need preconditioning.

Therefore, discretizing $r \to r_i = \{o, r_1, r_2, \ldots, r_{max} \equiv r_{N_r}\}$ with $N_r + 1$ equally spaced points (step size h), and replacing integrals with quadrature sums (with weight functions ϕ_k) yields the following for (8),

$$T_{ij} \frac{[\rho^+_{i+1,j} - \rho^+_{i-1,j}]}{2h} + \mathcal{G}_{ij}(\rho^+_{ij} - \rho^-_{ij}) + \Gamma'_j \mathcal{F}_{ij}\rho^+_{ij} - \Gamma'_j \sum_k \phi_k F_{jki}\rho^+_{ik} = 0 \tag{15a}$$

$$-T_{ij} \frac{[\rho^-_{i+1,j} - \rho^-_{i-1,j}]}{2h} + \Gamma'_j \mathcal{F}_{ij}\rho^-_{ij} - \Gamma'_j \sum_k \phi_k F_{jki}\rho^-_{ik} = 0 \tag{15b}$$

$$T_{ij} \frac{[\rho^+_{i+1,j} - \rho^+_{i-1,j}]}{2h} + \Gamma'_j \mathcal{F}_{ij}\rho^+_{ij} - \Gamma'_j \sum_k \phi_k F_{jki}\rho^+_{ik} = 0 \tag{15c}$$

$$-T_{ij} \frac{[\rho^-_{i+1,j} - \rho^-_{i-1,j}]}{2h} - |\mathcal{G}_{ij}|(\rho^+_{ij} - \rho^-_{ij}) + \Gamma' \mathcal{F}_{ij}\rho^-_{ij} - \Gamma'_j \sum_k \phi_k F_{jki}\rho^-_{ik} = 0 \tag{15d}$$

where $\Gamma_j \equiv \Gamma e^{-\lambda_j}$, $F_{jki} = F(\lambda_j, \mu_k; r_i)$, $\mathcal{F}_{ij} = \mathcal{F}(r_i, \lambda_j)$, $\mathcal{G}_{ij} = \frac{1}{r_i}\left(\frac{1}{r_i} - 2\lambda_j\right)$,

$|\mathcal{G}_{ij}| = \frac{1}{r_i}\left|\frac{1}{r_i} - 2\lambda_j\right|$, $T_{ij} = \frac{1}{r_i} - \lambda_j$ and $\rho^{\pm}_{ij}$ denotes $\rho^{\pm}(r_i,\lambda_j)$.

It will prove convenient to rearrange equations (15) into the order (15a,c), followed by (15b,d), so that the resultant coefficient matrix is positive definite (Golub and van Loan [30]). Then applying the boundary conditions on r yields,

$$-(1-\delta_{io})T_{ij_1}\rho^{+}_{i-1,j_1} - 2h\sum_{k_1}\left[\Gamma'_{j_1}\phi_{k_1}F_{j_1k_1i} - \delta_{k_1j_1}(\mathcal{G}_{ij_1} + \Gamma'_{j_1}\mathcal{F}_{ij_1})\right]\rho^{+}_{ik_1}$$

$$- 2h\,\Gamma'_{j_1}\sum_{k_2}\phi_{k_2}F_{j_1k_2i}\,\rho^{+}_{ik_2} - 2h\,\mathcal{G}_{ij_1}\,\rho^{-}_{ij_1} + (1-\delta_{N_r})\rho^{+}_{i+1,j_1}$$

$$= \delta_{io}\rho^{+}(r=o,\lambda_{j_1}) + \delta_{iN_r}\rho^{+}(r_{max},\lambda_{j_1}) \qquad (16a)$$

$$-(1-\delta_{io})T_{ij_2}\rho^{+}_{i-1,j_2} - 2h\,\Gamma'_{j_2}\sum_{k_1}\phi_{k_1}F_{j_2k_1i}\,\rho^{+}_{ik_1}$$

$$- 2h\sum_{k_2}\left[\Gamma'_{j_2}\phi_{k_2}F_{j_2k_2i} - \delta_{k_2j_2}\,\Gamma'_{j_2}\mathcal{F}_{ij_2}\right]\rho^{+}_{ik_2} + (1-\delta_{iN_r})\rho^{+}_{i+1,j_2}$$

$$= \delta_{io}\rho^{+}(r=o,\lambda_{j_2}) + \delta_{iN_r}\rho^{+}(r_{max},\lambda_{j_2}) \qquad (16b)$$

$$(1-\delta_{io})T_{ij_1}\rho^{-}_{i-1,j_1} - 2h\sum_{k_1}\left[\Gamma'_{j_1}\phi_{k_1}F_{j_1k_1i} - \delta_{k_1j_1}\,\Gamma'_{j_1}\mathcal{F}_{ij_1}\right]\rho^{-}_{ik_1}$$

$$- 2h\,\Gamma'_{j_1}\sum_{k_2}\phi_{k_2}F_{j_1k_2i}\,\rho^{-}_{ik_2} - (1-\delta_{N_r})\rho^{-}_{i+1,j_1}$$

$$= \delta_{io}\rho^{-}(r=o,\lambda_{j_1}) + \delta_{iN_r}\rho^{-}(r_{max},\lambda_{j_1}) \qquad (16c)$$

$$(1-\delta_{io})T_{ij_2}\rho^-_{ij_2} - 2h\,|\mathcal{G}_{ij_2}|\rho^+_{ij_2} - 2h\,\Gamma'_{j_2}\sum_{k_1}\phi_{k_1}F_{j_2k_1i}\,\rho^-_{ik_1}$$

$$- 2h\sum_{k_2}\left[\Gamma'_{j_2}\phi_{k_2}F_{j_2k_2i} - \delta_{k_2j_2}(|\mathcal{G}_{ij_2}| + \Gamma'_{j_2}\mathcal{F}_{ij_2})\right]\rho^-_{ik_2} - (1-\delta_{iN_r})\rho^-_{i+1j_2}$$

$$= \delta_{io}\rho^-(r=o,\lambda_{j_2}) + \delta_{iN_r}\rho^-(r_{max},\lambda_{j_2}) \qquad (16d)$$

and where the indices are defined: $1 \le i \le N_r-1$, $-N_c \le j_1 \le N_{b_1}$, $N_{b_1} \le j_2 \le N_{b_2}$ and $-N_c \le k_1 \le N_{b_1}$, $N_{b_1} \le k_2 \le N_{b_2}$. The energy range $[-\infty, \frac{1}{r}]$ has been discretized into three grids: $[-\lambda_{max},o]$, $[o, \frac{1}{2r_i}]$, $[\frac{1}{2r_i}, \frac{1}{r_i}]$ composed of $N_c + 1$, $N_{b_1} + 1$ and $N_{b_2} - N_{b_1}$ points, respectively. The total number of points in the energy grid is $N_c + N_{b_2}$. Hence the subscripts j_1, k_1 indicate that the energy is restricted to region I: $[-\lambda_{max}, \frac{1}{2r_i}]$, while j_2, k_2 *indicate that the energy is restricted to* region II: $[\frac{1}{2r_i}, \frac{1}{r_i}]$. The parameter λ_{max} represents the largest free ion energy considered. More details on the energy grid are given below.

Now, before applying the boundary conditions on λ (equations 9a,d)), a word is needed on continuity conditions. In equation (8) the λ,r phase space is divided into 2 regions. Since we assume that the unknowns $\rho^{\pm}(r,\lambda)$ are smooth functions of λ and r, we must insure that the computed solutions of (16) are continuous across the boundary between regions I and II. We do this by recognizing that (16a,b) are 2 equations for the *same* unknown when $j_1 = j_2 = N_{b_1}$. Therefore, we can add the two equations together and divide by 2. This insures that we will not have an overdetermined system of equations. In the case where j_1 and j_2 don't equal N_{b_1}, the appropriate terms from the k_1 and k_2 summations (i.e., the

last in k_1 and the first in k_2) must be added together in (16a,b). These two steps will insure that $\rho^+(r,\lambda)$ is continuous at $\lambda = 1/2r$. Analogous additions in equations (16c,d) will likewise insure that $\rho^-(r,\lambda)$ will be continuous at $\lambda = 1/2r$. Therefore, applying the steps above to insure continuity in the solution, and the boundary conditions on λ yields the following set of practical algebraic equations,

$$-(1-\delta_{io})T_{ij_1}\rho^+_{i-1,j_1} - \sum_{k_1}{}' \mathcal{A}^{(i)+}_{j_1k_1}\rho^+_{ik_1} - \mathcal{C}^{(i)+}_{j_1N_{b_1}}\rho^+_{iN_{b_1}} - \sum_{k_2}{}' \mathcal{A}^{(i)+}_{j_1k_2}\rho^+_{ik_2}$$

$$- 2h\,\mathcal{G}_{ij_1}\rho^-_{ij_1} + (1-\delta_{iN_r})\rho^+_{i+1,j_1} = \mathcal{B}^{(i)+}_{j_1} \qquad (17a)$$

$$-(1-\delta_{io})T_{ij_2}\rho^+_{i-1,j_2} - \sum_{k_1}{}' \mathcal{A}^{(i)+}_{j_2k_1}\rho^+_{ik_1} - \mathcal{C}^{(i)+}_{j_2N_{b_1}}\rho^+_{iN_{b_1}} - \sum_{k_2}{}' \mathcal{A}^{(i)+}_{j_2k_2}\rho^+_{ik_2}$$

$$+ (1-\delta_{iN_r})\rho^+_{i+1,j_2} = \mathcal{B}^{(i)+}_{j_2} \qquad (17b)$$

$$(1-\delta_{io})T_{ij_1}\rho^-_{i-1,j_1} - \sum_{k_1}{}' \mathcal{A}^{(i)-}_{j_1k_1}\rho^-_{ik_1} - \mathcal{C}^{(i)-}_{j_1N_{b_1}}\rho^-_{iN_{b_1}} - \sum_{k_2}{}' \mathcal{A}^{(i)-}_{j_1k_2}\rho^-_{ik_2}$$

$$- (1-\delta_{iN_r})\rho^-_{i+1,j_1} = \mathcal{B}^{(i)-}_{j_1} \qquad (17c)$$

$$(1-\delta_{io})T_{ij_2}\rho^-_{i-1,j_2} - 2h\,|\mathcal{G}_{ij_2}|\,\rho^+_{ij_2} - \sum_{k_1}{}' \mathcal{A}^{(i)-}_{j_2k_1}\rho^-_{ik_1} - \mathcal{C}^{(i)-}_{j_2N_{b_1}}\rho^-_{iN_{b_1}}$$

$$- \sum_{k_2}{}' \mathcal{A}^{(i)-}_{j_2k_2}\rho^-_{ik_2} - (1-\delta_{iN_r})\rho^-_{i+1,j_2} = \mathcal{B}^{(i)-}_{j_2} \qquad (17d)$$

where the coefficient matrix $\mathcal{A}$ and column vector $\mathcal{B}$ are defined as,

$$\mathcal{A}^{(i)+}_{j_1k_1} = 2h\left[\Gamma'_{j_1}\,\phi_{k_1}\,F_{j_1k_1i} - \delta_{k_1j_1}(\mathcal{G}_{ij_1} + \Gamma'_{j_1}\,\mathcal{F}_{ij_1})\right] \tag{18a}$$

$$\mathcal{A}^{(i)+}_{j_1k_2} = 2h\,\Gamma'_{j_1}\,\phi_{k_2}\,F_{j_1k_2i} \tag{18b}$$

$$\mathcal{A}^{(i)+}_{j_2k_1} = 2h\,\Gamma'_{j_2}\,\phi_{k_1}\,F_{j_2k_1i} \tag{18c}$$

$$\mathcal{A}^{(i)+}_{j_2k_2} = 2h\left[\Gamma'_{j_2}\,\phi_{k_2}\,F_{j_2k_2i} - \delta_{k_2j_2}\,\Gamma'_{j_2}\,\mathcal{F}_{ij_2}\right] \tag{18d}$$

$$\mathcal{A}^{(i)-}_{j_1k_1} = 2h\left[\Gamma'_{j_1}\,\phi_{k_1}\,F_{j_1k_1i} - \delta_{k_1j_1}\,\Gamma'_{j_1}\,\mathcal{F}_{ij_1}\right] \tag{18e}$$

$$\mathcal{A}^{(i)-}_{j_1k_2} = 2h\,\Gamma'_{j_1}\,\phi_{k_2}\,F_{j_1k_2i} \tag{18f}$$

$$\mathcal{A}^{(i)-}_{j_2k_1} = 2h\,\Gamma'_{j_2}\,\phi_{k_1}\,F_{j_2k_1i} \tag{18g}$$

$$\mathcal{A}^{(i)-}_{j_2k_2} = 2h\left[\Gamma'_{j_2}\,\phi_{k_2}\,F_{j_2k_2i} - \delta_{k_2j_2}(|\mathcal{G}_{ij_2}| + \Gamma'_{j_2}\,\mathcal{F}_{ij_2})\right] \tag{18h}$$

and,

$$\mathcal{B}^{(i)+}_{j_1} = \delta_{io}\rho^{+}(r=o,\lambda_{j_1}) + \delta_{iN_r}\rho^{+}(r_{max},\lambda_{j_1}) + \delta_{N_{b_2}k_2}\,2h\Gamma'_{j_1}\phi_{N_{b_1}}F_{j_1N_{b_2}i}\rho^{+}_{iN_{b_2}}$$

$$+ \delta_{k_1-N_c}\rho^{+}_{i,-N_c}\,2h\left[\Gamma'_{j_1}\,\phi_{-N_c}\,F_{j_1-N_ci} - \delta_{-N_cj_1}(\mathcal{G}_{ij_1} + \Gamma'_{j_1}\,\mathcal{F}_{ij_1})\right] \tag{19a}$$

$$\mathcal{B}^{(i)+}_{j_2} = \delta_{io}\rho^{+}(r=o,\lambda_{j_2}) + \delta_{iN_r}\rho^{+}(r_{max},\lambda_{j_2}) + \delta_{k_1-N_c}\,2h\Gamma'_{j_2}\phi_{-N_c}F_{j_2-N_ci}\rho^{+}_{i-N_c}$$

$$+ \delta_{k_2N_{b_2}}\rho^{+}_{iN_{b_2}}\left[2h\,\Gamma'_{j_2}\,\phi_{N_{b_2}}F_{j_2N_{b_2}i} - \delta_{k_2j_2}\,\Gamma'_{j_2}\,\mathcal{F}_{ij_2}\right] \tag{19b}$$

$$\mathcal{A}^{(i)-}_{j_1} = \delta_{io}\rho^{-}(\underline{r}=o,\lambda_{j_1}) + \delta_{iN_r}\rho^{-}(r_{max},\lambda_{j_1}) + \delta_{N_{b_2}k_2}\, 2h\Gamma'_{j_1}\Phi_{N_{b_2}}F_{j_1N_{b_2}i}\rho^{-}_{iN_{b_2}}$$

$$+ \delta_{k_1-N_c}\rho^{-}_{i,-N_c}\, 2h\left[\Gamma'_{j_1}\Phi_{-N_c}F_{j_1-N_c i} - \delta_{k_1j_1}\Gamma'_{j_1}\mathcal{F}_{ij_1}\right] \tag{19c}$$

$$\mathcal{A}^{(i)-}_{j_2} = \delta_{io}\rho^{-}(r=o,\lambda_{j_2}) + \delta_{iN_r}\rho^{-}(r_{max},\lambda_{j_2}) + \delta_{k_1-N_c}\, 2h\Gamma'_{j_2}\Phi_{-N_c}F_{j_2-N_c i}\rho^{-}_{i,-N_c}$$

$$+ \delta_{j_2N_{b_2}}\, 2h\,|\mathcal{F}_{ij_2}|(\rho^{+}_{i,N_{b_2}} - \rho^{-}_{i,N_{b_2}})$$

$$+ \delta_{k_2N_{b_2}}\, 2h\left[\Gamma'_{j_2}\Phi_{N_{b_2}}F_{j_2N_{b_2}i} - \delta_{k_2j_2}\Gamma'_{j_2}\mathcal{F}_{ij_2}\right]\rho^{-}_{iN_{b_2}} \tag{19d}$$

The elements of the coefficient matrix $\mathcal{A}$ which govern the continuity of the solutions $\rho^{\pm}$ at the boundary between regions I and II are denoted by $\mathcal{C}$ in (17) and are defined,

$$\mathcal{C}^{(i)+}_{j_1N_{b_1}} = 4h\,\Gamma'_{j_1}\Phi_{N_{b_1}}F_{j_1N_{b_1}i} - \delta_{j_1N_{b_1}}\,2h\,\Gamma'_{j_1}\mathcal{F}_{ij_1} \tag{20a}$$

$$\mathcal{C}^{(i)+}_{j_2N_{b_1}} = 4h\,\Gamma'_{j_2}\Phi_{N_{b_1}}F_{j_2N_{b_1}i} \tag{20b}$$

$$\mathcal{C}^{(i)-}_{j_1N_{b_1}} = 4h\,\Gamma'_{j_1}\Phi_{N_{b_1}}F_{j_1N_{b_1}i} - \delta_{j_1N_{b_1}}\,2h\,\Gamma'_{j_1}\mathcal{F}_{ij_1} \tag{20c}$$

$$\mathcal{C}^{(i)-}_{j_2N_{b_1}} = 4h\,\Gamma'_{j_2}\Phi_{N_{b_1}}F_{j_2N_{b_1}i} \tag{20d}$$

The index i in (17) is defined as before, while in (17a,c) j_1 is defined: $-N_c+1 \le j_1 \le N_{b_1}$, and in (17b,d) j_2 is defined: $N_{b_1}+1 \le j_2 \le N_{b_2}-1$. The primes on the k_1 and k_2 summations in (17) denote that the λ boundary terms are omitted (i.e., $k_1 = -N_c$ and $k_2 = N_{b_2}$). The primes also

indicate that the terms with $k_1 = N_{b_1}$ and $k_2 = N_{b_2}$ have been factored-out of the summation (and are represented by the $\mathcal{C}$ terms).

The algebraic equations (17) can be written in the familiar matrix notation,

$$\mathcal{A}\,\rho = \mathcal{B} \tag{21}$$

where $\mathcal{A}$ and $\mathcal{B}$ are given by (18,19), respectively, and ρ is the unknown column vector composed of the discretized elements of ρ^+ first, then ρ^-. The known column vector $\mathcal{B}$, composed of boundary conditions on $\rho^{\pm}$, has been written in full detail in (19) in order to show exactly how each boundary condition contributes to the problem. In practice, after application of (9), (19) will simplify considerably. From (18) it is clear that the coefficient matrix $\mathcal{A}$ is non-symmetric due to the presence of the $\mathcal{G}_{ij}$ and $|\mathcal{G}_{ij}|$ terms. The overall structure of the coefficient matrix is shown in figure 2.

The energy grid chosen was nonlinear due to the skew discontinuity present in the kernals $F(\lambda,\mu;r)$ (Flannery [22,23]). In particular, we use the 3tan(u) prescription of Bates and Mendaš [8] for the pivot points used in the Simpson's rule quadratures in (17). That is, the weights and pivots used in the energy quadratures are defined for the three grids as,

$$\lambda_k = 3\tan(k\xi), \qquad \phi_k = r_k\,\xi\,\sec^2(k\xi)$$

with,

(i) continuum part of region I: $-\lambda_{max} \le \lambda \le 0 \qquad -N_c \le k \le 0$

$$\xi = \tan^{-1}(\lambda_{max}/3)/N_c$$

$$r_k = \begin{cases} 1 & , k = -N_c,\ 0 \\ 4 & , k = \text{even integer in } (-N_c,0) \\ 2 & , k = \text{odd integer in } (-N_c,0) \end{cases}$$

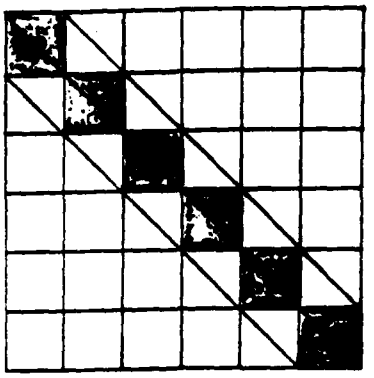

a

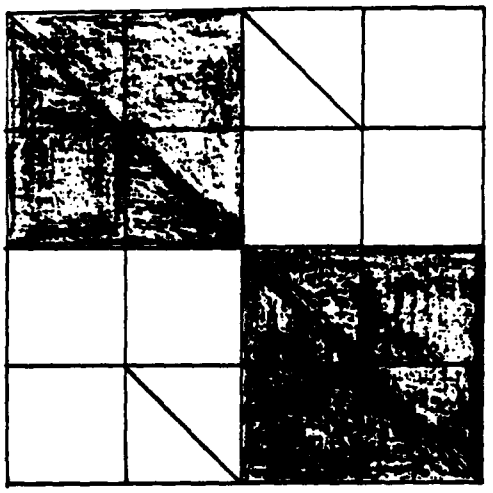

b

Figure 2: Structure of coefficient matrix $\mathcal{A}$ in equation (21). a) block tri-diagonal in r, b) non-symmetric, positive-definite in λ.

(ii) bound state part of region I: $0 \leq \lambda \leq \frac{1}{2r_i}$ $\quad 0 \leq k \leq N_{b_1}$

$$\xi = \tan^{-1}(1/6r_i)/N_{b_1}$$

$$r_k = \begin{cases} 1 & , k = 0, N_{b_1} \\ 4 & , k = \text{even integer in } (0,N_{b_1}) \\ 2 & , k = \text{odd integer in } (0,N_{b_1}) \end{cases}$$

and,

(iii) region II: $\frac{1}{2r_i} \le \lambda \le \frac{1}{r_i}$ $\quad N_{b_1} \le k \le N_{b_2}$

$$\lambda_k = 3\tan[\xi_{min} + (k-N_{b_1})\xi] \qquad \phi_k = r_k\,\xi\,\sec^2[\xi_{min} + (k-N_{b_1})\xi]$$

$$\xi_{min} = \tan^{-1}(1/6r_i) \qquad \xi = [\tan^{-1}(1/3r_i) - \tan^{-1}(1/6r_i)]/(N_{b_2}-N_{b_1})$$

$$r_k = \begin{cases} 1 & , k = N_{b_1}, N_{b_2} \\ 4 & , k = \text{even integer in } (N_{b_1}, N_{b_2}) \\ 2 & , k = \text{odd integer in } (N_{b_1}, N_{b_2}) \end{cases}$$

Denoting the total number of points in the energy quadrature by $N_\lambda \equiv N_c + N_{b_2} - 2$, and the total number of simultaneous equations in (21) by $N \equiv (N_r-1)\,2\,N_\lambda = 2(N_r-1)(N_c+N_{b_2}-2)$. A typical value for N is 20,988 for $N_r = 100$, $N_c = 36$ and $N_{b_2} = 72$. Hence, due to the very large sparse nature of the coefficient matrix $\mathcal{A}$, the use of direct techniques like Gaussian elimination to solve (21) will be totally out of the question because of the time and memory requirements involved. Therefore iterative techniques like Lanczos algorithms (Cullum and Willoughby [15], Golub and van Loan [30], accelerated successive overrelaxation methods (Young [42], Hageman and Young [32]) and Tchebychev iteration (Manteuffel [36,37]) should be used to solve (21).

Consequently, before continuing our discussion of the solution of (21), we will review some of the iterative techniques used to deal with large linear systems. For readers interested in a complete treatment consult the books listed in section IV - especially those by Young and Hageman and Young.

Iterative Methods for Large Linear Systems

Solve the matrix equation Ax = B where A is an N x N real, symmetric positive definite matrix, and x, B are column vectors of length N. Decompose A into three parts: a) it's diagonal elements (D), (b) all elements below the diagonal (C_L) and (c) all elements above the diagonal

(C_u). That is, we can write $A = D - C_L - C_u$. Now, scale the problem so the diagonal elements of the new coefficient matrix are 1. This can be done by multiplying by $D^{1/2}$,

$$(D^{-1/2} A D^{-1/2})(D^{1/2} x) = D^{-1/2} b \tag{22}$$

$$\rightarrow D^{-1/2}(D - C_L - C_u)D^{-1/2} = D^{-1/2} D D^{-1/2} - D^{-1/2}C_L D^{-1/2} - D^{-1/2} C_u D^{-1/2}$$

$$= I - L - L^t \tag{23}$$
$$\equiv I - B$$

where I is the identity matrix and $L \equiv D^{-1/2} C_L D^{-1/2}$, $B \equiv L + L^t$. Then, from (22), defining the column vectors $u \equiv D^{1/2} x$, $c \equiv D^{-1/2} b$ allows the original problem to be case into the suggestive form,

$$u = B u + c \tag{24}$$

which is then solved iteratively.

Two of the most widely used iterative methods are the Jacobi method,

$$u^{(n+1)} = B u^{(n)} + c \tag{25a}$$

and the Gauss-Seidel method,

$$u^{(n+1)} = L u^{(n+1)} + L^t u^{(n)} + c$$
$$= \mathcal{L} u^{(n)} + k \tag{25b}$$

where $k = (I - L)^{-1} c$, $\mathcal{L} = (I-L)^{-1} L^t$ and in (25) $u^{(n)}$ denotes the nth iteration of u. More recently variants on the Gauss-Seidel method have been developed to speed the convergence of the iteration procedure. One of the variants is the successive overrelaxation method (SOR),

$$u^{(n+1)} = \omega\,(L\,u^{(n+1)} + L^t\,u^{(n)} + c) + (1-\omega)\,u^{(n)}$$
$$= \mathcal{L}_\omega\,u^{(n)} + k_\omega \qquad (25c)$$

with $\mathcal{L}_\omega = (I - \omega L)^{-1}\,(\omega L^t + (1-\omega)I)$, $k_\omega = \omega(I-\omega L)^{-1}\,c$. The parameter ω is known as the acceleration parameter. When $\omega = 1$ (25c) reduces to the Gauss-Siedel method (25b). A generalization of the SOR method involves 2 SOR sweeps for each iteration of u, and is called the symmetric successive overrelaxation method (SSOR),

$$u^{(n+1/2)} = \mathcal{L}_\omega\,u^{(n)} + k_\omega^{(for.)} \qquad (25d)$$

$$u^{(n+1)} = \mathcal{U}_\omega\,u^{(n+1/2)} + k_\omega^{(back.)} \qquad (25e)$$

where the operator $\mathcal{L}_\omega$ is defined above, and $\mathcal{U}_\omega = (I - \omega L^t)^{-1}(\omega L + (1-\omega)I)$ and $k_\omega^{(for.)} = \omega(I - \omega L)^{-1}\,c$, $k_\omega^{(back.)} = \omega(I - \omega L^t)^{-1}\,c$. Equations (25d,e) can be combined into one iteration step by defining the operator $\mathcal{S}_\omega = \mathcal{U}_\omega\,\mathcal{L}_\omega$,

$$u^{(n+1)} = \mathcal{S}_\omega\,u^{(n)} + k_\omega \qquad (25f)$$

where $k_\omega = \omega\,(2-\omega)(I-\omega L^t)^{-1}(I-\omega L)^{-1}\,c$.

In the SOR and SSOR methods one must choose an acceleration parameter ω which will be optimal for a given coefficient matrix A. Two widely used methods of acceleration are Chebyshev acceleration and conjugate gradient acceleration. Writing the basic iteration procedure (24) as $u^{(n+1)} = \mathcal{G}\,u^{(n)} + k$, Chebyskev acceleration is defined,

$$u^{(n+1)} = \rho_{n+1}[(\tau\,\mathcal{G}\,u^{(n)} + k) + (1-\tau)u^{(n)}] + (1-\rho_{n+1})u^{(n-1)} \qquad (26a)$$

where $\tau = 2/[2-M(\mathcal{G})-m(\mathcal{G})]$ and,

$$\rho_{n+1} = \begin{cases} 1 & , n = s \\ (1 - \sigma^2/2)^{-1} & , n = s+1 \\ [1 - (\sigma/2)^2 \rho_n]^{-1} & , n \geq s+2 \end{cases}$$

with $\sigma = [M(\mathcal{G})-m(\mathcal{G})]/[2 - M(\mathcal{G})-m(\mathcal{G})]$, $M(\mathcal{G})$ = maximum eigenvalue of matrix $\mathcal{G}$, $m(\mathcal{G})$ = minimum eigenvalue of $\mathcal{G}$. The integer s is initially zero, then increased as the adaptive procedure proceeds (Grimes et al. [31]). That is, one can reassign the overrelaxation parameter ρ several times during the iteration process. A disadvantage of Chebyshev acceleration is that it requires estimates of the smallest and largest eigenvalues of $\mathcal{G}$ to be made.

Conjugate gradient acceleration is defined,

$$u^{(n+1)} = \rho_{n+1} (\gamma_{n+1} \delta^{(n)} + u^{(n)}) + (1 - \rho_{n+1})u^{(n-1)} \qquad (26b)$$

$$\delta^{(n+1)} = \rho_{n+1} (\gamma_{n+1} \mathcal{G} \delta^{(n)} + (1-\gamma_{n+1}) \delta^{(n)}) + (1 - \rho_{n+1})\delta^{(n-1)} \qquad (26c)$$

where $\delta^{(n)}$ is a pseudo-residual vector given by: $\delta^{(n)} = \mathcal{G} u^{(n)} + k - u^{(n)}$. The acceleration parameters ρ and γ are defined,

$$\rho_{n+1} = \begin{cases} 1 & , n = 0 \\ \dfrac{1}{1 - \left[\dfrac{\gamma_{n+1}}{\gamma_n \rho_n}\right] \dfrac{\delta^{(n)t} W^t W \delta^{(n)}}{\delta^{(n-1)t} W^t W \delta^{(n-1)}}} & , n \geq 1 \end{cases}$$

$$\gamma_{n+1} = \left[1 - \frac{\delta^{(n)t} W^t W \mathcal{G} \delta^{(n)}}{\delta^{(n)t} W^t W \delta^{(n)}}\right]^{-1}$$

where W is a nonsingular symmetrization matrix. For the Jacobi method $W = D^{1/2}$, while for the SSOR method $W = (1/\omega) D^{-1/2}(D - \omega C_L^t)$. While the

conjugate gradient acceleration method doesn't require estimation of the eigenvalues of $\mathcal{G}$, the number of arithmetic operations required for it's implementation is greater.

We have necessarily been selective and brief in our discussion of iterative methods due to the vastness of this area of linear algebra. The discussion of this subsection is based upon appendix A in the technical report of Grimes et al. [31]. Two excellent books which provide good introductions to this area are Young [42] and Hageman and Young [32] (others can be found in the list of general references in section IV). As for software which implements the iterative techniques discussed above (as well as others not discussed here), excellent packages are the ITPACK library (Grimes et al. [31]) and the package of Lanczos algorithms of Cullum and Willoughby [15].

So far we have only discussed iterative techniques for symmetric coefficient matrices $\mathcal{A}$. However, the central numerical problem of this lecture is to solve equation (21) for a large, sparse non-symmetric matrix $\mathcal{A}$. Unfortunately there is much less known in linear algebra about iterative techniques for non-symmetric matrices. One way to handle non-symmetric matrices $\mathcal{A}$ is to consider (instead of (21) for example) the associated equation $\mathcal{A}^t\mathcal{A}\rho = \mathcal{A}^t\mathcal{B}$, where $\mathcal{A}^t\mathcal{A}$ is a symmetric coefficient matrix. However, in many practical applications the condition number of $\mathcal{A}^t\mathcal{A}$ is much greater than that of $\mathcal{A}$ - thereby indicating that this technique will not necessarily yield a problem which will converge rapidly using one of the iterative techniques discussed above. Another way to deal with non-symmetric problems is to develop the appropriate generalizations of (25,26) directly (Young and Jea [43], Manteuffel [36,37]). However, these generalizations require knowledge of the eigenvalue spectrum of $\mathcal{G}$ which is difficult to obtain in practice. In summary then, while some progress has been made in linear algebra towards handling the non-symmetric case, much more work needs to be done in devising criteria by which one can select acceleration parameters which will be optimal for a given general coefficient matrix $\mathcal{G}$.

Returning now to our discussion of the numerical solution of (21) for non-symmetric $\mathcal{A}$, we will need to know the condition number $\kappa(\mathcal{A})$ for

the coefficient matrix $\mathcal{A}$ before using one of the iterative techniques above. The condition number of a matrix $\mathcal{A}$ is defined: $\kappa(\mathcal{A}) = ||\mathcal{A}|| \cdot ||\mathcal{A}^{-1}||$. Computing the condition number of the coefficient matrix in a given problem (e.g., equation (21)) is necessary because the iterative techniques discussed above (like SSOR) work best for well-conditioned matrices (i.e., those with small κ). Otherwise, the number of iterations required for convergence will increase greatly, and since κ provides a measure of the sensitivity of a given problem to round-off errors and perturbations, if κ is too large for a given $\mathcal{A}$, then iterative techniques will not work due to accumulation of round-off errors. Physically, the condition number of a matrix $\mathcal{A}$ provides a measure of the distance between $\mathcal{A}$ and the set of angular matrices. Hence, when $\kappa(\mathcal{A})$ is very large the matrix $\mathcal{A}$ is considered ill-conditioned, which means that the numerical solution u, of (24) say, will be very sensitive to round-off error which are unavoidably accumulated during the iteration process. More details about condition numbers in linear algebra can be found in Golub and van Loan [30].

Using the routine LFCRG in the IMSL library [33] to estimate the condition number $\kappa_1(\mathcal{A})$, via the algorithm of Cline et al. [14], of the coefficient matrix of equation (17) we find that $\kappa_1(\mathcal{A}) \simeq 4.20\ 10^{19}$. In contrast $\kappa_1(\mathcal{A}) = 1751.1$ for the coefficient matrix $\mathcal{A}$ resulting from the discretization of the quasi-equilibrium integral equation (29). This indicates that the condition number for the coefficient matrix of (17) needs to be reduced approximately 16 orders of magnitude before the iterative techniques (25,26) will become effective. This can be accomplished either by row scaling (Golob and van Loan [30]) or pre-conditioning (Faber and Manteuffel [17]) the coefficient matrix. Unfortunately, these calculations have not been completed at the time of writing but will be reported in a forthcoming paper (Flannery and Mansky [28]). Hence, it is still an open question whether the iterative techniques discussed above are effective in solving (17). However our discussion of the condition number $\kappa_1(\mathcal{A})$ of $\mathcal{A}$ given by (18) has revealed the underlying reason why the earlier work of [8], failed to converge quickly as a function of gas density N(Z). Also, by illustrating the structure of the coefficient matrix in figure 2 and equation (18), a

deeper insight into the role the gas density plays in the nonlinear pressure regime is obtained. In fact once the problem of the ill-condition of $\mathcal{A}$ is solved, a number of other problems in chemical physics should become ameniable to the iterative techniques discussed in this lecture including the prediction of microscopic three-body ion-neutral association rates (Bates and McKibben [7]), and the inclusion of non-thermal effects into ion-ion recombination (Bates et al. [6]).

Before ending section II we wish to discuss the numerical solution of integral equations briefly. This is necessary because much of the numerical analysis of PIDE's relies heavily upon the expertise gained in solving related one-dimensional integral equations. The IE we will use as an example will be the quasi-equilibrium integral equation arising in ion-ion recombination. We will necessarily be brief since the numerical analysis of integral equations (even one-dimensional ones) is a vast field and we only wish to highlight points about the numerical treatment of IE's which are related to our earlier discussion of PIDE's. For a complete discussion of the numerical treatment of IE's see Baker [2].

In discussing the quasi-equilibrium theory of ion-ion recombination it will prove useful to define the functions $\rho^S(r,\lambda)$ and $\rho^D(r,\lambda)$,

$$\rho^D(r,\lambda) = \frac{1}{2}\left[\rho^+(r,\lambda) - \rho^-(r,\lambda)\right] \tag{27a}$$

$$\rho^S(r,\lambda) = \frac{1}{2}\left[\rho^+(r,\lambda) - \rho^-(r,\lambda)\right] \tag{27b}$$

which describe physically the net and total numbers of ion pairs undergoing recombination at a given relative separation r and internal energy λ. Substituting (27) into (8) yields two coupled PIDE's valid for $-\infty < \lambda \leq \frac{1}{r}$,

$$\left(\frac{1}{r} - \lambda\right)\frac{\partial \rho^D(r,\lambda)}{\partial r} + \frac{1}{r}\left(\frac{1}{r} - 2\lambda\right)\rho^D(r,\lambda) = \Gamma' \int_{-\infty}^{1/r} \rho^S(r,\mu)F(\lambda,\mu,;r)d\mu - \Gamma' \mathcal{F}(r,\lambda)\rho^S(r,\lambda) \tag{28a}$$

$$\left(\frac{1}{r} - \lambda\right) \frac{\partial \rho^S(r,\lambda)}{\partial r} + \frac{1}{r}\left|\frac{1}{r} - 2\lambda\right|\rho^D(r,\lambda) = \Gamma' \int_{-\infty}^{1/r} \rho^D(r,\mu)F(\lambda,\mu,;r)d\mu$$

$$- \Gamma' \mathcal{F}(r,\lambda)\rho^D(r,\lambda) \qquad (28b)$$

In the quasi-equilibrium theory the motion of the center of mass of the ion pairs is taken to be in thermodynamic equilibrium with the third bodies, while a quasi-equilibrium distribution in highly excited internal energy states of the ion pairs is established effectively instantaneously due to collisions with the much more numerous third bodies. In the establishment of this distribution it is assumed that the distribution of separations of ion pairs does not effect the quasi-equilibrium distribution in internal energy. That is, the r dependence of the distributions $\rho^+(r,\lambda)$, $\rho^-(r,\lambda)$ is not influenced by the recombination proceeding in the plasma. Hence we can assume that the r-distributions of contracting and expanding ion pairs is in thermodynamic equilibrium, thereby implying that $\rho^D(r,\lambda) = 0$. This results in (28b) indicating that $\rho^S(r,\lambda)$ is a constant w.r.t. r. Multiplying (28a) by r^2 and integrating w.r.t. r yields the quasi-equilibrium integral equation for the distribution over internal energy states $\rho^S_{QE}(\lambda)$,

$$\int_{-\infty}^{\epsilon} F(\lambda,\mu)\rho^S_{QE}(\mu)d\mu = \rho^S_{QE}(\lambda) \int_{-\infty}^{\omega} F(\lambda,\mu)d\mu \qquad (29)$$

where ω is the maximum binding energy of an ion pair, and ϵ is the stabilization energy of an ion pair. We refer the reader to the original literature (Bates and Moffett [12], Bates and Flannery [5], Bates and Mendaš [11], and Flannery [22,23]) for the details.

Equation (29) is valid only in the low gas density limit where the flow of contracting and expanding ion pairs balance, at higher gas densities however a net contraction of ion pairs occurs so that the full PIDE (8) must be solved. We quote the expression for the recombination rate coefficient α for the low density limit from the original literature cited above,

$$\alpha/\alpha_T = \Gamma_o \int_{-\infty}^{\nu} d\lambda \int_{\nu}^{\omega} d\mu \; F(\lambda,\mu)[\rho_{QE}^S(\lambda) - \rho_{QE}^S(\mu)] \qquad (30)$$

where $\nu = -E/kT$ is an arbitrary energy level, and α_T is the Thomson rate coefficient (Thomson [40]). From (30) it is clear that once IE (29) is solved for the $\rho_{QE}^S(\lambda)$, a bi-cubic spline quadrature will yield α.

To solve the quasi-equilibrium integral equation (29) we impose the boundary conditions: $\rho_{QE}^S(\lambda \leq o) = 1$, $\rho_{QE}^S(\lambda \geq \epsilon) = 0$ yielding,

$$\int_o^{\epsilon} \rho_{QE}^S(\mu)\; F(\lambda,\mu)d\mu - \rho_{QE}^S(\lambda) \int_{-\infty}^{\omega} F(\lambda,\mu)d\mu = \int_{-\infty}^{o} F(\lambda,\mu)d\mu \qquad (31)$$

When (31) is discretized the result is a system of algebraic equations similar to (21) which can be solved either by iterative methods (SSOR) or direct techniques (Gaussian elimination), due to the much smaller size coefficient matrix $\mathcal{A}$ in the quasi-equilibrium case. As an example of the type of results obtained, we show in figures 3 and 4 the quasi-equilibrium distribution $\rho_{QE}^S(\lambda)$ and recombination rate α/α_T, respectively for the energy-transfer mechanisms of charge-transfer, hard-sphere and polarization collisions. We should also mention that, in addition to the smaller size, the quasi-equilibrium coefficient matrix is also symmetric - a fact which greatly helps in the numerical solution of (29). We have not discussed the numerical solution of the PIDE (28) in the same detail as that of (8), even though they are equivalent, because it results in a system of algebraic equations with a non-symmetric, nonpositive-definite coefficient matrix $\mathcal{A}$ - a problem much more difficult than (17). Finally, the quadrature rule used to determine the weights and pivots used in solving the quasi-equilibrium integral equation (31) were the same nonlinear Simpson's rule weights and pivots of Bates and Mendaš [8] discussed earlier. We conclude section II with a summary of the types of IE's found in the literature.

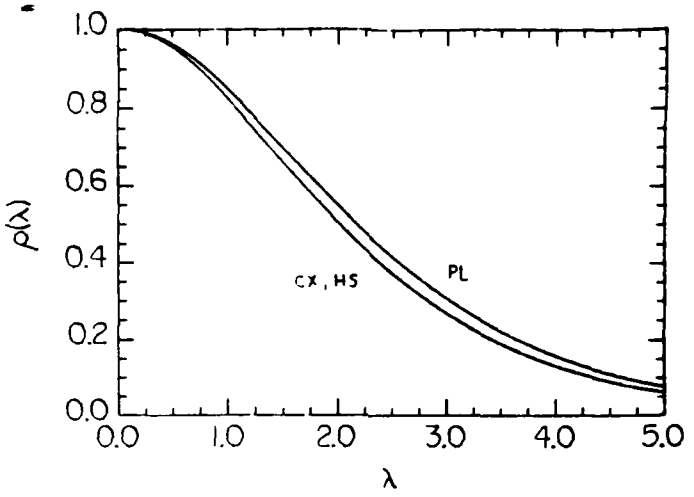

Figure 3: Quasi-equilibrium distribution function $\rho_{QE}(\lambda)$ for the case of a = 1/3 (m_1=m_2=m_3), and energy-change mechanisms of charge-transfer (CX), hard-sphere (HS) and polarization (PL) collisions.

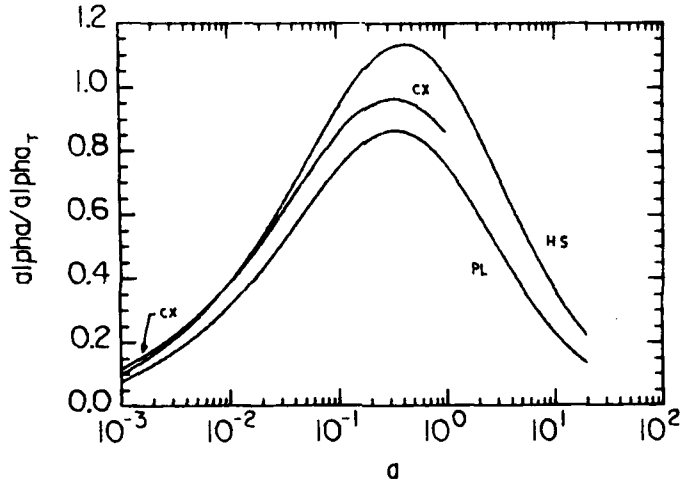

Figure 4: Quasi-Equilibrium recombination rate coefficient (α/α_T) versus mass ratio parameter (a) for energy-change mechanisms of charge-transfer (CX), hard-sphere (HS) and polarization (PL) collisions.

Numerical Solution of IE's

The three basic types of integral equations are Fredholm equations,

$$\int_a^b K(x,y)f(y)dy = g(x)f(x)$$

and Volterra equations of the first kind,

$$\int_o^t K(t,s)f(s)ds = g(t)$$

and second kind,

$$f(t) - \int_o^t K(t,s)f(s)ds = g(t)$$

where g is a known function, f is the unknown function and K is the kernal of the integral equation. We have already encountered Fredholm equations and Volterra equations of the 2nd-kind in (29) and (8), respectively. We will not encounter Volterra integral equations of the 1st-kind in this lecture. However, upon discretization, all three types of IE's above reduce to a problem of solving a system of linear algebraic equations. The particular technique used to solve the algebraic equations depends upon the structure of the coefficient matrix $\mathcal{A}$, which in turn depends on the behavior of the kernal K. Recalling our steps in the numerical solution of PIDE's, we find that steps (ii) - (iv) also provide a good prescription for the numerical solution of one-dimensional IE's. We have been brief in our summary of the numerical treatment of integral equations due again to the breadth of the area. For a complete introduction to the numerical solution of IE's see Baker [2] and Delves and Mohamed [16]. For an excellent account of Volterra equations see Linz [34].

III. Approximate Treatments of Ionic Recombination

As stated in the introduction, until the advent of super-computers, the direct solution of the PIDE's arising from the Boltzmann equation treatment of ionic recombination, was generally avoided due to the difficulty in solving systems of algebraic equations composed of 1000 or more equations and unknowns. The paper (Bates and Mendaš [9]) which originally derived the coupled PIDE's (8) solved them by a power series expansion in $\Lambda_{mfp.}$ which converged slowly with gas density and whose coefficients were difficult to compute in general. As discussed in section II, the slow convergence rate of the power series solution of (8) is directly related to the ill-conditioned nature of the coefficient matrix $\mathcal{A}$ in (21). Hence other methods of solving for the recombination rate α are needed. One such method which has proven quite successful is the Monte Carlo simulation of ion-ion recombination processes (Bates and Mendaš [10], and Morgan et al. [38]). We will not cover this type of calculation in this lecture since our main interest is in discussing techniques which lead to PDE's or PIDE's.

In this section we will discuss the Debye-Smoluchowski and diffusion equation approaches to ionic recombination. The starting point for the Debye-Smoluchowski equation is the macroscopic continuity equation for the number density of ion pairs, undergoing recombination of time t and separation R,

$$\frac{dn(\vec{R},t)}{dt} = \frac{\partial n(\vec{R},t)}{\partial t} + \vec{\nabla} \cdot \vec{J}(\vec{R},t) = 0 \qquad (32)$$

for $R \geq S \equiv$ sink radius, and is solved subject to the asymptotic boundary condition $n(R \to \infty,t) = \tilde{N}(X^+)\,\tilde{N}(Y^-)$ where $\tilde{N}$ is the equilibrium number density. The net current $\vec{J}(\vec{R},t)$ of ion pairs expanding at time t is,

$$\vec{J}(\vec{R},t) = -D\,\vec{\nabla}\, n(\vec{R},t) + (K/e)(\vec{\nabla} V)\, n(\vec{R},t) \qquad (33)$$

where V(R) is the interaction potential between X^+ and Y^-, and D, K are

the relative diffusion and mobility coefficients of X^+ and Y^- in a background gas Z. The introduction of a sink, with an assigned local three-body reaction rate α_3 at the surface, allows one to avoid dealing with the complicated collision kernels $F(\lambda,\mu;r)$ and full PIDE nature of (8) by replacing the problem with a phenomenological model. After substituting the current (33) into (32), and discretizing, the problem reduces to a boundary value problem involving a time-dependent diffusion equation in R. An example of the resultant solution is given in figure 5 which shows the time-dependent number density of ion pairs n(R,t) versus R for a specified sink radius. For further details on the Debye-Smoluchowski equation and ion-ion recombination see Flannery and Mansky [29].

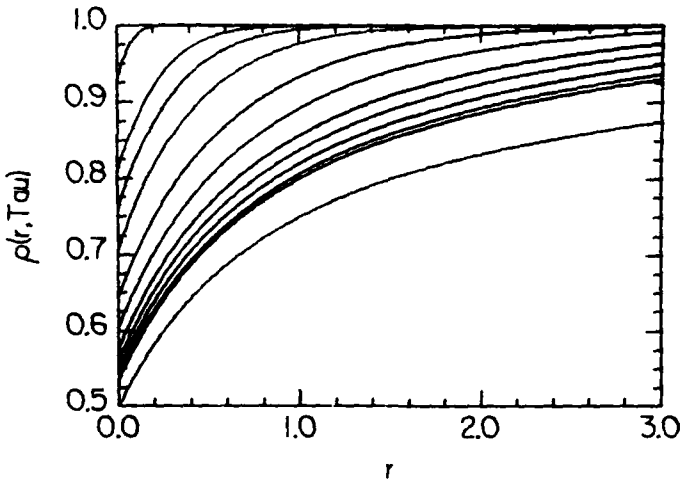

Figure 5: Solution of Debye-Smoluchowski equation for $\rho = n(r,\tau)/N_o \exp(-V/kT)$ $r \equiv R/S-1$, $\tau \equiv Dt/S^2$. τ ranges (from the top curve down) from 0.05, 0.5, 1, 2, 5, 10, 20, 30 to 100. The lowest curve is the steady state (equilibrium) distribution. Assigned parameters are $S = 0.5$, $\alpha_\infty/\alpha_{TR} = 0.5$ (see [29] for details).

Diffusion equations in energy have also been used to model ionic recombination since the work of Pitaevskii [39]. In fact, the quasi-equilibrium theory of ion-ion recombination discussed in section II can be considered a Markov process (Flannery [19]). Writing the quasi-equilibrium integral equation (29) in terms of energies E, E_i (with the time-dependence reinserted - see Flannery [30], p. 17),

$$\frac{\partial n(E,t)}{\partial t} = N(Z) \int_{-E_s}^{\infty} n(E_i,t)\, K(E_i,E)dE_i - n(E,t) \int_{-D}^{\infty} K(E,E_i)dE_i \qquad (34)$$

Combining the integrals in (34) and Taylor series expanding the resultant integrand results in the Fokker-Planck equation,

$$\frac{\partial n(E,t)}{\partial t} = - \frac{\partial}{\partial E} [A_1 n(E,t)] + \frac{1}{2} \frac{\partial^2}{\partial E^2} [A_2\, n(E,t)] \qquad (35)$$

where,

$$A_n = N(Z) \int_{-D}^{\infty} (E_f - E_i)^n\, K(E,E_f)dE_f$$

and one assumes that the energy-transfer between the ion-pairs and third bodies is small so that the Taylor series expansion of (34) converges. This necessarily limits the diffusion model to electron-ion recombination processes. As an example of the type of results obtained by the energy space diffusion equation, we show in figure 6 the steady-state distribution $\rho(\lambda)$ obtained by Pitaevskii compared with the corresponding results of the quasi-equilibrium theory. While Pitaevskii's treatment only becomes accurate in the limit of electron-ion recombination, it's similarity with the quasi-equilibrium results in figure 6, for the case of equal mass constitutents, is striking. For a more complete discussion of energy space diffusional theories of termolecular recombination see Flannery [26].

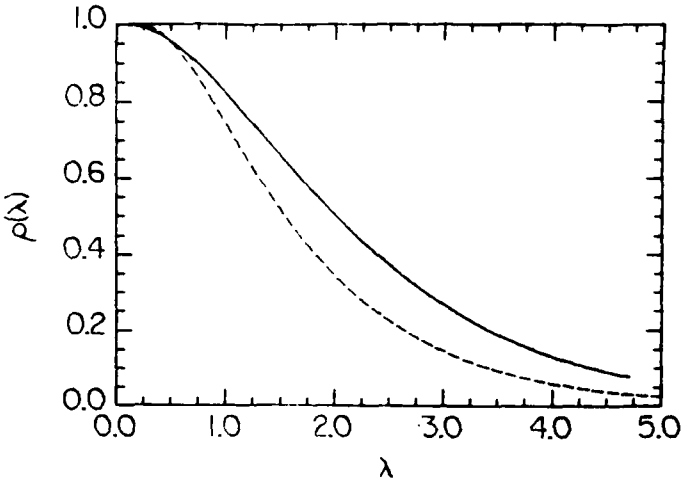

Figure 6: Comparison of quasi-equilibrium distribution (___) and Pitaevskii's distribution (---_ for the case of a = 1/3 and charge-transfer collisions.

IV. Conclusions and General References

In this lecture we have provided a detailed prescription for handling numerically the coupled partial integro-differential equations which arise from the Boltzmann equation treatment of ionic recombination. We have also given a brief summary of some of the approximate methods of treating ionic recombination. The reason for our detailed treatment of PIDE's is that there is little in either the physics or mathematics literature on how to tackle the problem of solving numerically a system of mult dimensional PIDEs (i.e., systems with more than 1 independent variable). In this lecture we have tried to fill this gap.

Our main conclusion is that iterative techniques are numerically the most efficient way of solving the large systems of algebraic equations which result from PIDE's like (8). While this is not entirely unexpected, it is the first time techniques like the SSOR have been applied to problems in ionic recombination. With resolution of the problem of the ill-conditioning of $\mathcal{A}$ in (21), a number of long-standing

problems in chemical physics will be able to be solved. We end this lecture with a list of general references which we have found useful on the subject of solving numerically IE's and PIDE's.

- Baker, C. T. H., 1977, The Numerical Treatment of Integral Equations, Oxford University Press.
- Cullum, J. K., and Willoughby, R. A., 1985, Lanczos Algorithms for Large Symmetric Eigenvalue Computations, Vol. I, Theory, Vol. II, Programs, Birkhauser (Boston).
- Delves, L. M. and Mohammed, J. L., 1985, Computational Methods for Integral Equations, Cambridge University Press.
- Feldstein, A., and Sopka, J. R., 1974, SIAM J. Numer. Analy. 11, 826-46.
- Golub, G. H., and van Loan, C. F., 1983, Matrix Computations, Johns Hopkins University Press.
- Hageman, L. A., and Young, D. M., 1981, Applied Iterative Methods, Academic Press.
- Linz, P., 1985, Analytical and Numerical Methods for Volterra Equations SIAM Press, (Philadelphia).
- Young, D. M., 1971, Iterative Solution of Large Linear Systems, Academic Press.
- Young, D. M., and Jea, K. C., 1980, Lin. Algebra Appl. 34, 159-94.
- Wilkinson, J., 1965, The Algebraic Eigenvalue Problem, Oxford Univ. Press.

Acknowledgements

This work is supported by AFOSR under grant No. 84-0233. The invitation to lecture, and the partial support received from Oak Ridge National Laboratory are also gratefully acknowledged.

References

1. Akhiezer, A. I., Akhiezer, I. A., Polovin, R. V., Sitenko, A. G., and Stepanov, K. N., 1975, Plasma Electrodynamics, Vol. 1, Linear Theory, Pergamon Press.
2. Baker, C. T. H., 1977, The Numerical Treatment of Integral Equations, Oxford University Press.

3. Balescu, R., 1963, Statistical Mechanics of Charged Particles, Interscience - Wiley.
4. ibid., 1975, Equilibrium and Nonequilibrium Statistical Mechanics, Wiley.
5. Bates, D. R., and Flannery, M. R., 1968, Proc. Roy. Soc. (Lon.) A 302, 367-83.
6. Bates, D. R., Hays, P. B., and Spevak, D., 1971, J. Phys. B: At. Mol. Phys. 4, 962-8.
7. Bates, D. R., and McKibbin, 1974, Proc. Roy. Soc. (Lon.) A 339, 13-28.
8. Bates, D. R., and Mendaš, I., 1975, J. Phys. B: At. Mol. Phys. 8, 1770-5.
9. ibid., 1978, Proc. Roy. Soc. (Lon.) A 359, 275-85.
10. ibid., 1978, Proc. Roy. Soc. (Lon.) A 359, 287-301.
11. ibid., 1982, J. Phys. B: At. Mol. Phys. 15, 1949-56.
12. Bates, D. R., and Moffett, 1966, Proc. Roy. Soc. (Lon.) A 291, 1-8.
13. Chapman, S. and Cowling, T. G., 1970, The Mathematical Theory of Non-Uniform Gases, Cambridge University Press, 3rd. ed.
14. Cline, A. K., Moler, C. B., Stewart, G. W., and Wilkinson, J. H., 1979, SIAM J. Numer. Analy. 16, 368-75.
15. Cullum, J. K., and Willoughby, R. A., 1985, Lanczos Algorithms for Large Symmetric Eigenvalue Computations, Vol. I, Theory, Vol. II, Programs, Birkhäuser (Boston).
16. Delves, L. M., and Mohamed, J. L., 1985, Computational Methods for Integral Equations, Cambridge University Press.
17. Faber, V., and Manteuffel, T. A., 1989, p. 37-61, in Transport Theory, Invariant Imbedding and Integral Equations, (P. Nelson, V. Faber, T. A. Manteuffel, D. A. Seth and A. B. White, Jr., eds.) Marcel Dekker.
18. Ferziger, J. H., and Kaper, H. G., 1972, Mathematical Theory of Transport Processes in Gases, North-Holland.
19. Flannery, M. R., 1971, Ann. Phys. (N.Y.) 67, 376-88.
20. ibid., 1972, Chap. 1, p. 1-90, in Case Studies in Atomic Collision Physics, Vol. 2, (E. W. McDaniel and M. R. C. McDowell, eds.), North-Holland.

21. ibid., 1973, Ann. Phys. (N.Y.) 79, 480-517.
22. ibid., 1980, J. Phys. B: At. Mol. Phys. 13, 3649-64.
23. ibid., 981, J. Phys. B: At. Mol. Phys. 14, 915-34.
24. ibid., 1982, Phil. Trans. Roy. Soc. (Lon.) A 304, 447-97.
25. ibid., 1987, J. Phys. B: At. Mol. Phys. 20, 4929-38.
26. ibid., 1987, J. Chem. Phys. 87, 6947-56.
27. Flannery, M. R., and Mansky E. J., 1988, J. Chem. Phys. 88, 4228-41.
28. ibid., 1989, "Kinetic Theory Foundations of Ion-Ion Recombination", J. Chem. Phys., to be submitted.
29. ibid., 1989, Chem. Phys. 132, 115-36.
30. Golub, G. H., and van Loan, C. F., 1983, Matrix Computations, Johns Hopkins University Press.
31. Grimes, R. G., Kincaid, D. R., and Young, D. M., 1979, ITPACK 2.0 User's Guide, CNA-150, Center for Numerical Analysis, Univ. Texas (Austin).
32. Hageman, L. A., and Young, D. M., 1981, Applied Iterative Methods, Academic Press.
33. IMSL Math/Library User's Manual, Vol. 1, 1989.
34. Linz, P., 1985, Analytical and Numerical Methods for Volterra Equations, SIAM Press (Philadelphia).
35. Mansky, E. J., 1985, Ph.D. thesis, Georgia Institute of Technology.
36. Manteuffel, T. A., 1977, Numer. Math. 28, 307-27.
37. ibid., 1978, Numer. Math. 31, 183-208.
38. Morgan, W. L., Whitten, B. L., and Bardsley, J. N., 1980, Phys. Rev. Lett. 45, 2021-4.
39. Pitaevskii, L. P., 1962, Soviet Phys. JETP 15, 919-21.
40. Thomson, J. J., 1924, Phil. Mag. 47, 337-78.
41. Tolman, R. C., 1938, The Principles of Statistical Mechanics, Oxford University Press.
42. Young, D. M., 1971, Iterative Solution of Large Linear Systems, Academic Press.
43. Young, D. M., and Jea, K. C., 1980, Lin. Algebra Appl. 34, 159-94.